Examining the development of brain structure in utero with fetal MRI, acquired as part of the Developing Human Connectome Project

Wilson, Sian

Awarding institution:
King's College London

A thesis submitted for the degree of

Doctor of Philosophy in Neuroscience

Examining the development of brain structure in utero with fetal MRI, acquired as part of the Developing Human Connectome Project

Siân Wilson

Centre for the Developing Brain,

MRC Centre for Neurodevelopmental Disorders,

Institute of Psychiatry, Psychology and Neuroscience,

King's College London, United Kingdom

July 2023

Contents

List of Figures

Abbreviations

CSD Constrained Spherical Deconvolution

CSF Cerebrospinal Fluid

dHCP Developing Human Connectome Project

DTI Diffusion Tensor Imaging

DWI Diffusion Weighted Imaging

EPI Echo Planar Imaging

FA Fractional Anisotropy

FDR False Discovery Rate

fMRI Functional Magnetic Resonance Imaging

GM Grey Matter

GW Gestational Week

HARDI High Angular Resolution Diffusion Imaging

ICA Independent Component Analysis

MD Mean Diffusivity

MRI Magnetic Resonance Imaging

MSMT-CSD Multi-shell Multi-tissue Constrained Spherical Deconvolution

ODF Orientation Density Function

RGC Radial Glial Cell

WM White Matter

Declaration

I, hereby declare that this thesis, entitled "Examining the development of brain structure in utero with fetal MRI", is a culmination of my own work and that all sources and external contributions have been acknowledged. The data collection for this project was an interdisciplinary collaboration between King's College London, Imperial College London and the University of Oxford. I was involved at multiple levels, including study design, quality control, image processing, data analysis and biological interpretation of the fetal data. All analysis included in this thesis was carried out by me, with feedback from my supervisors, thesis committee members, Daan Christiaens, Maximilian Pietsch, HyukJin Yun and Kiho Im. Two results chapters of this thesis have been peer-reviewed and published in the journals *PNAS (Wilson et al., 2021;* https://doi.org/10.1073/pnas.2023598118) and *eLife (Wilson et al., 2023;* https://doi.org/10.7554/eLife.83727). I declare that this thesis has not been submitted for any other degree, nor has it been submitted for publication elsewhere.

Acknowledgements

First and foremost, I am immensely grateful to Jonny, Tomoki & David, for being truly excellent supervisors. Thank you for restoring my faith in academia, allowing me to explore while keeping me focused, and for nurturing my confidence. My only criticism of this relationship is the unimpeachable bar it has set.

I owe an immeasurable amount of gratitude to the people, past and present, at the Centre for the Developing Brain, for the opportunity to work on the Developing Human Connectome Project. Their dedication to recruiting, acquiring and reconstructing the fetal MRI data within this thesis allowed me to explore unchartered imaging territory, surrounded by the most humble and helpful world-leading experts.

I would like to thank Laura Andreae & Tony Vernon, for taking a leap of faith in me and offering me a place on the MRC-CNDD PhD programme. Thank you to my thesis committee, Grainne McAlonan and Serena Counsell, your positive, constructive feedback always refuelled my enthusiasm and propelled me between projects.

Ellen Grant, Kiho Im and HyukJin Yun at Harvard Medical School, thank you for the opportunity to collaborate in a different research environment and for always welcoming my ideas.

This thesis would not have been possible without the unwavering support and kindness from my friends and family. A special thank you must go to my fellow PhD friends and sounding boards, Pavan, Anna, Dan & Jucha.

Finally to my Mum, Dad, Zoë & Rafe, thank you for your compassion, encouragement, and for uplifting me while keeping me grounded. You are my pillars and my guideposts.

To everyone who has been so supportive of me throughout this journey, I never imagined I would enjoy doing research as much as I have in the last 4 years.

Thank you,

Siân

Abstract

The human brain is an incredibly complex organ, and the study of it traverses many scales across space and time. The development of the brain is a protracted process that begins embryonically but continues into adulthood. Although neural circuits have the capacity to adapt and are modulated throughout life, the major structural foundations are laid in utero during the fetal period, through a series of rapid but precisely timed, dynamic processes. These include neuronal proliferation, migration, differentiation, axonal pathfinding, and myelination, to name a few. The fetal origins of disease hypothesis proposed that a variety of non-communicable diseases emerging in childhood and adulthood could be traced back to a series of risk factors effecting neurodevelopment in utero (Barker 1995). Since this publication, many studies have shown that the structural scaffolding of the brain is vulnerable to external environmental influences and the perinatal developmental window is a crucial determinant of neurological health later in life. However, there remain many fundamental gaps in our understanding of it.

The study of human brain development is riddled with biophysical, ethical, and technical challenges. The Developing Human Connectome Project (dHCP) was designed to tackle these specific challenges and produce high quality open-access perinatal MRI data, to enable researchers to investigate normal and abnormal neurodevelopment (Edwards et al., 2022). This thesis will focus on investigating the diffusion-weighted and anatomical (T2) imaging data acquired in the fetal period, between the second to third trimester (22 – 37 gestational weeks). The limitations of fetal MR data are ill-defined due to a lack of literature and therefore this thesis aims to explore the data through a series of critical and strategic analysis approaches that are mindful of the biophysical challenges associated with fetal imaging. A variety of analysis approaches are optimised to quantify structural brain development in utero, exploring avenues

to relate the changes in MR signal to possible neurobiological correlates. In doing so, the work in this thesis aims to improve mechanistic understanding about how the human brain develops in utero, providing the clinical and medical imaging community with a normative reference point.

To this aim, this thesis investigates fetal neurodevelopment with advanced in utero MRI methods, with a particular emphasis on diffusion MRI. Initially, the first chapter outlines a descriptive, average trajectory of diffusion metrics in different white matter fiber bundles across the second to third trimester. This work identified unique polynomial trajectories in diffusion metrics that characterise white matter development (Wilson et al., 2021). Guided by previous literature on the sensitivity of DWI to cellular processes, I formulated a hypothesis about the biophysical correlates of diffusion signal components that might underpin this trend in transitioning microstructure. This hypothesis accounted for the high sensitivity of the diffusion signal to a multitude of simultaneously occurring processes, such as the dissipating radial glial scaffold, commencement of pre-myelination and arborization of dendritic trees.

In the next chapter, the methods were adapted to address this hypothesis by introducing another dimension, and charting changes in diffusion properties along developing fiber pathways. With this approach it was possible to identify compartment-specific microstructural maturation, refining the spatial and temporal specificity (Wilson et al., 2023). The results reveal that the dynamic fluctuations in the components of the diffusion signal correlate with observations from previous histological work. Overall, this work allowed me to consolidate my interpretation of the changing diffusion signal from the first chapter. It also serves to improve understanding about how diffusion signal properties are affected by processes in transient compartments of the fetal brain.

The third chapter of this thesis addresses the hypothesis that cortical gyrification is influenced by both underlying fiber connectivity and cytoarchitecture. Using the same fetal imaging dataset, I analyse the tissue microstructural change underlying the formation of cortical folds. I investigate correlations between macrostructural surface features (curvature, sulcal depth) and tissue microstructural measures (diffusion tensor metrics, and multi-shell multi-tissue decomposition) in the subplate and cortical plate across gestational age, exploring this relationship both at the population level and within subjects. This study provides empirical evidence to support the hypotheses that microstructural properties in the subplate and cortical plate are altered with the development of sulci.

The final chapter explores the data without anatomical priors, using a data-driven method to extract components that represent coordinated structural maturation. This analysis aims to examine if brain regions with coherent patterns of growth over the fetal period converge on neonatal functional networks. I extract spatially independent features from the anatomical imaging data and quantify the spatial overlap with pre-defined neonatal resting state networks. I hypothesised that coherent spatial patterns of anatomical development over the fetal period would map onto the functional networks observed in the neonatal period.

Overall, this thesis provides new insight about the developmental contrast over the second to third trimester of human development, and the biophysical correlates affecting T2 and diffusion MR signal. The results highlight the utility of fetal MRI to research critical mechanisms of structural brain maturation in utero, including white matter development and cortical gyrification, bridging scales from neurobiological processes to whole brain macrostructure.

I. Introduction

1. Biological background

1.1 An introduction to in utero neurodevelopment

Neurodevelopment occurs as a precisely timed sequence of processes, from the onset of neurogenesis in the embryo to the refinement of neural circuits in adolescence. Each process is regulated and coordinated through a series of interactions with other histogenetic events, such that neurodevelopment progresses in a complex but sequential way. The procedural nature of neurodevelopment and consistency across individuals suggests that the fundamental biology is largely genetically determined in the earliest stages of life and becomes increasingly modulated by environmental factors with age. Extreme deviations or disruptions to these processes, from genetic or environmental causes, can significantly affect brain structure and function in childhood and even adulthood. Early developmental perturbations are thought to underpin many cognitive, behavioural, and neurodevelopmental disorders.

To investigate the general mechanisms of brain development, a variety of different research methods and model organisms have been used. In the human brain specifically, most work to date has relied on post-mortem histology, examining the brain slice-by-slice with immunohistochemistry methods, and in vivo neuroimaging. The following introductory chapter will summarise the current state of knowledge about the fundamental processes

involved in human neurodevelopment. This includes a timeline for the occurrence of different processes, which spatially and temporally overlap (Figure 1). This sequential progression of neurodevelopment and the interdependence of processes, underpins the transient features of the developing brain which are central to the work in this thesis.

Although brain development begins embryonically, for the purpose of this thesis, I will focus on the neurobiology of the time window covered by the Developing Human Connectome Project (dHCP) fetal dataset (20 - 37 gestational weeks). This will provide the relevant biological context to understand the signal changes in different MRI contrasts that accompany structural brain development.

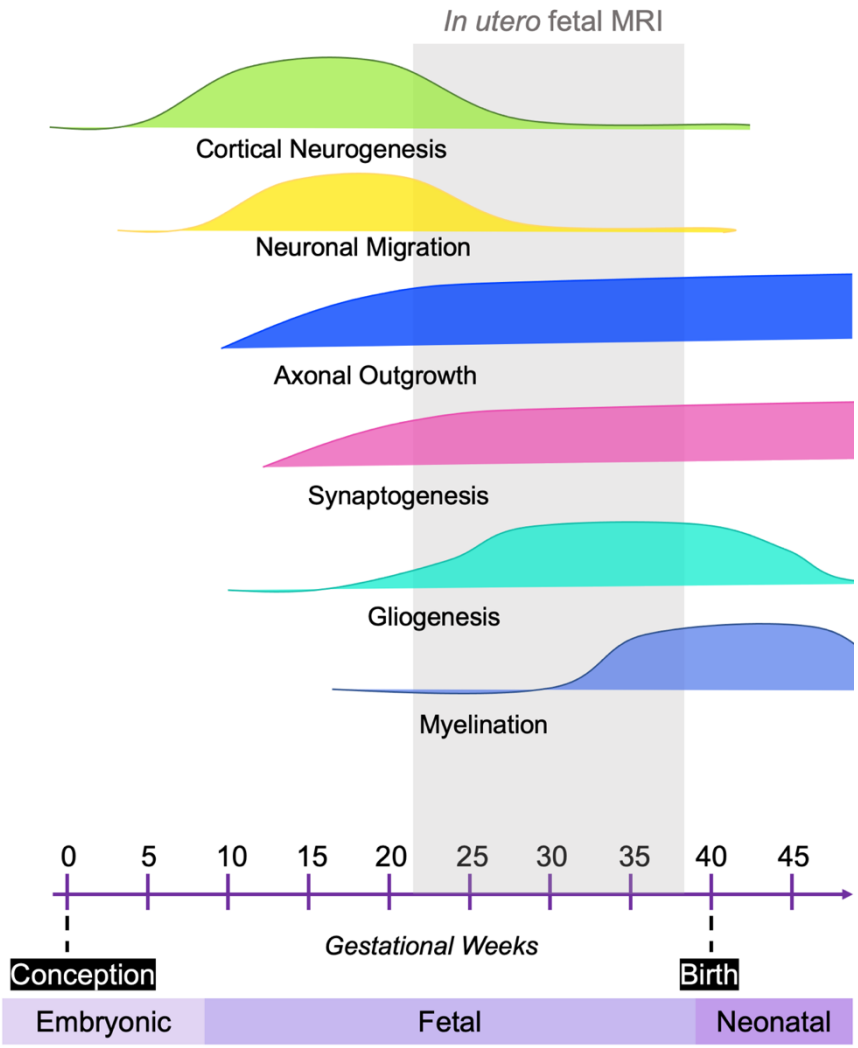

Figure 1. *Timeline for neurodevelopmental processes over the fetal period. The window of time where fetal MRI is acquired (in vivo) is highlighted in grey, to emphasise the co-occurrence of specific processes during that timeframe.*

1.2 Cell lineages and neuronal differentiation

The brain contains an extraordinary diversity of cell types, which all originate from the same neural stem cells. How billions of cells acquire their fate from a homogenous population of stem cells remains an active field of research (for a recent review, see Belmonte-Mateos and Pujades, 2022). The process of cellular differentiation requires stem cells to integrate signals in a noisy and dynamic environment, to drive electrophysiological, morphological, and transcriptional changes. A mixture of spatial information, intracellular factors and extracellular environmental cues are harmoniously integrated to alter gene expression and drive lineage progression in a stepwise manner, outlined in Figure 2.

The first neural stem cells, aka neuroepithelial cells, appear during the third week of embryonic growth, when they multiply and form a folded structure, the neural tube. Along the neural tube, the neuroepithelial cells are organised in specific locations and express a series of transcription factors, which together dictate the fate of their progeny. In the process of differentiation, cells regulate specific genes to alter their proteome and change their morphological features. For instance, neuroepithelial cells elongate and downregulate their epithelial features, stopping the expression of tight junction proteins to differentiate into radial glial cells (RGCs), which are bipolar-shaped neural progenitor cells. RGCs maintain a cell body in the ventricular zone as they elongate, and their processes extended towards the cortical plate. Both radial glial cells and neuroepithelial cells are classified as neural stem cells, sharing the expression of several

cellular markers (Alvarez-Buylla et al., 2001; Malatesta and Götz, 2013). Neural stem cells are tripotent, meaning that they can differentiate into 3 mature cell subtypes: neurons, astrocytes, and oligodendrocytes (Malatesta et al., 2000; Noctor et al., 2001).

The asymmetrical division of RGCs produces one radial glial cell and either one immature neuron or an intermediate progenitor. The pool of intermediate progenitor cells will then further divide to produce neurons. It is thought that the differentiation of radial glial cells is responsible for generating the vast neuronal diversity seen in the CNS. RGCs can differentiate into a diverse range neuronal subtypes in a position-dependent manner, according to the level of exposure to different molecular signals. The result is a mature neocortex, partitioned into structurally and functionally distinct "areas", with characteristic cellular organization and patterns of neuronal connectivity (for review, see Stiles and Jernigan, 2010).

At around 16 – 18 gestational weeks (GW), RGCs transition from being neurogenic to gliogenic and start to produce macroglia (astrocytes and oligodendrocytes), this is referred to as the 'neuron-glial switch' (Bayer and Altman, 1991). In the developing mammalian neocortex, gliogenesis begins with the production of immature astrocytes, followed by oligodendrocyte precursors (Jakovcevski et al., 2009) (oligodendrocytes discussed more in section 1.5.2). Although it is not fully understood what drives the gliogenic switch, evidence suggests a combination of extrinsic, intrinsic, and epigenetic signals affect the innate competence of precursor cells over time, such that there is a bias in favour of making neurons earlier in development, then glial cells later. For instance, in vitro work has shown that cortical precursors make neurons when cultured on embryonic cortical slices, but astrocytes when cultured on postnatal cortical slices (Morrow et al., 2001). RGCs also respond to extrinsic signals in their environment which regulate the appropriate timing of gliogenesis. Previous

studies have shown that multiple factors converge to promote the gliogenic switch, including cytokines, bone morphogenetic proteins (BMPs), and Notch ligands (Miller and Gauthier 2007).

1.3 Neuronal proliferation and migration

In the developing brain there is careful regulation over the timing and population size of different cell types, such that distinct cell fates can be specified within tight developmental windows. Genetic and epigenetic processes activate specific subsets of genes in a combinatorial manner at specific timepoints over the course of neurodevelopment, to specify neuronal subtypes and their patterns of connectivity. Neuronal migration ensures that neurons are in the right place at the right time, both for differentiation into the correct cellular identity and for the formation of neural circuits.

In humans, the onset of neurogenesis occurs embryonically at around 6-8 GW when neuroepithelial stem cells start switching to an asymmetric mode of cell division (Bryston 2006, Noctor 2001). Progenitor cells initially divide symmetrically, forming two additional progenitor cells, generating a population of proliferative units. This process continues up until ~ 6 GW, after which point the population of proliferative units is stabilised, and the progenitor cells begin to divide asymmetrically (into a stem cell and a postmitotic neuronal cell). After several weeks of asymmetric cell division there is an increased ratio of postmitotic neuronal cells to stem cells. Neuronal proliferation has two phases of growth during fetal development, rapid exponential growth between 10 – 20 GW followed by a slower growth phase from 20 GW to term. The highly proliferative fetal brain cellular architecture produces an estimate of $\sim 10^{10}$ cells by the end of the second trimester (Samuelson 2003).

Neuronal migration occurs with a similar overlapping timescale, it begins at ~10 GW and is largely complete by the end of the second trimester (Rakic 1990). Neuronal migration processes allow the nervous system to distribute billions of cells from their origin in the proliferative ventricular zone epithelium to widespread specific positions throughout the brain as it develops (Marin et al., 2010). Together these processes facilitate the creation of regionally specialised cytoarchitecture across the brain and the creation of complex neural circuits.

The first method of neuronal migration is known as somal migration, or movement by translocation of the cell body. This enables the early migrating neurons to move comparatively small distances in early development, up to around 10 GW (Volpe 2018). Subsequently, after more cellular scaffolding is in place, there are two main types of neuronal migration, radial and tangential (Hatten 1999; Marin and Rubenstein 2003). Radial migration occurs along a trajectory that is perpendicular to the ventricular zone, facilitated by radial glial cells forming a scaffold that supports the migration of neural progenitors from the ventricular zone to their destination. These cells originate from the same radial glial progenitors, such that the clonally related neuron migrates along the parent radial glial fiber (Walsh and Cepko 1988, 1990; Gray 1990).

Studies of cortical development in non-human primates have been crucial to our understanding of how neuronal proliferation and migration proceeds in early fetal development (Rakic, 1975, 1978, 1995). Different cell types appear to display a preferential mode of migration. Radial migration is the predominant mechanism for distributing glutamatergic pyramidal neurons throughout the brain. Pyramidal cells begin their journey in the ventricular zone and navigate into the cortex via radial migration pathways. These migration pathways are formed from

elongated radial glial cell projections that can extend between the ventricular zone and the pial surface in the developing primate brain (Rakic 1975, 1978). When the radial glial scaffold is misaligned, such as in the weaver mutant mouse, migrating neurons do not reach their final destination (Hatten et al., 1986).

On the other hand, GABAergic interneurons generated in the subpallium use tangential migration to reach their cortical destination (Corbin et al. 2001; Marin and Rubenstein 2001). Tangential migration occurs along a trajectory that is parallel to the ventricular zone and does not involve the use of the radial glial scaffold (Marin et al., 2010).

The developing cortical plate has a columnar organization, such that neurons are arranged in vertical layers, perpendicular to the surface. This feature of the cortex is critical for the formation of neural circuits and connectivity patterns that underpin functional activity in the adult brain. To elucidate how this organization arises, thymidine incorporation assays were used to study the birth, proliferation, migration of cells. These experiments revealed that neurons born in the earliest phases of development end up in the deepest layers of the cortex (Goldman 1983, Alvarez-Buylla and Nottebohm 1988, Alvarez-Buylla et al., 2001, Miller and Nowakowski, 1988). In other words, the columnar organisation forms in an inside-out manner, with the earliest migrating neurons settling in the deepest layers of the cortex and somas of newer cells adopting more superficial positions than their predecessors (Angevine and Sidman 1961; Rakic 1974).

One enduring hypothesis in developmental neuroscience, the ‘radial-unit hypothesis’, is that this columnar organization occurs as the result of the progeny from a single daughter cell migrating together in a column from the ventricular zone to the cortical plate (Rakic 1995,

2005). Rakic describes this hypothesis of cortical expansion as "the two-dimensional positional information that is contained within the proliferative zone is transformed into three-dimensional cortical architecture: the x and y axis of cell position within the horizontal plane is provided by the site of cell origin, whereas the z axis along the depth of the cortex is provided by the time of its origin" (Rakic 1995). However, studies in the developing ferret brain have shown that while some clonal populations of cells maintain regional specification, partially overlapping with other, other neighbouring clonal populations of neurons become widely dispersed through the cortex (Reid 1997; Ware 1999).

The processes discussed also appear in Figure 1, a visual reference to convey their overlapping occurrence, peaks, and troughs over gestation.

1.3.1 Radial glial cells

Radial glial cells (RGCs) were first discovered in the late 19th century, by histologists studying developmental neuroanatomy (Bergmann 1857; Magini 1888; Ramon y Cajal 1911, Golgi 1886). The introduction of the Golgi staining method enabled the visualisation of radial glial cells and the seminal work of Ramon y Cajal reported their elongated morphology, which lead to theories about their role in neurodevelopment (Figure 2a). Experiments conducted many decades later demonstrated that RGCs play a crucial role in the early organisation of the brain, providing a scaffold for migrating neurons to translocate through the cerebrum (Rakic 1971). This cell type has a profound effect on the diffusion MR signal over the second to third trimester, due to the strongly aligned nature of radially organised fibers.

Radial glial cells have extended processes to facilitate their guidance role (Figure 2b). RGCs can be broadly categorised into apical radial glial cells or basal radial glial cells, according to their highly polarised morphology and the orientation of their processes. The somas of apical RGCs are located in the ventricular zone and their basal processes extend to the pial surface, whereas basal RGCs have cell somas in the cortical wall (Figure 2c). Apical RGCs are positioned to interact with various molecular signals throughout the developing layers of the fetal brain, including signalling molecules from the ventricular zone. These different cellular morphologies confer differences in function and how RGC sub-types facilitate migration.

Although radial glial cells are present in all vertebrates, their relative abundance varies between species. They are abundant during development in gyrencephalic brains such as primates and ferrets, but considerably less prevalent in lissencephalic species such as rodents. Although their function appears to be largely developmental, the present evidence suggests that an RGC-like population persists through vertebrate development and can be found in certain specialized zones of the adult brain (Labusch et al., 2020; Lange et al., 2020; Doetsch et al., 1999). RGC-like cells in adults are thought to reside largely in a quiescent state but can intermittently re-enter the cell cycle, proliferate and engage in neurogenesis when appropriate cellular signals are transmitted (Abbott and Nigussie 2020; Zambusi and Ninkovic, 2020; Lange et al., 2020). In this way they can replenish the neural tissue with new neurons when required.

RGCs can divide symmetrically to self-renew and produce more radial glial cells or asymmetrically, to produce intermediate progenitor cells or neurons (Haubensak et al., 2004; Noctor et al., 2004; Rowitch and Kriegstein, 2010). Over the course of development, the gene expression profile within RGCs changes and subsequently effects cellular morphology and function. Their behaviour is also heavily influenced by extracellular environmental signals

(Götz et al., 2002), and the task of precisely characterising these cellular populations remains an ongoing challenge for developmental biologists, as more markers are being discovered to identify RGC sub-types (Pollen et al., 2015; Eze et al., 2021). There are specific sub-populations of RGCs found in different brain regions at different developmental timepoints, suggesting a strictly defined spatiotemporal specificity to their role.

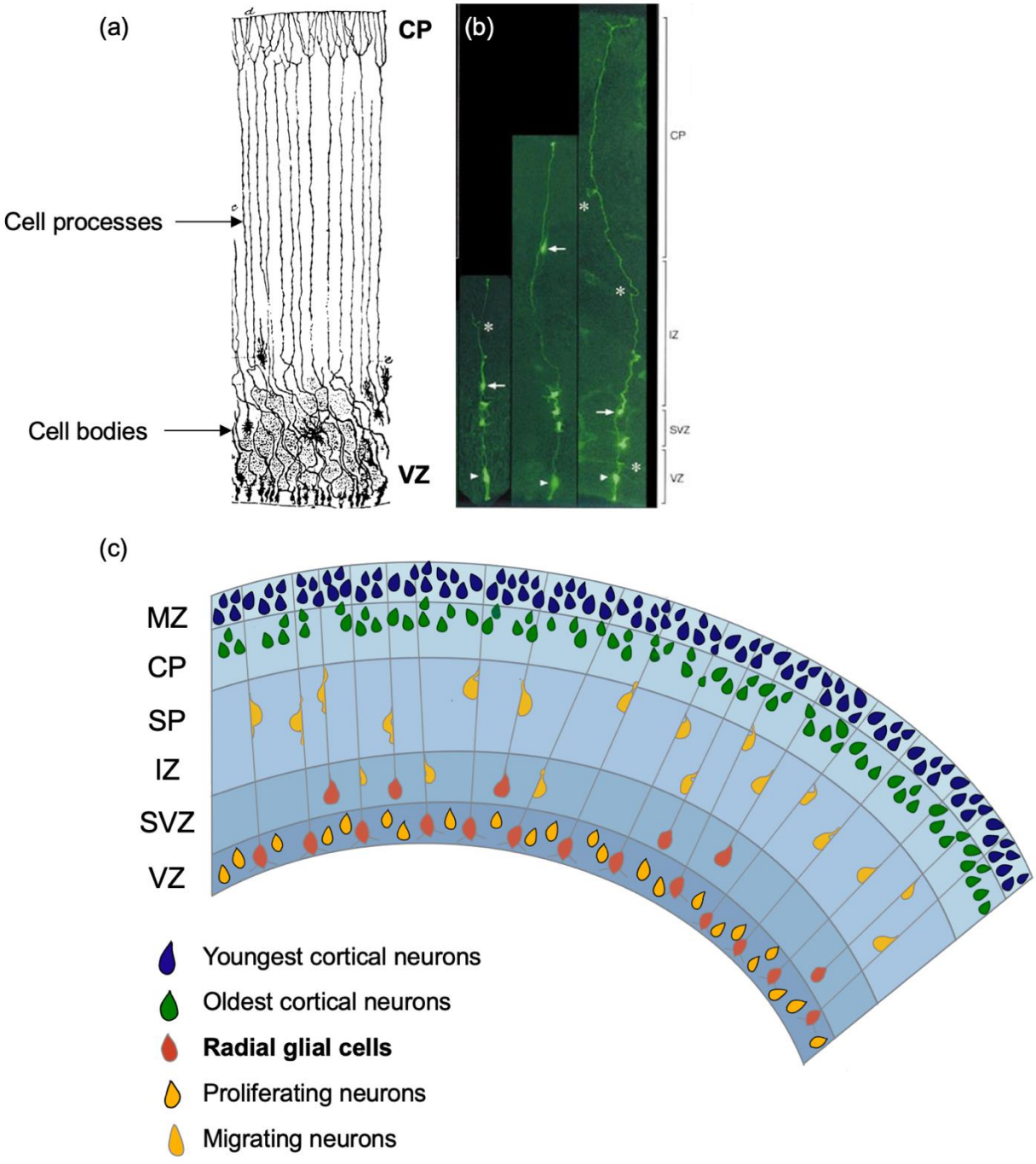

Figure 2. *(a) Illustration of radial glial cells from the neonatal rabbit cerebral cortex, stained using the Golgi method. Cell bodies located in the ventricular zone (VZ) and processes extend to the cortical plate (CP) (Adapted from Ramón y Cajal, 1909) (b) Radial clonal units 72 hours after retroviral infection with Green Fluorescent Protein (GFP). Arrowheads denote typical appearance of radial glia-like cell body. Asterisks highlights association of radial fibers with blood vessels. Arrows point to migrating neuron associated with a related radial fiber. Adapted from Noctor et al., 2001 (c) Schematic of RGC positioning relative to other cell layers and migrating neurons in fetal brain.*

1.4 Transient laminar organization

Several regions of the central nervous system have a 'laminar organisation', where cells adopt an orderly arrangement in distinct and defined layers which are conserved between individuals. The maturation of the cerebral cortex proceeds via the sequential development of transient laminar compartments, which have critical roles facilitating different neurodevelopmental processes at specific points in gestational time (Figure 3). They are categorised as 'transient' because they only exist for small window of developmental time, during which they serve a specific purpose and then they dissipate or rather, evolve into a more permanent feature of brain structure. The unique biophysical properties of these compartments effect MR contrast at different stages in fetal development, such that the boundaries between layers are visible in fetuses during specific gestational weeks. An understanding of the evolution of these zones is fundamental to much of the work that will be presented in this thesis (Figure 3).

The deepest zone closest to the centre of the brain is the ventricular zone, where neural progenitor cells are produced. The first neurons to migrate out of the ventricular zone, via somal

translocation, form the pre-plate. At around 10 GW, this region splits into a multi-layered structure, upon the arrival of the cortical plate neurons in a superficial layer, the marginal zone.

By 14 GW there is an established organisation of different layers, which includes (in order of most-least superficial), the marginal zone, the cortical plate, the subplate, the intermediate zone, the subventricular zone and the ventricular zone (Figure 3). The subventricular zone is formed as the ventricular neuroepithelium expands and first post-mitotic cells migrate away from it. The subventricular zone is also the region that produces the most glial cells. Over time, these glial cells become distributed throughout the next layer, the intermediate zone, and form the scaffold that enables radial migration of neurons through the developing brain. Superficial to the intermediate zone is the subplate, a hydrophilic compartment full of extracellular matrix that is the site of early spontaneous functional activity and synaptogenesis. The most superficial layer of the fetal brain is the cortical plate, which develops into the multi-laminar neocortex by term.

These compartments are a crucial consideration for MRI studies for several reasons. The first, because the biological processes occurring within them have distinct biophysical properties and therefore, profoundly impact the MR signal intensity. The second, because they appear and disappear during the second to third trimester, and as a result the underlying biology affecting MR signal is not uniform across time. Specific attention will be given to the subplate layer and intermediate zone as these areas are the precursors of white matter, which is a focus of thesis.

1.4.1 The subplate

The fetal subplate has the largest volume of all transient compartments over the fetal period (Figure 3) (Kostovic and Vasung 2009). This subplate is prominent across the cerebrum between ~15 and ~34 GW, and remnants of it persist in some brain regions postnatally (Kostović et al., 2014). In its peak abundance, the subplate zone is approximately four times wider the cortical plate (Vasung et al., 2020). The subplate contains a combination of migratory neurons, glia, axon growth cones, extracellular matrix, axonal guidance molecules and morphogens. The abundance of hydrophilic extracellular matrix leads to easy visualisation of the subplate as a hyperintense band on T2w images in the late second to early third trimester (Rutherford 2009). The role of the subplate in neurodevelopment is far-reaching but remains enigmatic, as it is involved in many crucial developmental processes.

Neurons destined for the subplate are the most mature neurons in the developing cerebrum during the second trimester (Volpe 2018). Their relatively mature physiology helps to explain the importance of subplate neurons in cerebral organizational events. They have an elaborate dendritic arbour with spines that can receive synaptic inputs from ascending thalamic afferents and distant cortical sites. Numerous studies have demonstrated that both subplate neurons and other molecular components of the subplate, such as radial glial processes, are critical for the axonal guidance, facilitating the pathfinding of thalamocortical axons (Hoerder-Suabedissen and Molnár, 2015; Kostović et al., 2015, 2019; Molnár et al., 2019). In the late second trimester, the subplate functions as a ‘waiting compartment’ for thalamocortical axons before they select their cortical plate target (Kanold and Luhmann, 2010, Kostović and Judaš, 2010). Ablating the subplate impairs the ability of thalamocortical fibers to form synapses in the cortical plate and prevents somatosensory circuit development (Tolner et al., 2012).

The mature physiology of subplate neurons makes them capable of firing action potentials during the fetal period (Allendoerfer and Shatz, 1994; Luhmann and Khazipov, 2018). This spontaneous activity shapes the first cortical circuits by facilitating cell specialisation, neuronal differentiation and enabling connectivity between brain areas before cortico-cortical pathways are established (Kanold, 2019; Luhmann and Khazipov, 2018; Hoerder-Suabedissen and Molnár, 2015, 2013; Allendoerfer and Shatz, 1994; Luhmann and Khazipov, 2018). Experimental data suggests that in the early preterm phase of development, external environmental stimuli are relayed to the subplate via thalamic inputs, which modulates subplate activity and influences the development of cortical circuits (Allendoerfer and Shatz, 1994, Kanold and Luhmann, 2010).

Apoptosis of subplate neurons takes place in the third trimester, and the subplate gradually dissipates as its components become reorganized, differentiated, or dissolved. It is estimated that 90% of subplate neurons have disappeared after approximately the sixth month of postnatal life. The pattern of disappearance varies slightly between cortical areas, and subplate remnants exist for longer in some brain areas than others. By 6 postnatal months, there is no longer any distinct subplate zone contrast on MR images, however there are interstitial neurons embedded into the white matter which are believed to be surviving descendants of fetal subplate neurons (Kostovic and Rakic 1980, Luskin and Shatz, 1985).

1.4.2 The intermediate zone

This heterogeneous compartment was first termed the ‘intermediate zone’ to describe its location between the deeper proliferative layers and superficial post-migratory cells in the

cortical plate (Kershman 1938). It receives considerably less attention in the literature than the subplate but is an important compartment containing the cellular substrates of white matter fibers. There is divergent literature about the precise timeline of its emergence or a general definition of its contents in terms of cellular processes taking place (Byrston 2008). There is a consensus that the intermediate zone contains migratory neurons, moving both radially and tangentially, and large bundles of both afferent and efferent growing axons.

In early development, the intermediate zone is traversed by cells generated in the ventricular zone, which then migrate relatively rapidly and synchronously in waves to the developing cortical plate, mediated by radial glial scaffolding. Initially, the system has a uniformly radial alignment, and in the ventricular zone the radial glial fibers appear to separate columns of germinating cells. As the fetal brain develops, there is a rapid expansion of the intermediate zone, and the radial glial cells form fascicles of fibers, which arc in the medial-lateral direction, forming more curved trajectories to guide neurons along (Gadisseux 1989). Then in the superior boundary of the intermediate zone where it interfaces with the subplate, the radial glial fibers become inflected again to a radial alignment, perpendicular to the pial surface.

In the second to third trimester, the intermediate zone is the host of the astrocytes and preoligodendrocytes that form the cellular basis of the myelin sheath (Rakic, 1972; Kostovic and Rakic, 1990; Bystron et al., 2008). The intermediate zone transforms into white matter as pre-myelination commences around the start of the third trimester.

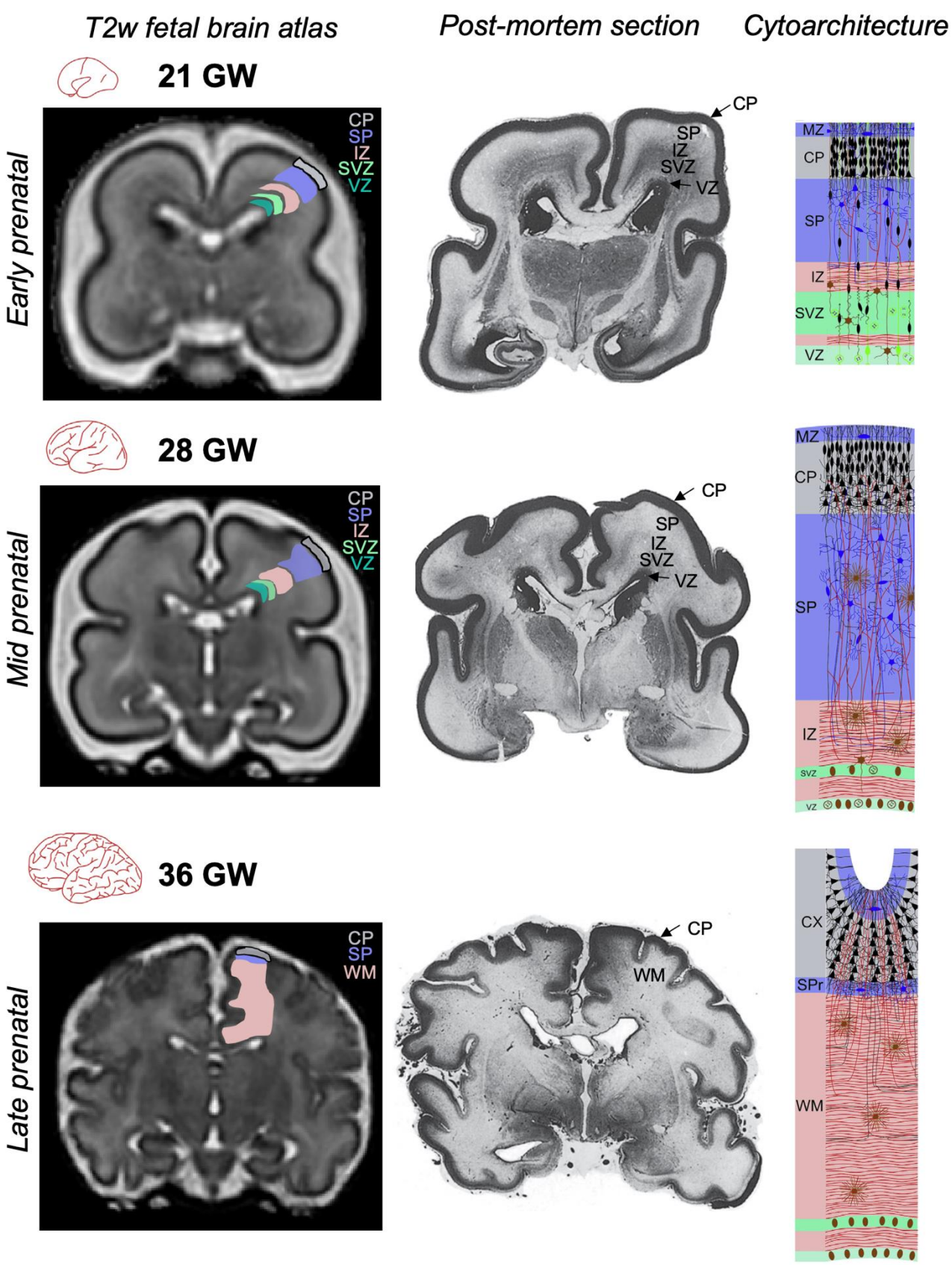

Figure 3. *Developing and dissipating transient fetal brain compartments at early, mid and late prenatal windows (21, 28 and 36 GW). Three columns represent MR signal average (atlas) in*

specific gestational week, equivalent histological section, and a schematic of cytoarchitecture adapted with permission from Kostovic and Judas 2015. Each panel is labelled with the compartments (CP = cortical plate, SP = subplate, IZ = intermediate zone, SVZ = sub-ventricular zone, VZ = ventricular zone, WM = white matter).

1.5 Myelination

1.5.1 Oligodendrocytes and myelinogenesis

Oligodendrocytes are myelin-producing glial cells, which begin developing in the human fetal brain during the second trimester of gestation. Oligodendrocytes have the highest turnover rate of all cell types in the central nervous system; therefore, all stages of precursor cells exist throughout adult life (Dawson et al., 2003). Much of our understanding about their lineage progression is from the study of rodents, using a variety of molecular biology techniques to map the genetics and proteomics of mouse neurodevelopment (He et al., 2001; Marshall and Goldman, 2002; Kessaris et al., 2006).

Oligodendrocyte lineage proceeds through four basic stages, beginning with the progenitors, followed by preoligodendrocytes, immature oligodendrocytes, and mature oligodendrocytes. The myelin sheath in the CNS is constructed by oligodendrocytes extending and modifying their cellular processes to form a tightly wrapped multi-layered structure around axons. The extension and stabilisation of the myelin sheath around axons is mediated by interactions with other cells, including signalling between neurons and astrocytes.

Upon discovering that a single oligodendrocyte can myelinate several axons, it was hypothesised that each axon regulates its own myelination (Friede, 1972). Experimental evidence now suggests that there is reciprocal signalling between neurons and astrocytes that directs the production of the myelin sheath, shapes axonal structure and conduction, and maintains the survival of oligodendrocytes (Hartline and Colman 2007, Duncan et al., 2021). It is estimated that each oligodendrocyte can extend its processes to approximately 50 different axons (Edgar and Garbern 2004). There is a synergy between the oligodendrocyte and developing axon, such that the axonal cytoskeleton does not form properly in the absence of myelin (Brady 1999).

There are specific gene expression markers that can be used to identify each stage of oligodendrocyte differentiation, which have allowed researchers to characterise the proportional ratio of each cell type during the second to third trimester. Pre-oligodendrocytes are proliferative, O4+ multipolar cells which account for 90% of the total population of oligodendrocytes up to 28 GW. The O4+ cells progress into immature oligodendrocytes, which are O1+ cells. Although O1+ cells first appear in the human fetal brain in the second trimester, there is a large spike in their abundance between 27-30 GW, and their ratio shifts from ~10% to 40% of the total oligodendrocyte population (Back et al., 2002).

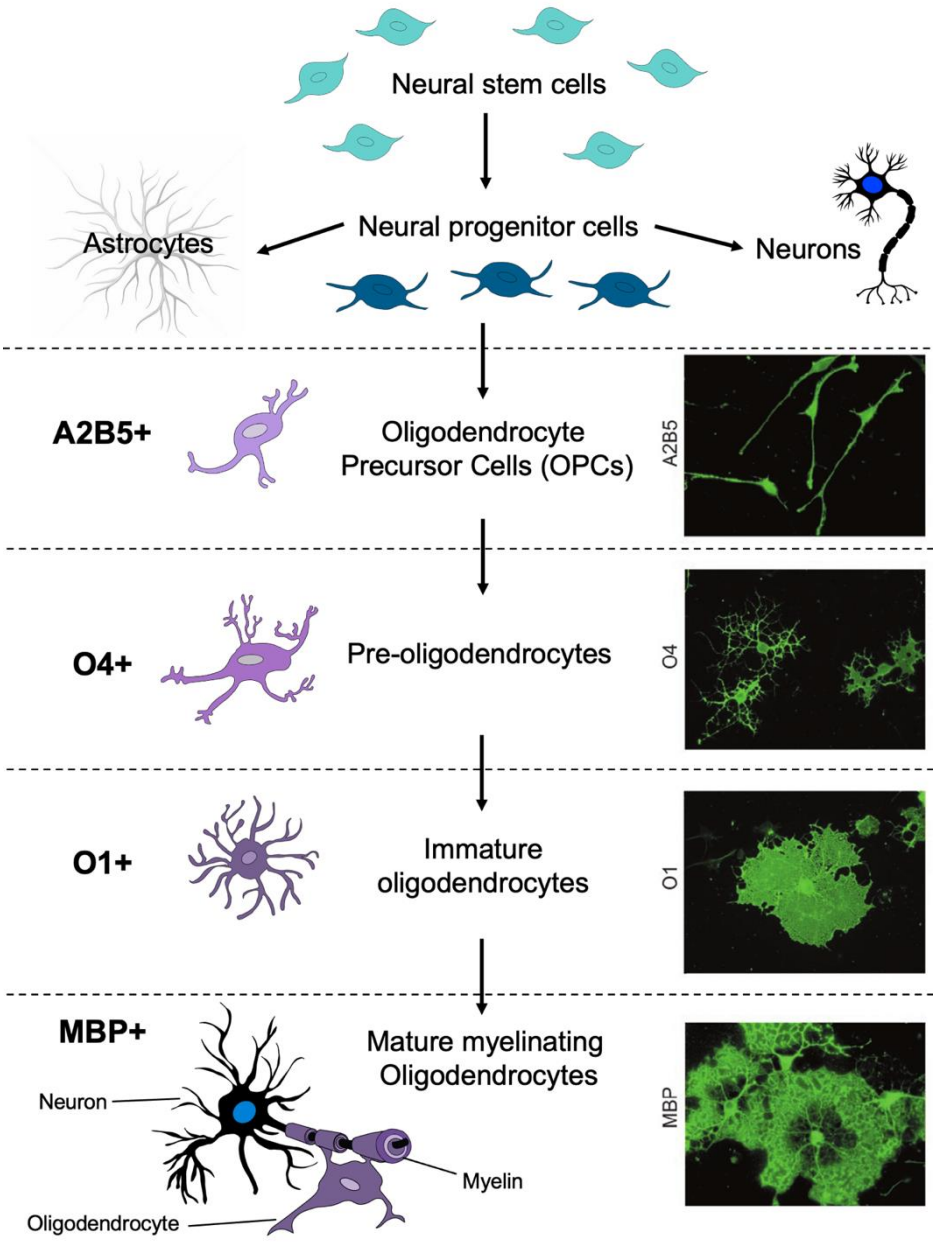

Figure 4. *Lineage progression of neural stem cells into astrocytes, neurons, and oligodendrocytes. Oligodendrocyte differentiation is marked by the expression of particular proteins (eg. O4, O1, MBP), used to identify the relative abundance of different cell types. Right panel shows cells of oligodendrocyte lineage in cell culture. Oligodendrocyte precursors were isolated from rat forebrain. The immunolabelling highlights the lineage-dependent expression of antigens (A2B5, O4, O1 and MBP). Adapted with permission from Wang et al., 2022*

It is hypothesised that a series of extrinsic factors, including axon-dependent trophic factors, are required to trigger a switch, converting immature oligodendrocytes to a myelinating phenotype. There is no apparent contact between immature oligodendrocytes and axons before the onset of myelinogenesis. Once contact is made between these cell types at the start of the third trimester (~30 GW), O1+ cells develop cellular processes and wrap around axons (Figure 4). They also start to display more mature biochemistry, producing myelin-associated markers such as MBP and transitioning into mature oligodendrocytes. This phase is referred to as pre-myelination, and it has a significant effect on diffusion MR signal (Counsell et al., 2002, Dudink et al., 2007, 2010, Wilson et al, 2021, 2023). The ensheathment of axons reduces the free diffusion of water molecules, leading to a quantifiable difference in diffusion MR image contrast in the fetal brain. The final stage in oligodendrocyte lineage progression is the differentiation into mature oligodendrocytes, which express MBP and proteolipid protein (Figure 4). Mature oligodendrocytes become the dominant population postnatally and are the cellular substrates of mature myelin.

The different phases in this lineage progression are key to understanding the mechanisms of white matter injury in premature infants (Volpe 2001). A series of studies in sheep, pigs and rodents suggested that immature oligodendrocytes are vulnerable to damage from hypoxic insult, whereas the mature oligodendrocytes are resistant (Rees 1997, Yue 1997, Ikeda 1998, Uehara 1999). In preterm sheep, the pattern of white matter injury was determined by the topographic distribution of the immature oligodendrocytes within ischemic areas (Volpe 2018). This concept also extends to the specific vulnerabilities of different white matter tracts. Acute diseases in early postnatal life, can preferentially affect fast myelinating tracts. On the other

hand, disease processes that extend over longer periods are more likely to affect the white matter pathways which have a protracted process of myelination.

The vulnerability of differentiating oligodendrocytes to excitotoxicity is thought to be due to the overexpression of AMPA and NMDA receptors in the preoligodendrocytes of cerebral white matter. The high permeability of these receptors to calcium means that during ischemia, the activation of these receptors can lead to excessive cytosolic accumulation of calcium, disrupting cellular processes and triggering cell death.

1.5.2 Myelin

Myelin is a concentrically laminated, proteolipid structure that wraps around, or 'ensheaths', axons to increase their conduction velocity, enhancing the speed of action potential propagation (Figure 5a). Myelin in the central nervous system is generated by oligodendrocytes, and myelin in the peripheral nervous system is made by Schwann cells.

The low capacitance and highly conductive nature of myelin is due to several features of its structure. The lipid-rich composition of myelin segments gives the axon high transverse resistance and low electrical capacitance. Another important structural feature of myelin are the nodes of Ranvier, gaps of approximately 1 μm between adjacent myelin membranes, where the axon is exposed to the extracellular space. At the nodes, there is a high density of voltage-gated sodium channels, together with other cell adhesion molecules and cytoskeletal proteins that are responsible for action potential generation (Poliak and Peles, 2003). The concentration of specialised molecular structure at the nodes means that transmembrane currents only occur at the nodes where the axonal membrane is exposed (Susuki 2008). The arrangement of

voltage-gated sodium channels at nodes flanked by insulating myelin sheath, causes the action potential in myelinated nerve fibers to jump from one node to the next. This mechanism is called ‘saltatory conduction’, and it facilitates the rapid propagation of electrical impulses down axons.

The composition of myelin changes throughout the lifespan and the biophysical properties of myelin underpin the major MRI contrast changes in the perinatal period. The initial proteolipid bilayer deposited around axons does not share the same biochemical composition as the mature myelin sheath of the adult brain. The pre-myelin laid down in the fetal and early postnatal brain is a transitional membrane, representing an intermediate between the oligodendrocyte cell membrane and mature compact myelin (Barkovich 2000). This earliest form of myelin generally has less MBP, and more cyclic nucleotide phosphodiesterase. As this sheath matures, the water content decreases, and the lipid and protein content increases. The mature myelin sheath is estimated to be approximately 70% lipid and 20-30% protein (Brady 1999, Morrell 1999, Van der Knaap 2005). The protein content of myelin is mostly myelin basic protein (MBP) (30%), proteolipid protein (PLP) (50%), and cyclic nucleotide phosphodiesterase (4%).

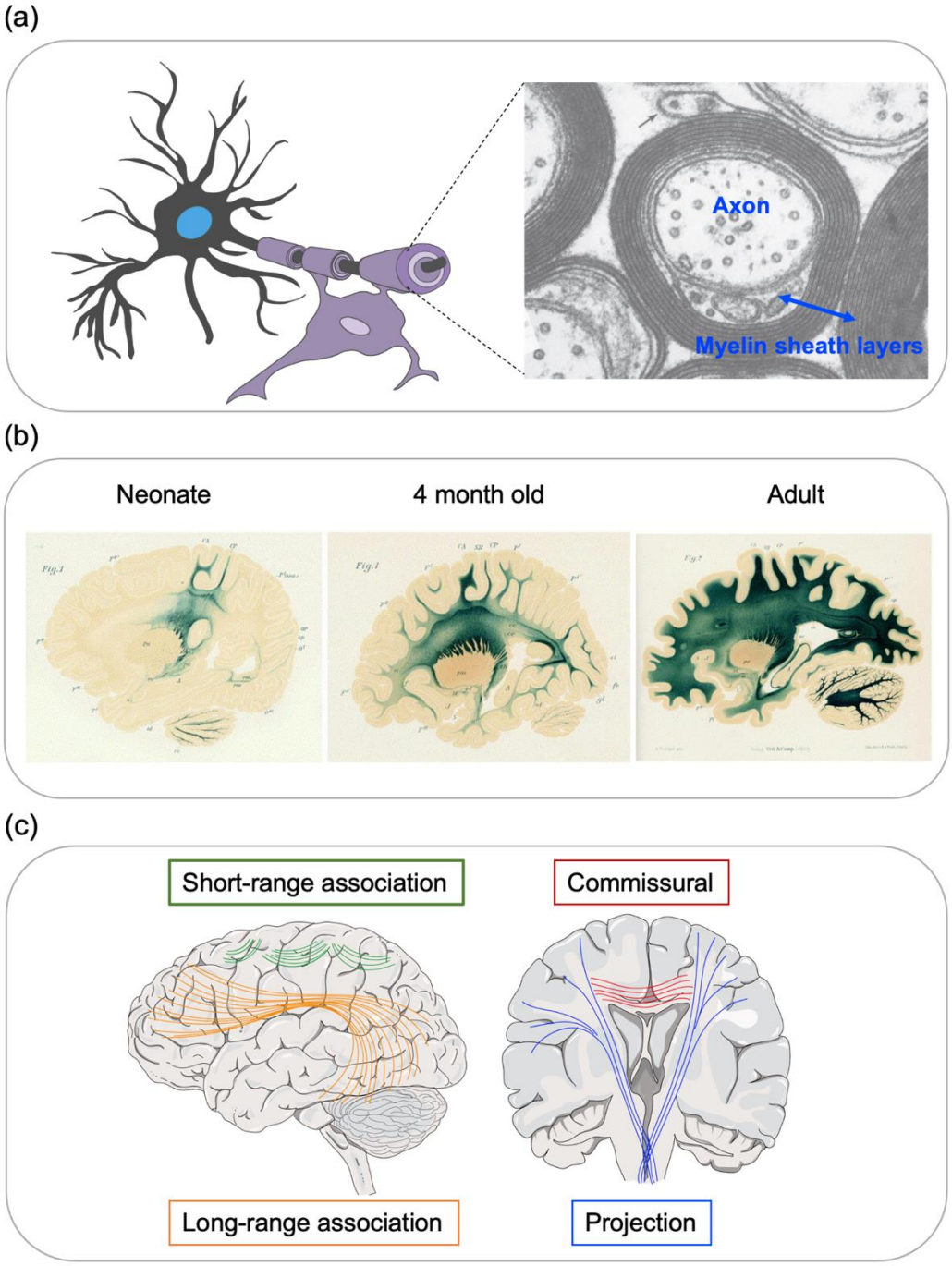

Figure 5. The structure of myelin and the developmental timeline of myelination *(a) (Left) Schematic showing a neuron and oligodendrocyte wrapping the axon in myelin. (Right) An electron micrograph showing the cross-section of an axon, ensheathed by layers of myelin. Adapted from Mackay and Laule, 2016. (b) Weigert staining to show the development of myelin sheaths. In the neonate, the spread of myelin begins in primary sensory and motor cortical areas, before spreading to other cortical areas. The later myelinating areas are frontal*

and parietal cortical areas. Adapted from Fleschig 1920. (c) Example of different types of white matter fiber bundle in the human brain, including short- and long-range association fibers, commissural and projection fibers. Adapted from asccc-oeri.org.

1.5.3 Myelination timeline

The progression of myelination at the macro-scale is closely tied to the lineage progression of oligodendrocytes at the molecular level. Although myelination begins in the fetal period, it is largely a postnatal process, peaking in the first year of postnatal life and continuing into adulthood. By two years old, the brain is almost completely myelinated, except for some small fibers that will never myelinate. Experience-dependent myelination, modulated by functional activity and environmental cues also persists into adulthood (Fields, 2008). Despite the theories and evidence to suggest that myelination is activity-dependent, no correlation has been found between myelination and functional maturation at the systems level in developing networks.

Myelination of the CNS occurs in a complex but consistent and organised spatiotemporal pattern specific to each vertebrate species (Figure 5b). The peripheral nervous system myelinates first, followed by the CNS. Within the CNS, there is a regional variation in both the time of onset and rate of myelination for different tracts, such that some are fast myelinators and others slow. The spinal cord myelinates first at 12-14 GW, followed by the brain stem, cerebellum and cortex (Barkovich, 1988, Weidenheim, 1992, Kinney 1984). Many major tracts which form in the second trimester, such as the corticospinal tract and corpus callosum, are only myelinated postnatally in the brain. There are few, isolated brain areas where mature myelin can be detected at term, mainly in the cerebellum and posterior limb of the internal capsule (Figure 5b). A seminal characterisation of perinatal myelination by Kinney and co-

workers highlighted general rules to describe the pattern of myelination in development (Brody et al., 1987, Kinney et al., 1988):

(1) Myelination of proximal pathways occurs before distal pathways

(2) Sensory before motor

(3) Projection pathways myelinate before higher level associative pathways

(4) Central cerebral sites myelinate before cerebral poles

(5) Occipital regions myelinate before frontotemporal regions

1.5.4 White matter fiber bundles

There is an important distinction to make in the fetal brain between the presence of axonal fiber bundles and their myelination. Neuroanatomical studies of the fetal period will describe the emergence of white matter, as the time when the fibers exist in the brain between their origin and termination point, however this is distinct from the time point when they become myelinated, which is mostly a postnatal process. Structural refinements to these fiber bundles, such as axonal pruning, also take place across the lifespan and are modulated by a variety of environmental factors.

White matter pathways are organized systematically throughout the brain and can be classified according to the type of brain regions they connect. There are three major classes of fiber bundle, commissural, projection and association (Figure 5c).

1. Commissural fibers.

   Cross the midline, connecting the same cortical area between left and right hemispheres (eg. corpus callosum). These pathways support functional integration (Aralasmak et al.,

2006; Catani et al., 2002), memory and executive function (Voineskos et al., 2012; Zahr et al., 2009)

2. Projection fibers.

Afferent and efferent fibers between the cortex and the deep grey nuclei, brainstem, cerebellum, and spinal cord. In this way, they carry information between the cerebrum and the rest of the body and are mainly involved in motor and sensory function. (eg. corticospinal tract, thalamic radiations)

3. Association fibers.

Connect between cortical regions within the same hemisphere. These can be subdivided into two types: long-range and short-range (U-fibers) (eg. cingulum, superior and inferior longitudinal fasciculi, uncinate fasciculus). Association fibers support cognitive processes, including executive function, language, visuospatial functions, and memory (Duffau, 2015; Friederici, 2009; Mabbott et al., 2009; Thiebaut de Schotten et al., 2012; Voineskos et al., 2012; Wendelken et al., 2015).

Immunohistochemistry and diffusion MRI work suggests that the primitive axons of all these types of fiber bundle are present in the first trimester (Huang et al., 2009; Takahashi et al., 2012; Dubois et al., 2014). Inter-hemispheric corpus callosum axons are evident around 13–14 GW (Rakic and Yakovlev, 1968; Ren et al., 2006). Immature axons of the cortico-cortical association tracts, such as the Inferior longitudinal fasciculus have been reported between 15-17 GW (Kostovic 2006; Huang 2006). Organization of the brain's wiring, and increasing coherence of the brain's fiber bundles, is thought to mostly occur during the second half of

pregnancy, but its exact temporal progression is still poorly described in humans. Overall, white matter development is a protracted process but the reason for this remains elusive.

1.6 Cortical gyrification

The human brain has a characteristic pattern of folds, made up of specifically positioned grooves (the sulci) and ridges (the gyri). Sulci are categorised as either primary, secondary, or tertiary. The primary sulci develop first and occupy specific positions across the brain, these include the major landmarks such as the central sulcus and sylvian fissure. Secondary branches then begin to form off the primary sulci, followed later by the tertiary folds. Cortical folding, or gyrification, optimizes the efficiency of brain circuitry, by bringing interconnected cortical areas closer together to minimize wiring and increase the speed of information transmission (Fernandez et al., 2016). Gyrification also allows the expansion of cortical surface area within the confined space of the skull. Most of this areal expansion occurs during early brain development, when there is extensive cellular proliferation and expansion of the neural cell population which leads to rapidly increasing brain volume (Kapellou *et al.*, 2006, Chenn and Walsh, 2002; Fernandez et al., 2016; Rakic, 2009).

The brain transitions quickly from a relatively smooth, lissencephalic structure at mid-gestation, to period of rapid gyrification, which begins at approximately 26 GW when the bulk of neuronal proliferation and migration has finished (Figure 6). Primary folds start to appear around 20 GW, the first secondary folds around 32 GW and tertiary folds around term. All major primary and secondary convolutions are present by term (39 GW), creating complex folding patterns across the surface of cortical hemispheres. The brain continues to fold postnatally, peaking in early adolescence (White *et al.*, 2010; Tamnes *et al.*, 2017). There is a relatively consistent timeline for the emergence of primary sulci between individuals, starting

in the central region, followed by the parietal, temporal and occipital lobes, then the frontal lobe (Dubois, et al. 2008).

There are also stable patterns in the position and orientation of primary sulci between individuals, and more variation is introduced at the level of secondary and tertiary sulci. This has led researchers to hypothesise that the formation of early developing primary sulcal patterns is under genetic control, although the precise mechanisms for this are not fully understood (Im and Grant, 2019). There are inter-species differences in the extent and patterns of cortical folding that have led to numerous theories about why some species have gyrencephalic brains and others do not (Thompson, 1942). One such theory is that by allowing an expanded surface area to fit into the skull, gyrification enables greater complexity in human brain function.

The mechanistic basis of cortical folding is complex and numerous theories have been proposed, however these are largely based on animal data and computational simulations. The most popular hypotheses include cranial pressure, axonal tension, and differential growth between cortical layers (Thompson, 1942; Richman *et al.*, 1975; Van Essen, 1997; Kriegstein, Noctor and Martínez-Cerdeño, 2006). Van Essen's tension-based hypothesis about cortical morphogenesis proposes that axonal and glial fibers exert a radial force on the cortex as they develop, allowing the cortex to remain thin while surface area expands and a distinctive pattern of folds forms (Van Essen, 1997). This theory accounts for strongly connected brain regions being closer together and the compaction of white matter, enhancing conduction speed and efficiency (Van Essen 1997). Van Essen expanded on this to suggest that the axonal tension in cortico-cortical fibers drives folding, pulling in the cerebral mantle (Van Essen 2020). The foundations of this theory have been challenged by numerous subsequent studies. One study conducted in the developing ferret demonstrated that the patterns of mechanical stress were not

directed across developing gyri, and therefore did not suggest a casual role for axonal tension (Xu et al 2010).

An alternative theory is the differential cortical growth hypothesis (Richmane et al., 1975, Toro et al., 2005, Tallinen et al., 2014). Tallinen et al., modelled this as an emergent property of a mechanical system where two materials with different physical properties (different cellular layers of the fetal brain) are growing at different rates, the system becomes unstable and changes shape, forming cortical folds. Most of the evidence supporting this theory is based on simulations and mechanical modelling techniques (Tallinen et al., 2016, Nie et al., 2010, Bayley et al., 2013, Budday et al 2014) as opposed to empirical evidence.

The different cellular processes that occur during the time window that cortical folding takes place would suggest that there is not one uniform mechanism to explain the formation of all cortical folds, rather there are differences in the biology underpinning the formation of primary folds compared to tertiary folds. The rapid onset of gyrification in the fetal brain is also accompanied by other developmental processes such as ingrowth of axons, neuronal differentiation, and synaptogenesis. Whether these overlapping processes influence one another remains unclear, and the final chapter of this thesis addresses the hypothesis that there is a causal relationship between microstructural change in fetal compartments and gyrification, using diffusion imaging and surface reconstructions of anatomical data.

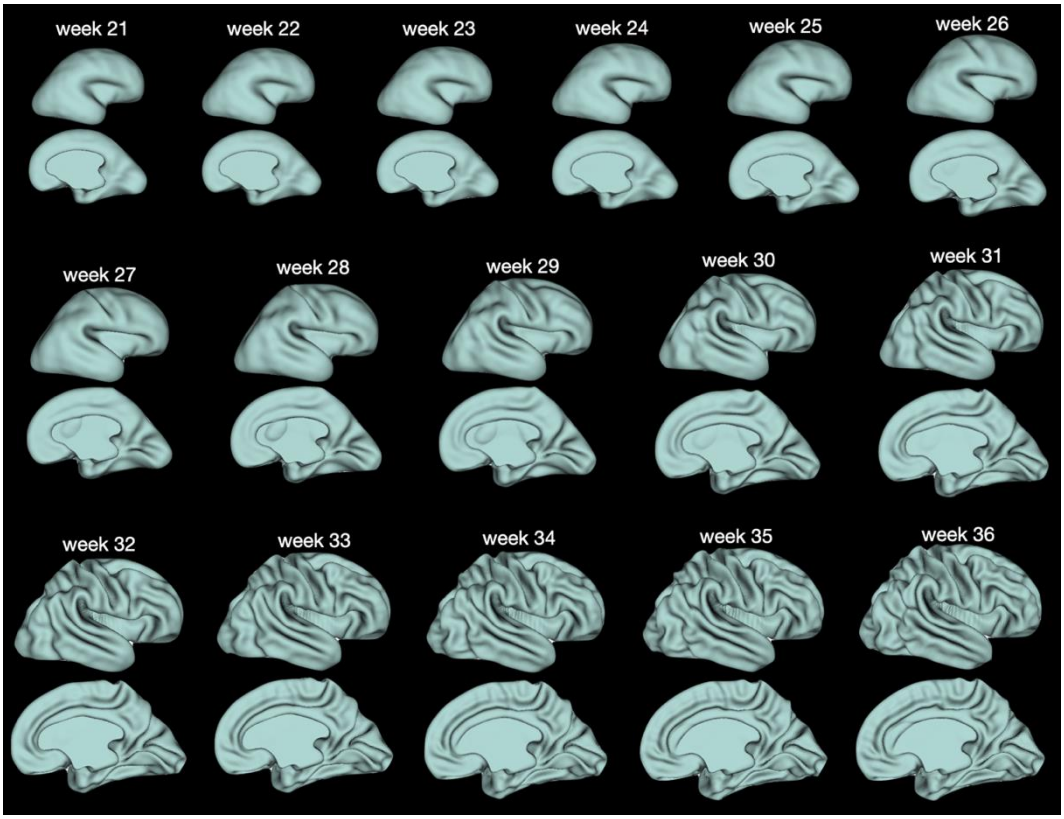

Figure 6. *Cortical folding across the second to third trimester, between 21 and 36 gestational weeks. Surface template derived from the dHCP fetal cohort, averaging among subjects within each gestational week.*

2. Methodological background

2.1 Magnetic Resonance Imaging

The phenomenon of nuclear magnetic resonance (NMR) was first discovered in 1946 (Purcell, 1946, Bloch, 1946). Over 30 years later, the first magnetic resonance images were produced when Lauterbur discovered a way to spatially encode the signal generated by NMR (Lauterbur, 1973, Hawkes et al., 1980). Since its conception, MRI has provided an invaluable clinical and diagnostic tool, for which novel applications continue to emerge, supported by technological advances. The sections below will provide an overview of the general principles of MRI as they pertain to multi-slice multi-echo spin echo sequences, one of the most popular imaging techniques for clinical purposes.

2.1.1 Basic principles of MRI

The principle of magnetic resonance is derived from the “spin” property of certain nuclei, such as the hydrogen nucleus, ^{1}H. The H nucleus induces a magnetic moment, generating a local magnetic field with north and south poles, behaving like a bar magnet. When a magnetic field is applied (B_0), the ^{1}H nucleus will either align parallel (adopting a low energy spin state) or perpendicular to the external field (adopting a high energy state). The ratio of spins, aligned vs anti aligned, follows a Boltzmann distribution, and the ratio approaches 1 as temperature increases. This "Boltzmann ratio," is determined by the population difference of nuclear spin energy levels at a given magnetic field strength and temperature. In the context of human

biology, in an MRI scanner with a 1.5T field strength, for 10 million proteins at body temperature there are approximately 7 more in the aligned state than anti-aligned.

Nuclei with spin have an angular momentum and rotate or 'precess' around the B_0 axis, a behaviour called Larmor precession. The rate of precession around the field direction is referred to as the Larmor frequency, which is proportional to the strength of an applied magnetic field. This property is exploited in MRI, by applying radio frequency pulses, perpendicular field to B_0 (B_1), and exciting the H nuclei within the magnetic field (B_0).

Obtaining an image of a human subject involves placing them in a spatially homogenous B_0 field inside a scanner, that provides uniform coverage and magnetization of the tissues of interest. When the perpendicular radiofrequency (RF) pulse is applied, the magnetic moment tilts away from B_0, as the nuclei absorb the energy of this pulse and transition between high and low energy states. Removing the RF pulse causes the nuclei to return to thermal equilibrium and realign themselves with B_0. The absorption and relaxation process emits energy, inducing an RF signal known as the free-induction-decay (FID) signal, which can be measured using a conductive field coil in an MR scanner. These properties of ^1H nuclei underpin the principle of 'nuclear magnetic resonance', each nuclei will resonate at a characteristic frequency for a given magnetic field strength, for example in a 3T scanner, ^1H nuclei resonate at a frequency of 127.7 MHz.

'Magnetic resonance imaging' involves creating an image from these signals, which requires a spatial encoding to localise their origins in three dimensions. This is facilitated by three encoding gradients, slice selection, phase encoding (PE) and frequency encoding (FE), which are applied to B_0 with linearly varying intensity, direction, and duration, thus affecting the

frequency and phase of proton precession. After this combination of different gradients is applied, the resulting phase and frequency of the signal can be used to determine the spatial information by applying a series of Fourier transforms, which convert the raw 2D 'k-space' data into a 3D reconstructed volume in 'image space'.

2.1.2 T1 and T2 weighting

Common imaging modalities for quantifying differences in brain anatomy are T_1 and T_2 weighted imaging. These two types of image contrast are dependent on the longitudinal relaxation time (T_1) and the transverse relaxation time (T_2). This relaxation time refers to the behaviour of nuclei as they return to thermal equilibrium after absorbing the energy from the RF pulse, described above. T_1 signal can therefore be manipulated by varying the time between RF pulses.

In the brain, the varying magnetic properties of different tissue types leads to image contrast between CSF, grey and white matter. There are longer T_1 relaxation times in water-rich CSF, leading to lower signal intensity and darker areas in MR images. Whereas a higher fat content quickly realigns with the B_0, and therefore T_1 relaxation is shorter in white matter, resulting in a higher signal intensity and brighter areas of the image. Grey matter regions have a signal intensity that is an intermediate between the two.

On the other hand, with T_2 weighted images, the relaxation is known as spin-spin relaxation, which takes place when there is a loss of phase coherence between ^1H nuclei in the transverse plane. ^1H nuclei in tissue with higher fat content have a shorter T_2 relaxation time, compared to water-rich tissues.

2.2 Diffusion Weighted Imaging (DWI)

2.2.1 Biological principles of DWI

Brownian motion describes the random movement of water molecules due to thermal energy. In diffusion imaging, the signal contrast is due to the difference in Brownian motion of water molecules between biological tissue types. In homogenous water-rich tissues, such as CSF, this motion is random and equally likely in all directions (isotropic) (Figure 7a). When a biological membrane is introduced, such as in the grey and white matter tissues, the diffusion of water molecules becomes more restricted (Figure 7a). Furthermore, in coherent white matter fiber bundles, diffusion is restricted more in the perpendicular direction than the parallel direction. This preferential diffusion in a specific direction is termed 'anisotropic'. The different properties of water molecules in the intra and extracellular space around these biological tissues forms the basis of contrast in DWI volumes. This imaging technique has high clinical utility, and DWI sequences were initially developed for imaging acute cerebral ischemia in stroke patients, as the image contrast can highlight regions of white matter injury (Moseley et al., 1990).

2.2.2 DWI Acquisition

DWI contrast is generated from the combination of an underlying T_2-weighted reference image, and a diffusion-weighted component. To optimise the acquisition time and minimise the effect of motion, diffusion weighted volumes in the dHCP were acquired with single-shot spin-echo echo-planar imaging (EPI) (Mansfield, 1977), the most frequently used imaging

method for dMRI. However, with this faster imaging technique, there is a trade-off of lower image resolution (Cohen, 1998). This technique rapidly alternates the phase and frequency encoding gradients, allowing for large amounts of information to be encoded in the order of 100 ms, minimizing the background phase variation due to subject motion. To accelerate volume coverage along the slice direction, multi-banded RF pulses are used, acquiring multiple slices simultaneously. The number of simultaneously excited slices dictates the number of bands required in the RF pulse.

The DWI component involves the application of diffusion gradients either side of the 180 RF pulse (Stejskal and Tanner, 1965) (Figure 7b). After the first diffusion gradient is applied, the spins are phase shifted. The second diffusion gradient will rephase the protons if they are stationary and under the influence of the same spatially encoded gradient field. This basic principle underlies why different biological tissues exhibit a different contrast following the application of these gradients.

In cell dense tissues, with low extracellular matrix and restricted diffusion, water molecules are not displaced between sensitizing gradients. Therefore, the rephasing gradient cancels the phase shifts produced by the dephasing gradient, there is no net loss of the T2 signal, and the DWI signal is hyperintense. Whereas in tissues with less restricted diffusion of water molecules, the protons move around in the time window between the application of gradients. Therefore, the protons are not rephased when the second gradient is applied, leading to signal loss in the T2 and low DWI signal (Figure 7b).

Several key parameters define a diffusion acquisition sequence. The diffusion weighting of the gradient, or ‘b value’ is proportional to the square of the amplitude (G) and duration (δ), of the applied gradient, separated by time interval (Δ). This is described by the Stejskal-Tanner

equation (Stejskal and Tanner, 1965) (Figure 7c). A higher b-value is achieved by increasing the gradient amplitude, duration, and interval time between pulses.

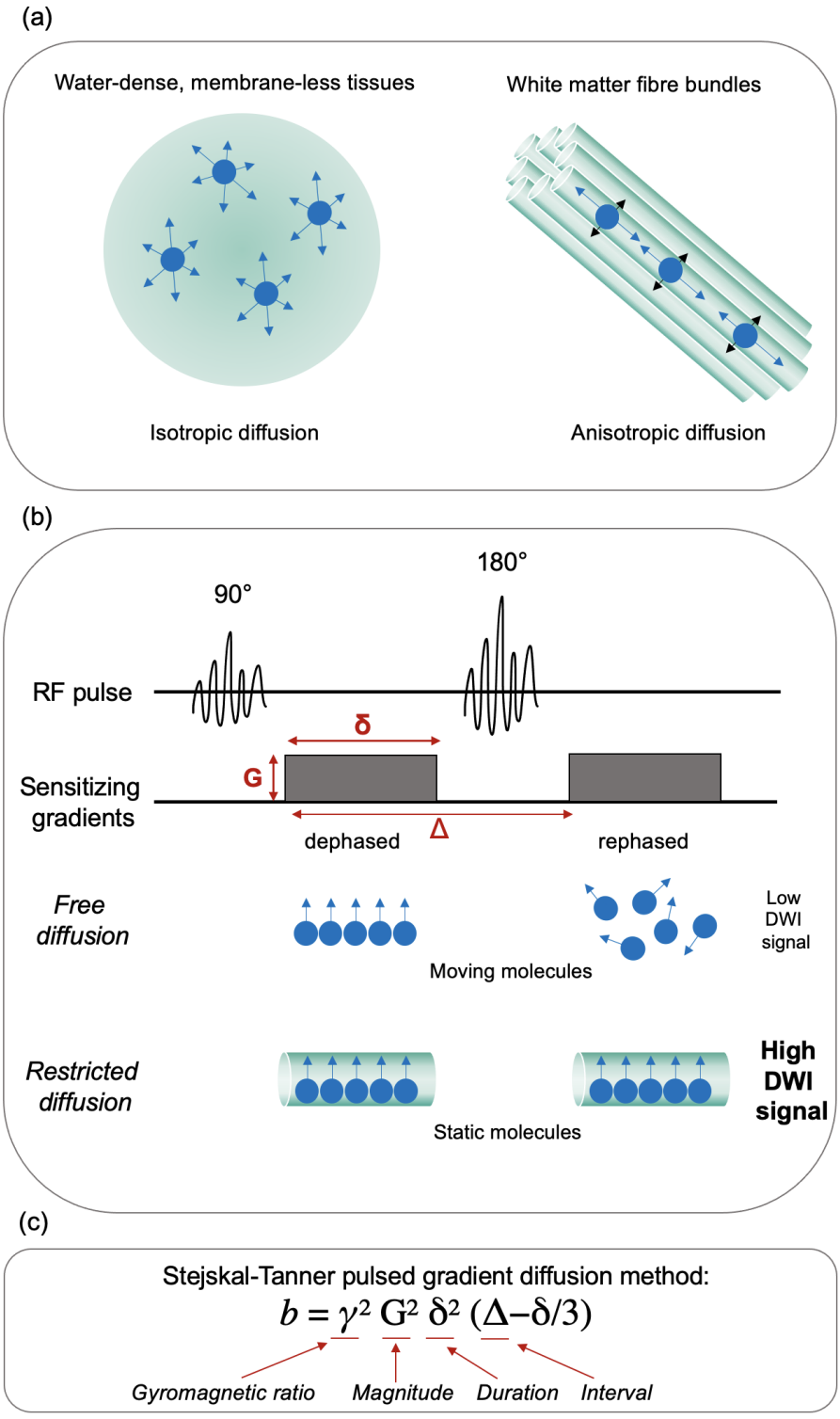

Figure 7. *Principles of DWI acquisition and contrast. (a) Diffusion of water molecules can be more or less restricted between different biological tissue types. In white matter fiber bundles, diffusion is anisotropic, and has strong directionality. In the CSF, water molecules can freely diffuse in every direction. (b) The sensitizing gradients applied either side of RF pulses will only rephase static protons that are not displaced in the interval time. This is the principle of DWI contrast. Freely diffusing molecules will move between the diffusion gradient pulses, leading to attenuated T2 signal and lower DWI signal, vice versa for protons in a diffusion-restricted environment. (c) Stejskal and Tanner equation that describes the parameters affecting the b-shell value, or the diffusion gradient strength, including gyromagnetic ratio (g) magnitude/amplitude (G), duration (d) and time interval between sensitizing gradients (D).*

Different biological tissues have unique b-value dependencies, such that the contrast between tissues changes at different b values. At higher b values, the diffusion signal is more specific to membranous tissue types with anisotropic diffusion, such as the white matter. This property is exploited by certain advanced diffusion modelling methods such as multi-shell multi-tissue constrained spherical deconvolution (described below).

The trade-off at higher b values is that there is greater suppression of the signal by stronger diffusion gradients, leading to a lower signal:noise ratio. This is particularly a limiting factor with fetal DWI acquisition because of the inherently low SNR in the abdominal environment. The sequence design process takes this into consideration and is further discussed in the General Methods section.

Diffusion gradients can also be applied in multiple different directions, to capture the displacement of water molecules in specific orientations. When more directions are acquired,

this increases the angular resolution of the data and allows the orientational properties of white matter fibers to be estimated. This technique is referred to as High Angular Resolution Diffusion Imaging (HARDI) (Berman et al., 2013). HARDI was used in the dHCP to image the neonatal and fetal brain (Hutter et al., 2017), permitting higher order models to extract directional-resolved information about developing tissue properties, or 'microstructure'.

2.2.2 Diffusion modelling

2.2.2.1 Diffusion Tensor Imaging

To interpret and quantify the signal in diffusion-weighted images, various models have been developed that deconvolve the diffusion signal. One of the most frequently used models in the neuroimaging field is diffusion tensor imaging (DTI) (Basser et al., 1994). The diffusion tensor is calculated by solving the Stejskal-Tanner equation, which describes the relationship between signal intensity before and after the diffusion sensitizing gradient is applied (Stejskal and Tanner, 1965). This produces a diffusion tensor matrix, which is a positive-definite symmetric 3x3 matrix. It has 3 perpendicular eigenvectors and 3 positive eigenvalues ($\lambda 1$, $\lambda 2$, $\lambda 3$). The principle eigenvector represents the direction of fastest diffusion, or the principle diffusion direction, i.e an estimate of the orientation of a specific white matter tract. The tensor eigenvalues represent the magnitude of the diffusion in the direction of each eigenvector, i.e the structural integrity or maturity of a tract. By applying the diffusion tensor model, it is possible to generate maps that estimate the underlying microstructure, the mean diffusivity (MD) and the fractional anisotropy (FA). MD is calculated by averaging the three eigenvalues:

$$MD = (\lambda 1+\lambda 2+\lambda 3)/3$$

FA is the normalized variance of the three eigenvalues, (where 0 = isotropic diffusion and 1 = anisotropic diffusion):

$$\mathrm{FA} = \frac{1}{\sqrt{2}} \frac{\sqrt{\left(\lambda_1 \widehat{-} \lambda\right)^2 + \left(\lambda_2 \widehat{-} \lambda\right)^2 + \left(\lambda_1 \widehat{-} \lambda\right)^2}}{\sqrt{\lambda_1^2 + \lambda_2^2 + \lambda_3^2}}$$

If a voxel contains densely packed, straight parallel fibers, such as in undamaged white matter bundles, the FA will be high and the tensor is shaped as an ellipsoid, representing a strong principal direction of diffusion. When FA is low, such as in the CSF, the tensor is represented by a sphere, conveying isotropic diffusion.

The major caveat of the tensor model is its inability to represent multiple fiber orientations within a voxel (Wiegel 2000, Alexander 2001, 2002). This is an important consideration for imaging in the early developing brain, as crossing fibers are highly abundant (Jeurissen, 2013). The tensor model in this context is confounded by the incoherent nature of immature axonal bundles, transient cellular structures, and increased partial volume effect in smaller brains. This is discussed further in the General Methods section.

Despite these caveats, DTI is still the most prevalent modelling approach both in research and in clinical practice, because of its simplicity, robustness, and fast computation.

2.2.2.2 Multi-shell multi-tissue constrained spherical deconvolution (MSMT-CSD)

Since DTI has reduced validity in regions with crossing fiber populations, researchers have refined approaches to model and interpret the DWI signal. In this thesis, and for the fetal imaging context, a suitable alternative to DTI is Multi-Shell Multi-Tissue Constrained

Spherical Deconvolution (MSMT-CSD). There is information at the higher angular frequencies which is not adequately captured with DTI, because there are more directions acquired with HARDI than are required for DTI modelling. Whereas CSD is an alternative model that can resolve multiple fiber orientations within a voxel (Tournier et al., 2004).

The assumptions of CSD are that there is no diffusion between fiber populations, and that all fibers share the same diffusion characteristics within fiber bundles, what separates them is solely their orientation. The first step is the estimation of a response function, sampling the data directly in a voxel containing a single coherent fiber population, such as the corpus callosum. This response function can be averaged using the same region of interest across a population to obtain an average response function, that approximates the diffusion profile of a colinear fiber bundle for the specific dataset.

The relationship between the diffusion signal and the response function (R) is described by equation X, where the HARDI signal (S) is effectively a weighted sum of all fiber populations (f_i), for a given b-value and azimuth relative to the fiber axis (θ). A_i is the rotation of the response function onto the direction of the fiber population (θ, ϕ).

$$S(b, \theta, \phi) = \sum_i f_i A_i(R(b, \theta))$$

The diffusion signal and the response function can be represented using spherical harmonics. Equation Y is the spherical convolution of the response function, which approximates the fiber orientation density function (ODF) $f(\theta, \phi)$.

$$S(b, \theta, \phi) = f(\theta, \phi) * R(b, \theta)$$

The coefficients of the response function form a spherical convolution matrix, which is a set of linear matrix vector multiplications relating the ODF coefficients to the signal intensities in

the DWI volume. The ODF represents the density of fibers as a function of the direction they are aligned in (θ, ϕ).

For the CSD model to be applicable for non-white matter tissue types, more than one response function is required. To manage this, a newer method, multi-shell multi-tissue CSD (MSMT-CSD) was developed, which uses multi-shell DWI to deconvolve the diffusion signal into multiple tissue types in the brain (Jeurissen et al., 2014). This model assumes that the white matter response function is anisotropic, whereas the grey matter and CSF response functions are isotropic. For this method, a minimum of two shells in addition to b = 0 are required. The response functions are estimated in each shell for each tissue type, then averaged across shells, exploiting the unique b value dependencies of the different tissue types (demonstrated in Figure 8). This produces a multi-tissue ODF and maps that convey the contributions from each tissue type to the overall diffusion signal (Figure 8). The ODFs can also be averaged across subjects. One such application of this is to create an atlas, representing the average contributions of tissue and fluid in each voxel, in each gestational week (Figure 8c) (Pietsch et al., 2019). This atlas space can be a beneficial starting point for tractography by improving the signal:noise ratio in the fetal data (Figure 8c).

In adults, specific response functions can be evaluated using the unique diffusion signal in grey matter, white matter, and CSF voxels. In the developing fetal brain, the biophysical properties of immature grey and white matter are more difficult to distinguish, therefore in this thesis the diffusion signal is decomposed with only two distinct ‘tissue’ and ‘fluid’ response functions.

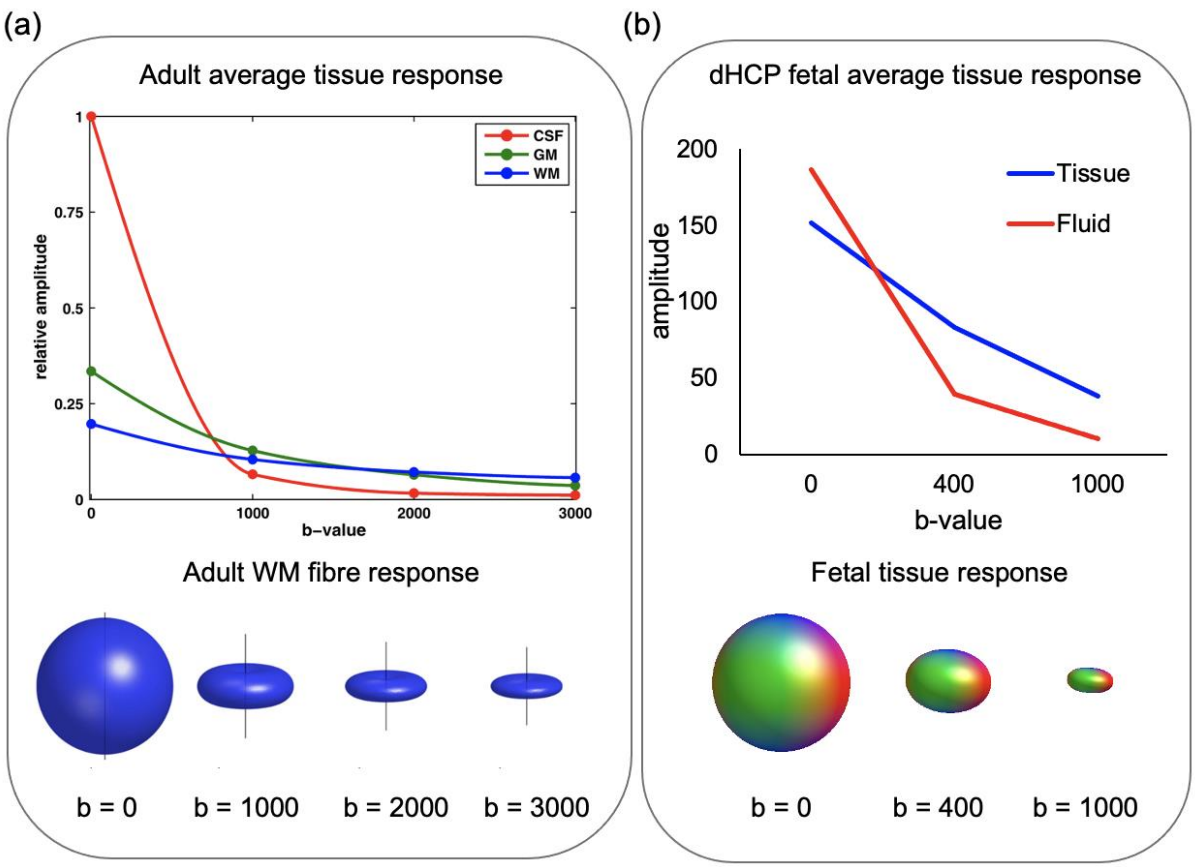
(a)
Adult average tissue response
CSF
GM
WM
relative amplitude
b–value
Adult WM fibre response
b = 0
b = 1000
b = 2000
b = 3000
(b)
dHCP fetal average tissue response
Tissue
Fluid
amplitude
b-value
Fetal tissue response
b = 0
b = 400
b = 1000

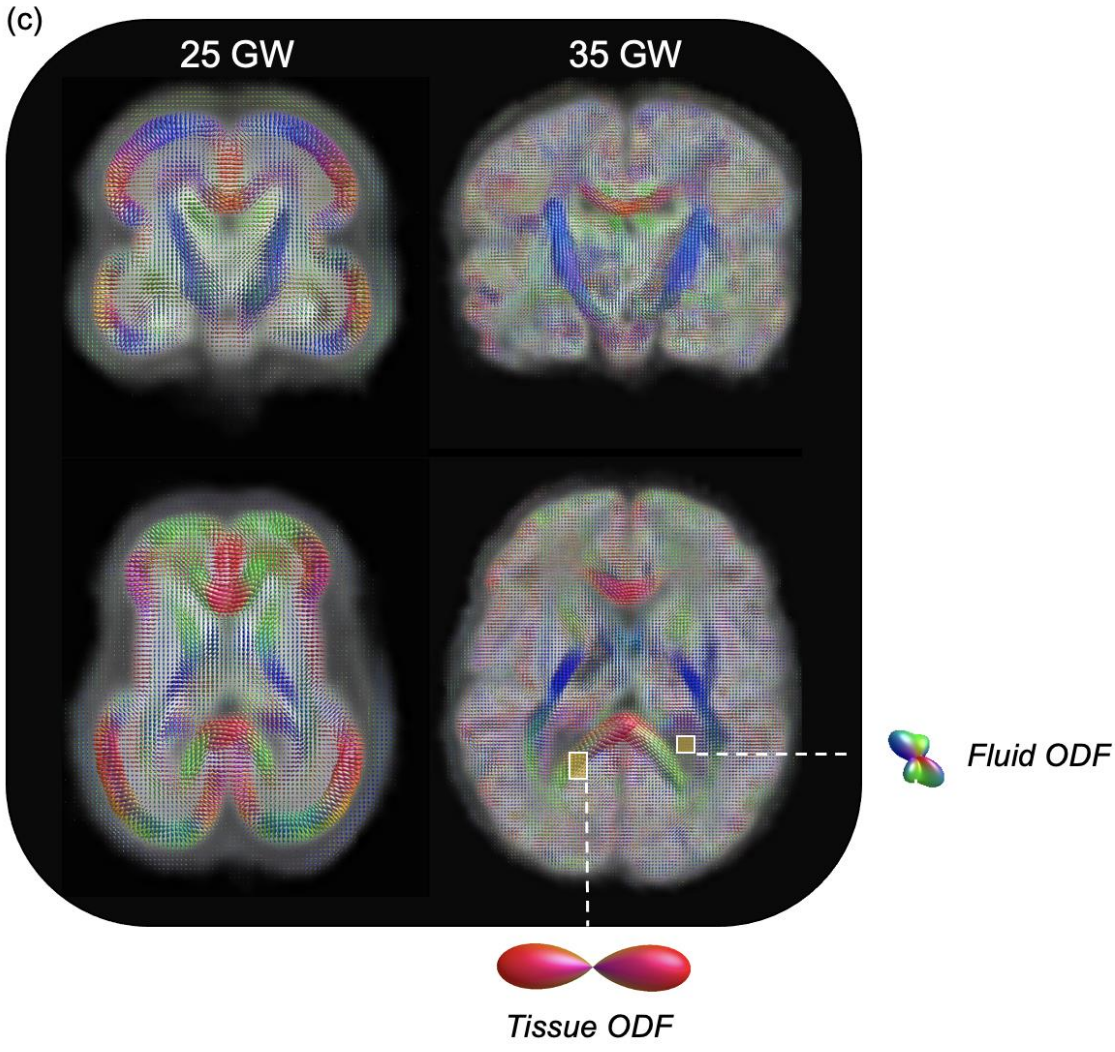
(c)
25 GW
35 GW
Fluid ODF
Tissue ODF

Figure 8. *Tissue and fluid response amplitudes at different b-shells (a) Adapted with permission from Jeurissen et al., 2014, average relative signal amplitude per tissue type as a function of b-value in the adult brain (top); average angular WM fiber responses as a function of b-value (bottom). (b) A replication of (a) using the dHCP fetal diffusion data, acquired with three b shells (0, 400,1000). It is possible to decompose the diffusion signal into tissue and fluid components using MSMT-CSD.*

3. The neuroradiology of the fetal brain

3.1 The short history of in utero MRI

The first evidence of fetal MRI in the literature came shortly after the first successful adult scans (Smith et al., 1983, 1984), where 15 mothers were scanned during the first trimester of pregnancy to test the validity of this imaging method for routine clinical use. Several years later, fetal MRI was used in conjunction with ultrasound, aiming to identify clinical abnormalities in utero (Levine, 1997, 1998, Hubbard et al., 1999). The primary motivation for the use of MRI in the perinatal window was to facilitate earlier detection and more precise classification of abnormalities during pregnancy, to improve clinical treatment planning and neurodevelopmental outcome.

As fetal image acquisition and reconstruction have become more advanced, so has the quality of fetal MR data. This increases the utility of the data for both clinical and research purposes, to address fundamental research questions about human brain development in vivo. For example, the development of single-shot rapid acquisition sequence with refocused echoes (HASTE), was a significant leap for the imaging field as it enabled much faster image acquisition times (Tsuchiya et al., 1996; Yamashita et al., 1997). Unpredictable, large amounts of fetal motion and the sensitivity of EPI methods to spatial distortions, mean that research progress and quality is closely tied to methodological advances reducing scan time and improving motion and distortion correction algorithms (Jakab et al., 2015, Fogtmann et al., 2014; Kim et al., 2010; Kurugol et al., 2017; Kuklisova-Murgasova 2012; Hutter et al., 2018; Cordero-Grande 2018; Christiaens 2019).

Despite its relatively recent introduction to the field of medical imaging and neuroscience, studies using fetal MRI modalities have cemented it as a valuable research tool, in addition to its clinical utility for abnormality detection. Structural imaging studies over the past decade have achieved cohorts large enough to be representative of a population norm, to assess age-related development in brain structure, some exceeding 150 fetuses (Andescavage 2016). Previous work has delineated timelines for cortical folding, volumetric growth of deep brain structures, and characterised transient fetal compartments (Garel et al., 2001; Kyriakopoulou et al., 2012, 2017; Glenn, 2009; Rajagopalan et al., 2011). In utero functional imaging studies have successfully measured spontaneous functional activity and demonstrated the presence of coordinated network organisation between brain regions in the second and third trimester (Turk et al., 2019; Thomason et al., 2017; Karolis et al., 2023). Applying these advanced techniques and interpreting their results requires an understanding of the underlying biology that leads to MR contrast changes.

3.2 The biophysical correlates of MR signal change over the second to third trimester

3.2.1 Investigating developing brain structure with T2-weighted imaging.

The structural changes in the fetal brain at the micro and macro level lead to profound differences in the morphology and MR signal over the second to third trimester (Figure 9). The brain-wide age-related changes are easily visualised in structural and DWI contrasts, observable both at the individual subject level and in atlases that average the MR signal for each gestational week (Figure 9).

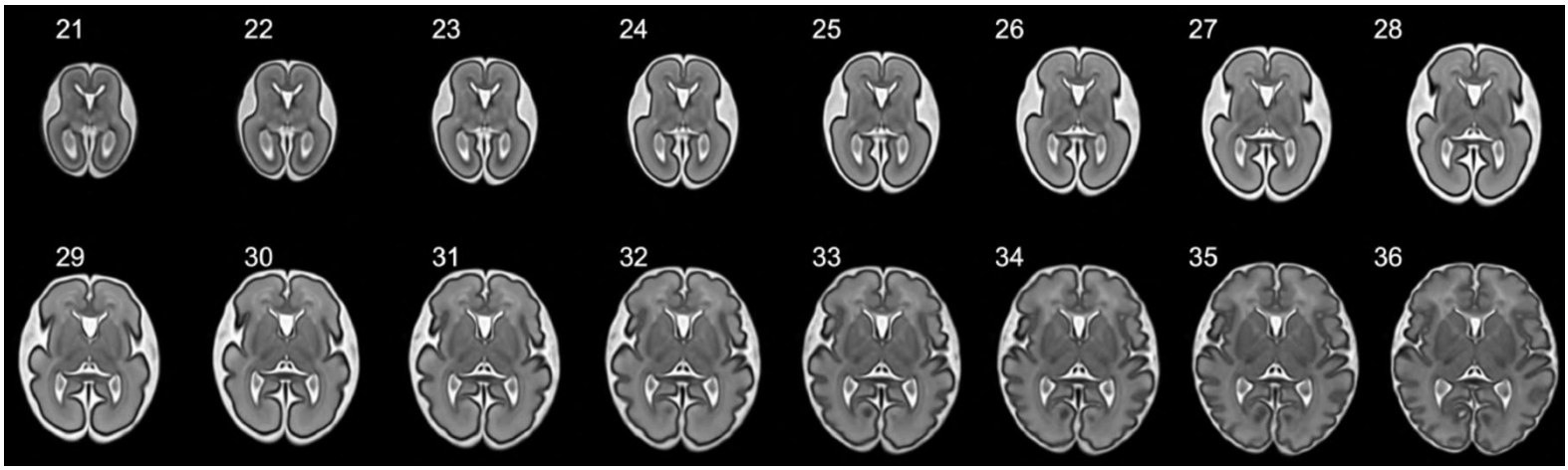

Figure 9. *T2w atlas of fetal development using the dHCP cohort between 21 and 36 GW, with permission from A.U (https://doi.gin.g-node.org/10.12751/g-node.ysgsy1/)*

There are major maturational changes in the brain that are observable on T2w imaging contrast. The proportional ratio of tissue:CSF increases with gestational age, as the ventricles decrease in size and cortical surface area grows considerably, taking up a larger proportion of the space inside skull. In the early-prenatal phase, between 21 – 25 GW, the fetal brain is characterised by a lack of structural complexity, both in terms of the smooth cortical surface and the uniform contrast within the cortical boundary (Figure 9). There is a lack of contrast between the subcortical grey and white matter, only the hypo-intense cortical plate is clearly observed. There is a broad hyperintense band beneath the cortical plate, which represents the hydrophilic subplate.

The mid-prenatal window (27-31 GW) is marked by the hyperintensity in the internal capsule and the periventricular cross-roads. The basal ganglia are more clearly visualised as contrast between the deep grey matter structures and the white matter starts to increase with age. This period is also marked by the onset of gyrification and the macrostructure of the brain noticeably

changes on a weekly basis. Sylvian fissures are easily recognized, and the surface starts to form broad gyri and shallow sulci, which then extend more deeply into the white matter. The late prenatal period (32 GW – term) is characterised by more rapid gyrification, and development of major primary sulci such that they are all present at term. At this point the brain more closely resembles the structural features of the adult cerebral cortex, and contrast between tissue types increases as pre-myelination commences.

3.2.2 T2w-derived metrics

MRI's increasing popularity as a research tool, has been accompanied by the development of metrics to quantify aspects of neurodevelopment. Manipulating and quantifying MR signal in more advanced ways has led to more complex interpretations of signal change. This allows researchers to link imaging data more robustly to the underlying biology, and research in this field becomes less observational and more mechanistic.

A commonly used, simple metric to describe the fetal brain is volume. Volumetric analysis is conducted to describe the change in size and morphology of brain regions, including deep grey matter structures, white matter bundles and overall brain volume. Brain volumes are a popular and simple approach to describe brain growth. They are routinely used in clinical practice, as traditional ultrasound methods are reliant on volumetric growth charts to identify abnormal development during pregnancy.

Structural imaging studies over the past decade have used image segmentation techniques to delineate different brain regions from the imaging contrast and quantified normative age-related development in brain structure (Andescavage 2016). Previous work has delineated

timelines for cortical folding, volumetric growth of deep brain structures, and characterised the size and relative abundance of transient fetal compartments (Garel et al., 2001; Kyriakopoulou et al., 2012,2017; Glenn, 2009; Rajagopalan et al., 2011). Measuring volumetric change is also essential to the diagnosis and understanding of perinatal abnormalities such as ventriculomegaly, characterised by enlarged ventricular volume (Kyriakopoulou et al., 2014).

The reconstruction of surfaces from segmented T2w volumes allows the characterisation of macrostructural features, using metrics that describe the development of the cerebral cortex and surface mantle. These metrics include gyrification index, mean curvature, sulcal depth, cortical thickness, and surface area. Together they provide valuable information about whole-brain growth, in healthy development and to characterise abnormalities over the second to third trimester. The patterns of sulcal emergence, timing and individual variability have been described (Im and Grant 2019; Yun 2020) and have implications for understanding folding abnormalities, such as the delayed gyrification in infants with congenital heart disease (Kelly et al., 2017).

3.2.3 DWI signal in transient fetal compartments

Complementary to the T2w contrast, the structural development of the brain can also be characterised using DWI. There are drastic differences in microstructural properties of the developing tissues, that can be quantified using different models (discussed previously in Section 2.2.2). This is robustly illustrated with an ODF atlas, which represents the magnitude and directionality of the diffusion. It can provide a visual tool to compare early, mid and late fetal neurodevelopment (Figure 8).

The two-compartment decomposition takes average response functions of white matter, using a corpus callosum mask in the oldest fetal subjects, for a region with strongly aligned, uniform, high fiber density and CSF, taking the average response function in the ventricles (Figure 8a). The diffusion signal is then deconvolved (MSMT-CSD), relative to the response functions of these distinct compartments and normalised across all subjects. With DWI atlases, representing the average ODF in each voxel, the different biophysical properties of each transient compartment of the fetal brain are clearly visualised, and the developing white matter bundles emerge with strong tissue-like signal prior to myelination (Figure 8a).

The relative abundance of subplate, intermediate zone and ventricular zones is apparent from the ODF estimation of the diffusion signal, which can be visually segmented according to the polar plot characteristics that are congruent with the Nissl stain, labelling neuronal tissue in histological sections of the brain (Figure 10). The cortical plate is characterised by strong radial alignment of cells in the early and mid-prenatal period, which is represented by the strong tissue-like signal in the ODF atlas and a dark purple Nissl stain. The lamination of the cortical plate in the late prenatal window, together with dendritic branching and more mature neuronal morphology reduces the anisotropic diffusion and the microstructure is less preferentially aligned in a specific direction, this is visible in the changing ODF feature of the cortical plate (Figure 10). The transient compartments are distinct in early and mid-prenatal ODF representations (Figure 10b, c), but the microstructural maturity is more uniform by the late prenatal phase (Figure 10d). As described in Section 1.4, the disappearance of the hydrophilic subplate, which appears as a more fluid-like signal, is apparent between mid and late prenatal window (Figure 10c,d), as subplate neurons become incorporated into the subcortical white matter as interstitial neurons.

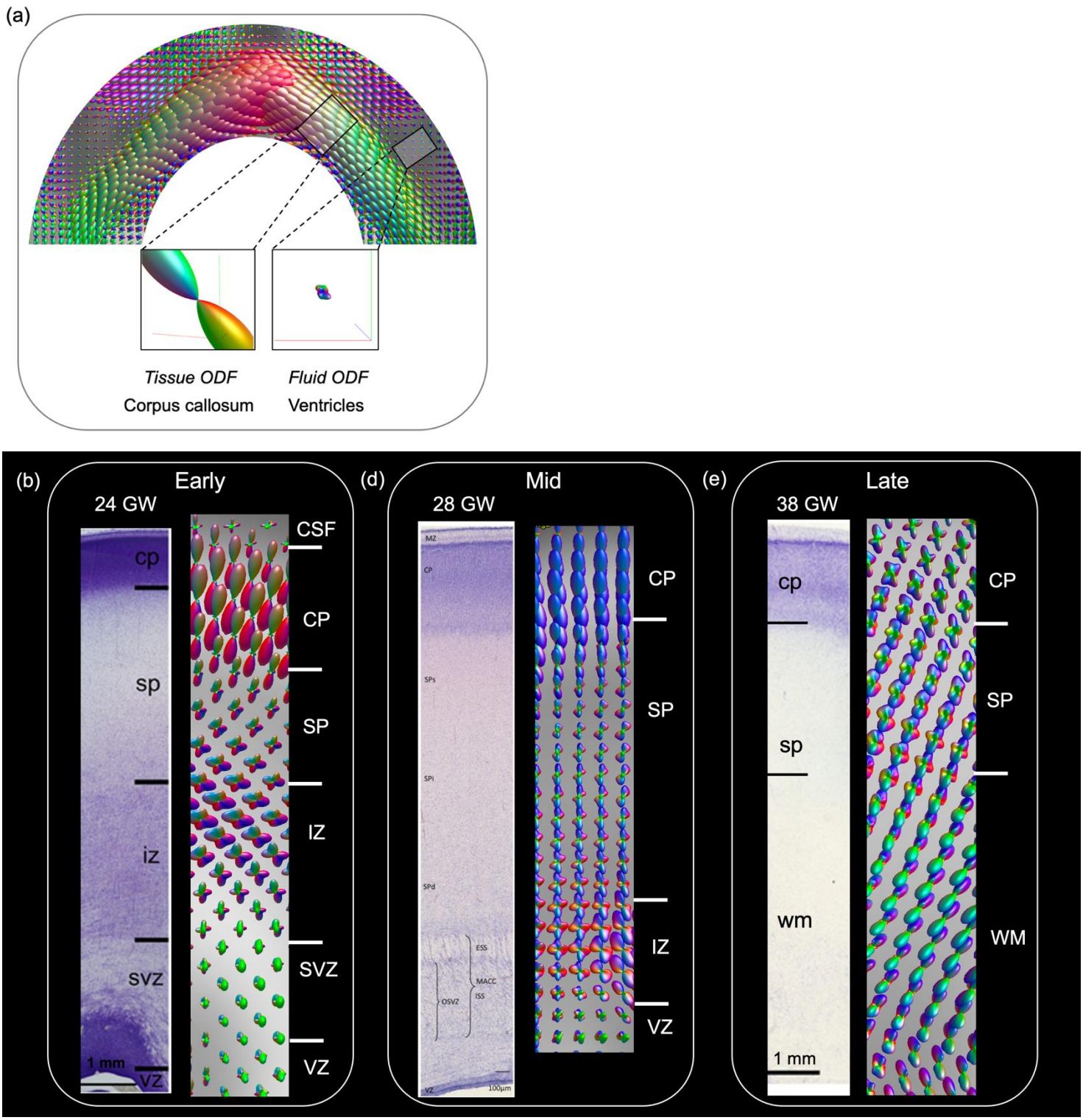

Figure 10. Histology vs. ODF atlas representation of transient compartments (a) *Close-up axial view of the corpus callosum and ventricles in 36 GW ODF atlas, highlighting the ODFs in the regions used to derive response functions. Strong uniform alignment of white matter fibers in the corpus callosum, where the tissue fraction is modelled. Fluid fraction is the*

reciprocal and is based on the response function in the fluid-filled ventricles. ***(b)(c)(d)*** *Nissl stain histological sections vs. coronal section ODF atlas of fetal brain development, derived from weekly averaging of the ODFs using the dHCP cohort. (a) (b) and (c) represent the early, mid and late prenatal developmental stages. The changing characteristics of the ODF between fetal layers match up with histology denoted boundaries. (b) The prominence of the subplate is visible in both nissl stains and the ODF, where three sublaminas can be distinguished within the subplate: superficial SP (SPs), intermediate subplate (SPi) and deep subplate (SPd). Zones are labelled as follows, cp, cortical plate; sp, subplate zone; iz, intermediate zone; svz, subventricular zone; vz, ventricular zone. (a) and (c) Histology sections adapted with permission from Judas et al., 2013, (b) adapted from Kostovic, 2020.*

3.3 State of the field: in utero diffusion imaging

Compared to other fields in neuroscience, fetal diffusion imaging is a novel approach and there are very few sites in the world that have the technical expertise and equipment to acquire this data, resulting in a narrow range of published literature. Diffusion imaging is generally the modality of choice for exploring white matter development, as the MR contrast is related to the directed movement of water in brain tissue. In the fetal brain, many of the cellular processes underpinning white matter development occur over the second to third trimester and this leads to dynamic and complex diffusion signal changes across time. Disentangling and summarising these signal changes is challenging and has led to mixed and inconsistent results describing white matter maturation. There is also a lack of generalizability in previous studies which have included fetuses with brain abnormalities or ex utero preterm infants, and are therefore not representative of typical in utero development in the second to third trimester (Maas et al., 2004, Huppi 1998, McKinstry et al., 2002).

It is relevant to the work presented in this thesis to highlight the limitations of previous studies published using diffusion imaging, to emphasise the uniqueness of the dHCP and how it represents a giant leap in the fetal neuroimaging field.

3.3.1 Constraints and limitations of previous in utero DWI studies

1. Data quality

Acquiring diffusion imaging of a moving fetus that is of high enough quality for research use is extremely challenging. Previously published studies, including atlases of diffusion maps, are confounded by low signal:noise ratio and large amounts of spatial distortion. The barriers to acquiring and reconstructing high quality fetal MR images are more comprehensively described in the subsequent general methods section. The dHCP motion and distortion correction algorithms have tackled these problems and designed pipelines that specifically address fetal imaging artefacts, significantly improving data quality for advanced imaging analysis.

2. Cohort size

The expertise and funding requirements to setup in utero imaging limit the number of sites worldwide capable of carrying out these studies. Recruiting pregnant women is also challenging, due to general safety concerns about MRI scans and time constraints with other prenatal appointments. In addition, due to the high signal attenuation with abdominal imaging, there is a low success rate of scanning fetal cohorts. A large proportion (up to

50%) of imaging data is excluded from the analysis due to artefacts, motion, and poor imaging quality. Overall, this has restricted the fetal imaging studies to relatively small cohort sizes in the past, making it difficult to explore developmental trajectories across age and account for heterogeneity within a population.

3. Using clinical populations and premature infants

With smaller cohort sizes, previous studies have not had stringent exclusion criteria for radiological and clinical abnormalities, including these cases in the analysis cohort. Similarly, cohorts of infants born prematurely have been used in the past to describe the neurobiology of the second to third trimester (McKinstry et al., 2002; Dubois 2008, 2015). However, it is well established that prematurity is associated with various alterations in brain structure and function (Dimitrova et al., 2020; Ball et al 2012, 2014, 2015), confounding the results presented by these studies.

4. Single shell, low-angular resolution acquisition

The acquisition sequences used to acquire fetal diffusion imaging in the past have often been restricted to a single b shell, or a limited number of angles in which the diffusion gradients are applied. With single-shell data, researchers are limited to more simple modelling approaches and by extension, simpler interpretation of the diffusion signal. Previous work has used diffusion modelling techniques that are applied to adult datasets, eg. DTI, which are less well-suited to characterising the unique physiology and dynamic signal changes in the fetal brain. The multi-shell DWI acquisition sequence used by the dHCP was designed using a data-driven approach to capture as much information content

as possible in the fetal brain, it includes an optimised number of b shells, gradient strengths and directions specific to the fetal context, described further in the General Methods Section 4.3.2 (Christiaens et al., 2019a,b, Tournier et al., 2019). This advanced multi-shell acquisition improves the angular resolution and permits the use of multi-shell multi-tissue model (MSMT-CSD) to describe the complex signal changes more comprehensively over the second to third trimester.

5. Inconsistency and lack of reproducibility

The lack of reproducibility between neuroimaging studies is largely due to data harmonization issues between MR scanners at different sites, using different acquisition and pre-processing pipelines on the data (Kelly 2022). Within the last two decades in the fetal imaging field, there has been a lack of consensus about trajectories in diffusion-derived metrics across the second to third trimester, and a variety of different trends have been reported between cohorts. This inconsistency is likely due to a combination of all the aforementioned issues and challenges associated with in utero imaging.

To characterise white matter development, typical analysis pipelines involve estimation of fiber pathways with tractography and then calculating an average diffusion tensor metric across an entire tract. Some found weak linear correlations between diffusion tensor metrics and gestational age (Bui 2006, Kasprian 2008, Khan 2019, Jaimes 2020). Others fitted a 2^{nd} or 3^{rd} order polynomial to describe the relationship (Schneider et al. 2007, Zanin et al 2011). Some found no trend at all (Mitter 2015, Jakab 2017). All these studies were conducted with small cohort sizes, of less than 50 fetal subjects, with low angular resolution imaging, making it difficult to resolve the many crossing fiber bundles in the fetal brain.

Previous work in adults has demonstrated that DTI measurements are highly site-specific and inconsistent (Fortin et al., 2017), and this effect is likely to be heightened by the noisier nature of fetal MR signal.

II. General Methods

4. The Developing Human Connectome Project

4.1 Overview

The Developing Human Connectome Project (dHCP) is a collaborative, interdisciplinary project between Kings College London, the University of Oxford and Imperial College London. The dHCP aims to acquire high quality, open-access, multi-modal neuroimaging data to characterise the structural and functional development of the brain at the earliest stages of life. The multi-modal imaging data, along with genetics, sociodemographic and cognitive information, will be publicly released to the research community.

Over the course of the dHCP, specialist techniques and methods have been developed to optimise every stage of the perinatal imaging process, from the acquisition to the image segmentation. Dedicated pipelines that account for the unique biophysical properties of the fetal and neonatal brain facilitate higher quality analysis and research output, describing normal and abnormal neurodevelopment with levels of accuracy and precision that were previously unobtainable. In addition to the data itself, these bespoke pipelines for image reconstruction, processing and analysis are freely available online to encourage reproducibility.

The following section will outline information about the dHCP fetal cohort, beginning with sociodemographic characteristics and followed by technical summaries about each step in the pipeline to prepare the data. This section will describe how the data is processed from the scanner and prepared for use in advanced imaging analysis.

4.2 Cohort sociodemographic information

The dHCP fetal cohort were recruited and scanned in St Thomas Hospital, London. Pregnant women between 21-37 weeks GA that consented to the study and were healthy enough to participate were included. Most fetal subjects were also followed up at birth, and information on sex, birth weight and gestational age at birth was collected (Figure 11). The sex ratio was 1.15 male: female, and birth weight and gestational age at birth were normally distributed. The total number of fetal datasets acquired is 307, however at each stage of the reconstruction and analysis pipeline subjects were excluded due to missing imaging modalities, registration failures and uncorrected residual motion/distortion (see Section 5.5 Quality Control). The subset of the cohort used in each results chapter required specific exclusion criteria, which are outlined in the corresponding methods sections.

One of the fundamental aims of the dHCP was to create a normative reference to understand early development. To achieve this requires a diverse sociodemographic cohort. The ethnicity and socioeconomic data collected suggests that the sample is broadly representative of the diversity in London (Figure 11). Index of multiple deprivation (IMD), an approach to quantify the relative deprivation of an area, was calculated using online lookup tool (https://www.fscbiodiversity.uk/imd/) (Figure 12). IMD is a cumulative score, based on weighted indices that are broadly indicative of socioeconomic status, it includes data on

income, employment, education, skills and training, health and disability, barriers to housing and services, as well as crime rate. Higher IMD values indicate higher deprivation.

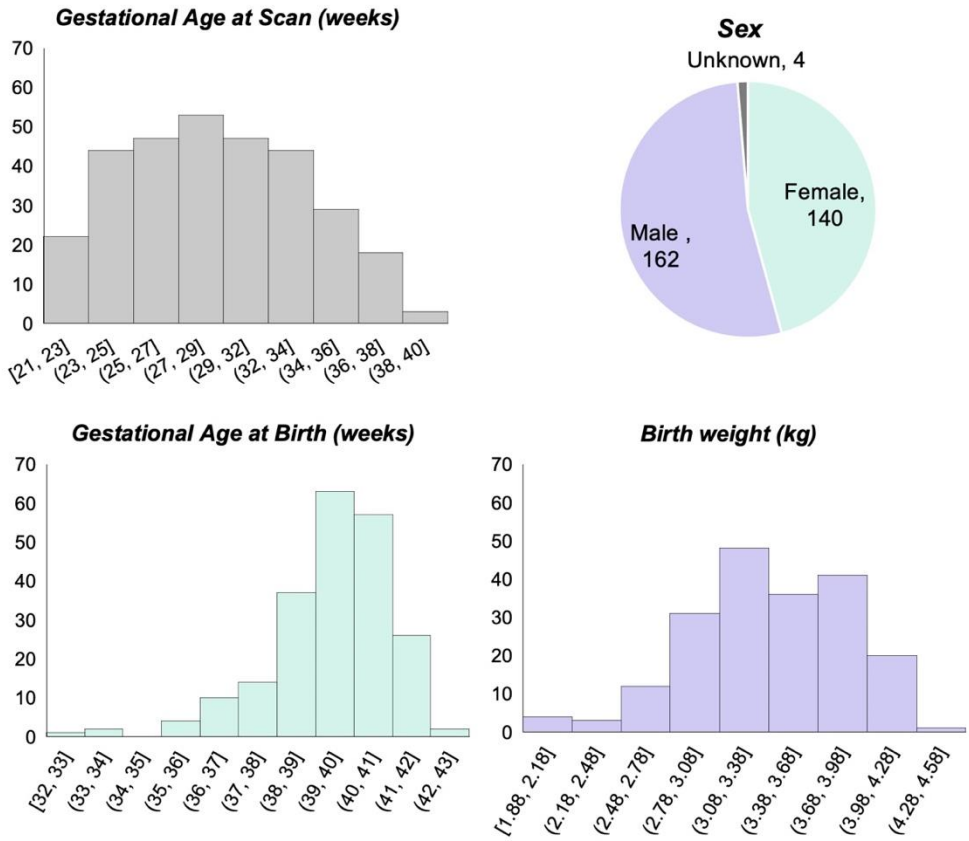

Figure 11. *Perinatal information about the dHCP fetal cohort, including gestational age at scan, gestational age at birth, birth weight and sex.*

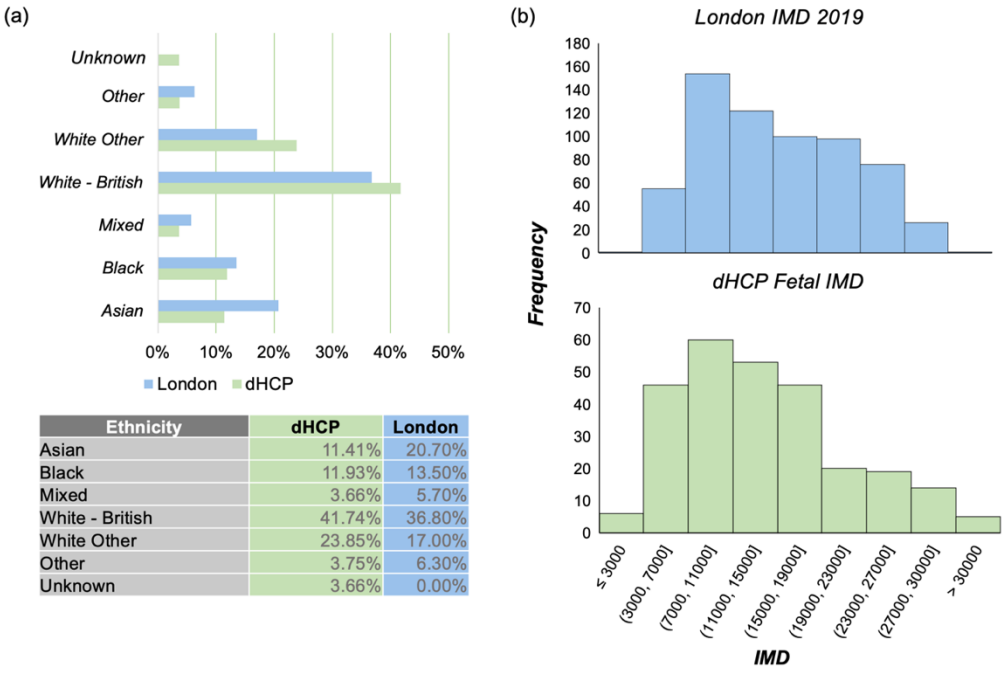

Ethnicity	dHCP	London
Asian	11.41%	20.70%
Black	11.93%	13.50%
Mixed	3.66%	5.70%
White - British	41.74%	36.80%
White Other	23.85%	17.00%
Other	3.75%	6.30%
Unknown	3.66%	0.00%

Figure 12. Ethnic and IMD distribution a) *Comparison between dHCP cohort (green) and London (blue) percentage and distribution of ethnicities.* ***b)*** *Index of multiple deprivation distribution between London and dHCP fetal cohort*

4.3 Acquisition, reconstruction, and pre-processing pipelines

4.3.1 T2w acquisition and image reconstruction

Adaptations were made to the current mainstay acquisition protocols to specifically accommodate the fetal context, focussing on improving SNR and to minimise the effect of motion. Images were acquired on a Philips Achieva 3T system with a 32-channel cardiac coil. The dHCP fetal acquisition protocol is described in full by Price et al., 2019, and included T1w and fMRI. For the scope of this thesis, only the T2w and DWI acquisition will be described.

Briefly, T2w volumes were acquired with a single shot turbo spin echo (ssTSE) sequence with TE=250ms, TR=2265ms, acquisition resolution 1.1x1.1x2.2mm (-1.1mm gap), from 6 stacks (Price et al., 2019). The 'single- shot' refers to the use of a single excitation slice-selective pulse prior to a series of spin echoes, which minimises intra-scan T2 motion artefacts, providing strong contrast between tissue and fluid in the intermittent periods of quiescent fetal motion (Gholipour et al., 2015).

All datasets were reconstructed by L.C.G to 0.5x0.5x0.5mm resolution using a custom-built, fully automated slice-to-volume reconstruction pipeline (Cordero-Grande et al. 2019, ISMRM). The pipeline uses stacks of 2D single-shot slices and a deep learning network to localise the brain in each slice. A global search is done (x,y and z dimensions) and a rigid transform is applied to realign any mismatched boundaries (Figure 13a). Despite the fetal data having inconsistent slices and high amounts of motion, there was an extremely high success

rate when this approach was piloted on preliminary data (129/133 cases successfully reconstructed) (Figure 13 b,c).

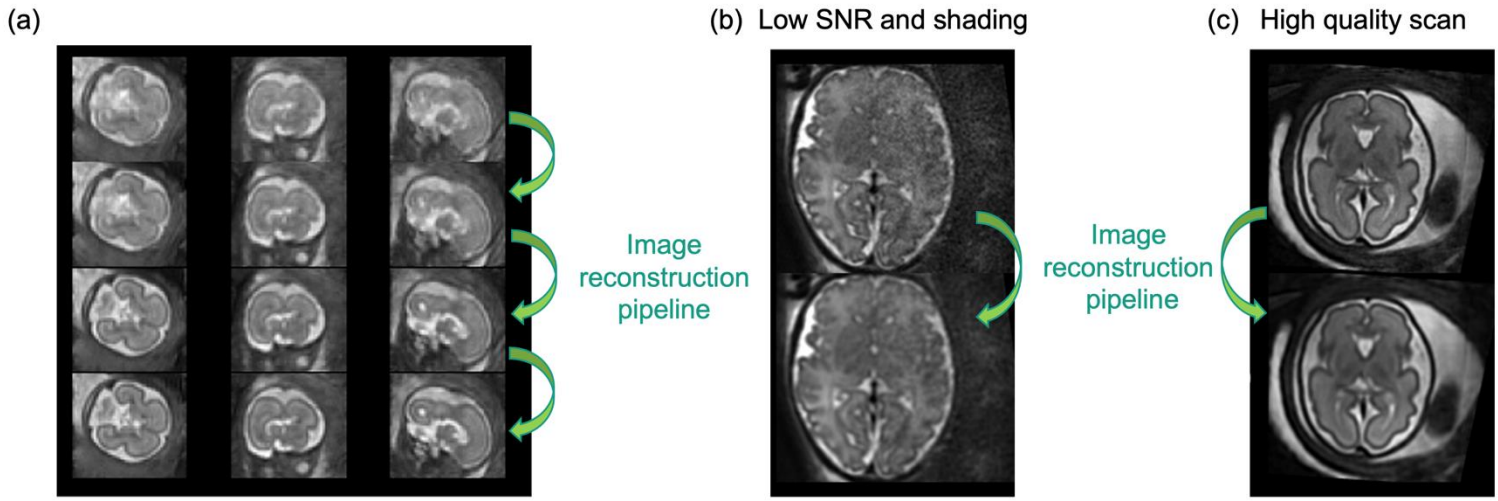

Figure 13. *Image reconstruction pipeline (a) Different stages of alignment showing the progression of images through the reconstruction pipeline. (b) Example of a case with low SNR and shading, before and after image reconstruction (c) High quality case example reconstruction. Adapted with permission from L.C.G*

Imaging analysis has the potential to be confounded by the presence of non-uniform signal intensity variations across the field of view, which are not anatomically significant. This is referred to as a bias field, and there are several approaches that have been developed to correct it. For the fetal data, the reconstructed T2w volumes were intensity normalised and run through N4 bias field correction (Tustison et al., 2010), similar to the pipeline used for the dHCP neonatal data (Schuh et al., 2018).

To extract the brain from surrounding erroneous tissues, a convolutional neural network (CNN) model, U-Net (Ronneberger, Fischer and Brox, 2015) was used, trained on manually edited individual brain masks (by A.U). Extracted-brains were then segmented using a fetal-optimised version of the Developing brain Region Annotation With Expectation-Maximization (Draw-

EM) module of the Medical Image Registration ToolKit (MIRTK) (https://biomedia.doc.ic.ac.uk/software/mirtk/) (Makropoulos et al., 2018). Cortex, white matter, and CSF probability maps were extracted, together with labels for the ventricles and deep grey matter structures (Figure 14). These segmentations were used to facilitate image registration and other data analysis steps, such as anatomically constrained tractography (see Results Chapter 2).

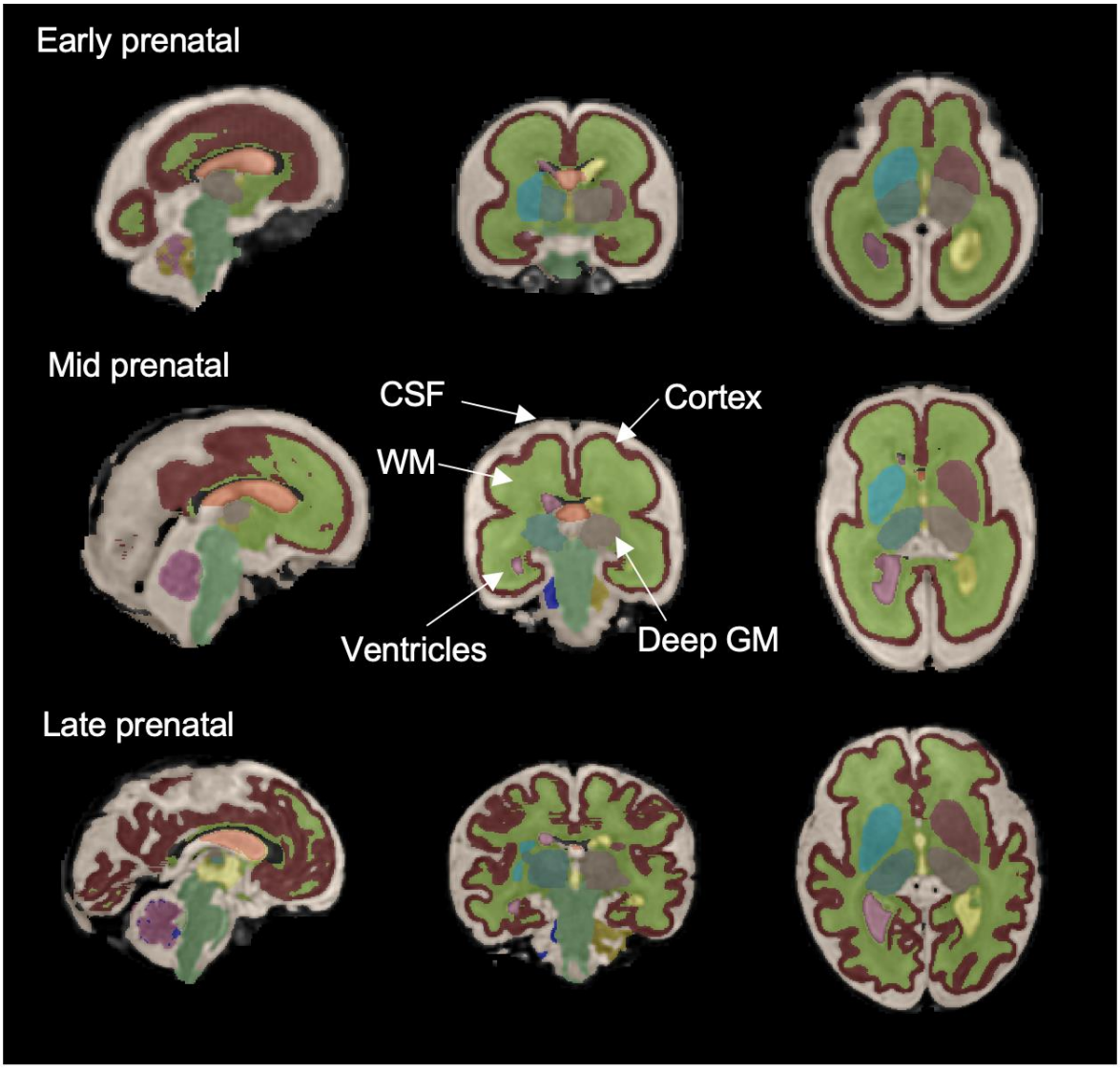

Figure 14. *Examples of the Draw-EM image segmentation tool in exemplary subjects in the early, mid and late prenatal phase of development.*

4.3.2 Diffusion Weighted Imaging

In utero DWI was acquired with a combined spin- and field-echo (SAFE) sequence, TE=76ms, TR=5810ms and 2.0x2.0x2.0mm acquisition resolution, with three diffusion gradients (15 b=0 s/mm^2, 46 b=400 s/mm^2 and 80 b=1000 s/mm^2). Each of these sequence parameters were decided on after being tested and optimised specifically for fetal imaging (see HARDI section below).

4.3.2.1 Spin- and Field-Echo (SAFE) sequence

Instead of acquiring all slices in each volume with a single diffusion weighting, the dHCP acquisition sequence interleaves slices with low and high b-values within each stack (Hutter et al., 2018). This method addresses challenges of motion and distortion in fetal imaging. Firstly, by allowing a higher sampling rate of low b-value slices, this improves the robustness of motion correction. Secondly, slice-level encoding enables dynamic estimation of b0 field maps, to account for the non-uniform field inhomogeneities between slices in fetal MRI. This dynamic estimation of the b0 field map facilitates dynamic distortion correction on a slice-by-slice basis (Cordero-Grande 2018).

4.3.2.2 High Angular Resolution Diffusion-Weighted Imaging (HARDI)

Hardware of MRI scanners has been updated and improved in recent years which allows the acquisition of multi-shell diffusion data. It is possible to apply diffusion gradients in multiple directions, at different strengths, or b-shell values. The dHCP fetal cohort were acquired with 15 b=0 s/mm^2, 46 b=400 s/mm^2 and 80 b=1000 s/mm^2. To choose the b-shell parameters for this acquisition, a data-driven approach was used (Tournier et al., 2015). This optimisation method was also used for the dHCP neonatal data release, and is comprehensively described in

Tournier et al., 2015. Briefly, this framework estimates the information content from mean images of the raw diffusion MRI signal at different b-shells. It then uses a singular value decomposition to examine the diffusion signal in terms of response functions for different tissue types in each of the b-shells, calculating the effect sizes for each observed component in the decomposition. Using this information, it identifies the set of acquisition parameters (number of shells, b-shell values, number of directions per shell) that provide optimal sensitivity to the different components of the diffusion signal (Tournier et al., 2015).

The trade-off at higher b values is that there is greater suppression of the signal by stronger diffusion gradients, leading to a lower signal:noise ratio. In the fetal brain, at higher b-shell values there is very little signal, due to a combination of higher noise and relatively immature microstructure in early neurodevelopment. This lead to the decision to not acquire anything higher than b = 1000.

4.3.3 Image reconstruction, distortion, and motion correction

Diffusion volumes were reconstructed to 2.0mm resolution using an automated pipeline, implemented with MRtrix3 (Tournier et al., 2019). The steps in this pipeline include Generalized Singular Value Shrinkage (GSVS), Marcenko-Pastur Principal Component Analysis (MP-PCA) image denoising and Rician bias correction (Veraart 2016), followed by data-driven dynamic distortion correction. Images were undistorted on a shot-by-shot basis, using single slice estimations of the b0 field maps (Hutter et al., 2018, Cordero-Grande 2018). Intensity inhomogeneities were then corrected with the ANTs N4 bias field correction algorithm (Tustison et al., 2010). The bias field was estimated from the mean b = 0 image, then applied to the rest of the image series.

DWI volumes were then run through a slice-to-volume motion correction algorithm, based on a multi-shell spherical harmonics and radial decomposition (SHARD) representation of the diffusion signal (Deprez et al., 2020, Christiaens et al. 2021). SHARD tackles the problem of large motion between slices, that need to be aligned within and across diffusion-weighted contrasts. SHARD is based on algorithms that represent multi-shell dMRI data as a linear combination of orthogonal components, to estimate the unknown motion traces in a set of slices and reconstruct the motion-corrected signal in scattered slices both within and across shells.

This method was originally tested in dHCP neonatal data, then subsequently trialled with the fetal data. This reconstruction framework was successful in most of the fetal cohort, even in severely motion-corrupted subjects (Figure 15). SHARD was able to recover slice-level motion and successfully corrects slice dropouts in fetal and neonatal data. The distortion and motion correction steps were performed by L.C.G and D.C.

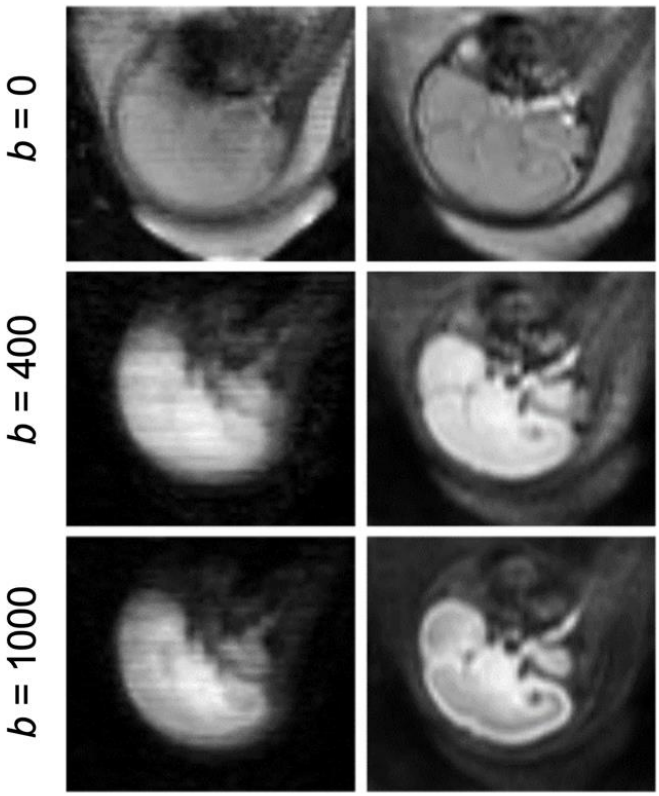

Figure 15. *Example in utero images pre and post SHARD correction at different b-shells (b = 0, b = 400, b = 1000). Adapted with permission from D.C.*

4.4 Image registration

All the analysis techniques described in this thesis required alignment between imaging modalities for each subject (eg. T2 and DWI), and for some methods described in this thesis, it was necessary to align all subjects to a common space, in the same coordinate system. I optimised image registration methods for the fetal context, in order to accurately map between subject and template space across gestational ages. The unique macro and microstructural features of the fetal brain at different gestational ages lead to series of age-dependent errors. For example, with increasing structural detail in the cortex, there was substantial blurring in cortical areas in older subjects. However, in younger subjects, the higher proportion of fluid in the abdomen lead to more motion, and rotation of the fetus, therefore the registration quality in youngest subjects was often compromised by this. Therefore, the resulting pipeline to

transform between modalities and subjects in this cohort was a compromise between factors to ensure a uniform approach could be used across all subjects. However, image registration in the fetal data remains imperfect compared to the quality in neonatal and adult transformations.

Reconstructed fetal volumes were often rotated out-of-plane in the x, y and z directions. The global search function in FLIRT was able to correct this for most subjects, but including a CNN step further increased the success rate overall in the cohort.

The mean b1000 shell has the highest contrast at the boundary between the cortex and the subplate (Figure 15), which is useful for boundary-based registration (BBR). BBR uses the segmented white-matter boundaries of the T2 data to drive the alignment at the grey/white matter boundary. It spatially transforms a mesh of the DWI volume until its vertices align with the maximal intensity gradient across white and grey matter in the T2. BBR is especially effective in the fetal brain as it is robust to spatial intensity inhomogeneities (eg. due to partial voluming) in the diffusion data because it calculates tissue intensity gradients in the anatomical image.

For the diffusion and T2 registration to template space, a framework was decided on that delivers the most reliable results for the fetal dataset and is described below:

1. Reorientation of T2 to a standard plane used a dedicated transformer convolutional neural network (CNN) (Wright et al., 2018).
2. Alignment of DWI to T2 volumes within-subject used the mean b1000 shell (calculated using MRtrix3), and FLIRT boundary-based registration (BBR) in FSL (Greve and Fischl, 2009), with six degrees of freedom, normalised mutual information cost function and a global search in the x, y and z axis to orient the fetal volumes correctly (Jenkinson and Smith, 2001; Jenkinson et al., 2002).

3. Non-linear registration between T2 and age-matched template (Uus et al., 2023), used the ANTs toolbox, two channel (T2w + cortex probability maps), Symmetric Diffeomorphic Image Registration with Cross Correlation (Avants 2008).
4. Warps were concatenated to create a single transform between native DWI and T2 atlases.

4.5 Quality control

Following initial assessment by expert fetal radiologists to check for clinical abnormalities, all reconstructed imaging volumes were assessed for the presence of residual or uncorrected artefacts. To ensure only datasets of sufficient quality are analysed, each step in the pre- and post-processing pipelines involved visual assessment and quality control.

After the diffusion data was processed with the SHARD pipeline, summary metrics for each subject were reviewed (Figure 16). These metrics quantify the gradient of motion parameters over time and the percentage of slice dropouts in the data (Christiaens et al., 2021).

Image sharpness, residual distortion, and motion artefacts were visually assessed and scored between 0 and 3, based on the mean b=0, b=400, and b=1000 images. The scoring system was as follows: 0=failure, brain outside field of view, 1=banding and large distortion, 2=blurring but no major artefacts, 3=relatively high quality.

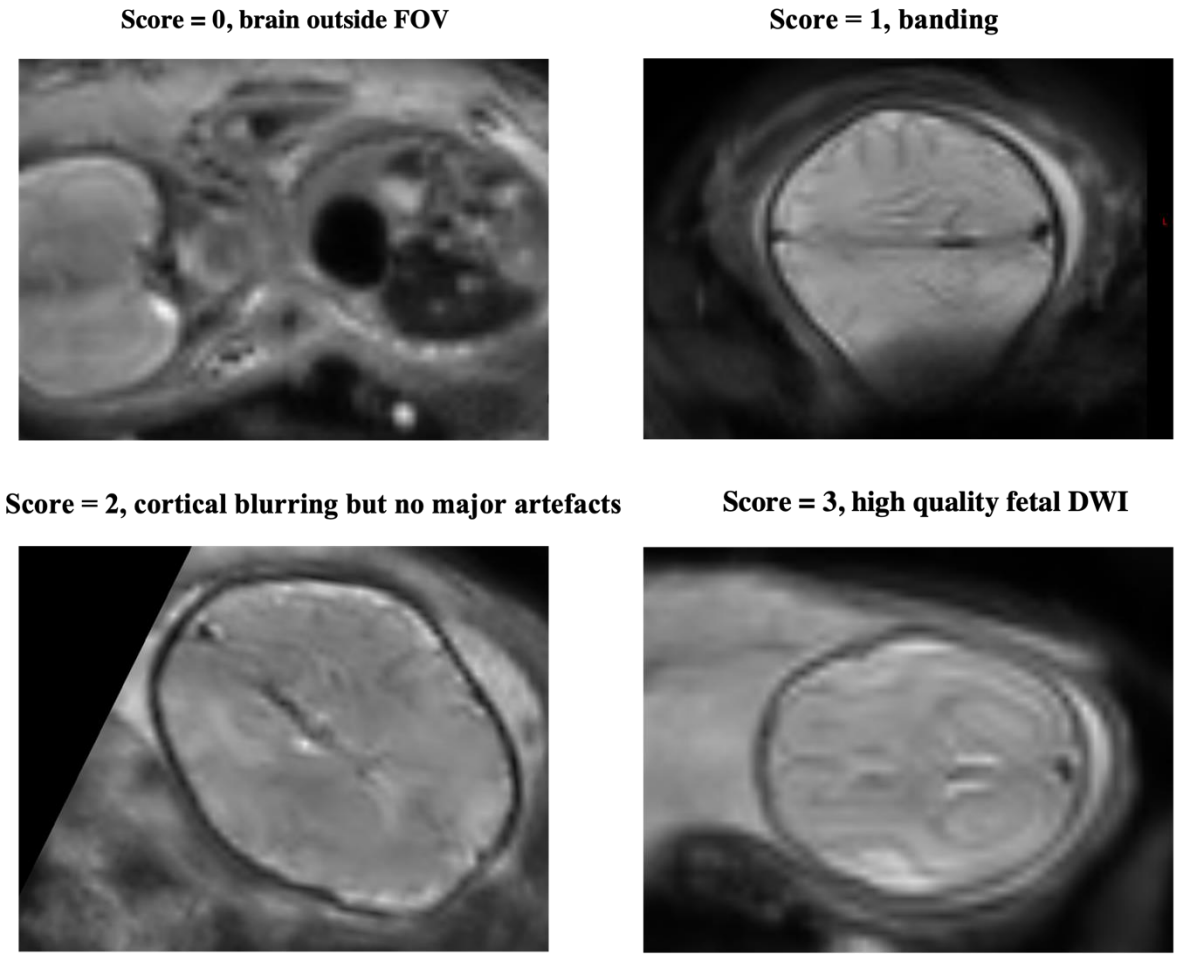

Figure 16. *Examples of QC scoring scale for subjects, between 0 and 3, with 0 = failure, (e.g. subject moved out of the field of view) to 3 = high quality.*

As an additional check to explore if the extent of motion affected our results, we correlated the indices derived from the SHARD pipeline with GA (Figure 17). There are three output parameters per subject, which are signal-to-noise ratio (SNR), rotation, and translation. SNR represents the mean b=0 signal/mean noise level, measured in the reconstruction mask using MP-PCA denoising. Rotation reflects the mean change in rotation of the subject pose between slices (degrees). Translation is the mean change in translation of the subject pose between slices (mm).

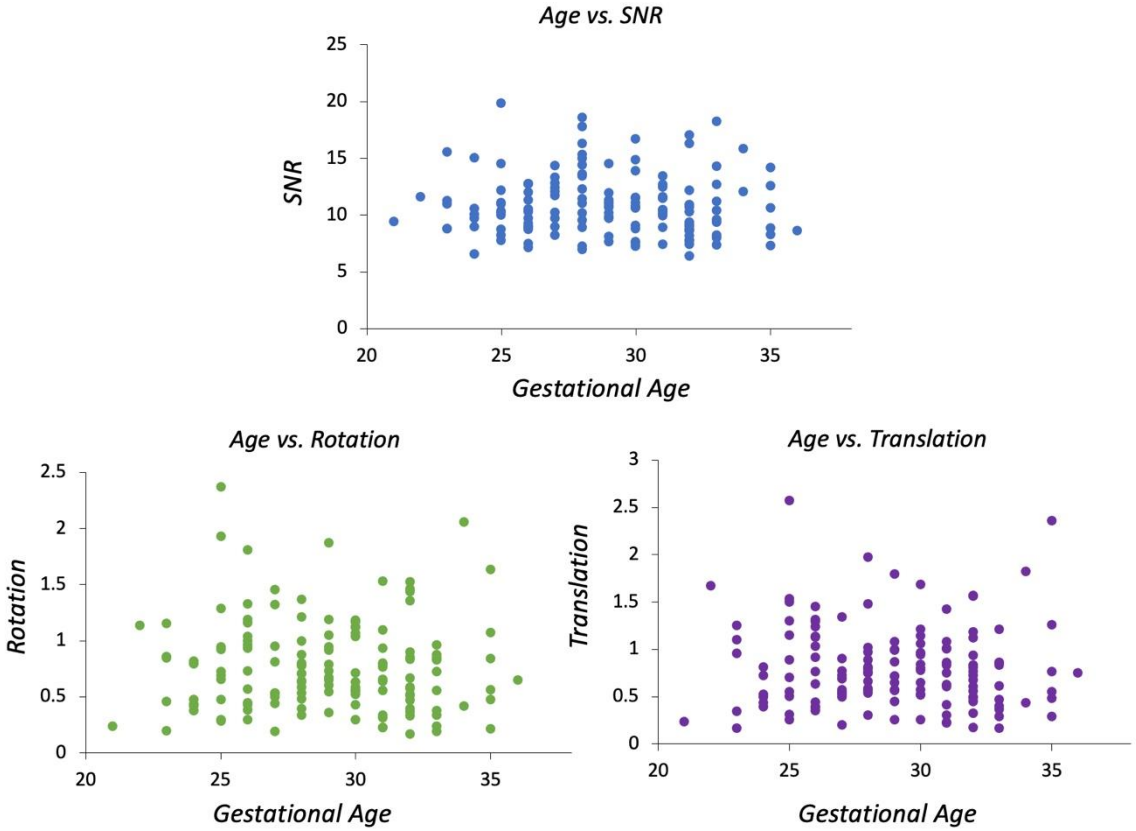

Figure 17. *Correlations between spherical harmonics and radial decomposition (SHARD)-derived indices describing subject motion and gestational age (signal-to-noise ratio (SNR), rotation and translation).*

4.6 Diffusion modelling

As described in the Methodological Background, the interpretation and quantification of diffusion MR signal requires the application of various models to deconvolve the signal. In this thesis, two different approaches to modelling the DWI signal were used, the more traditional diffusion tensor imaging (DTI) method (Basser et al., 1994) and multi-shell multi-tissue constrained spherical deconvolution (MSMT-CSD) (Jeurissen et al., 2014).

4.6.1 Diffusion Tensor Imaging (DTI)

Modelling the diffusion signal with DTI allows us to compare our findings with previous fetal MR literature, and more broadly with other MR studies. Although there is evidence to suggest it does not capture the wealth of information in the diffusion signal like other models, and cannot resolve the presence of crossing fibers, it remains the most widespread and clinically utilised model (see Background, 2.2.2.1).

The diffusion tensor was estimated by extracting the b=0 and b=1000 volumes for each subject, using the iteratively reweighted linear least squares estimator in MRtrix3 (Tournier et al., 2019). Subsequently FA/MD maps were calculated from the tensor (Basser et al., 1994) (Figure 18).

4.6.2 Multi-shell multi-tissue constrained spherical deconvolution (MSMT-CSD)

Since the creation of the tensor model, other more advanced models have been devised that exploit the information from different b-values to estimate how the restricted and unrestricted

diffusion between tissue types makes up the diffusion signal. One such model, that is better suited to modelling HARDI data, is the MSMT-CSD model (see Background, 2.2.2.2). The adult HARDI signal can be separated into CSF, white matter, and grey matter components (Jeurissen et al., 2014). However, the fetal brain has high fluid content and less contrast between tissue types, particularly in the early fetal stages (Figure 16). There is also heterogenous contrast between tissues as the microstructure matures with age. For these reasons, we adopted a two-compartment model approach, decomposing the DWI signal using two signal fingerprints or 'response functions', the CSF (fluid) and white matter (tissue), modelled off the voxels in the ventricles and the corpus callosum (see Methodological Background, Figure 8a).

For MSMT-CSD derived metrics, in each subject, white matter response functions were extracted using masks of areas with relatively mature white matter (corpus callosum) using the 'tournier' algorithm (Tournier et al., 2019; Tournier et al., 2013). CSF responses were extracted using masks of the ventricles using the 'dhollander' algorithm in MRtrix3 (Jeurissen et al., 2014; Tournier et al., 2019; Tournier et al., 2013). To obtain group-average response functions, the white matter response functions of the oldest 20 subjects were averaged (approximating relatively mature white matter), and the CSF group-average response function was calculated from the whole cohort. Using these two average response functions, the dMRI signal of all subjects was subsequently deconvolved into a tissue and fluid component, using the tournier algorithm applied via the MRtrix3 software package (Tournier et al., 2019), and resulting components were intensity normalised for each subject (Raffelt et al., 2011). The tissue and fluid component maps were normalised to 1, for ease of interpretation, then labelled and tissue and fluid 'fraction' (Figure 18).

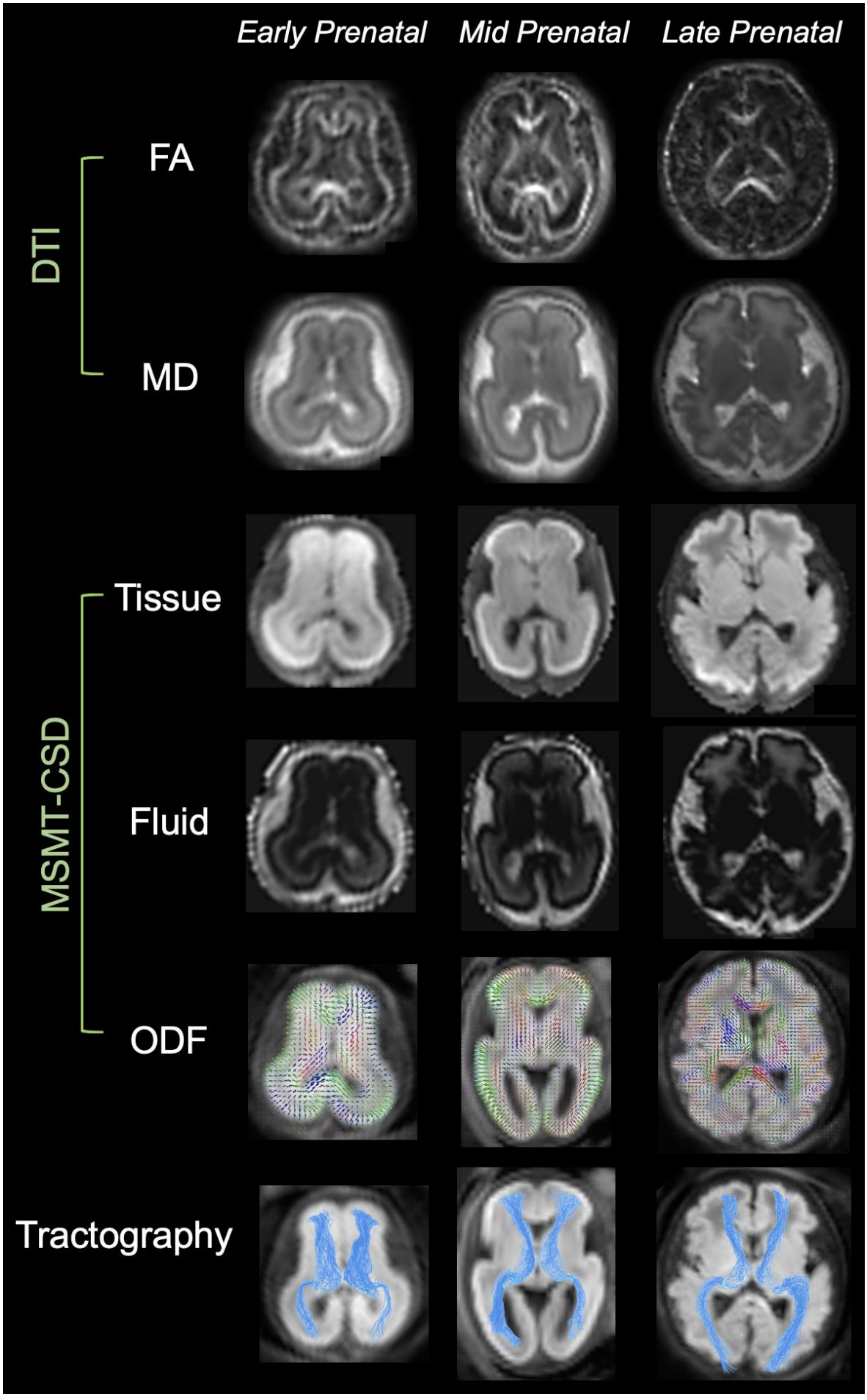
Early Prenatal
Mid Prenatal
Late Prenatal
DTI
FA
MD
MSMT-CSD
Tissue
Fluid
ODF
Tractography

Figure 18. *Individual subject maps of diffusion metrics, from the early (24 GW), mid (27 GW), and late (34 GW) prenatal stages. First two rows are derived from the diffusion tensor (DTI) model (FA, MD), subsequent rows are derived from MSMT-CSD (Tissue and fluid fraction), and ODFs. Bottom row is example of tractography at individual subject level, to estimate the optic radiation and anterior thalamic radiation.*

4.6 Tractography

After applying a model to the DWI signal to estimate the orientations and relative contributions of fiber populations within a voxel, tractography algorithms can be used to approximate and reconstruct white matter fiber bundles. For fiber tracking in the fetal brain, CSD was the most suitable model choice, implemented via MRtrix3 software (https://www.mrtrix.org/) (Tournier et al., 2019, Jeurissen et al., 2014) as it can model different ODF peaks within a value, affording tractography algorithms multiple pathways out of a voxel (Tournier et al., 2007, Jeurissen et al., 2014). In contrast, if the diffusion signal is modelled with DTI, the tractography algorithm can only follow one eigenvector in each voxel, and DTI is incapable of resolving crossing fibers. This crossing-fiber problem is a significant confound for modelling microstructure in the fetal brain, which contains incoherent axons and glial scaffolding during the early and mid fetal stages (Kostovic et al., 2012).

Tractography algorithms fall under two broad categories, deterministic and probabilistic. Deterministic tractography was one of the first algorithms to be developed (Basser et al., 2000). Streamlines are generated by following the principle eigenvector of the diffusion tensor in each voxel, in a stepwise manner between a seed and target region. One limitation of this approach

is the lack of information about the error in the tracking procedure in any given experiment (Parker 2010). The probabilistic approaches address this limitation (Parker 2004; Jones, 2008), by accounting for sources of uncertainty and calculating a confidence level or 'probability', for each streamline pathway. To estimate the fiber orientations within a given voxel, probability density functions (PDFs) are used to capture the expected distribution of potential fiber orientations. Probabilistic algorithms are therefore better equipped to cope with crossing-fibers and the natural fanning of individual fibers within a bundle.

In the fetal brain, to combat the low SNR and variability between subjects, probabilistic tractography was used on the ODF templates to generate a structural connectome to estimate fiber pathways on a weekly basis. Warps between native and template space could then be used to propagate the tracts into whichever space was required for the analysis. Using ODF templates for tractography ensured a standardised region of interest was used for subjects of the same age in subsequent microstructural analysis.

Co-registration between the T2 and diffusion atlases allowed us to propagate the accurate T2-derived tissue segmentations of the cortex, white matter, and deep grey matter to the ODF atlas. These tissue boundaries facilitated anatomically constrained tractography, which utilises the segmentations as biologically realistic priors, constraining streamline generation and aiming to overcome some of the common tractography pitfalls (Smith et al., 2012).

Whole-brain structural connectomes of 100 M streamlines were generated in each gestational week (Smith et al., 2012; Tournier et al., 2019). The connectomes were filtered down to 10 M streamlines using the SIFT algorithm (Smith et al., 2013; Tournier et al., 2019), so that the number of streamlines connecting the two regions was approximately proportional to the cross-

sectional area of the fibers connecting them (Smith et al., 2013). For specific tracts of interest, this connectome was filtered down using anatomical understanding about the origin and termination of tracts, with Draw-EM segmentations of sub-cortical grey matter and cortical regions mentioned previously. Additional manually drawn masks were used to exclude spurious streamlines that projected away from the expected path of the tract (e.g. to exclude callosal fibers from the corticospinal tract).

Tractography was never used as a quantitative method to assess tract morphology, for example, the diameter of fiber bundles. This would lead to erroneous results, as smaller fetal brains often had higher streamline connectivity in their tractograms. A clear example of this is the anterior thalamic radiation in the tractography example in Figure 15, the largest tract diameter is in the youngest subject, in the early prenatal period, which does not reflect current understanding of fetal white matter biology (Figure 18). Rather, it is more likely this result is a methodological consequence of using a fixed number of streamlines for connectome generation in all templates. It may also be due to the tractography parameters, and the use of a probabilistic algorithm. Streamlines are more likely to be created between origin and termination points when there is a smaller distance between them. Where tractography is used in this thesis, the specific parameters and precise methods are described more completely in the Results Chapters.

5. Challenges and limitations of in utero imaging

The difficulty of imaging the fetal brain can be attributed to a number of interconnected factors, this section will aim to provide a non-exhaustive summary of some of the key issues and constraints, and how the study design of the dHCP was implemented to overcome them.

Although diffusion MRI is a relatively well-established neuroimaging method, very few studies have been conducted successfully using this imaging modality in utero, due to the difficulty of acquiring high quality data. This can be attributed to dMRI being an inherently low signal:noise technique, as large gradients are applied to amplify dephasing and therefore attenuate the signal. The in utero context, within the abdomen, introduces more noise to this already sensitive technique along with a series of different artefacts. Artefacts and motion compromise the quality of imaging for both clinical and research applications, requiring dedicated post-processing algorithms to overcome.

5.1 Fetal environment and maternal habitus

The innate biology of the fetal and maternal environment introduces a series of different challenges, which both impose constraints on acquisition sequences and introduce a variety of artefacts. There is significant signal attenuation between the magnetic coil and the fetal brain due to the presence of different maternal tissues and amniotic fluid. This signal loss would be even more prominent in a mother with a high body mass index (BMI) or a large amount of

subcutaneous fat, and a thicker abdominal wall. Furthermore, magnetic field inhomogeneities exist at the boundaries between different biological tissues, such as brain and air, or brain and bone. In the abdominal imaging context, the problem is multiplied by the presence of numerous different fetal and maternal organs, such as the placenta, the maternal gut and maternal blood vessels. The large difference in magnetic susceptibility between fetal tissue and pockets of air in the maternal gut induces local static field shifts and inhomogeneities in the magnetic field, which can create artefacts in the reconstructed volume (Christiaens et al., 2021).

5.2 Motion

Diffusion imaging is highly sensitive to motion, due to the application of large gradients which amplify dephasing and introduce signal attenuation during slice-acquisition. Motion during the acquisition can also lead to misalignment between slices, inconsistent stacks and signal dropout. For a technique which is already sensitive to motion, there are compounding effects of the in-utero environment, which complicates the process of designing suitable acquisition, reconstruction and motion correction pipelines. The uncontrollable and unpredictable nature of fetal movement, as well as motion from maternal breathing can introduce phase errors, dynamically changing distortions, and mismatched slices. Overall, these issues result in a high exclusion rate for data analysis, because in some subjects the motion and distortion are too large to be fully corrected by currently available algorithms (Christiaens et al., 2019, Christiaens et al., 2021).

5.3 Safety and comfort

The rapid gradient switching in EPI leads to high acoustic noise, which needs to be reduced as much as possible to avoid any harm to the developing fetus or cause distress, as no additional hearing protections can be offered to the fetus apart from the abdominal wall. Peripheral nerve stimulation (PNS) is also a potential side effect of the rapid gradient switching, and there is greater risk in pregnant mothers with higher BMI. Sequences must be designed to minimise both of these factors, however this puts constraints on the readout bandwidth of the acquisition.

Maintaining the high safety standards for mother and developing fetus throughout scanning are imperative, but comfort is also a key consideration to encourage involvement in research and facilitate the recruitment of pregnant participants. In the late second to third trimester, it becomes more challenging to maintain the comfort of the mother for the duration of the scan. This motivates minimising the total scan time as much as possible, imposing limitations on the acquisition sequence such as the number of diffusion encodings that can be acquired.

Overall, this series of interdependent factors comprises a circular problem, which imposes many constraints and challenges for image acquisition. A series of trade-offs must be made which impact the spatial and temporal resolution, as well as the susceptibility to artefacts.

5.4 Partial voluming

The partial-volume effect occurs when there is more than one tissue type within a voxel. The signal intensity in that voxel becomes dependent on the proportions of each tissue type present. It is a confound that becomes more or less relevant as a function of imaging resolution and the biological tissues of interest. The small size of the fetal brain means that the partial volume effect is increased, as voxel dimensions are typically larger than the biological structures of

interest. Furthermore, the extent to which partial voluming effects data analysis changes across the gestational time window, as the fetal brain volume increases rapidly.

An exemplary scenario in the fetal brain is the quantification of microstructure in the cortical plate. The thickness of the cortical plate increases in the second trimester, from ~ approximately 0.5 – 2.0 mm, peaking around 28 – 31 gestational weeks depending on the region (Kostovic et al., 2014). Therefore, for much of the analysis window, the 2 mm voxel size is larger than the cortical plate itself, leading to inevitable partial-volume effects. Measures such as cortical thickness and microstructural properties in the fetal brain will always be prone to a partial volume effect, which must be given due consideration when choosing analysis approaches and in the interpretation of results.

III. Aims and hypotheses.

The literature reviewed thus far represents a summary about current understanding of neurodevelopment during the second to third trimester. Most of this knowledge is derived from research using model organisms and post-mortem tissue. To translate research findings between animal models and the human brain, so they can be impactful to modern medicine, it is necessary to use non-invasive, clinically available technology such as MRI. With MRI it is possible to capture the biology of healthy developing fetuses in vivo.

As highlighted in the previous section, very few studies have successfully imaged the fetal brain at scale, across a diverse population and produced reliable imaging data. By exploiting the dHCP's bespoke acquisition and pipelines, uniquely designed to combat the challenges of fetal imaging, using open-access data, the chapters in this thesis aim to establish a reproducible and reliable quantitative description of structural brain maturation, at the micro and macro scale. Part of this process involves investigating the available analysis approaches and optimising them for the fetal context.

The specific aims of this thesis are:

1. Delineate the developing brain's association, projection, and callosal white matter pathways. Quantify the maturational trajectories for different tracts and relate them to histological knowledge.
2. Examine the emergence of thalamocortical white matter over the second to third trimester by quantifying microstructure along the tracts in fetal compartments.

3. Relate critical neurobiological transitions occurring in the second to third trimester to changes in the MR signal and provide a normative reference to complement histological knowledge.
4. Using surface reconstructions and diffusion data, quantify the relationship between maturing microstructure of the cortex and coritical gyrification.
5. Explore data-driven decomposition methods to link structural and functional network maturation.

In relation to the above aims, I hypothesised that:

1. Maturational trajectories in diffusion signal would be distinct and unique for different tracts. This will reflect their unique, heterogenous development in terms of the underlying biology.
2. The cellular biology of fetal compartments will affect the MR contrast in a dynamic but predictable way, which can be quantified as smooth transitions in diffusion signal properties across the second to third trimester.
3. There is a causal link between the development of microstructure in fetal brain layers (subplate and cortical plate) and the formation of cortical folds. This can be quantified by analysing local neighbourhoods across the brain within individual subjects.
4. The structure and function of primary cortical areas co-matures in the fetal brain and these networks show the highest spatial overlap between modalities.

IV. Results

Chapter 7.

Development of white matter pathways over the second to third trimester in the human fetal brain.

Wilson et al., 2021 PNAS

Development of human white matter pathways in utero over the second and third trimester

Siân Wilson[a,b], Maximilian Pietsch[a], Lucilio Cordero-Grande[a,c,d], Anthony N. Price[a], Jana Hutter[a], Jiaxin Xiao[a], Laura McCabe[a], Mary A. Rutherford[a], Emer J. Hughes[a], Serena J. Counsell[a], Jacques-Donald Tournier[a], Tomoki Arichi[a,e,f,1], Joseph V. Hajnal[a], A. David Edwards[a,b], Daan Christiaens[a,g,2], and Jonathan O'Muircheartaigh[a,h,i,2]

[a]Centre for the Developing Brain, School of Biomedical Engineering and Imaging Sciences, King's College London, London, SE1 7EH, United Kingdom; [b]Centre for Neurodevelopmental Disorders, Kings College London, London, SE1 1UL, United Kingdom; [c]Biomedical Image Technologies, ETSI Telecomunicación, Universidad Politécnica de Madrid, 28040 Madrid, Spain; [d]Biomedical Research Networking Center in Bioengineering, Biomaterials and Nanomedicine (CIBER-BBN), 28029 Madrid, Spain; [e]Children's Neurosciences, Evelina London Children's Hospital, Guy's and St Thomas' NHS Foundation Trust, London SE1 7EH, United Kingdom; [f]Department of Bioengineering, Imperial College London, London SW7 2AZ, United Kingdom; [g]Department of Electrical Engineering (ESAT/PSI), Katholieke Universiteit Leuven, 3001 Leuven, Belgium; [h]Department of Forensic and Neurodevelopmental Sciences, King's College London, London SE5 8AF, United Kingdom; and [i]Department of Neuroimaging, Institute of Psychiatry, Psychology and Neuroscience, King's College London, London SE5 8AF, United Kingdom

Edited by David C. Van Essen, Washington University in St. Louis School of Medicine, St. Louis, MO, and approved March 28, 2021 (received for review November 26, 2020)

During the second and third trimesters of human gestation, rapid neurodevelopment is underpinned by fundamental processes including neuronal migration, cellular organization, cortical layering, and myelination. In this time, white matter growth and maturation lay the foundation for an efficient network of structural connections. Detailed knowledge about this developmental trajectory in the healthy human fetal brain is limited, in part, due to the inherent challenges of acquiring high-quality MRI data from this population. Here, we use state-of-the-art high-resolution multishell motion-corrected diffusion-weighted MRI (dMRI), collected as part of the developing Human Connectome Project (dHCP), to characterize the in utero maturation of white matter microstructure in 113 fetuses aged 22 to 37 wk gestation. We define five major white matter bundles and characterize their microstructural features using both traditional diffusion tensor and multishell multitissue models. We found unique maturational trends in thalamocortical fibers compared with association tracts and identified different maturational trends within specific sections of the corpus callosum. While linear maturational increases in fractional anisotropy were seen in the splenium of the corpus callosum, complex nonlinear trends were seen in the majority of other white matter tracts, with an initial decrease in fractional anisotropy in early gestation followed by a later increase. The latter is of particular interest as it differs markedly from the trends previously described in ex utero preterm infants, suggesting that this normative fetal data can provide significant insights into the abnormalities in connectivity which underlie the neurodevelopmental impairments associated with preterm birth.

fetal | diffusion MRI | white matter | tractography

In the human fetus, the brain's major white matter pathways develop over the second to third trimester of gestation in an extremely rapid yet distinctly hierarchical order (1, 2). The structure and the integrity of these white matter connections have an integral role in supporting the efficiency and coordination of functional networks. Current understanding about these processes has been largely reliant on postmortem data (2–6). Fetal MRI can capture whole-brain development in its living, functioning state, thereby providing crucial additional insight into normal growth. In the case of white matter in particular, this can include detailed investigation of developing long-range connections and region-specific trajectories.

The importance of better understanding this key period is emphasized by the high prevalence of cognitive and motor problems in children born preterm. In these infants, early exposure to the ex utero environment likely influences later trajectories of neurodevelopment (7–9). Multiple lines of evidence suggest that white matter abnormalities are the dominant pathology, further suggesting that this specific tissue type is both at a critical stage in its development and vulnerable to external influences (10–15). In this context, characterization of in utero maturation of white matter has a critical role as a normative reference.

Precise characterization of in vivo fetal development of white matter tracts using noninvasive methods such as MRI is challenging due to difficulties inherent to acquiring imaging data from this population, such as addressing image artifacts related to maternal tissue and constant fetal motion, as well as recruiting enough subjects to account for population heterogeneity and age effects (11, 16–27). Previous studies are also difficult to generalize as representing typical development as they have included clinical populations with brain abnormalities or ex utero preterm infants (8, 28, 29). All existing studies have used diffusion-tensor imaging (DTI) to describe changes in microstructure (30); however, the results have been inconsistent. While some studies have reported linear relationships between DTI metrics and gestational age (GA) (16, 22, 23, 31), others have fit nonlinear models (18, 32) and others still have found no clear age-dependence (19, 21).

In this study, we address the limitations of DTI and challenges of fetal imaging using a state-of-the-art high angular resolution multishell diffusion-weighted MRI (dMRI) acquisition, as well as a

Significance

This work uses state-of-the-art acquisition and analysis methods developed specifically for fetal MRI to delineate the developing brain's association, projection, and callosal white matter pathways. We describe unique, heterogenous maturational trajectories for different tracts, suggesting that regionally distinct biological mechanisms are at play in building the structural connectome in utero.

Author contributions: S.W., M.A.R., T.A., J.V.H., A.D.E., D.C., and J.O. designed research; S.W., A.N.P., J.H., L.M., M.A.R., E.J.H., T.A., J.V.H., and J.O. performed research; M.P., L.C.-G., A.N.P., J.H., J.-D.T., J.V.H., and D.C. contributed new reagents/analytic tools; S.W., M.P., J.X., S.J.C., T.A., A.D.E., D.C., and J.O. analyzed data; and S.W., M.P., L.C.-G., S.J.C., T.A., A.D.E., D.C., and J.O. wrote the paper.

The authors declare no competing interest.

This article is a PNAS Direct Submission.

[1]To whom correspondence may be addressed. Email: tomoki.arichi@kcl.ac.uk.

[2]D.C. and J.O. contributed equally to this work.

This article contains supporting information online at https://www.pnas.org/lookup/suppl/doi:10.1073/pnas.2023598118/-/DCSupplemental.

Published May 10, 2021.

reconstruction and processing pipeline developed specifically for studying challenging fetal data as part of the developing Human Connectome Project (dHCP) (http://www.developingconnectome.org) (33, 34). We applied newly developed and optimized methods for in utero tractography and microstructure estimation in a large cohort of 113 healthy fetuses from 22 to 37 wk GA. With these methods, we were able to delineate specific white matter bundles including the left and right corticospinal tracts (CST) (an example of a projection tract), the optic radiations (ORs) and inferior longitudinal fasciculus (ILF) (examples of association tracts), and the corpus callosum (CC) (example of a commissural tract). These specific tracts were selected due to known differences in their developmental trajectories and because their injury or abnormal development has been implicated in the pathophysiology of neurodevelopmental disorders or intellectual disability (10, 12, 35). This study represents the largest and most detailed in utero characterization of maturational changes in white matter microstructure across the second to third trimester of human gestation and represents a valuable resource for improving our understanding of the neuropathophysiology underlying neurodevelopmental disorders.

Results

Normative Trends for Whole-Brain Growth and FA in the Fetal Cohort. Fetal dMRI data were collected in 151 subjects (age 22 to 38 wk) as part of the dHCP (details presented in *SI Appendix*, section 1). All fetal brain images were reviewed and reported by an experienced perinatal neuroradiologist as showing appropriate appearances with no evidence of brain injury and/or malformation. Each subject was processed using the dHCP preprocessing pipeline, which includes specific measures to account for the existence of unpredictable fetal motion, geometric distortion of echo planar imaging, signal intensity inhomogeneities caused by differences in fetal position, and poor signal to noise ratio due to the small size of the fetal head and its distance from the coil (36, 37). Of the total 151 subjects that were manually assessed, 38 subjects failed due to excessive motion during acquisition (details of quality checking criteria presented in *SI Appendix*, section 1).

To verify that the data set showed normal expected trends in volumetric growth, we calculated the relationship between whole-brain volume of each subject and GA. Consistent with existing literature, we found a strong linear increase in volume across our study period ($R2 = 0.78$, $P < 0.001$, Fig. 1*B*) (38). Whole-brain mean FA similarly showed a positive linear relationship with GA (Fig. 1*C*).

Projection, Association, and Commissural White Matter Microstructure from 22 to 37 wk GA. Next, we estimated individual orientation density functions (ODFs) in MRtrix3 using constrained spherical deconvolution (details presented in *SI Appendix*, section 2). This method improves tractography estimations by addressing the challenge of resolving crossing fiber populations within a voxel, which can confound other commonly used methods like diffusion tensor imaging (39, 40). Individual subject ODFs were first compiled into average templates for each gestational week and then probabilistic streamline tractography was used at three-weekly intervals (22, 26, 29, 32, and 35 gestational weeks) to delineate five different white matter pathways (splenium and genu of the CC, CSTs, ILFs, ORs) (regions of interest and paths are described in *SI Appendix*, sections 3.1–3.4). Tractography was successful in all cases with the exception of the OR, which was difficult to estimate in the youngest 22 gestational week template, but could be reliably identified at all other ages (Fig. 2). Template-to-subject warps were then used to transform tracts from the age-matched template to individual subject space (details in *SI Appendix*, section 3).

White Matter Bundles Have Distinct Maturational Trajectories. To place our results in the context of prior studies looking at white matter development, we first used diffusion tensor metrics; FA and mean diffusivity (MD) to estimate changes in the underlying

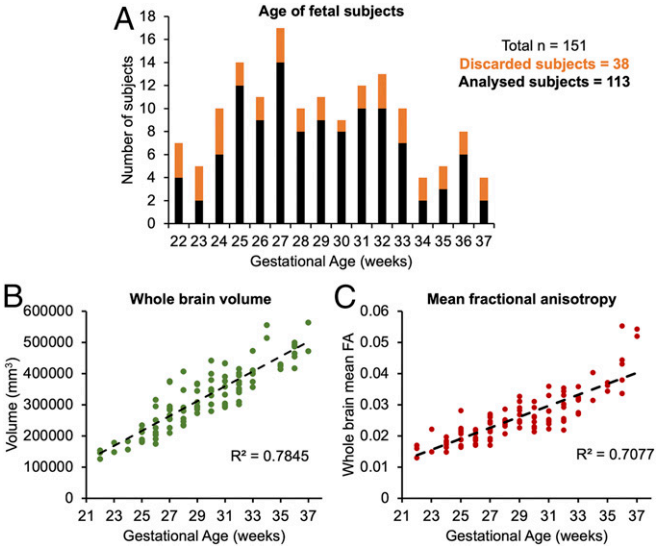

Fig. 1. (*A*) Distribution of subjects used in the study according to their GA (black), including those discarded at the tractography stage (orange). (*B*) The whole-brain volume of each subject plotted according to GA. (*C*) The mean FA across the whole brain in each subject, plotted according to GA.

microstructure of each tract. Mean FA and MD showed distinct maturational trajectories within different white matter tracts (Fig. 3). The relationship between GA and tensor metrics was best described by a second degree polynomial fit (as defined by Akaike Information Criterion [AIC]) in the majority of the delineated tracts (Fig. 3), with the exception of FA and MD in the splenium and MD in CST, where the relationship was linear (CST: FA AIC weight (wi) = 0.6; ILF: FA wi = 0.64, MD = 0.70; OR: FA wi = 0.72, MD = 0.73; Genu: FA wi = 0.54, MD wi = 0.71).

As expected, and in keeping with there being complex developmental changes in the white matter across our study period, relationships between FA/MD and GA were significant for all the tracts ($P < 0.01$). There were no significant differences between the left and right hemispheres for any of the delineated tracts ($P > 0.1$). Of particular interest, distinct maturational trends of FA/MD were seen within different sections of the CC, with a linear relationship between FA and GA in the splenium ($\rho = 0.36$) but a more complex relationship in the genu, with FA values first decreasing from 22 to 30 wk GA and then increasing thereafter toward full term gestation (Fig. 3). The inverse of this relationship was seen in MD values, with a linear decrease in the splenium ($\rho = -0.3$) and a similar nonlinear relationship in the genu with a peak at ~30 wk followed by a decline toward term. As with the splenium of the CC, a downward trend in FA from 22 to 30 wk, then a steady incline from 30 wk toward term was identified in the CST, ILF, and OR (Fig. 3). Similarly, inverse trends were seen in these white-matter tracts in the relationship between MD and GA, with an initial rise from 22 to 30 wk followed by a decrease toward full term. The exception was the CST, which showed a strong negative correlation ($\rho = -0.75$). For completeness, the axial and radial diffusivities underlying each tract were also computed, and these plots can be found in the supplementary information section.

Validating Tensor Metrics Using Multishell, Multitissue Modeling. Given the relatively small size of the fetal brain, it is plausible that partial-voluming of tissue might have affected the estimated FA and MD values underlying the tracts, especially if streamlines traverse voxels, which contain both white and gray matter or cerebrospinal fluid (CSF) (41). To specifically address these partial-voluming effects and see whether they are responsible for our observed

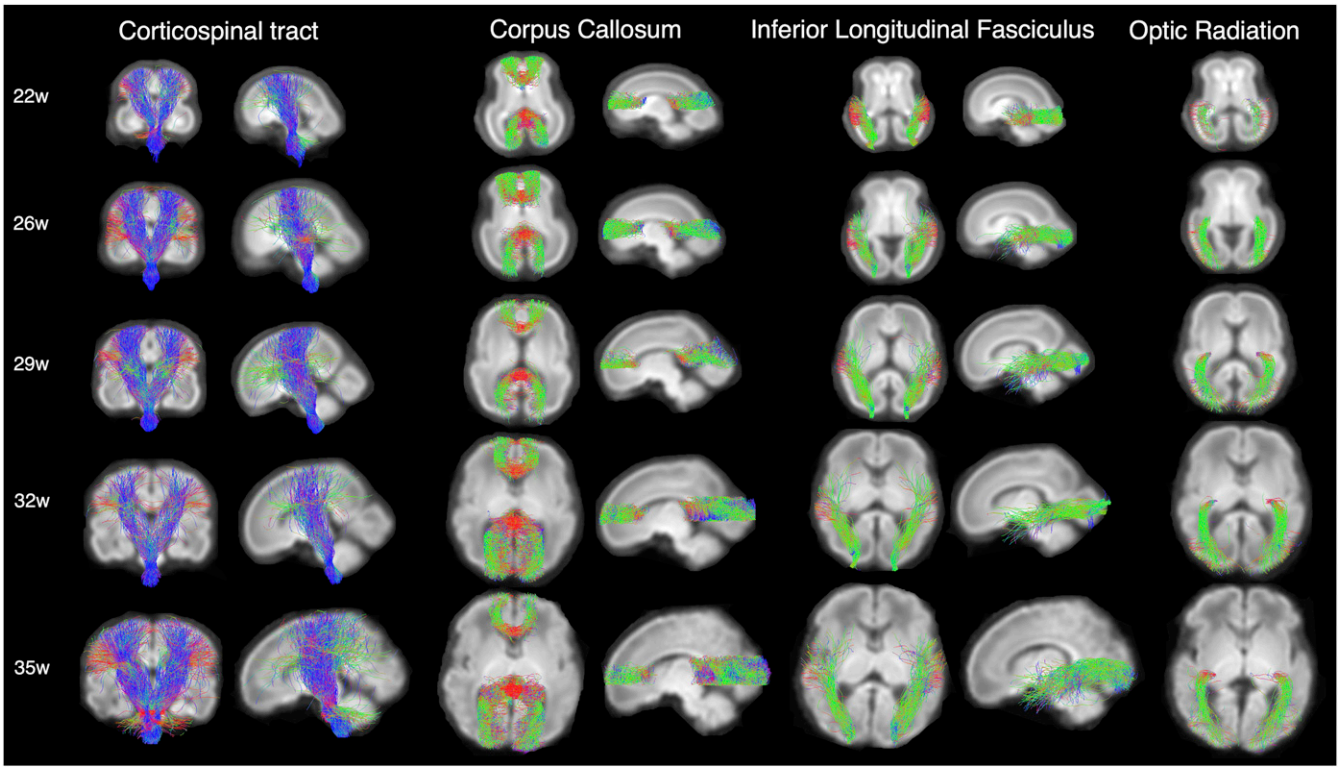

Fig. 2. White matter pathways estimated using targeted probabilistic streamline tractography in ODF templates constructed by averaging individual subject ODFs for each gestational week. The color coding of tractography connections is based on a standard red-green-blue code applied to the vector between the end-points of each structure (green for anterior–posterior, red for right–left and blue for dorsal–ventral).

maturational trends, we applied a multishell multitissue constrained spherical deconvolution model to the DWI data (details presented in *SI Appendix*, section 2), which uses the unique b-value dependencies of signal in white matter and CSF to delineate intravoxel contributions of brain tissue and fluid (11, 40). As would be expected, this analysis identified a strong positive linear trend between the fraction of fluid and MD in all of the delineated tracts (Fig. 4) and a positive relationship between mean FA and the tissue anisotropy (Fig. 4). Importantly, these linear trends suggest that the observed nonlinear maturational trends in our data cannot be attributed to simple partial voluming effects. To highlight the similarities between MD and fluid fraction trends over GA, a plot displaying the relationship between fluid fraction and GA can be found in the *SI Appendix*, Fig. S2).

Discussion

In this work, we used in utero dMRI to report in vivo brain white-matter development in a population of 113 fetuses aged 22

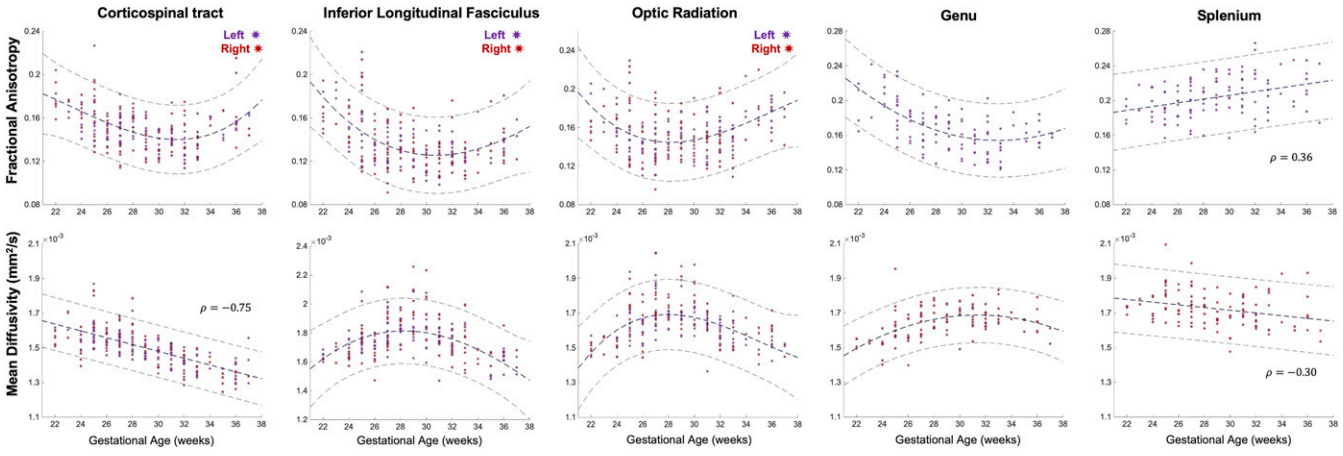

Fig. 3. Mean FA and MD values underlying the left (red) and right (purple) CST, ILF, OR, Genu, and splenium for each fetal subject, plotted according to the GA of the subject in weeks. A second degree polynomial curve is fitted for the FA in the CST, ILF, OR, and Genu, the MD in the ILF, OR, and Genu (navy dashed line). The MD in the CST and the FA/MD in the splenium have linear relationships with GA, described by a Spearman's rank correlation coefficient (ρ). Dashed lines above and below represent the 95% confidence interval.

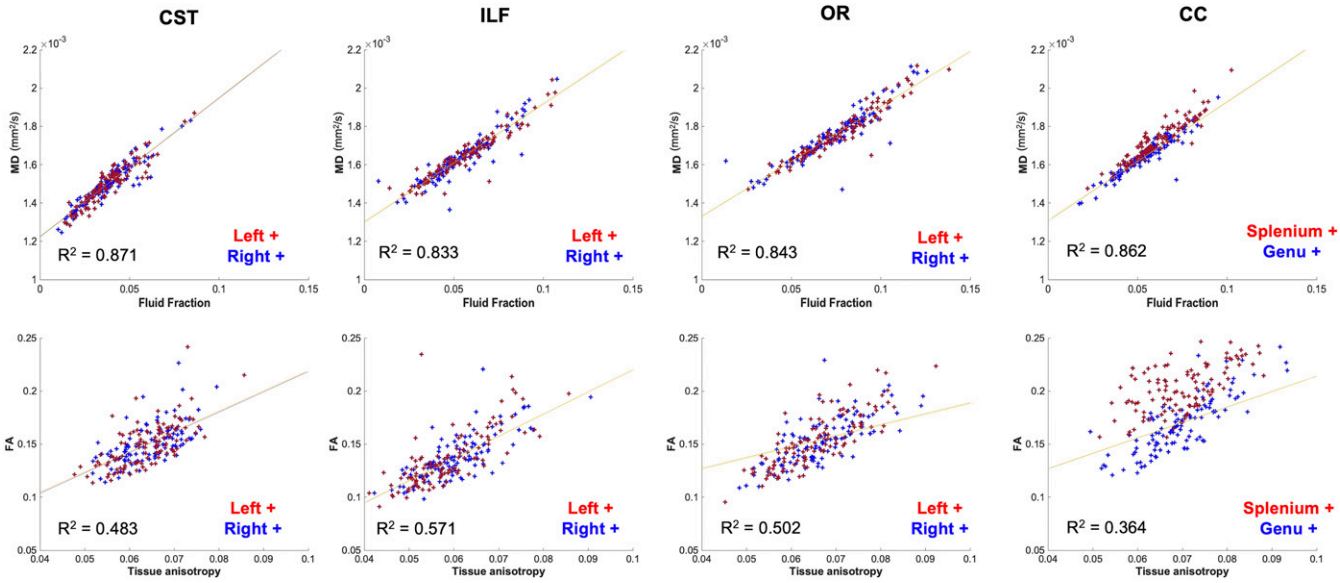

Fig. 4. (*Top row*) partial correlations between tract-average MD and volume fraction of the fluid component (significant relationship for all partial correlations, $P < 0.01$). (*Bottom row*) Mean FA value of the tract plotted against the square root of the power in the l = 2 band of the tissue component (tissue anisotropy) values in voxels traversed by each tract (significant relationship for all partial correlations, $P < 0.05$).

to 37 wk gestation as part of the open-access dHCP. In addition to representing the largest ever cohort of fetuses studied in this way, we used state-of-the-art acquisition and analysis methods, which have enabled the most detailed delineation of the fetal brain's white-matter pathways to date. Using these methods, we have studied the brain's major association, projection, and commissural fibers and demonstrate that each have distinct developmental ontogenies, with several showing nonlinear changes in tract microstructure across our study period.

In accordance with postmortem studies describing the presence of commissural and projection fibers as early as the first trimester of gestation, we were able to identify both the genu and the splenium of the CC, the CST, and the ILF in our study population from 22 wk GA onward (Fig. 2) (4, 24, 42–44). Immature axons within the cortico-cortical association tracts have also been seen as early as 15 wk gestation, with the first appearance of the ILF reported around 15 to 17 wk GA (4, 24). In our data, the only white-matter tract which was challenging to delineate at the earliest 22 wk GA time point was the OR, with few streamlines reaching the back of the occipital lobe. This finding is consistent with electron microscopy studies, which report that while the OR is evident from the lateral geniculate nucleus to the subplate by 11 to 13 wk GA (45–47), synapses in the cortical plate are only evident at 23 to 25 wk GA (46, 48).

To provide a comparison with previous studies, which have reported white matter microstructural metrics derived from the widely used tensor model, we quantitively assess changes over the fetal period using FA and MD (30, 49, 50). We observed a linear increase between GA and FA at a whole-brain level, reflecting overall reduction in water content and increasing proportion of white matter relative to gray matter over this timeframe. This simple linear relationship at a whole-brain level highlights that the tracts have unique and distinct trajectories, which are influenced by more complex processes than just overall tissue and fluid balance in the brain. In contrast to our findings, the majority of previous fetal and preterm neonatal diffusion studies have reported linear increases in FA and decreases in MD over their study periods (16, 22, 23, 31). However, many of these study populations have very few subjects under the age of 28 wk, and some have only studied the last trimester of gestation (16, 23, 31). The reported linear increase in FA and decrease in MD in the third trimester in these previous studies therefore corresponds to the changes in FA and MD that we observe in our data between ∼29 and 37 wk in the CST, ILF, OR, and splenium of the CC.

Some prior investigations into fetal white matter development have also found nonlinear relationships between MD and GA (18, 22, 32). As with our results, Schneider et al. found that a second degree polynomial fit best described changes in MD in different white matter regions across the brain (32). Khan et al. also found an increase in MD toward 30 wk gestation followed by a sharp decrease toward term in the cortical plate (22).

The tract-specific maturational trends we observe likely also reflect the known regional differences in white-matter maturation across the brain (2, 51, 52). Tensor metrics are highly sensitive to different biological processes, and therefore the unique trends we observe are likely to have resulted from a combination of multiple factors (29, 53, 54). In our data, a negative linear correlation between MD and GA was seen only in the CST and splenium, which could represent simple reductions in water content and increasing fiber organization in these particular tracts over the third trimester (16, 22, 23, 31). Since histology and ex vivo DTI studies suggest that both the CST and CC tracts are among the earliest to form (24, 42, 55), it is plausible based on this histological evidence that by 22 wk gestation these tracts are already coherently organized and that MD is predominantly being affected by the reduction in water content over our study age range. In contrast, within the ILF, OR, and Genu, the initial increase in MD could be explained by tortuous fibers becoming more coherent over this period, making water diffusion less hindered in the principle direction of the fiber pathway (18). In addition, before 30 wk gestation, there is less tissue organization and there are larger extracellular spaces between fibers to allow for cellular migration, which could further contribute to higher MD values (32). In keeping with this, histological studies have described an abundance of extracellular matrix (ECM) between white-matter fiber bundles in the second trimester, which significantly decreases by 35 wk gestation (56). Since the ECM has high water content, it is possible that its relative abundance around fibers has an effect on MD values and significantly contributes to the trends we observe.

Although FA in older cohorts is often used as a proxy for the degree of integrity or myelination, the white-matter pathways in this study are still relatively immature at birth (57). Biochemical markers of mature myelin (myelin-basic protein) are largely expressed postnatally in the cerebral cortex and then increase substantially in the first 2 y of life (51, 58). However, unmyelinated white-matter tracts still show signal intensity changes consistent with anisotropic water diffusion (59), so it is possible that the increases in FA we observe are due to active axonal outgrowth and initial ensheathment of axons by premyelin sheaths, generated by immature oligodendrocytes (OLs) (58, 60). In agreement with this, OL lineage progression has been shown to affect FA values (61), and the percentage of immature OLs in the cerebral white matter increases markedly from 30 wk gestation (62). Back et al. also identify the first signs of pre-OL ensheathment of axons at ~30 wk gestation (60), coinciding with the transition in our FA trends for the CST, ILF, OR, and Genu. Of further interest, Xu et al. also identified 30 to 31 wk gestation as a transitional point from high angular resolution diffusion imaging (HARDI)-defined radial coherence to cortico-cortical coherence, indicating the emergence of cortico-cortical association fibers (63). These MRI findings were correlated with histology, where they additionally observed the transformation of radial glial fibers into astrocytes (63). Together, these observations indicate that there are several developmental processes that transition around 30 wk gestation, which are likely to have had an effect on the FA values and are contributing to the unique trends we describe in Fig. 3.

Our results additionally support existing evidence that there is heterogeneity in the development of the different compartments of the CC (51). In our data, the precise neurobiological underpinnings of these differing trajectories between the genu and the splenium cannot be determined just with dMRI data alone. Developing callosal fibers grow through complex pathways and cross the midline using different substrates in transient fetal structures such as the callosal septa. The callosal septa are prominent between 18 and 34 wk, and their biochemical composition is dynamically over this period, including changes in the expression of axonal guidance molecules, cellular matrix, and ECM constituents, which are likely to affect tensor metrics (64, 65). Previous studies have also identified differences in the growth rate of different sections of the CC, with the genu growing at a faster rate than the body and the splenium during fetal development, but then after birth, mature myelination is observed in the splenium before the genu (55, 51, 66, 67). Kinney et al. additionally report a difference in the delay between the onset and maturation of myelin between the anterior and posterior sections of the CC, which might further contribute to the different trends we observe in FA/MD between the two distinct sections. Therefore, it is possible that the initial higher FA values in the genu at 22 wk are reflective of a faster growth rate over the fetal period. The premyelin phase then initiates first in the splenium, resulting in a higher FA in comparison with the genu at full-term age (51). Based on our findings, future studies would benefit from further delineation of the CC into different compartments through combination with histology for more specificity.

Developing white matter is known to be vulnerable to adverse influences related to the extrauterine environment, and early damage leads to significant life-long neurocognitive impairments (7, 68, 69). A comprehensive characterization of in utero normal white matter development is therefore a critically important reference point for comparison with data from preterm infants. In addition to enabling more detailed and reliable tractography, continuing advances in dMRI and processing pipelines can also now provide more information about the underlying microstructural changes. This can give new insight into the mechanisms of white-matter injury, such as why certain tracts appear more susceptible to damage than others and how this is influenced by timing of the related insult (54, 70, 71). In a wider sense, the combination of in utero dMRI with ex utero imaging and histological studies can therefore provide a comprehensive understanding about the role of aberrant early development in the pathophysiology of neurodevelopmental disorders originating in the perinatal period.

To address partial-voluming effects and understand if they could explain the trends seen in our data, we applied a multishell multitissue constrained spherical deconvolution model, which uses the unique b-value dependencies of signal in white matter and CSF to delineate intravoxel contributions of brain tissue and fluid (40, 72). In adults, this more complex approach to modeling voxel-wise diffusion has been shown to improve the precision of fiber orientation estimations at tissue interfaces (73). As seen in neonatal cohorts, partial voluming between tissue and fluid is present in fetal dMRI data to varying degrees throughout the brain and as a function of maturation (34). In the tissue-specific ODFs, we found a strong positive linear relationship in all tracts between the MD value and the fluid fraction, verifying the expected relationship between MD and voxel-wise fluid density. Based on this result, we propose that partial voluming effects alone cannot explain the observed nonlinear U-shaped relationships between GA and FA and MD values.

The image acquisition and processing pipelines used in this study were specifically designed to address the unique challenges associated with fetal and neonatal neuroimaging within the dHCP (http://www.developingconnectome.org/). The advances within this project have both significantly reduced data loss and markedly increased the signal to noise ratio and sensitivity, ultimately offering improved biological interpretation. While there is a large body of literature to support that measuring white-matter structural integrity with DTI has clinical relevance (29, 54, 71, 74), tensor metrics do not provide direct visualization of fiber bundles and therefore findings must be complemented by existing knowledge from histology. However, the noninvasive nature of dMRI allows whole-brain three-dimensional visualization, thus enabling studies investigating the development of long-range connectivity across the entire brain network and comparisons of regional differences in brain development. Through combining state-of-the-art acquisition and methodology, we have sufficient sensitivity to highlight different developmental trajectories within specific white-matter tracts and in doing so provide valuable insights about a fundamental stage in early human brain development.

In summary, we describe the largest study to date in a healthy fetal cohort using dMRI methods to characterize the fundamental processes underlying healthy white-matter development across the late second to third trimesters of human gestation. Our large cohort covers a wide age range and only includes healthy fetuses with no evidence of brain injury, which is in marked contrast to previous reports that have studied narrower windows in development and included fetuses with abnormalities. Our results and the associated data represent a valuable resource, which is being made publicly available, and is representative of healthy white-matter development in utero, which can be compared with that of clinical populations at risk of neurodevelopmental difficulties such as those born preterm.

Methods

Fetal dMRI data were collected in 151 subjects as part of the dHCP (Fig. 1*A*). Raw data were preprocessed using a bespoke pipeline (details described in *SI Appendix*) that includes denoising, bias correction, dynamic distortion correction, and slice-to-volume motion. Only images that passed quality control were included in this study.

For each subject, the $b = 0$ and $b = 1{,}000$ volumes were extracted and used to estimate the diffusion tensor and calculate FA/MD maps (details in *SI Appendix*).

We then estimated ODFs for each subject in MRtrix3 (https://www.mrtrix.org/). Individual subject ODFs were compiled into weekly templates (details in *SI Appendix*). Probabilistic streamline tractography was used to estimate the five different tracts; streamlines were guided by specific seed regions, waypoints, and exclusion zones based on the known neuroanatomy of the tracts (details in *SI Appendix*). Tracts were overlaid onto the FA and MD

maps, and then the mean FA and MD values were calculated within the overlaid streamlines. The AIC (75) was used to evaluate the most suitable model across different degrees of polynomial fit (1–4) to describe the relationship between GA and FA/MD.

To model the data using a multishell multitissue approach, subject-specific white matter response functions were extracted and the oldest 20 subjects were averaged to obtain a group-average response function of relatively mature white matter (details in *SI Appendix*). A group-average CSF response function was calculated from the whole cohort of subjects. All subjects' dMRI signals were deconvolved into tissue ODF and fluid components using multishell multitissue constrained spherical deconvolution and the two corresponding group-average response functions. Tracts were overlaid onto the normalized fluid ODF (to approximate the fluid fraction in each voxel) and onto the square root of the power in the $l = 2$ band of the tissue ODF (representing tissue anisotropy). The mean CSF fraction and mean tissue anisotropy for each tract was calculated.

Data Availability. Anonymized open-access fetal MRI data used in this work are available on request and will be released in full as part of the dHCP fetal data release (http://www.developingconnectome.org).

ACKNOWLEDGMENTS. We thank the patients who agreed to participate in this work and the staff of St. Thomas' Hospital London. This work was supported by the European Research Council under the European Union Seventh Framework Programme (FP/2007-2013)/ERC Grant Agreement No. 319456. We acknowledge infrastructure support from the National Institute for Health Research (NIHR) Mental Health Biomedical Research Centre (BRC) at South London and Maudsley NHS Foundation Trust, King's College London, and the NIHR-BRC at Guy's and St Thomas' NHS Foundation Trust. We also acknowledge grant support in part from the Wellcome Engineering and Physical Sciences Research Council (EPSRC) Centre for Medical Engineering at King's College London (WT 203148/Z/16/Z) and the Medical Research Council (UK) (MR/K006355/1 and MR/L011530/1). J.O. is supported by a Sir Henry Dale Fellowship jointly funded by the Wellcome Trust and the Royal Society (Grant 206675/Z/17/Z). J.O. and A.D.E. received support from the Medical Research Council Centre for Neurodevelopmental Disorders, King's College London (Grant MR/N026063/1). T.A. was supported by an MRC Clinician Scientist Fellowship (MR/P008712/1). Support for this work was also provided by the NIHR-BRC at Kings College London, Guy's and St Thomas' NHS Foundation Trust in partnership with King's College London, and King's College Hospital NHS Foundation Trust.

1. F. H. Gilles, A. Leviton, E. C. Dooling, Eds., "Myelinated tracts: Growth patterns" in *The Developing Human Brain: Growth and Epidemiologic Neuropathology*, (Elsevier Science, 1983), pp. 118–185.
2. B. A. Brody, H. C. Kinney, A. S. Kloman, F. H. Gilles, Sequence of central nervous system myelination in human infancy. I. An autopsy study of myelination. *J. Neuropathol. Exp. Neurol.* **46**, 283–301 (1987).
3. P. L. Yakovlev, A. R. Lecours, "The myelogenetic cycles of regional maturation of the brain" in *Resional Development of the Brain in Early Life*, A. Minkowski, Ed. (Oxford, Blackwell, 1967), pp. 3–70.
4. I. Kostović, M. Judaš, Prolonged coexistence of transient and permanent circuitry elements in the developing cerebral cortex of fetuses and preterm infants. *Dev. Med. Child Neurol.* **48**, 388–393 (2006).
5. I. Kostović, N. Jovanov-Milosević, The development of cerebral connections during the first 20-45 weeks' gestation. *Semin. Fetal Neonatal Med.* **11**, 415–422 (2006).
6. S. A. Bayer, J. Altman, *The Human Brain During the Second Trimester* (Taylor & Francis, 2005).
7. A.-M. Childs *et al*., American journal of neuroradiology. *AJNR Am. J. Neuroradiol.* **20**, 1349–1357 (2001).
8. L. C. Maas *et al*., Early laminar organization of the human cerebrum demonstrated with diffusion tensor imaging in extremely premature infants. *Neuroimage* **22**, 1134–1140 (2004).
9. S. A. Back, White matter injury in the preterm infant: Pathology and mechanisms. *Acta Neuropathol.* **134**, 331–349 (2017).
10. J. J. Volpe, Brain injury in premature infants: A complex amalgam of destructive and developmental disturbances. *Lancet Neurol.* **8**, 110–124 (2009).
11. D. Batalle *et al*., Early development of structural networks and the impact of prematurity on brain connectivity. *Neuroimage* **149**, 379–392 (2017).
12. C. Nosarti *et al*., Preterm birth and structural brain alterations in early adulthood. *Neuroimage Clin.* **6**, 180–191 (2014).
13. M. Allin *et al*., Cognitive maturation in preterm and term born adolescents. *J. Neurol. Neurosurg. Psychiatry* **79**, 381–386 (2008).
14. L. J. Woodward, J. O. Edgin, D. Thompson, T. E. Inder, Object working memory deficits predicted by early brain injury and development in the preterm infant. *Brain* **128**, 2578–2587 (2005).
15. B. Larroque *et al*.; EPIPAGE Study group, Neurodevelopmental disabilities and special care of 5-year-old children born before 33 weeks of gestation (the EPIPAGE study): A longitudinal cohort study. *Lancet* **371**, 813–820 (2008).
16. T. Bui *et al*., Microstructural development of human brain assessed in utero by diffusion tensor imaging. *Pediatr. Radiol.* **36**, 1133–1140 (2006).
17. G. Kasprian *et al*., In utero tractography of fetal white matter development. *Neuroimage* **43**, 213–224 (2008).
18. E. Zanin *et al*., White matter maturation of normal human fetal brain. An in vivo diffusion tensor tractography study. *Brain Behav.* **1**, 95–108 (2011).
19. C. Mitter, D. Prayer, P. C. Brugger, M. Weber, G. Kasprian, In vivo tractography of fetal association fibers. *PLoS One* **10**, e0119536 (2015).
20. A. Jakab, R. Tuura, C. Kellenberger, I. Scheer, In utero diffusion tensor imaging of the fetal brain: A reproducibility study. *Neuroimage Clin.* **15**, 601–612 (2017).
21. G. Lockwood Estrin *et al*., White and grey matter development in utero assessed using motion-corrected diffusion tensor imaging and its comparison to ex utero measures. *MAGMA* **32**, 473–485 (2019).
22. S. Khan *et al*., Fetal brain growth portrayed by a spatiotemporal diffusion tensor MRI atlas computed from in utero images. *Neuroimage* **185**, 593–608 (2019).
23. C. Jaimes *et al*., In vivo characterization of emerging white matter microstructure in the fetal brain in the third trimester. *Hum. Brain Mapp.* **41**, 3177–3185 (2020).
24. H. Huang *et al*., White and gray matter development in human fetal, newborn and pediatric brains. *Neuroimage* **33**, 27–38 (2006).
25. H. Huang, L. Vasung, Gaining insight of fetal brain development with diffusion MRI and histology. *Int. J. Dev. Neurosci.* **32**, 11–22 (2014).
26. D. Batalle *et al*., Different patterns of cortical maturation before and after 38 weeks gestational age demonstrated by diffusion MRI in vivo. *Neuroimage* **185**, 764–775 (2019).
27. J. H. Gilmore, R. C. Knickmeyer, W. Gao, Imaging structural and functional brain development in early childhood. *Nat. Rev. Neurosci.* **19**, 123–137 (2018).
28. R. C. McKinstry *et al*., Radial organization of developing preterm human cerebral cortex revealed by non-invasive water diffusion anisotropy MRI. *Cereb. Cortex* **12**, 1237–1243 (2002).
29. P. S. Hüppi *et al*., Microstructural development of human newborn cerebral white matter assessed in vivo by diffusion tensor magnetic resonance imaging. *Pediatr. Res.* **44**, 584–590 (1998).
30. P. J. Basser, J. Mattiello, D. LeBihan, MR diffusion tensor spectroscopy and imaging. *Biophys. J.* **66**, 259–267 (1994).
31. K. Keunen *et al*., Early human brain development: Insights into macroscale connectome wiring. *Pediatr. Res.* **84**, 829–836 (2018).
32. J. F. Schneider *et al*., Diffusion-weighted imaging in normal fetal brain maturation. *Eur. Radiol.* **17**, 2422–2429 (2007).
33. E. J. Hughes *et al*., A dedicated neonatal brain imaging system. *Magn. Reson. Med.* **78**, 794–804 (2017).
34. M. Pietsch *et al*., A framework for multi-component analysis of diffusion MRI data over the neonatal period. *Neuroimage* **186**, 321–337 (2019).
35. J. O'Muircheartaigh *et al*., Modelling brain development to detect white matter injury in term and preterm born neonates. *Brain* **143**, 467–479 (2020).
36. D. Christiaens *et al*., Scattered slice SHARD reconstruction for motion correction in multi-shell diffusion MRI. *Neuroimage* **225**, 117437 (2021).
37. M. Deprez *et al*., Higher order spherical harmonics reconstruction of fetal diffusion MRI with intensity correction. *IEEE Trans. Med. Imaging* **39**, 1104–1113 (2020).
38. A. Gholipour, J. A. Estroff, C. E. Barnewolt, S. A. Connolly, S. K. Warfield, Fetal brain volumetry through MRI volumetric reconstruction and segmentation. *Int. J. CARS* **6**, 329–339 (2011).
39. J. D. Tournier, F. Calamante, A. Connelly, Robust determination of the fibre orientation distribution in diffusion MRI: Non-negativity constrained super-resolved spherical deconvolution. *Neuroimage* **35**, 1459–1472 (2007).
40. B. Jeurissen, J. D. Tournier, T. Dhollander, A. Connelly, J. Sijbers, Multi-tissue constrained spherical deconvolution for improved analysis of multi-shell diffusion MRI data. *Neuroimage* **103**, 411–426 (2014).
41. A. L. Alexander, K. M. Hasan, M. Lazar, J. S. Tsuruda, D. L. Parker, Analysis of partial volume effects in diffusion-tensor MRI. *Magn. Reson. Med.* **45**, 770–780 (2001).
42. H. Huang *et al*., Anatomical characterization of human fetal brain development with diffusion tensor magnetic resonance imaging. *J. Neurosci.* **29**, 4263–4273 (2009).
43. E. Takahashi, R. D. Folkerth, A. M. Galaburda, P. E. Grant, Emerging cerebral connectivity in the human fetal brain: An MR tractography study. *Cereb. Cortex* **22**, 455–464 (2012).
44. J. Dubois *et al*., The early development of brain white matter: A review of imaging studies in fetuses, newborns and infants. *Neuroscience* **276**, 48–71 (2014).
45. P. Rakic, Prenatal development of the visual system in rhesus monkey. *Philos. Trans. R. Soc. Lond. B Biol. Sci.* **278**, 245–260 (1977).
46. I. Kostovic, P. Rakic, Developmental history of the transient subplate zone in the visual and somatosensory cortex of the macaque monkey and human brain. *J. Comp. Neurol.* **297**, 441–470 (1990).
47. J. A. De Carlos, D. D. M. O'Leary, Growth and targeting of subplate axons and establishment of major cortical pathways. *J. Neurosci.* **12**, 1194–1211 (1992).
48. M. E. Molliver, I. Kostović, H. van der Loos, The development of synapses in cerebral cortex of the human fetus. *Brain Res.* **50**, 403–407 (1973).
49. P. J. Basser, J. Mattiello, D. LeBihan, Estimation of the effective self-diffusion tensor from the NMR spin echo. *J. Magn. Reson. B.* **103**, 247–254 (1994).
50. S. K. Song *et al*., Dysmyelination revealed through MRI as increased radial (but unchanged axial) diffusion of water. *Neuroimage* **17**, 1429–1436 (2002).

51. H. C. Kinney, B. A. Brody, A. S. Kloman, F. H. Gilles, Sequence of central nervous system myelination in human infancy. II. Patterns of myelination in autopsied infants. *J. Neuropathol. Exp. Neurol.* **47**, 217–234 (1988).
52. P. Flechsig, Anatomie des menschlichen gehirns und rückenmarks auf myelogenetischer grundlage. *Journal of Mental Science* **67**, 210–211 (1921).
53. P. Mukherjee *et al*., Normal brain maturation during childhood: Developmental trends characterized with diffusion-tensor MR imaging. *Radiology* **221**, 349–358 (2001).
54. J. Neil, J. Miller, P. Mukherjee, P. S. Hüppi, Diffusion tensor imaging of normal and injured developing human brain–A technical review. *NMR Biomed.* **15**, 543–552 (2002).
55. P. Rakic, P. I. Yakovlev, Development of the corpus callosum and cavum septi in man. *J. Comp. Neurol.* **132**, 45–72 (1968).
56. R. I. Milos *et al*., Developmental dynamics of the periventricular parietal crossroads of growing cortical pathways in the fetal brain–In vivo fetal MRI with histological correlation. *Neuroimage* **210**, 116553 (2020).
57. J. J. Volpe *et al*., *Volpe's Neurology of the Newborn* (Elsevier, 2017).
58. R. L. Haynes *et al*., Axonal development in the cerebral white matter of the human fetus and infant. *J. Comp. Neurol.* **484**, 156–167 (2005).
59. D. M. Wimberger *et al*., Identification of "premyelination" by diffusion-weighted MRI. *J. Comput. Assist. Tomogr.* **19**, 28–33 (1995).
60. S. A. Back, N. L. Luo, N. S. Borenstein, J. J. Volpe, H. C. Kinney, Arrested oligodendrocyte lineage progression during human cerebral white matter development: Dissociation between the timing of progenitor differentiation and myelinogenesis. *J. Neuropathol. Exp. Neurol.* **61**, 197–211 (2002).
61. A. Drobyshevsky *et al*., Developmental changes in diffusion anisotropy coincide with immature oligodendrocyte progression and maturation of compound action potential. *J. Neurosci.* **25**, 5988–5997 (2005).
62. S. A. Back *et al*., Late oligodendrocyte progenitors coincide with the developmental window of vulnerability for human perinatal white matter injury. *J. Neurosci.* **21**, 1302–1312 (2001).
63. G. Xu *et al*., Radial coherence of diffusion tractography in the cerebral white matter of the human fetus: Neuroanatomic insights. *Cereb. Cortex* **24**, 579–592 (2014).
64. M. Culjat, N. J. Milošević, Callosal septa express guidance cues and are paramedian guideposts for human corpus callosum development. *J. Anat.* **235**, 670–686 (2019).
65. N. Jovanov-Milosević, V. Benjak, I. Kostović, Transient cellular structures in developing corpus callosum of the human brain. *Coll. Antropol.* **30**, 375–381 (2006).
66. R. Achiron, A. Achiron, Development of the human fetal corpus callosum: A high-resolution, cross-sectional sonographic study. *Ultrasound Obstet. Gynecol.* **18**, 343–347 (2001).
67. A. J. Barkovich, B. O. Kjos, D. E. Jackson Jr, D. Norman, Normal maturation of the neonatal and infant brain: MR imaging at 1.5 T. *Radiology* **166**, 173–180 (1988).
68. O. Kapellou *et al*., Abnormal cortical development after premature birth shown by altered allometric scaling of brain growth. *PLoS Med.* **3**, e265 (2006).
69. C. Raybaud, T. Ahmad, N. Rastegar, M. Shroff, M. Al Nassar, The premature brain: Developmental and lesional anatomy. *Neuroradiology* **55**, 23–40 (2013).
70. J. J. Volpe, Neurobiology of periventricular leukomalacia in the premature infant. *Pediatr. Res.* **50**, 553–562 (2001).
71. P. S. Hüppi *et al*., Microstructural brain development after perinatal cerebral white matter injury assessed by diffusion tensor magnetic resonance imaging. *Pediatrics* **107**, 455–460 (2001).
72. J. D. Tournier *et al*., MRtrix3: A fast, flexible and open software framework for medical image processing and visualisation. *Neuroimage* **202**, 116137 (2019).
73. K. G. Schilling *et al*., Histological validation of diffusion MRI fiber orientation distributions and dispersion. *Neuroimage* **165**, 200–221 (2018).
74. S. P. Miller *et al*., Serial quantitative diffusion tensor MRI of the premature brain: Development in newborns with and without injury. *J. Magn. Reson. Imaging* **16**, 621–632 (2002).
75. H. Akaike, "Information theory and an extension of the maximum likelihood principle" in *Springer Series in Statistics (Perspectives in Statistics)*, E. Parzen, K. Tanabe, G. Kitagawa, Eds. (Springer, New York, NY, 1973), pp. 199–213.

Chapter 8.

Spatiotemporal tissue maturation of thalamocortical pathways in the human fetal brain.

Wilson et al., 2023, eLIFE.

RESEARCH ARTICLE

Spatiotemporal tissue maturation of thalamocortical pathways in the human fetal brain

Siân Wilson[1,2], Maximilian Pietsch[1], Lucilio Cordero-Grande[1,3,4], Daan Christiaens[1,5], Alena Uus[6], Vyacheslav R Karolis[1], Vanessa Kyriakopoulou[1], Kathleen Colford[1], Anthony N Price[1], Jana Hutter[1], Mary A Rutherford[1], Emer J Hughes[1], Serena J Counsell[1], Jacques-Donald Tournier[1], Joseph V Hajnal[1], A David Edwards[1,2], Jonathan O'Muircheartaigh[1,2,7,8]*, Tomoki Arichi[1,2,9,10]*

[1]Centre for the Developing Brain, School of Biomedical Engineering and Imaging Sciences, King's College London, London, United Kingdom; [2]Centre for Neurodevelopmental Disorders, King's College London, London, United Kingdom; [3]Biomedical Image Technologies, ETSI Telecomunicación, Universidad Politécnica de Madrid, Madrid, Spain; [4]Biomedical Research Networking Center in Bioengineering, Biomaterials and Nanomedicine (CIBER-BBN), Madrid, Spain; [5]Department of Electrical Engineering (ESAT/PSI), Katholieke Universiteit Leuven, Leuven, Belgium; [6]Department of Biomedical Engineering, School Biomedical Engineering and Imaging Sciences, King's College London, St. Thomas' Hospital, London, United Kingdom; [7]Department of Forensic and Neurodevelopmental Sciences, King's College London, London, United Kingdom; [8]Department of Neuroimaging, Institute of Psychiatry, Psychology and Neuroscience, King's College London, London, United Kingdom; [9]Children's Neurosciences, Evelina London Children's Hospital, Guy's and St Thomas' NHS Foundation Trust, London, United Kingdom; [10]Department of Bioengineering, Imperial College London, London, United Kingdom

***For correspondence:** jonathanom@kcl.ac.uk (JO'M); tomoki.arichi@kcl.ac.uk (TA)

Competing interest: The authors declare that no competing interests exist.

Funding: See page 14

Received: 26 September 2022
Preprinted: 25 October 2022
Accepted: 31 March 2023
Published: 03 April 2023

Reviewing Editor: Finnegan J Calabro, University of Pittsburgh, United States

Abstract The development of connectivity between the thalamus and maturing cortex is a fundamental process in the second half of human gestation, establishing the neural circuits that are the basis for several important brain functions. In this study, we acquired high-resolution in utero diffusion magnetic resonance imaging (MRI) from 140 fetuses as part of the Developing Human Connectome Project, to examine the emergence of thalamocortical white matter over the second to third trimester. We delineate developing thalamocortical pathways and parcellate the fetal thalamus according to its cortical connectivity using diffusion tractography. We then quantify microstructural tissue components along the tracts in fetal compartments that are critical substrates for white matter maturation, such as the subplate and intermediate zone. We identify patterns of change in the diffusion metrics that reflect critical neurobiological transitions occurring in the second to third trimester, such as the disassembly of radial glial scaffolding and the lamination of the cortical plate. These maturational trajectories of MR signal in transient fetal compartments provide a normative reference to complement histological knowledge, facilitating future studies to establish how developmental disruptions in these regions contribute to pathophysiology.

Editor's evaluation

This study presents important new findings regarding prenatal thalamocortical development. The authors present convincing evidence, while overcoming substantial methodological challenges, in

charting prenatal brain development in vivo. This work will be of interest to pediatric and developmental neuroscientists and neuroradiologists.

Introduction

Thalamocortical connections provide important inputs into the developing cortex during the second half of human gestation, where they play a key role in guiding cortical areal differentiation and establishing the circuitry responsible for sensory integration across the lifespan (***Jones, 2007***; ***Price et al., 2006***; ***Schummers et al., 2005***; ***Sharma et al., 2000***; ***Sur and Rubenstein, 2005***). Their importance is highlighted by previous work implicating disruptions to thalamocortical development during the perinatal period in the pathophysiology of neurodevelopmental disorders, such as schizophrenia (***Klingner et al., 2014***; ***Marenco et al., 2012***), bipolar disorder (***Anticevic et al., 2014***), and autism (***Nair et al., 2013***). Altered thalamocortical connectivity has also been described in preterm infants, and was used to predict cognitive outcome (***Ball et al., 2013***; ***Ball et al., 2015***; ***Toulmin et al., 2021***), highlighting the specific vulnerability of these pathways during the second to third trimester. Although thalamocortical development has been studied in rodents and non-human primates (***Brody et al., 1987***; ***Kostović and Jovanov-Milosević, 2006***; ***Molnár and Blakemore, 1995***; ***Yakovlev et al., 1960***) and post-mortem human tissue (***Krsnik et al., 2017***; ***Takahashi et al., 2012***; ***Wilkinson et al., 2017***), little is known about in vivo white matter maturation during fetal development.

White matter development in the late second and third trimesters of human gestation (between 21 and 37 weeks) is characterised by a sequence of precisely timed biological processes occurring in transient compartments of the fetal brain. These processes include the migration of neurons along the radial glial scaffold, accumulation of thalamocortical axons in the superficial subplate, innervation of the target cortical area, conversion of radial glial cells into astrocytes, and ensheathment of axonal fibres (***Krsnik et al., 2017***; ***Molliver et al., 1973***; ***Kostović et al., 2002***, ***Kostovic and Judas, 2006***). The challenge for in vivo neuroimaging studies is to disentangle the effect of these different neurobiological processes on the diffusion magnetic resonance imaging (dMRI) signal, to improve mechanistic insight about the transformation of transient fetal compartments into segments of developing white matter (Kostovic 2012).

Recent advances in diffusion weighted imaging now allow in vivo characterisation and estimation of white matter development during the fetal period. Tractography has been used to estimate the fetal brain's major white matter bundles and quantitatively characterise the evolution of the microstructure across the second half of gestation (***Bui et al., 2006***; ***Zanin et al., 2011***; ***Jaimes et al., 2020***; ***Jakab et al., 2015***; ***Keunen et al., 2018***; ***Khan et al., 2019***; ***Machado-Rivas et al., 2021***; ***Wilson et al., 2021***). Advanced acquisition and analysis methods enable the relative contribution of constituent tissue and fluid compartments to the diffusion signal to be estimated (***Jeurissen et al., 2014***; ***Pietsch et al., 2019***). Using this approach, previous work has identified non-linear trends in diffusion metrics over the second to third trimester (***Wilson et al., 2021***). Namely, we observed an initial decrease in tissue fraction within developing white matter between 22 and 29 weeks, which could be due to the radial glial scaffold disassembling (***Rakic, 2003***). Subsequently, we observed an increase from 30 to 36 weeks, potentially linked to more coherent fibre organisation, axonal outgrowth, and ensheathment (***Wimberger et al., 1995***; ***Back et al., 2002***; ***Haynes et al., 2005***), increasing the structural integrity of maturing white matter. Interpreting these trends is especially challenging in the rapidly developing fetal brain, because of the high sensitivity and low specificity of diffusion metrics to various co-occurring biological processes.

We hypothesise that the biological processes occurring in different fetal compartments leads to predictable changes in diffusion metrics along tracts, reflecting the appearance and resolution of these transient zones. When a mean value across the whole tract is calculated, sensitivity to the unique neurobiological properties of each transient compartment is lost. For example, in the early prenatal and mid prenatal period, the subplate is a highly water-rich compartment containing extracellular matrix, whereas the cortical plate and the deep grey matter are relatively cell dense (***Kostović, 2020***). We therefore predict that the tissue fraction would be higher in the deep grey matter and the cortical plate and lower in the subplate. We investigate this by characterising the entire trajectory of tissue composition changes between the thalamus and the cortex, to explore the role of transient fetal brain developmental structures on white matter maturational trajectories.

We acquired diffusion weighted imaging from 140 fetuses over a wide gestational age (GA) range (21–37 weeks) and use tractography to delineate five distinct thalamocortical pathways. To investigate whether the immature axonal bundles can be traced back to specific and distinct locations within thalamus, we parcellate the thalamus according to streamline connectivity (***Behrens et al., 2003***). We find consistent and distinct origins of different tracts, resembling the adult topology of thalamic nuclei (***Toulmin et al., 2015***; ***Behrens et al., 2003***) as early as 23 weeks' gestation. We then apply a multi-shell multi-tissue constrained spherical deconvolution (MSMT-CSD) diffusion model (***Jeurissen et al., 2014***) and derive tissue and fluid fraction values, charting tract-specific maturational profiles over the second to third trimester. We overlay the tracts on an atlas of transitioning fetal compartments and correlate changes in the dMRI signal across time with critical neurodevelopmental processes, such as the dissolution of the subplate and lamination of the cortical plate. We demonstrate that along-tract sampling of diffusion metrics can capture temporal and compartmental differences in the second to third trimester, reflecting the maturing neurobiology of the fetal brain described in histological studies. With these methods, we provide a detailed, accurate reference of the unique developing microstructure in each tract that improves mechanistic insight about fibre maturation, bridging the gap between MRI and histology.

Results

Estimating thalamocortical pathways using probabilistic streamline tractography

High-angular-resolution multi-shell diffusion weighted imaging (HARDI) was acquired from 140 fetuses between 21 and 37 gestational weeks (70 male, 70 female) as part of the Developing Human Connectome Project (dHCP). Data were corrected for fetal head motion and other imaging artefacts (***Christiaens et al., 2021***). Individual subject orientation density functions (ODFs) were then computed using cohort-specific fluid and 'tissue' response functions and compiled to generate weekly diffusion templates (see Materials and methods). The diffusion templates were then registered to a T2-weighted brain atlas (***Gholipour et al., 2017***) of tissue segmentations, used to generate anatomically constrained whole-brain connectomes for each gestational week

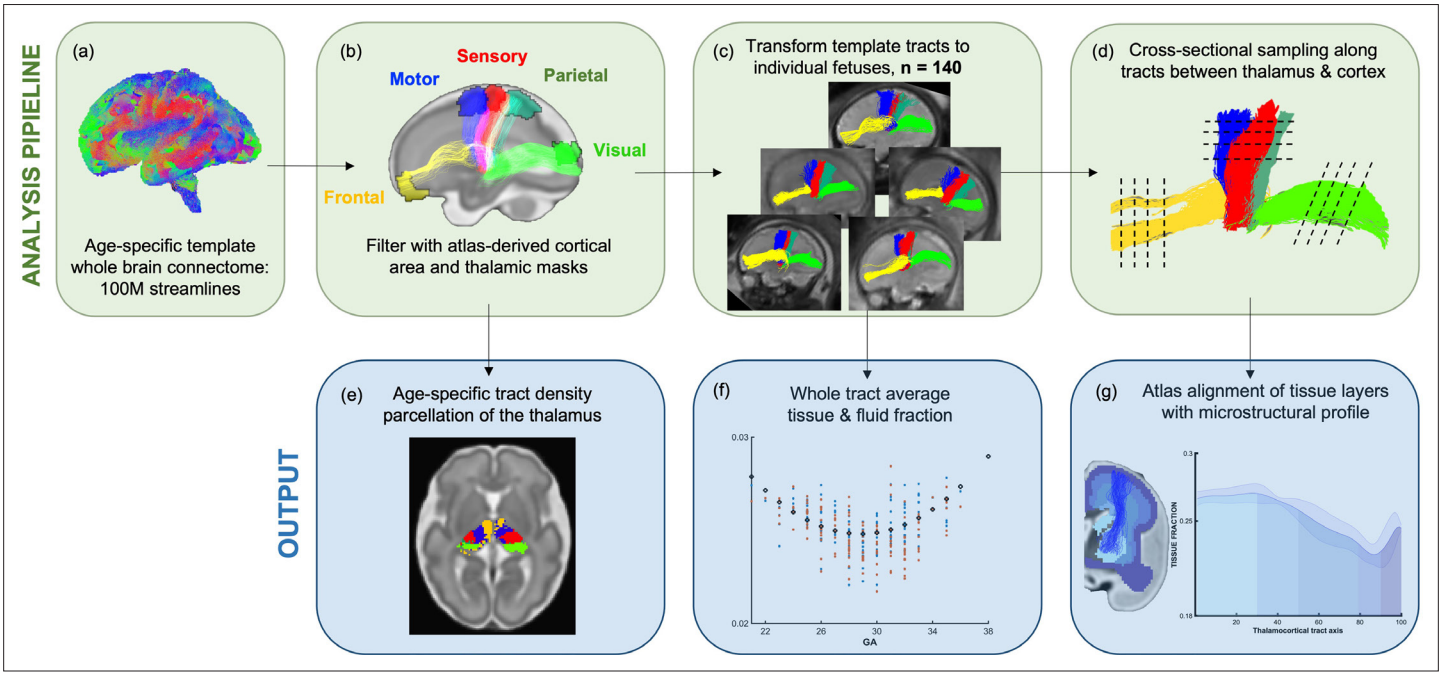

Figure 1. Methods pipeline to estimate and quantify thalamocortical tracts development. (Top row) (**a**) Whole-brain connectomes generated for each gestational week template. (**b**) Atlas-defined masks of the thalamus and cortical areas were used to extract white matter pathways of interest from the connectomes. (**c**) These pathways were transformed to the native fetal diffusion space, (**d**) the values were sampled along the tract. (**f**) Whole-tract average diffusion metrics were calculated or (**g**) values sampled along the tract were aligned to an atlas of transient fetal compartments.

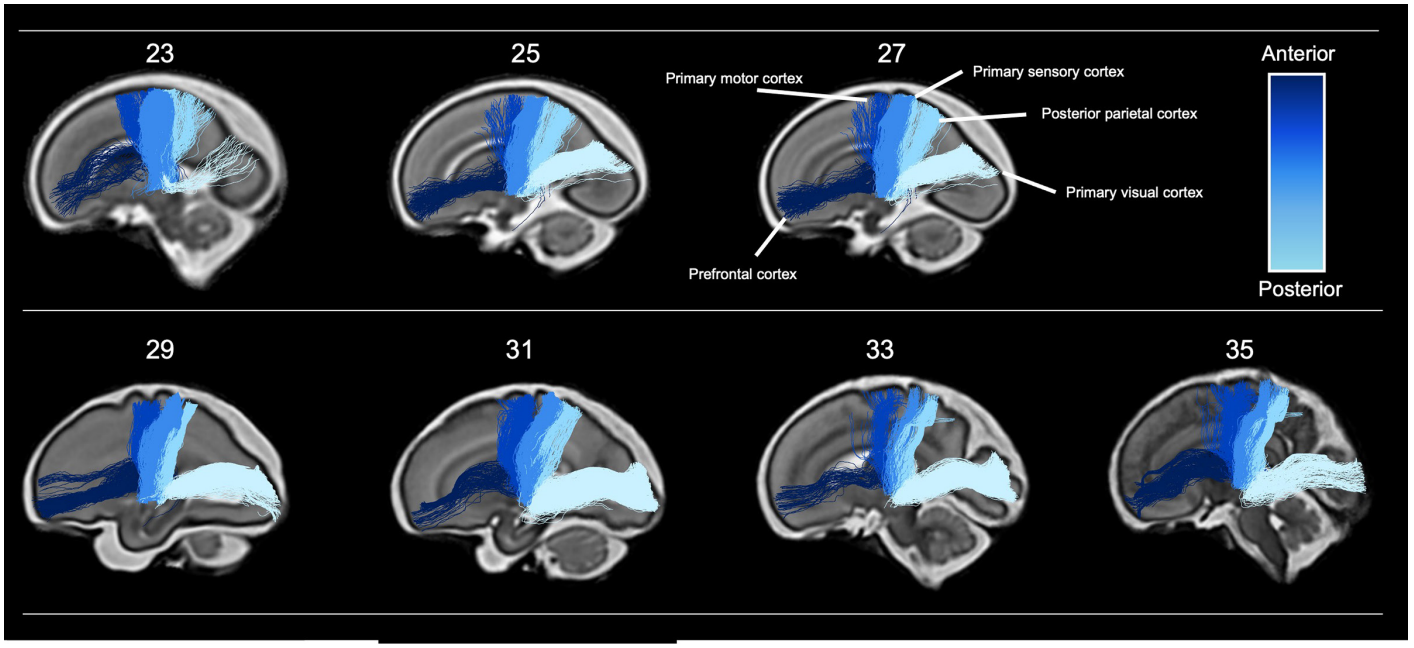

Figure 2. Tractography of thalamocortical pathways in different gestational week templates across the second to third trimester. Tracts project to five different cortical areas, the prefrontal cortex, primary motor cortex, primary sensory cortex, posterior parietal cortex, and primary visual cortex, coloured according to the anterior-posterior axis.

(***Smith et al., 2012***; ***Tournier et al., 2019***). To constrain our investigation, we selected thalamocortical pathways that are at a critical stage in their development and are vulnerable to external influences in the second to third trimester (***Batalle et al., 2017***; ***Nosarti et al., 2014***; ***Raybaud et al., 2013***), the anterior thalamic radiation (AT), thalamic-motor tract (TM), thalamic-sensory tract (TS), posterior parietal tract (PP), and optic radiation (OR). The connectomes were filtered down to the pathways of interest using inclusion regions defined by the T2 atlas, including the thalamus and specific cortical areas (***Figure 1***). These included the primary motor cortex, primary sensory cortex, posterior parietal cortex, dorso-lateral prefrontal cortex, and the primary visual cortex. With this method, we were able to delineate five major thalamocortical pathways in each gestational week. To keep regions of interest more consistent across the cohort, we grouped all cases into 2-weekly intervals, starting at 23 weeks (***Figure 2***), replicating methods used previously (***Wilson et al., 2021***).

Structural connectivity parcellation of the fetal thalamus resembles adult topology of thalamic nuclei

Tract density imaging (***Calamante et al., 2010***) was used in each ODF template to explore whether the different cortical areas were connected to distinct, specific regions of the thalamus (***Figure 3a***). We found that for all ages, there was symmetrical topographical representation of the cortical regions of interest in the thalamus. Furthermore, they spatially corresponded to the adult organisation of thalamic nuclei, demonstrated by the schematic (***Figure 3a***) which is based on Morel's thalamus and other connectivity-derived parcellations from adult imaging studies (***Morel et al., 1997***; ***Najdenovska et al., 2018***; ***Niemann et al., 2000***). The tract projecting to the prefrontal cortex was connected to the anterior thalamus and in the younger ages (23–29 weeks) also to the medial thalamus. In the older templates (31, 33, and 35 weeks), frontal connectivity was more localised to the anterior thalamus and less evident in the medial area. There were distinct but neighbouring areas in the ventral thalamus connecting to the sensory and motor cortical areas, the motor-connected thalamic region being more frontal. The connectivity of the posterior parietal area was in the posterior part of the thalamus, and the most posterior voxels in the thalamic mask projected to the primary visual cortex.

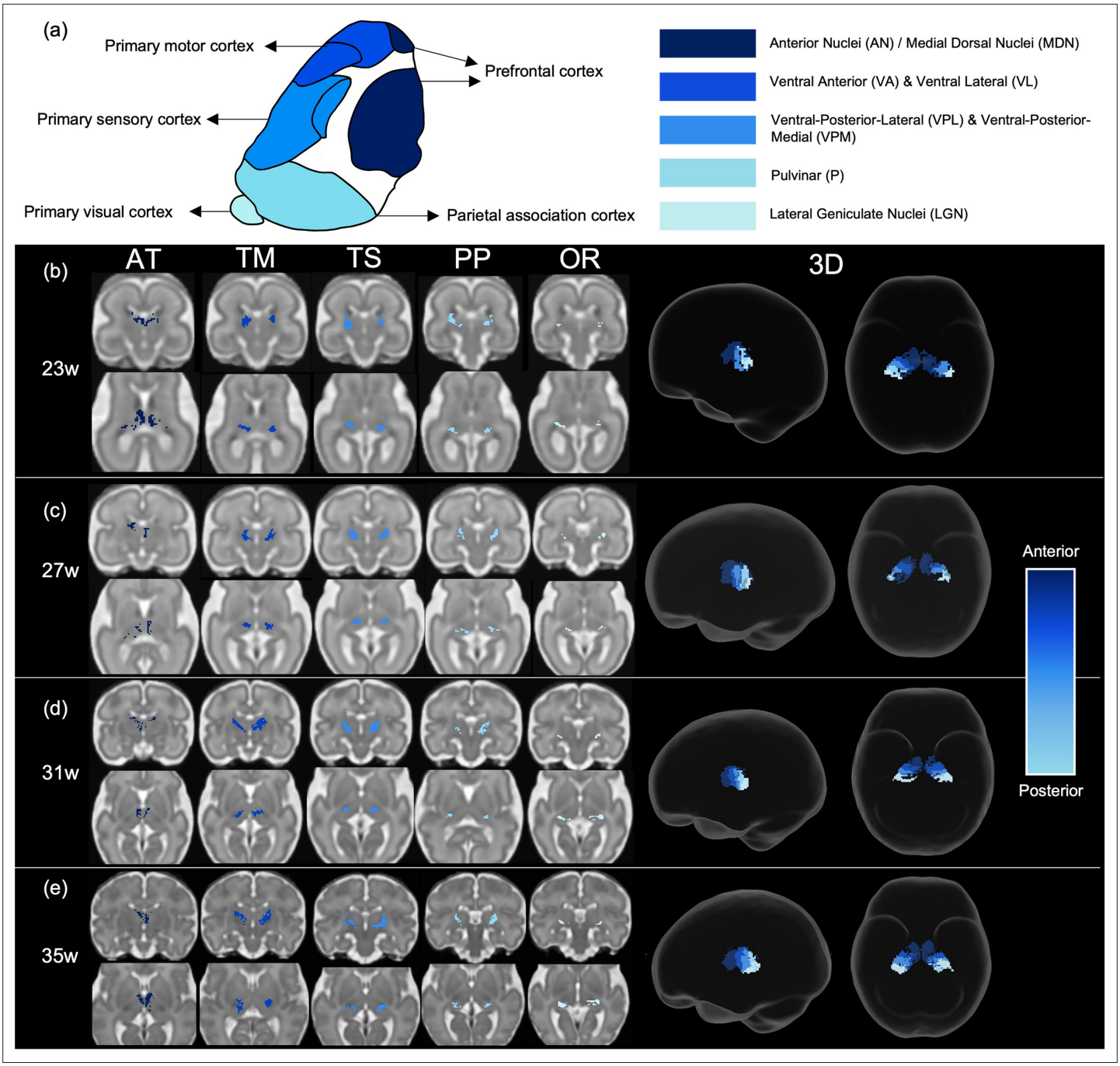

Figure 3. Tract density imaging parcellation of thalamus at different fetal ages. (**a**) A schematic of expected cortical connectivity arrangement across the thalamus, based on Morel's parcellation of the adult thalamic nuclei. (**b**) Axial slices of thalamic parcellation, thresholded for the top 20% of voxels, colour-coded according to streamline connectivity of different tracts at 23 weeks, (**c**) 27 weeks, (**d**) 31 weeks, and (**e**) 35 weeks.

Whole-tract average diffusion metrics have a characteristic U-shaped trend across the second to third trimester

The thalamocortical pathways were transformed from the age-matched templates to the native subject space for 140 fetal subjects (***Figure 4a***). The MSMT-CSD-derived voxel-average tissue and fluid ODF values were sampled along the warped group-average streamline tracts. Tract-specific values were derived by averaging these for each tract in each subject, replicating the approach that has been used in previous fetal studies (***Wilson et al., 2021***). The values for each tract were plotted against the GA

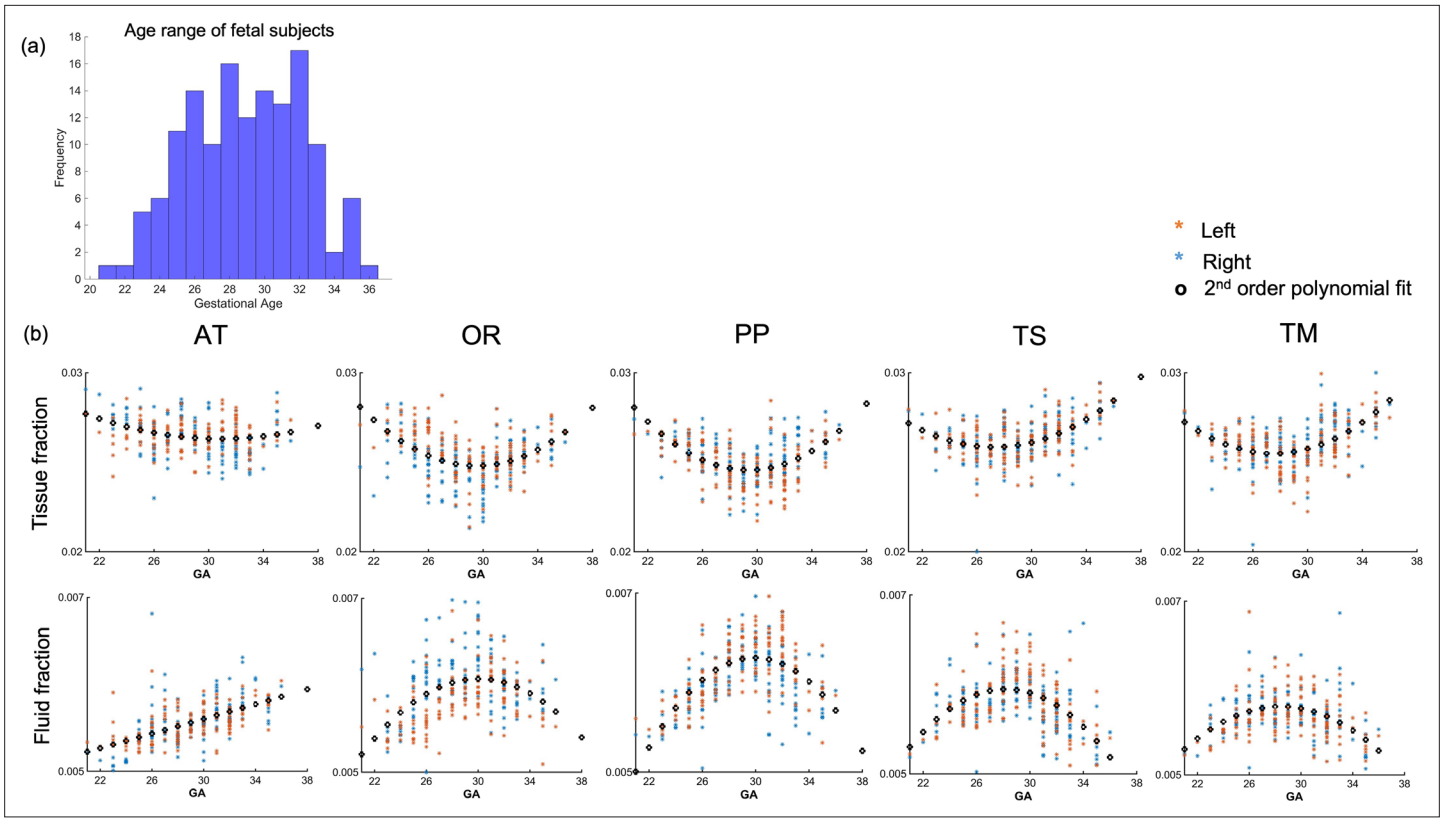

Figure 4. Diffusion metric age trajectories for each tract. (**a**) Distribution of age among the fetal cohort (n=140) in gestational weeks. (**b**) Whole-tract average tissue (top) and fluid fractions (bottom) for each subject in the left (orange) and right (blue) hemisphere, plotted against gestational age (GA) of the subject, best fit by second-order polynomials (AT = anterior thalamic radiation, OR = optic radiation, PP = posterior parietal tract, TS = thalamic-sensory tract, TM = thalamic-motor tract).

The online version of this article includes the following figure supplement(s) for figure 4:

Figure supplement 1. Whole-tract average of diffusion tensor metrics in the fetal cohort (n=140), fractional anisotropy (FA), and mean diffusivity (MD), in thalamocortical tracts across gestational age (every other week shown).

of the subject. The Akaike information criterion suggested second-order polynomial relationships for all tracts for both tissue and fluid fraction metrics, except the fluid fraction in the AT which is linear (***Figure 4b***). Diffusion tensor metrics also displayed similar age-related polynomial trends (***Figure 4—figure supplement 1***). We compared male vs. female (two-sample test) in each gestational week and found no significant differences (p>0.1).

Along-tract sampling reveals evolving properties of fetal brain transient compartments

To explore the origins of these trends in diffusion metrics, the values of tissue and fluid fraction were sampled in subject space at 100 equidistant intervals between the thalamus and the cortex. Tissue and fluid fraction are scaled jointly per scan such that they are approximately reciprocal of one another across the brain using a cubic polynomial spatial model (***Pietsch et al., 2019***). In each subject, we sampled the tissue and fluid fraction values beneath the streamlines from the thalamus to the cortex, plotting the microstructural tissue composition against the distance from the thalamus (***Figure 5***). We found that trajectories changed gradually between gestational weeks, and therefore we grouped them to match previous histological studies that define this fetal period according to three developmental windows, early (21–25.5 weeks), mid (26–31.5 weeks), and late (32–36 weeks) prenatal period (***Kostović, 2020***; ***Appendix 1—figures 5 and 6***). When comparing the microstructural profiles of all the tracts in the different periods, the motor, sensory, and parietal tracts shared similar trajectories, whilst those in the AT and OR tracts were more distinct (***Figure 5a, b, and c*** and ***Figure 5—figure supplement 1a,b***).

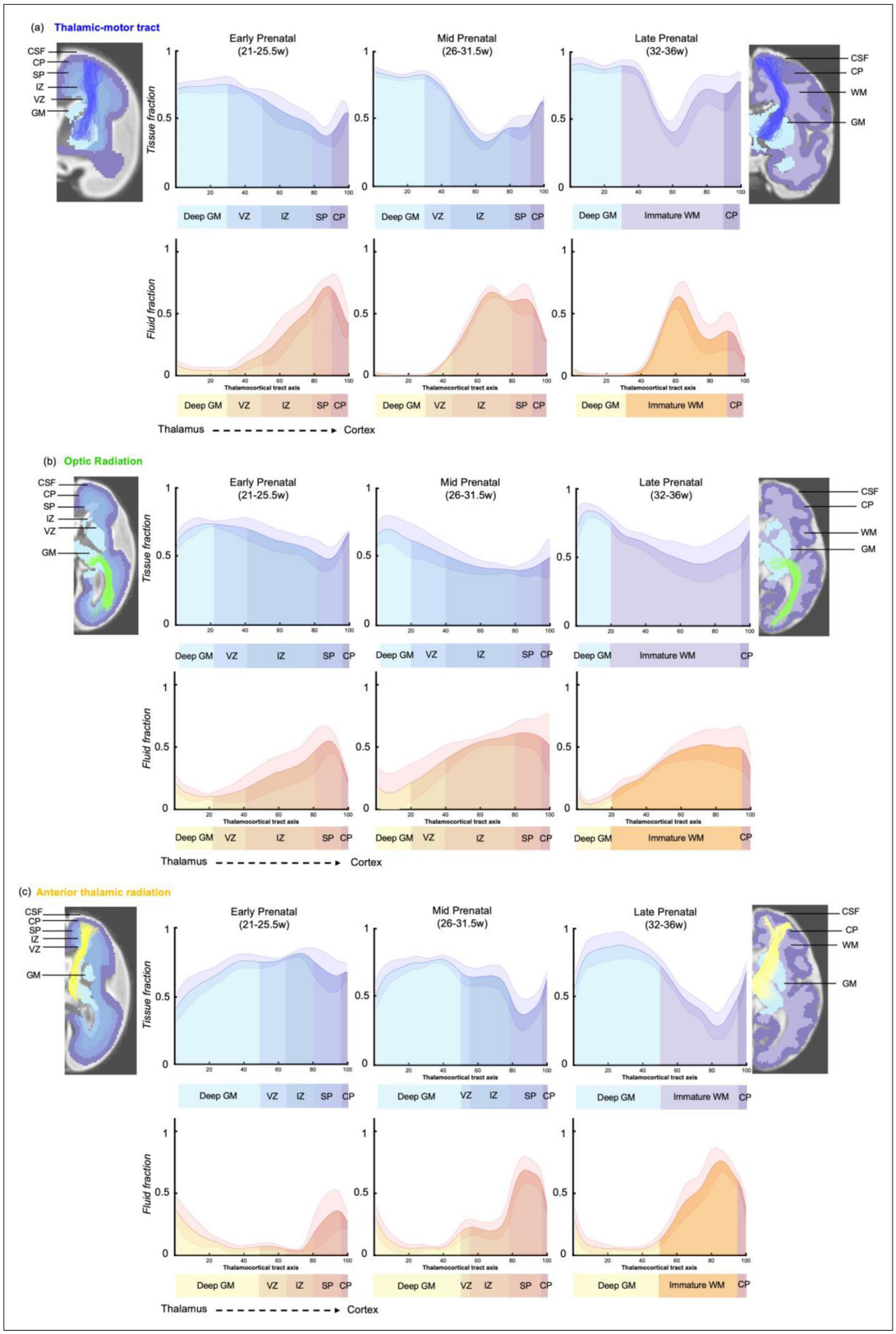

Figure 5. Microstructural composition of fetal compartments traversed by developing thalamic white matter. Tracts were overlayed on the atlas of fetal compartments (examples highlight the difference between fetal brain structure in early prenatal [25 weeks] on far left, and late prenatal [35 weeks] on far right). Tissue fraction trends (top row) and fluid fraction trends (bottom row), normalised to 1, between the thalamus and cortex (thalamocortical tract axis)

Figure 5 continued on next page

Figure 5 continued

for the (**a**) thalamic-motor tract, (**b**) optic radiation, and (**c**) anterior thalamic radiation. Subjects were grouped by age, and average trajectories plotted for early prenatal (22–25.5 weeks), mid prenatal (26–31.5 weeks), late prenatal (32–36 weeks). Error bars represent the standard deviation among all subjects in each group. Atlas-derived tissue boundaries are marked on the trajectories to reveal the changing tissue properties of each layer between early, mid, and late prenatal development (cortical spinal fluid = CSF, cortical plate = CP, subplate = SP, intermediate zone = IZ, ventricular zone = VZ, deep grey matter = GM, immature white matter = WM).

The online version of this article includes the following figure supplement(s) for figure 5:

Figure supplement 1. Microstructural composition of fetal compartments traversed by developing thalamic white matter.

To improve our ability to corroborate changes in the dMRI signal with observations from histological studies, we mapped the maturational trajectories to an atlas of fetal brain compartments (***Gholipour et al., 2017***) and overlayed the boundaries of these compartments on the tissue and fluid fraction trajectories (***Figure 5***). By overlaying the tracts on the atlas, and corroborating each sampling segment with an atlas region, we could characterise the diffusion properties of the different fetal compartments independent of their change in size across gestation. Tissue fraction values in the deep grey matter and the cortical plate areas increased with GA in all tracts. This increase was most marked in the tracts terminating in superior areas of the brain (motor, sensory, and superior parietal cortex) (***Figure 5a*** TM, ***Figure 5—figure supplement 1*** (a) TS and (b) PP). The tissue fraction of the ventricular and intermediate zones decreased between the early and mid prenatal period, in all tracts. This decrease was very pronounced in the motor, sensory, and superior parietal tracts. The subplate tissue fraction changes were more tract specific. In the subplate of sensorimotor and parietal tracts, there was initially a very high fluid fraction and low tissue fraction, which transitions across the second to third trimester, increasing in tissue fraction from early to mid and then to late prenatal. Whereas in the AT, there was a decrease in subplate tissue fraction with GA (and a reciprocal increase in fluid fraction). In the OR, the subplate tissue fraction decreases between early and mid prenatal to then increase again in late prenatal. Highest tissue fractions were generally observed in the ventricular zone, with the lowest tissue fraction in the subplate area. To statistically test if there was a difference between the values in each compartment across GA, we correlated the tissue fraction values against age for each of the 100 sampling points. After correcting for multiple comparisons, points 1–16, 24–42, and 70–100 had significant linear correlations with age. Sampling points 43–69 had significant second-order polynomial relationships with age.

Discussion

In this work, we studied in utero development of five distinct thalamocortical pathways using state-of-the-art dMRI methods and bespoke pre-processing pipeline (***Christiaens et al., 2019a***; ***Cordero-Grande et al., 2019***; ***Hutter et al., 2018a***; ***Pietsch et al., 2019***; ***Wilson et al., 2021***) in 140 fetuses aged 21–37 weeks' gestation. We show that these pathways connect to distinct thalamic nuclei, which could be clearly defined at group level even at 23 weeks. To disentangle the impact of different neurobiological processes on diffusion metrics, we characterised the tissue composition profile along each of the thalamocortical tracts as they traverse the different developmental tissue layers of the fetal brain. We used MSMT-CSD to model this fetal DWI dataset because it does not mandate a specific set of b-values. The technique exploits the unique b-value dependencies of different tissue types, and so depends inherently on the characteristics of the tissue in the fetal brain. The distinct properties of different fetal compartments after the application of MSMT-CSD are highlighted by the ODFs (***Appendix 1—figure 4***). Readers are directed to ***Tournier et al., 2019***, for a more comprehensive review of the optimisation process involved to select appropriate b-shell values for the acquisition.

We found that the spatiotemporal changes in the diffusion signal reflected known developmental processes that take place between the early, mid, and late prenatal period. The early period is characterised by higher tissue fractions in the middle of the tract, where there is a radial scaffold for migrating neurons. As this scaffold dissipates in the mid prenatal period, this is accompanied by a reduction in the tissue fraction in the middle of the tract, and an increase in tissue fraction towards the termination of the tracts as the neurons of the cortical plate mature. Finally in the late prenatal period,

we observe the highest tissue fraction values at the start and end of the axis, as the pre-myelination phase of white matter development commences. This study demonstrates how the dMRI signal can be modelled to create in vivo spatiotemporal trajectories which relate to underlying neurobiological properties and are consistent with described trends from post-mortem histology (***Kostović, 2020***).

Early embryonic patterning of gene expression and cell division in the thalamus provide a template for specialised nuclei to emerge over the course of development, such that specific cells eventually occupy distinct locations within the thalamus (***Clascá et al., 2012***; ***Nakagawa, 2019***, ***Kostovic and Goldman-Rakic, 1983***). Rodent studies labelling the embryonic thalamus demonstrated that there is a characteristic topography of thalamic projections which roughly exists at their time of arrival; anterior to posterior movement along the convexity of the cortex is represented in a medial-to-lateral axis within the thalamus, while ventral-dorsal movement across the cortex is represented in an anterior-to-posterior axis within the thalamus (***Molnár et al., 1998***; ***Molnár et al., 2012***). Thalamocortical tracts emerge over the same timescale as the thalamus parcellates and matures into its specialised group of nuclei (***Clascá et al., 2012***). Although the topography of thalamic nuclei and their cortical connectivity is acquired embryonically, no in vivo parcellation of the thalamus in the fetal brain has been published. Using tract density imaging, we observed that the cortical areas were connected to specific thalamic regions, organised in an anterior-posterior axis. This anterior-posterior representation of cortical connectivity in the thalamus was consistent across the second to third trimester and is in accordance with the topology of thalamic nuclei described in rodent studies and histology (***Molnár and Blakemore, 1995***; ***Molnár et al., 1998***).

In addition, our fetal structural connectivity parcellation resembles the functionally derived thalamic parcellation in neonates, supporting the view that there is a strong association between structure and function in thalamocortical circuitry that begins early in life (***Johansen-Berg et al., 2005***; ***Toulmin et al., 2015***; ***Alcauter et al., 2014***). However, it is worth noting that this thalamic parcellation is dependent on streamline count through a voxel, and in the fetal brain streamlines are prone to spurious detection. This limitation is particularly relevant in the youngest fetuses, where we observe an extremely dense connectome (due to a fixed number of streamlines in a smaller brain) but there are very few coherent axonal bundles, so tracts might be overrepresented in the thalamic parcellation. The topography of thalamic nuclei is also not static during the embryonic and fetal period (***Le Gros Clark, 1936***), as pulvinar size increases and the dorsal lateral geniculate nucleus shifts its position from dorsolateral to ventromedial (***Rakic, 1977***; ***Mojsilović and Zecević, 1991***). However, the image resolution of this study and the timespan in development over which this data was collected limit us from visualising these differences across age.

Recent studies characterising developing white matter pathways using human fetal MRI identified second-order polynomial maturational trends in diffusion metrics unique to this developmental period (***Wilson et al., 2021***; ***Machado-Rivas et al., 2021***). Here, we replicated these methods with a different group of tracts and found the same U-shaped trends in thalamocortical white matter development. The inflection point at around 29–30 weeks was hypothesised to be the result of the dissipating radial glial scaffold followed by the pre-myelination phase of white matter development (***Wilson et al., 2021***; ***Machado-Rivas et al., 2021***). The sensitivity of HARDI to radially organised structure in the fetal brain has been described by previous studies (***Miyazaki et al., 2016***; ***Takahashi et al., 2012***; ***Xu et al., 2014***) combining it with post-mortem tissue analysis to show that radially coherent diffusion signal corresponded to radial glial fibres in the early prenatal period, transitioning to cortico-cortical fibres around 30 weeks, coinciding with the appearance of astrocytes (***Takahashi et al., 2012***; ***Xu et al., 2014***). However, with whole-tract average values, it is not possible to establish the precise effect of different neurodevelopmental processes on diffusion metrics across gestation.

To address this ambiguity, we characterised the entire trajectory of tissue composition changes between the thalamus and the cortex. We found that age-related changes in the tissue and fluid fraction along the tracts concurred with histological observations (***Kostović and Judas, 2010***). During the early prenatal period (22–25.5 GW), neuronal precursors migrate along the radial glial scaffold from proliferative zones to their destination in the cortical plate and thalamocortical axons accumulate in the superficial subplate, entering a 'waiting phase', forming transient synaptic connections (***Ghosh et al., 1990***; ***Kostovic and Rakic, 1984***; ***Kostovic and Rakic, 1990***). In terms of the diffusion signal, this strongly aligned microstructure of the radial glia is represented in our results by a higher tissue fraction in the transient compartments containing the most migratory cells (such as the VZ, IZ)

(**Kostović and Judas, 2010**). Conversely, we observe the lowest tissue fraction in the early prenatal SP, which predominantly contains hydrophilic extracellular matrix, as demonstrated by rodent and non-human primate studies (**Allendoerfer and Shatz, 1994**; **Miller et al., 2014**; **Molnár and Hoerder-Suabedissen, 2016**).

By the mid prenatal period (26–31.5 weeks), we observe increased tissue fraction in the cortical plate, coinciding with the innervation of the cortical plate by thalamocortical axons, increasing soma volume and dendritic branching of CP neurons and CP synaptogenesis (**Huttenlocher, 1979**; **Mrzljak et al., 1992**; **Huttenlocher and Dabholkar, 1997**). We also observe increased tissue fraction in the SP zone in the mid prenatal period, consistent with histological observations of increased coherence of axonal fibres between cortical areas (**Takahashi et al., 2012**; **Xu et al., 2014**). The tissue fraction in the VZ and IZ decreases compared to the early prenatal period, corresponding to the timeframe when the radial glial scaffold dissipates (**Kinney et al., 1988**; **Back et al., 2001**; **Haynes et al., 2005**).

From the mid to late prenatal period, there is a marked increase in tissue fraction in last third of the axis between thalamus and cortex. By this point in development, the radial glia have converted into oligodendrocyte precursor cells which ensheath the axonal fibres to commence pre-myelination, enhancing the structural integrity of the fibre pathways (**Back et al., 2001**; **Back et al., 2002**; **Haynes et al., 2005**; **Kinney et al., 1988**; **Kinney et al., 1994**). A previous study in perinatal rabbits has shown that this oligodendrocyte lineage progression correlates with diffusion metrics (**Drobyshevsky et al., 2005**), suggesting it is likely to contribute to the increased tissue fraction we observe in the late prenatal period. The tissue fraction increase in the CP area is consistent in time with the lamination of the CP, the elaboration of thalamocortical terminals in layer IV, and a rapid growth of basal dendrites of layer III and V pyramidal neurons (**Kostović and Jovanov-Milosević, 2006**; **Krsnik et al., 2017**; **Molliver et al., 1973**). These high tissue fraction values at the origin and termination of the tracts suggest co-maturation between ascending and descending pathways between the thalamus and cortex to eventually form continuous, structurally mature fibre bundles. This concept was proposed in the 1990s by Blakemore and Molnar, termed the 'handshake hypothesis'. They suggested that thalamocortical pathways ascending through the internal capsule project to their cortical targets with assistance from reciprocal descending cortical pathways (**Molnár and Blakemore, 1995**). We hypothesise that continuing this analysis over subsequent weeks into the neonatal period would lead to an increasing tissue fraction in the middle of the axis, as fibre bundles become more uniformly structurally mature and the subplate completely resolves (**Kinney et al., 1988**; **Haynes et al., 2005**; **Kostović and Jovanov-Milosević, 2006**).

We observed that tracts terminating superiorly (motor, sensory, and parietal) shared very similar trajectories in the early, mid, and late periods. However, the OR and the AT had more distinct trajectories. The microstructural change along the AT suggests increasing tissue fraction between the deep grey matter, VZ and IZ. We hypothesise that the high tissue fraction in the IZ is due to densely packed ascending and descending bundles within the anterior limb of the internal capsule (**Emos et al., 2022**). The precise timeline for outgrowth and intermingling of the thalamocortical and corticothalamic projections remains ambiguous, and appears to be different between rodents and non-human primates (**Alzu'bi et al., 2019**).

On the other hand, the OR traverses the deep parietal lobe along the border of the lateral ventricle and has smoother transitions in tissue fraction between the fetal compartments. This is likely due to the tract area running more parallel to the tissue interfaces. Another explanation for the regional differences in microstructural properties is the variation in subplate remnants. In the late prenatal trajectories, all tracts except the OR have a large dip in tissue fraction along the tract. In the primary visual cortex, the subplate disappears during the final weeks of gestation, whereas in the somatosensory cortex there are still subplate neurons present in term-born neonates (**Kostovic and Rakic, 1990**) and the subplate of the pre-frontal associative cortex gradually disappears over the 6 postnatal months. Therefore, the peaks of fluid fraction in the frontal and sensory trajectories might reflect the lasting presence of subplate in these areas (**Kostović and Jovanov-Milosević, 2006**; **Kostovic and Rakic, 1990**).

There are several important considerations to our work which may limit the interpretation of our findings. MRI has an inherently low signal:noise ratio as signal attenuation is deliberately introduced and EPI acquisitions are highly susceptible to motion and distortion artefacts. Furthermore, the biophysical properties of the fetal environment introduce a series of additional inter-dependent

challenges for acquiring high-quality dMRI data (***Christiaens et al., 2019a***; ***Christiaens et al., 2019b***, ***Tournier et al., 2020***). In utero imaging methods must adapt and account for unpredictable, sometimes abrupt motion of fetus, in addition to the motion introduced by maternal breathing. Achieving even coverage of the magnetic coil is challenging due to varying fetal and maternal positions inside the scanner, introducing unique bias fields for every subject. The dHCP acquisition protocol and preprocessing pipelines have incorporated dynamic distortion and motion correction algorithms that were designed to specifically tackle the unique artefacts-associated imaging fetuses (***Deprez et al., 2020***; ***Cordero-Grande et al., 2018***; ***Cordero-Grande et al., 2019***; ***Christiaens et al., 2019a***; ***Christiaens et al., 2019b***; ***Hutter et al., 2018b***; ***Price et al., 2019***). However, even after the extensive correction procedures, there is still some residual motion and distortion in the data. For a more extensive and comprehensive review of challenges associated specifically with in utero diffusion imaging and constructive suggestions to address them, readers are directed to ***Christiaens et al., 2019b***.

The conclusions that can be drawn from analysing the diffusion MR signal are limited more generally by the level of noise and lack of directionality in the signal, and therefore we are not able to distinguish between ascending and descending thalamic projections as they develop. The fibre-tracking process itself is also very sensitive to the residual motion and distortion in fetal data, producing highly variable results in terms of streamline count per tract. Therefore, the metrics generally used in this field to investigate fibre bundle morphology, such as streamline count, a proxy for 'innervation density', are not an accurate, quantitative measure (***Calamante, 2019***) and cannot be reliably used to assess fibre morphology. Consequently, we have just used tractography to delineate regions of interest and used the signal contrast in the diffusion maps to quantify microstructure.

The methods described allow the direct study of the maturational effects of the subplate and intermediate zones, which are known to represent critical substrates for early synaptogenesis and the spatial guidance of thalamocortical axons (***Ghosh et al., 1990***). Damage to this essential structural framework for developing cortical circuitry has been implicated in the origins of numerous developmental disorders and is suspected to underly the altered structural and functional connectivity of the thalamus in preterm infants (***Back and Volpe, 1997***; ***Volpe, 2001***; ***Volpe, 2009***; ***Hüppi et al., 2001***; ***Counsell et al., 2003***; ***Hadders-Algra et al., 2017***; ***Mathur and Inder, 2009***; ***Toulmin et al., 2015***; ***Ball et al., 2012***; ***Ball et al., 2015***). It is therefore critical to use clinically relevant tools, such as in utero MRI, to relate the microstructural properties of these transient fetal compartments to neurobiological processes. This improves mechanistic insight about both healthy white matter maturation and the developmental origins of white matter pathologies.

With this study we explore the development of thalamocortical white matter by quantifying microstructure in the different layers of the fetal brain. Using diffusion metrics, we characterise the emergence of structural connectivity from the thalamus to spatially and functionally distinct cortical brain regions. We observe correlations between the transitioning tissue components and key neurobiological processes in white matter development. By providing a detailed normative reference of MR signal change during the second to third trimester, this will help future studies to identify if the tissue properties of specific compartments are affected by preterm birth or other perinatal injury. To this effect, all fetal MRI data is made available to the research community.

Materials and methods

Sample

The study was approved by the UK Health Research Authority (Research Ethics Committee reference number: 14/LO/1169) and written parental consent was obtained in every case for imaging and open data release of the anonymised data. All data was acquired in St Thomas Hospital, London, United Kingdom. The sociodemographic characteristics of this sample are representative of the diversity in the London population (see ***Appendix 1—figure 1***).

Acquisition, pre-processing, and quality control

GA was determined by sonography at 12 post-ovulatory weeks as part of routine clinical care. Three-hundred fetal MRI datasets were acquired with a Philips Achieva 3T system, with a 32-channel cardiac coil in maternal supine position. dMRI data was collected with a combined spin echo and field echo (SAFE) sequence (***Hutter et al., 2018a***, ***Cordero-Grande et al., 2018***) at 2 mm isotropic resolution,

using a multi-shell diffusion encoding that consists of 15 volumes at b=0 s/mm^2, 46 volumes at b=400 s/mm^2, and 80 volumes at b=1000 s/mm^2 lasting 14 min (***Christiaens et al., 2019a***). For more insight on the choice of b-shell values for this acquisition, readers are directed to ***Appendix 1—figure 4*** (***Tournier et al., 2019***). The protocol also included the collection of structural T2w, T1w, and fMRI data, for a total imaging time of approximately 45 min (***Price et al., 2019***).

dMRI data were processed using a bespoke pipeline (***Christiaens et al., 2019a***) that includes generalised singular value shrinkage image denoising and debiasing from complex data (***Cordero-Grande et al., 2019***), dynamic distortion correction of susceptibility-induced B0 field changes using the SAFE information (***Ghiglia and Romero, 1994***; ***Cordero-Grande et al., 2018***; ***Hutter et al., 2018b***) and slice-to-volume motion correction based on a multi-shell spherical harmonics and radial decomposition (SHARD) representation (***Christiaens et al., 2021***). Quality control (QC) was implemented using summary metrics based on the gradient of the motion parameters over time and the percentage of slice dropouts in the data (***Christiaens et al., 2021***). This was followed up with expert visual assessment, which considered any residual or uncorrected artefacts. Image sharpness, residual distortion, and motion artefacts were visually assessed and scored between 0 and 3, with 0 (=failure, e.g. because the subject moved out of the field of view) to 3 (=high quality), based on the mean b=0, b=400, and b=1000 images and the ODFs estimated with MSMT-CSD. See ***Appendix 1—figure 2*** for examples of subjects that were excluded. Both DWI and T2 for each fetus were required to facilitate co-registration to template space via a structural intermediate. After co-registration, the QC scores were checked and validated again by different authors (MP, AU, SW), only subjects scoring 2 or 3 that were well aligned in T2 space were admitted to this study. Based on the above criteria, 140 of the 300 subjects that were pre-processed were classified as high-quality reconstructions for both DWI and T2 modalities. Post hoc analysis was also conducted to check if any motion-related parameters correlate with GA (***Appendix 1—figure 3***).

Diffusion modelling and template generation

All diffusion processing and tractography was done using MRtrix3 (***Tournier et al., 2019***). To deconvolve the tissue and fluid components of the diffusion data, white matter and cortical spinal fluid (CSF) response functions were estimated for each subject using T2-based tissue segmentations as inclusion areas. White matter response functions were extracted from areas of relatively mature white matter (corticospinal tract and corpus callosum) using the 'tournier' algorithm and CSF responses using the 'dhollander' algorithm in MRtrix3 (***Jeurissen et al., 2014***; ***Tournier et al., 2019***; ***Tournier et al., 2013***). The white matter response functions of the oldest 20 subjects were averaged to obtain a group-average response function of relatively mature white matter, whilst a group-average CSF response function was calculated from the whole cohort of subjects. dMRI signal of all subjects was subsequently deconvolved into tissue ODF and fluid components using MSMT-CSD and the group-average white matter and CSF response functions (***Jeurissen et al., 2014***), and resulting components were intensity normalised for each subject (***Raffelt et al., 2011***). Subject ODFs warped into weekly templates through a series of coarse pose normalisation and non-linear diffeomorphic image registration steps (***Jenkinson et al., 2002***; ***Raffelt et al., 2011***; ***Pietsch, 2018***). These transformations were composed to obtain pairs of inverse consistent diffeomorphic subject-to-template and template-to subject warps.

Connectome generation and tractography

The ODF templates were co-registered to the Boston T2-fetal atlas (***Gholipour et al., 2017***) using non-linear registration (***Avants et al., 2008***). The tissue segmentations of the cortex, white matter, and deep grey matter were used for anatomically constrained tractography to generate whole-brain structural connectomes of 100 M streamlines in each gestational week (***Smith et al., 2012***; ***Tournier et al., 2019***). The connectomes were filtered down to 10 M streamlines using the SIFT algorithm (***Smith et al., 2013***; ***Tournier et al., 2019***), so that the number of streamlines connecting the two regions are approximately proportional to the cross-sectional area of the fibres connecting them (***Smith et al., 2013***). In each weekly template, thalamocortical pathways of interest were defined in both hemispheres by filtering the connectome using seed regions derived from the Boston T2-fetal atlas (***Gholipour et al., 2017***), including the thalamus, primary motor cortex, primary sensory cortex, posterior parietal cortex, dorso-lateral prefrontal cortex, and primary visual cortex. We also used

additional ROIs to exclude spurious streamlines that were projecting away from the expected path of the tract (e.g. to exclude callosal fibres from the TM).

Tract density parcellation of thalamus

Tckmap was used to identify which voxels in the thalamus mask were traversed by the streamlines of each tract (***Calamante et al., 2010***). The tract density maps were merged using FSL (***Jenkinson et al., 2012***) and a colour-coded parcellation volume was constructed reflecting the maximum density tract for each voxel. For visualisation, the tract density maps for each tract were thresholded at 80%, only to include voxels with the highest streamline connectivity.

Extracting tissue and fluid fraction values

To extract diffusion metrics for analysis, tracts were transformed from the templates to age-matched subject space to be overlaid onto the normalised fluid ODF and the normalised tissue ODF. The mean value within the segmented tracts was calculated to give the tissue and fluid fractions.

Microstructural profiling

In each template, thalamocortical tracts were filtered so all the streamlines for each tract were of the same length, to ensure even sampling intervals along them. All template tracts were then registered into a standard space and resampled to 100 points, before being transformed to individual subjects and overlaid on the normalised tissue and fluid fraction maps. The average value for each sampling point was calculated to create a microstructural profile along the path between the thalamus and the cortical plate. To provide a reference for microstructural differences between fetal brain compartments, tracts were overlaid on the atlas-derived tissue parcellations. The value of the tissue labels underlying the tract were used to establish which sampling points corresponded to each fetal compartment. These boundaries between compartments were then used to label the plots in ***Figure 5***.

Acknowledgements

We thank the patients who agreed to participate in this work and the staff of St Thomas' Hospital London. This work was supported by the European Research Council under the European Union Seventh Framework Programme (FP/2007–2013)/ERC Grant Agreement No. 319456. We acknowledge infrastructure support from the National Institute for Health Research (NIHR) Mental Health Biomedical Research Centre (BRC) at South London and Maudsley NHS Foundation Trust, King's College London, and the NIHR-BRC at Guy's and St Thomas' NHS Foundation Trust. We also acknowledge grant support in part from the Wellcome Engineering and Physical Sciences Research Council (EPSRC) Centre for Medical Engineering at King's College London (WT 203148/Z/16/Z) and the Medical Research Council (UK) (MR/K006355/1) and (MR/L011530/1). SW was supported by PhD funding from the UK Medical Research Council/Sackler Foundation (MR/P502108/1). JO is supported by a Sir Henry Dale Fellowship jointly funded by the Wellcome Trust and the Royal Society (206675/Z/17/Z). JO, MR, ADE, JO, and TA received support from the Medical Research Council Centre for Neurodevelopmental Disorders, King's College London (MR/N026063/1). TA was supported by an MRC Clinician Scientist Fellowship (MR/P008712/1). VK and TA were supported by an MRC Transition Support Award (MR/V036874/1). Support for this work was also provided by the NIHR-BRC at Kings College London, Guy's and St Thomas' NHS Foundation Trust in partnership with King's College London, and King's College Hospital NHS Foundation Trust.

Additional information

Funding

Funder	Grant reference number	Author
European Research Council	Seventh Framework Programme: FP/2007/2013	Maximilian Pietsch Lucilio Cordero-Grande Daan Christiaens Vyacheslav R Karolis Vanessa Kyriakopoulou Anthony N Price Jana Hutter Emer J Hughes Jacques-Donald Tournier Joseph V Hajnal A David Edwards
Wellcome Trust	Sir Henry Dale Fellowship: 206675/Z/17/Z	Jonathan O'Muircheartaigh
Medical Research Council Centre for Neurodevelopmental Disorders	MR/N0266063/1	Siân Wilson Jonathan O'Muircheartaigh Mary A Rutherford A David Edwards Tomoki Arichi
Medical Research Council	Translation support fellowship: MR/V036874/1	Vyacheslav R Karolis Tomoki Arichi
Wellcome / EPSRC Centre for Biomedical Engineering, Kings College London	WT 203148/Z/16/Z	Anthony N Price Jana Hutter Jacques-Donald Tournier Joseph V Hajnal
Medical Research Council	Clinician Scientist Fellowship MR/P008712/1	Tomoki Arichi
Medical Research Council	MR/K006355/1	Siân Wilson Maximilian Pietsch Lucilio Cordero-Grande Daan Christiaens Alena Uus Vyacheslav R Karolis Vanessa Kyriakopoulou Kathleen Colford Anthony N Price Jana Hutter Mary A Rutherford Emer J Hughes Serena J Counsell Jacques-Donald Tournier Joseph V Hajnal A David Edwards Jonathan O'Muircheartaigh Tomoki Arichi
Medical Research Council	MR/L011530/1	Serena J Counsell

The funders had no role in study design, data collection and interpretation, or the decision to submit the work for publication. For the purpose of Open Access, the authors have applied a CC BY public copyright license to any Author Accepted Manuscript version arising from this submission.

Author contributions

Siân Wilson, Conceptualization, Formal analysis, Validation, Investigation, Visualization, Methodology, Writing – original draft, Writing – review and editing; Maximilian Pietsch, Data curation, Software, Formal analysis, Methodology, Writing – review and editing; Lucilio Cordero-Grande, Data curation, Software, Methodology, Writing – review and editing; Daan Christiaens, Data curation, Formal analysis, Methodology, Writing – review and editing; Alena Uus, Data curation, Methodology; Vyacheslav R Karolis, Formal analysis, Investigation, Methodology, Writing – review and editing; Vanessa

Kyriakopoulou, Kathleen Colford, Anthony N Price, Emer J Hughes, Data curation; Jana Hutter, Data curation, Writing – review and editing; Mary A Rutherford, Data curation, Funding acquisition; Serena J Counsell, Data curation, Investigation, Writing – review and editing; Jacques-Donald Tournier, Data curation, Software, Formal analysis; Joseph V Hajnal, Resources, Data curation, Funding acquisition, Methodology, Project administration; A David Edwards, Supervision, Funding acquisition, Investigation, Methodology, Project administration, Writing – review and editing; Jonathan O'Muircheartaigh, Conceptualization, Resources, Data curation, Supervision, Funding acquisition, Validation, Investigation, Methodology, Project administration, Writing – review and editing; Tomoki Arichi, Conceptualization, Resources, Data curation, Formal analysis, Supervision, Funding acquisition, Validation, Investigation, Methodology, Project administration, Writing – review and editing

Author ORCIDs
Siân Wilson http://orcid.org/0000-0003-4617-3583
Serena J Counsell http://orcid.org/0000-0002-8033-5673
A David Edwards http://orcid.org/0000-0003-4801-7066
Tomoki Arichi http://orcid.org/0000-0002-3550-1644

Ethics
Human subjects: The study was approved by the UK Health Research Authority (Research Ethics Committee reference number: 14/LO/1169) and written parental consent was obtained in every case for imaging and open data release of the anonymized data.

Decision letter and Author response
Decision letter https://doi.org/10.7554/eLife.83727.sa1
Author response https://doi.org/10.7554/eLife.83727.sa2

Additional files

Supplementary files
- MDAR checklist

Data availability
Developing Human Connectome project data is open-access and available for download following completion of a data-usage agreement via: http://www.developingconnectome.org/. Data is also available at: https://nda.nih.gov/edit_collection.html?id=3955.

The following dataset was generated:

Author(s)	Year	Dataset title	Dataset URL	Database and Identifier
Uus A, Kyriakopoulou V, Cordero Grande L, Pietsch M, Price A, Wilson S, Patkee P, Karolis V, Schuch A, Gartner A, Williams L, Hughes E, Arichi T, O'Muircheartaigh J, Hutter J, Robinson E, Tournier JD, Rueckert D, Counsell SJ, Rutherford MA, Deprez M, Hajnal JV, Edwards AD	2023	Multi-channel spatio-temporal MRI atlas of normal fetal brain development (dHCP project)	https://doi.org/10.12751/g-node.ysgsy1	G-Node Open Data, 10.12751/g-node.ysgsy1

The following previously published dataset was used:

Author(s)	Year	Dataset title	Dataset URL	Database and Identifier
Gholipour A, Rollins CK, Velasco-Annis C, Ouaalam A, Akhondi-Asl A, Afacan O, Ortinau C, Clancy S, Limperopoulos C, Yang E, Estroff JA, Warfield SK	2017	A normative spatiotemporal MRI atlas of the fetal brain for automatic segmentation and analysis of early brain growth	http://crl.med.harvard.edu/research/fetal_brain_atlas/	Harcard CRL/fetal brain atlas, fetal_brain_atlas/

References

Alcauter S, Lin W, Smith JK, Short SJ, Goldman BD, Reznick JS, Gilmore JH, Gao W. 2014. Development of thalamocortical connectivity during infancy and its cognitive correlations. *The Journal of Neuroscience* **34**:9067–9075. DOI: https://doi.org/10.1523/JNEUROSCI.0796-14.2014, PMID: 24990927

Allendoerfer KL, Shatz CJ. 1994. The subplate, a transient neocortical structure: Its role in the development of connections between thalamus and cortex. *Annual Review of Neuroscience* **17**:185–218. DOI: https://doi.org/10.1146/annurev.ne.17.030194.001153, PMID: 8210173

Alzu'bi A, Homman-Ludiye J, Bourne JA, Clowry GJ. 2019. Corrigendum: Thalamocortical afferents innervate the cortical subplate much earlier in development in primate than in rodent. *Cerebral Cortex* **29**:5316. DOI: https://doi.org/10.1093/cercor/bhz056, PMID: 31037284

Anticevic A, Cole MW, Repovs G, Murray JD, Brumbaugh MS, Winkler AM, Savic A, Krystal JH, Pearlson GD, Glahn DC. 2014. Characterizing thalamo-cortical disturbances in schizophrenia and bipolar illness. *Cerebral Cortex* **24**:3116–3130. DOI: https://doi.org/10.1093/cercor/bht165, PMID: 23825317

Avants BB, Epstein CL, Grossman M, Gee JC. 2008. Symmetric diffeomorphic image registration with cross-correlation: Evaluating automated labeling of elderly and neurodegenerative brain. *Medical Image Analysis* **12**:26–41. DOI: https://doi.org/10.1016/j.media.2007.06.004, PMID: 17659998

Back SA, Volpe JJ. 1997. Cellular and molecular pathogenesis of periventricular white matter injury. *Mental Retardation and Developmental Disabilities Research Reviews* **3**:96–107. DOI: https://doi.org/10.1002/(SICI)1098-2779(1997)3:1<96::AID-MRDD12>3.0.CO;2-M

Back SA, Luo NL, Borenstein NS, Levine JM, Volpe JJ, Kinney HC. 2001. Late oligodendrocyte progenitors coincide with the developmental window of vulnerability for human perinatal white matter injury. *The Journal of Neuroscience* **21**:1302–1312. DOI: https://doi.org/10.1523/JNEUROSCI.21-04-01302.2001, PMID: 11160401

Back SA, Luo NL, Borenstein NS, Volpe JJ, Kinney HC. 2002. Arrested oligodendrocyte lineage progression during human cerebral white matter development: Dissociation between the timing of progenitor differentiation and myelinogenesis. *Journal of Neuropathology and Experimental Neurology* **61**:197–211. DOI: https://doi.org/10.1093/jnen/61.2.197, PMID: 11853021

Ball G, Boardman JP, Rueckert D, Aljabar P, Arichi T, Merchant N, Gousias IS, Edwards AD, Counsell SJ. 2012. The effect of preterm birth on thalamic and cortical development. *Cerebral Cortex* **22**:1016–1024. DOI: https://doi.org/10.1093/cercor/bhr176, PMID: 21772018

Ball G, Boardman JP, Aljabar P, Pandit A, Arichi T, Merchant N, Rueckert D, Edwards AD, Counsell SJ. 2013. The influence of preterm birth on the developing thalamocortical connectome. *Cortex; a Journal Devoted to the Study of the Nervous System and Behavior* **49**:1711–1721. DOI: https://doi.org/10.1016/j.cortex.2012.07.006, PMID: 22959979

Ball G, Pazderova L, Chew A, Tusor N, Merchant N, Arichi T, Allsop JM, Cowan FM, Edwards AD, Counsell SJ. 2015. Thalamocortical connectivity predicts cognition in children born preterm. *Cerebral Cortex* **25**:4310–4318. DOI: https://doi.org/10.1093/cercor/bhu331, PMID: 25596587

Batalle D, Hughes EJ, Zhang H, Tournier JD, Tusor N, Aljabar P, Wali L, Alexander DC, Hajnal JV, Nosarti C, Edwards AD, Counsell SJ. 2017. Early development of structural networks and the impact of prematurity on brain connectivity. *NeuroImage* **149**:379–392. DOI: https://doi.org/10.1016/j.neuroimage.2017.01.065, PMID: 28153637

Behrens TEJ, Johansen-Berg H, Woolrich MW, Smith SM, Wheeler-Kingshott CAM, Boulby PA, Barker GJ, Sillery EL, Sheehan K, Ciccarelli O, Thompson AJ, Brady JM, Matthews PM. 2003. Non-Invasive mapping of connections between human thalamus and cortex using diffusion imaging. *Nature Neuroscience* **6**:750–757. DOI: https://doi.org/10.1038/nn1075, PMID: 12808459

Brody BA, Kinney HC, Kloman AS, Gilles FH. 1987. Sequence of central nervous system myelination in human infancy. I. An autopsy study of myelination. *Journal of Neuropathology and Experimental Neurology* **46**:283–301. DOI: https://doi.org/10.1097/00005072-198705000-00005, PMID: 3559630

Bui T, Daire JL, Chalard F, Zaccaria I, Alberti C, Elmaleh M, Garel C, Luton D, Blanc N, Sebag G. 2006. Microstructural development of human brain assessed in utero by diffusion tensor imaging. *Pediatric Radiology* **36**:1133–1140. DOI: https://doi.org/10.1007/s00247-006-0266-3, PMID: 16960686

Calamante F, Tournier JD, Jackson GD, Connelly A. 2010. Track-density imaging (TDI): Super-resolution white matter imaging using whole-brain track-density mapping. *NeuroImage* **53**:1233–1243. DOI: https://doi.org/10.1016/j.neuroimage.2010.07.024, PMID: 20643215

Calamante F. 2019. The seven deadly SINS of measuring brain structural connectivity using diffusion MRI streamlines fibre-tracking. *Diagnostics* **9**:115. DOI: https://doi.org/10.3390/diagnostics9030115, PMID: 31500098

Christiaens D, Cordero-Grande L, Price AN, Hutter J, Hughes E, Counsell SJ, Tournier JD, Hajnal JV. 2019a. Fetal diffusion MRI acquisition and analysis in the developing Human Connectome Project. ISMRM Annual Meeting & Exhibition. .

Christiaens D, Slator PJ, Cordero-Grande L, Price AN, Deprez M, Alexander DC, Rutherford M, Hajnal JV, Hutter J. 2019b. In utero diffusion MRI: Challenges, advances, and applications. *Topics in Magnetic Resonance Imaging* **28**:255–264. DOI: https://doi.org/10.1097/RMR.0000000000000211, PMID: 31592992

Christiaens D, Cordero-Grande L, Pietsch M, Hutter J, Price AN, Hughes EJ, Vecchiato K, Deprez M, Edwards AD, Hajnal JV, Tournier JD. 2021. Scattered slice SHARD reconstruction for motion correction in multi-shell diffusion MRI. *NeuroImage* **225**:117437. DOI: https://doi.org/10.1016/j.neuroimage.2020.117437, PMID: 33068713

Clascá F, Rubio-Garrido P, Jabaudon D. 2012. Unveiling the diversity of thalamocortical neuron subtypes. *European Journal of Neuroscience* **35**:1524–1532. DOI: https://doi.org/10.1111/j.1460-9568.2012.08033.x, PMID: 22606998

Cordero-Grande L, Price AN, Ferrazzi G, Hutter J, Christiaens D, Hughes E, Hajnal JV. 2018. Spin And Field Echo (SAFE) dynamic field correction in 3T fetal EPI. Joint Annual Meeting ISMRM-ESMRMB. Paris, France.

Cordero-Grande L, Christiaens D, Hutter J, Price AN, Hajnal JV. 2019. Complex diffusion-weighted image estimation via matrix recovery under general noise models. *NeuroImage* **200**:391–404. DOI: https://doi.org/10.1016/j.neuroimage.2019.06.039, PMID: 31226495

Counsell SJ, Allsop JM, Harrison MC, Larkman DJ, Kennea NL, Kapellou O, Cowan FM, Hajnal JV, Edwards AD, Rutherford MA. 2003. Diffusion-Weighted imaging of the brain in preterm infants with focal and diffuse white matter abnormality. *Pediatrics* **112**:1–7. DOI: https://doi.org/10.1542/peds.112.1.1, PMID: 12837859

Deprez M, Price A, Christiaens D, Lockwood Estrin G, Cordero-Grande L, Hutter J, Daducci A, Tournier JD, Rutherford M, Counsell SJ, Cuadra MB, Hajnal JV. 2020. Higher order spherical harmonics reconstruction of fetal diffusion MRI with intensity correction. *IEEE Transactions on Medical Imaging* **39**:1104–1113. DOI: https://doi.org/10.1109/TMI.2019.2943565, PMID: 31562073

Drobyshevsky A, Song S-K, Gamkrelidze G, Wyrwicz AM, Derrick M, Meng F, Li L, Ji X, Trommer B, Beardsley DJ, Luo NL, Back SA, Tan S. 2005. Developmental changes in diffusion anisotropy coincide with immature oligodendrocyte progression and maturation of compound action potential. *The Journal of Neuroscience* **25**:5988–5997. DOI: https://doi.org/10.1523/JNEUROSCI.4983-04.2005, PMID: 15976088

Emos MC, Khan Suheb MZ, Agarwal S. 2022. Neuroanatomy, Internal Capsule. StatPearls Publishing.

Ghiglia DC, Romero LA. 1994. Robust two-dimensional weighted and unweighted phase unwrapping that uses fast transforms and iterative methods. *Journal of the Optical Society of America A* **11**:107. DOI: https://doi.org/10.1364/JOSAA.11.000107

Gholipour A, Rollins CK, Velasco-Annis C, Ouaalam A, Akhondi-Asl A, Afacan O, Ortinau CM, Clancy S, Limperopoulos C, Yang E, Estroff JA, Warfield SK. 2017. A normative spatiotemporal MRI atlas of the fetal brain for automatic segmentation and analysis of early brain growth. *Scientific Reports* **7**:476. DOI: https://doi.org/10.1038/s41598-017-00525-w, PMID: 28352082

Ghosh A, Antonini A, McConnell SK, Shatz CJ. 1990. Requirement for subplate neurons in the formation of thalamocortical connections. *Nature* **347**:179–181. DOI: https://doi.org/10.1038/347179a0, PMID: 2395469

Hadders-Algra M, Boxum AG, Hielkema T, Hamer EG. 2017. Effect of early intervention in infants at very high risk of cerebral palsy: a systematic review. *Developmental Medicine and Child Neurology* **59**:246–258. DOI: https://doi.org/10.1111/dmcn.13331, PMID: 27925172

Haynes RL, Borenstein NS, Desilva TM, Folkerth RD, Liu LG, Volpe JJ, Kinney HC. 2005. Axonal development in the cerebral white matter of the human fetus and infant. *The Journal of Comparative Neurology* **484**:156–167. DOI: https://doi.org/10.1002/cne.20453, PMID: 15736232

Hüppi PS, Murphy B, Maier SE, Zientara GP, Inder TE, Barnes PD, Kikinis R, Jolesz FA, Volpe JJ. 2001. Microstructural brain development after perinatal cerebral white matter injury assessed by diffusion tensor magnetic resonance imaging. *Pediatrics* **107**:455–460. DOI: https://doi.org/10.1542/peds.107.3.455, PMID: 11230582

Huttenlocher PR. 1979. Synaptic density in human frontal cortex-developmental changes and effects of aging. *Brain Research* **163**:195–205. DOI: https://doi.org/10.1016/0006-8993(79)90349-4, PMID: 427544

Huttenlocher PR, Dabholkar AS. 1997. Regional differences in synaptogenesis in human cerebral cortex. *The Journal of Comparative Neurology* **387**:167–178. DOI: https://doi.org/10.1002/(sici)1096-9861(19971020)387:2<167::aid-cne1>3.0.co;2-z, PMID: 9336221

Hutter J, Christiaens DJ, Schneider T, Cordero-Grande L, Slator PJ, Deprez M, Price AN, Tournier J-D, Rutherford M, Hajnal JV. 2018a. Slice-level diffusion encoding for motion and distortion correction. *Medical Image Analysis* **48**:214–229. DOI: https://doi.org/10.1016/j.media.2018.06.008, PMID: 29966941

Hutter J, Slator PJ, Christiaens D, Teixeira RPAG, Roberts T, Jackson L, Price AN, Malik S, Hajnal JV. 2018b. Integrated and efficient diffusion-relaxometry using zebra. *Scientific Reports* **8**:15138. DOI: https://doi.org/10.1038/s41598-018-33463-2, PMID: 30310108

Jaimes C, Machado-Rivas F, Afacan O, Khan S, Marami B, Ortinau CM, Rollins CK, Velasco-Annis C, Warfield SK, Gholipour A. 2020. In vivo characterization of emerging white matter microstructure in the fetal brain in the third trimester. *Human Brain Mapping* **41**:3177–3185. DOI: https://doi.org/10.1002/hbm.25006, PMID: 32374063

Jakab A, Pogledic I, Schwartz E, Gruber G, Mitter C, Brugger PC, Langs G, Schöpf V, Kasprian G, Prayer D. 2015. Fetal cerebral magnetic resonance imaging beyond morphology. *Seminars in Ultrasound, CT, and MR* **36**:465–475. DOI: https://doi.org/10.1053/j.sult.2015.06.003, PMID: 26614130

Jenkinson M, Bannister P, Brady M, Smith S. 2002. Improved optimization for the robust and accurate linear registration and motion correction of brain images. *NeuroImage* **17**:825–841. DOI: https://doi.org/10.1016/s1053-8119(02)91132-8, PMID: 12377157

Jenkinson M, Beckmann CF, Behrens TEJ, Woolrich MW, Smith SM. 2012. FSL. *NeuroImage* **62**:782–790. DOI: https://doi.org/10.1016/j.neuroimage.2011.09.015, PMID: 21979382

Jeurissen B, Tournier JD, Dhollander T, Connelly A, Sijbers J. 2014. Multi-tissue constrained spherical deconvolution for improved analysis of multi-shell diffusion MRI data. *NeuroImage* **103**:411–426. DOI: https://doi.org/10.1016/j.neuroimage.2014.07.061, PMID: 25109526

Johansen-Berg H, Behrens TEJ, Sillery E, Ciccarelli O, Thompson AJ, Smith SM, Matthews PM. 2005. Functional-anatomical validation and individual variation of diffusion tractography-based segmentation of the human thalamus. *Cerebral Cortex* **15**:31–39. DOI: https://doi.org/10.1093/cercor/bhh105, PMID: 15238447

Jones EG. 2007. The thalamus. (2nd ed.). Cambridge University Press.

Keunen K, van der Burgh HK, de Reus MA, Moeskops P, Schmidt R, Stolwijk LJ, de Lange SC, Išgum I, de Vries LS, Benders MJ, van den Heuvel MP. 2018. Early human brain development: Insights into macroscale connectome wiring. *Pediatric Research* **84**:829–836. DOI: https://doi.org/10.1038/s41390-018-0138-1, PMID: 30188500

Khan S, Vasung L, Marami B, Rollins CK, Afacan O, Ortinau CM, Yang E, Warfield SK, Gholipour A. 2019. Fetal brain growth portrayed by a spatiotemporal diffusion tensor MRI atlas computed from in utero images. *NeuroImage* **185**:593–608. DOI: https://doi.org/10.1016/j.neuroimage.2018.08.030, PMID: 30172006

Kinney HC, Brody BA, Kloman AS, Gilles FH. 1988. Sequence of central nervous system myelination in human infancy. II. Patterns of myelination in autopsied infants. *Journal of Neuropathology and Experimental Neurology* **47**:217–234. DOI: https://doi.org/10.1097/00005072-198805000-00003, PMID: 3367155

Kinney HC, Karthigasan J, Borenshteyn NI, Flax JD, Kirschner DA. 1994. Myelination in the developing human brain: Biochemical correlates. *Neurochemical Research* **19**:983–996. DOI: https://doi.org/10.1007/BF00968708, PMID: 7800125

Klingner CM, Langbein K, Dietzek M, Smesny S, Witte OW, Sauer H, Nenadic I. 2014. Thalamocortical connectivity during resting state in schizophrenia. *European Archives of Psychiatry and Clinical Neuroscience* **264**:111–119. DOI: https://doi.org/10.1007/s00406-013-0417-0, PMID: 23892770

Kostovic I, Goldman-Rakic PS. 1983. Transient cholinesterase staining in the Mediodorsal nucleus of the thalamus and its connections in the developing human and monkey brain. *The Journal of Comparative Neurology* **219**:431–447. DOI: https://doi.org/10.1002/cne.902190405, PMID: 6196382

Kostovic I, Rakic P. 1984. Development of prestriate visual projections in the monkey and human fetal cerebrum revealed by transient cholinesterase staining. *The Journal of Neuroscience* **4**:25–42. DOI: https://doi.org/10.1523/JNEUROSCI.04-01-00025.1984, PMID: 6693940

Kostovic I, Rakic P. 1990. Developmental history of the transient subplate zone in the visual and somatosensory cortex of the macaque monkey and human brain. *The Journal of Comparative Neurology* **297**:441–470. DOI: https://doi.org/10.1002/cne.902970309, PMID: 2398142

Kostović I, Judas M, Rados M, Hrabac P. 2002. Laminar organization of the human fetal cerebrum revealed by histochemical markers and magnetic resonance imaging. *Cerebral Cortex* **12**:536–544. DOI: https://doi.org/10.1093/cercor/12.5.536, PMID: 11950771

Kostović I., Jovanov-Milosević N. 2006. The development of cerebral connections during the first 20-45 weeks' gestation. *Seminars in Fetal & Neonatal Medicine* **11**:415–422. DOI: https://doi.org/10.1016/j.siny.2006.07.001, PMID: 16962836

Kostovic I, Judas M. 2006. Prolonged coexistence of transient and permanent circuitry elements in the developing cerebral cortex of fetuses and preterm infants. *Developmental Medicine and Child Neurology* **48**:388–393. DOI: https://doi.org/10.1017/S0012162206000831, PMID: 16608549

Kostović I, Judas M. 2010. The development of the subplate and thalamocortical connections in the human foetal brain. *Acta Paediatrica* **99**:1119–1127. DOI: https://doi.org/10.1111/j.1651-2227.2010.01811.x, PMID: 20367617

Kostović I. 2020. The enigmatic fetal subplate compartment forms an early tangential cortical nexus and provides the framework for construction of cortical connectivity. *Progress in Neurobiology* **194**:101883. DOI: https://doi.org/10.1016/j.pneurobio.2020.101883, PMID: 32659318

Krsnik Ž, Majić V, Vasung L, Huang H, Kostović I. 2017. Growth of thalamocortical fibers to the somatosensory cortex in the human fetal brain. *Frontiers in Neuroscience* **11**:233. DOI: https://doi.org/10.3389/fnins.2017.00233, PMID: 28496398

Le Gros Clark WE. 1936. The topography and homologies of the hypothalamic nuclei in man. *Journal of Anatomy* **70**:203–214.

Machado-Rivas F, Afacan O, Khan S, Marami B, Velasco-Annis C, Lidov H, Warfield SK, Gholipour A, Jaimes C. 2021. Spatiotemporal changes in diffusivity and anisotropy in fetal brain tractography. *Human Brain Mapping* **42**:5771–5784. DOI: https://doi.org/10.1002/hbm.25653, PMID: 34487404

Marenco S, Stein JL, Savostyanova AA, Sambataro F, Tan HY, Goldman AL, Verchinski BA, Barnett AS, Dickinson D, Apud JA, Callicott JH, Meyer-Lindenberg A, Weinberger DR. 2012. Investigation of anatomical thalamo-cortical connectivity and fMRI activation in schizophrenia. *Neuropsychopharmacology* **37**:499–507. DOI: https://doi.org/10.1038/npp.2011.215, PMID: 21956440

Mathur A, Inder T. 2009. Magnetic resonance imaging -- insights into brain injury and outcomes in premature infants. *Journal of Communication Disorders* **42**:248–255. DOI: https://doi.org/10.1016/j.jcomdis.2009.03.007, PMID: 19406431

Miller JA, Ding S-L, Sunkin SM, Smith KA, Ng L, Szafer A, Ebbert A, Riley ZL, Royall JJ, Aiona K, Arnold JM, Bennet C, Bertagnolli D, Brouner K, Butler S, Caldejon S, Carey A, Cuhaciyan C, Dalley RA, Dee N, et al. 2014. Transcriptional landscape of the prenatal human brain. *Nature* **508**:199–206. DOI: https://doi.org/10.1038/nature13185, PMID: 24695229

Miyazaki Y, Song JW, Takahashi E. 2016. Asymmetry of radial and symmetry of tangential neuronal migration pathways in developing human fetal brains. *Frontiers in Neuroanatomy* **10**:2. DOI: https://doi.org/10.3389/fnana.2016.00002, PMID: 26834572

Mojsilović J, Zecević N. 1991. Early development of the human thalamus: Golgi and nissl study. *Early Human Development* **27**:119–144. DOI: https://doi.org/10.1016/0378-3782(91)90033-y, PMID: 1802659

Molliver ME, Kostović I, van der Loos H. 1973. The development of synapses in cerebral cortex of the human fetus. *Brain Research* **50**:403–407. DOI: https://doi.org/10.1016/0006-8993(73)90741-5, PMID: 4705508

Molnár Z, Blakemore C. 1995. How do thalamic axons find their way to the cortex? *Trends in Neurosciences* **18**:389–397. DOI: https://doi.org/10.1016/0166-2236(95)93935-q, PMID: 7482804

Molnár Z, Adams R, Blakemore C. 1998. Mechanisms underlying the early establishment of thalamocortical connections in the rat. *The Journal of Neuroscience* **18**:5723–5745. DOI: https://doi.org/10.1523/JNEUROSCI.18-15-05723.1998, PMID: 9671663

Molnár Z, Garel S, López-Bendito G, Maness P, Price DJ. 2012. Mechanisms controlling the guidance of thalamocortical axons through the embryonic forebrain. *The European Journal of Neuroscience* **35**:1573–1585. DOI: https://doi.org/10.1111/j.1460-9568.2012.08119.x, PMID: 22607003

Molnár Z, Hoerder-Suabedissen A. 2016. Regional scattering of primate subplate. *PNAS* **113**:9676–9678. DOI: https://doi.org/10.1073/pnas.1611194113, PMID: 27551078

Morel A, Magnin M, Jeanmonod D. 1997. Multiarchitectonic and stereotactic atlas of the human thalamus. *The Journal of Comparative Neurology* **387**:588–630. DOI: https://doi.org/10.1002/(sici)1096-9861(19971103)387:4<588::aid-cne8>3.0.co;2-z, PMID: 9373015

Mrzljak L, Uylings HB, Kostovic I, van Eden CG. 1992. Prenatal development of neurons in the human prefrontal cortex. II. A quantitative Golgi study. *The Journal of Comparative Neurology* **316**:485–496. DOI: https://doi.org/10.1002/cne.903160408, PMID: 1577996

Nair A, Treiber JM, Shukla DK, Shih P, Müller RA. 2013. Impaired thalamocortical connectivity in autism spectrum disorder: A study of functional and anatomical connectivity. *Brain* **136**:1942–1955. DOI: https://doi.org/10.1093/brain/awt079, PMID: 23739917

Najdenovska E, Alemán-Gómez Y, Battistella G, Descoteaux M, Hagmann P, Jacquemont S, Maeder P, Thiran JP, Fornari E, Bach Cuadra M. 2018. In-vivo probabilistic atlas of human thalamic nuclei based on diffusion-weighted magnetic resonance imaging. *Scientific Data* **5**:180270. DOI: https://doi.org/10.1038/sdata.2018.270, PMID: 30480664

Nakagawa Y. 2019. Development of the thalamus: From early patterning to regulation of cortical functions. *Wiley Interdisciplinary Reviews. Developmental Biology* **8**:e345. DOI: https://doi.org/10.1002/wdev.345, PMID: 31034163

Niemann K, Mennicken VR, Jeanmonod D, Morel A. 2000. The morel stereotactic atlas of the human thalamus: Atlas-to-MR registration of internally consistent canonical model. *NeuroImage* **12**:601–616. DOI: https://doi.org/10.1006/nimg.2000.0650, PMID: 11112393

Nosarti C, Nam KW, Walshe M, Murray RM, Cuddy M, Rifkin L, Allin MPG. 2014. Preterm birth and structural brain alterations in early adulthood. *NeuroImage. Clinical* **6**:180–191. DOI: https://doi.org/10.1016/j.nicl.2014.08.005, PMID: 25379430

Pietsch M. 2018. *Advanced Diffusion MRI Analysis Methods for Neonatal Imaging* King's College.

Pietsch M, Christiaens D, Hutter J, Cordero-Grande L, Price AN, Hughes E, Edwards AD, Hajnal JV, Counsell SJ, Tournier JD. 2019. A framework for multi-component analysis of diffusion MRI data over the neonatal period. *NeuroImage* **186**:321–337. DOI: https://doi.org/10.1016/j.neuroimage.2018.10.060, PMID: 30391562

Price DJ, Kennedy H, Dehay C, Zhou L, Mercier M, Jossin Y, Goffinet AM, Tissir F, Blakey D, Molnár Z. 2006. The development of cortical connections. *The European Journal of Neuroscience* **23**:910–920. DOI: https://doi.org/10.1111/j.1460-9568.2006.04620.x, PMID: 16519656

Price AN, Cordero-Grande L, Hughes E, Hiscocks S, Green E, McCabe L, Hutter J, Ferrazzi G, Deprez M, Roberts T, Christiaens D, Duff E, Karolis V, Malik S, Rutherford M, Edwards AD, Hajnal JV. 2019. The developing Human Connectome Project (dHCP): fetal acquisition protocol. ISMRM Annual Meeting & Exhibition. .

Raffelt D, Tournier JD, Fripp J, Crozier S, Connelly A, Salvado O. 2011. Symmetric diffeomorphic registration of fibre orientation distributions. *NeuroImage* **56**:1171–1180. DOI: https://doi.org/10.1016/j.neuroimage.2011.02.014, PMID: 21316463

Rakic P. 1977. Prenatal development of the visual system in rhesus monkey. *Philosophical Transactions of the Royal Society of London. Series B, Biological Sciences* **278**:245–260. DOI: https://doi.org/10.1098/rstb.1977.0040, PMID: 19781

Rakic P. 2003. Elusive radial glial cells: historical and evolutionary perspective. *Glia* **43**:19–32. DOI: https://doi.org/10.1002/glia.10244, PMID: 12761862

Raybaud C, Ahmad T, Rastegar N, Shroff M, Al Nassar M. 2013. The premature brain: developmental and lesional anatomy. *Neuroradiology* **55 Suppl 2**:23–40. DOI: https://doi.org/10.1007/s00234-013-1231-0, PMID: 23832006

Schummers J, Sharma J, Sur M. 2005. Bottom-up and top-down dynamics in visual cortex. *Progress in Brain Research* **149**:65–81. DOI: https://doi.org/10.1016/S0079-6123(05)49006-8, PMID: 16226577

Sharma J, Angelucci A, Sur M. 2000. Induction of visual orientation modules in auditory cortex. *Nature* **404**:841–847. DOI: https://doi.org/10.1038/35009043, PMID: 10786784

Smith RE, Tournier JD, Calamante F, Connelly A. 2012. Anatomically-constrained tractography: improved diffusion MRI streamlines tractography through effective use of anatomical information. *NeuroImage* **62**:1924–1938. DOI: https://doi.org/10.1016/j.neuroimage.2012.06.005, PMID: 22705374

Smith RE, Tournier JD, Calamante F, Connelly A. 2013. SIFT: spherical-deconvolution informed filtering of tractograms. *NeuroImage* **67**:298–312. DOI: https://doi.org/10.1016/j.neuroimage.2012.11.049, PMID: 23238430

Sur M, Rubenstein JLR. 2005. Patterning and plasticity of the cerebral cortex. *Science* **310**:805–810. DOI: https://doi.org/10.1126/science.1112070, PMID: 16272112

Takahashi E, Folkerth RD, Galaburda AM, Grant PE. 2012. Emerging cerebral connectivity in the human fetal brain: an mr tractography study. *Cerebral Cortex* **22**:455–464. DOI: https://doi.org/10.1093/cercor/bhr126, PMID: 21670100

Toulmin H, Beckmann CF, O'Muircheartaigh J, Ball G, Nongena P, Makropoulos A, Ederies A, Counsell SJ, Kennea N, Arichi T, Tusor N, Rutherford MA, Azzopardi D, Gonzalez-Cinca N, Hajnal JV, Edwards AD. 2015. Specialization and integration of functional thalamocortical connectivity in the human infant. *PNAS* **112**:6485–6490. DOI: https://doi.org/10.1073/pnas.1422638112, PMID: 25941391

Toulmin H, O'Muircheartaigh J, Counsell SJ, Falconer S, Chew A, Beckmann CF, Edwards AD. 2021. Functional thalamocortical connectivity at term equivalent age and outcome at 2 years in infants born preterm. *Cortex; a Journal Devoted to the Study of the Nervous System and Behavior* **135**:17–29. DOI: https://doi.org/10.1016/j.cortex.2020.09.022, PMID: 33359978

Tournier JD, Calamante F, Connelly A. 2013. Determination of the appropriate B value and number of gradient directions for high-angular-resolution diffusion-weighted imaging. *NMR in Biomedicine* **26**:1775–1786. DOI: https://doi.org/10.1002/nbm.3017, PMID: 24038308

Tournier JD, Smith R, Raffelt D, Tabbara R, Dhollander T, Pietsch M, Christiaens D, Jeurissen B, Yeh CH, Connelly A. 2019. MRtrix3: a fast, flexible and open software framework for medical image processing and visualisation. *NeuroImage* **202**:116137. DOI: https://doi.org/10.1016/j.neuroimage.2019.116137, PMID: 31473352

Tournier J-D, Christiaens D, Hutter J, Price AN, Cordero-Grande L, Hughes E, Bastiani M, Sotiropoulos SN, Smith SM, Rueckert D, Counsell SJ, Edwards AD, Hajnal JV. 2020. A data-driven approach to optimising the encoding for multi-shell diffusion MRI with application to neonatal imaging. *NMR in Biomedicine* **33**:e4348. DOI: https://doi.org/10.1002/nbm.4348, PMID: 32632961

Volpe JJ. 2001. Neurobiology of periventricular leukomalacia in the premature infant. *Pediatric Research* **50**:553–562. DOI: https://doi.org/10.1203/00006450-200111000-00003, PMID: 11641446

Volpe JJ. 2009. The encephalopathy of prematurity -- brain injury and impaired brain development inextricably intertwined. *Seminars in Pediatric Neurology* **16**:167–178. DOI: https://doi.org/10.1016/j.spen.2009.09.005, PMID: 19945651

Wilkinson M, Kane T, Wang R, Takahashi E. 2017. Migration pathways of thalamic neurons and development of thalamocortical connections in humans revealed by diffusion mr tractography. *Cerebral Cortex* **27**:5683–5695. DOI: https://doi.org/10.1093/cercor/bhw339, PMID: 27913428

Wilson S, Pietsch M, Cordero-Grande L, Price AN, Hutter J, Xiao J, McCabe L, Rutherford MA, Hughes EJ, Counsell SJ, Tournier J-D, Arichi T, Hajnal JV, Edwards AD, Christiaens D, O'Muircheartaigh J. 2021. Development of human white matter pathways in utero over the second and third trimester. *PNAS* **118**:e2023598118. DOI: https://doi.org/10.1073/pnas.2023598118, PMID: 33972435

Wimberger DM, Roberts TP, Barkovich AJ, Prayer LM, Moseley ME, Kucharczyk J. 1995. Identification of "premyelination" by diffusion-weighted MRI. *Journal of Computer Assisted Tomography* **19**:28–33. DOI: https://doi.org/10.1097/00004728-199501000-00005, PMID: 7529780

Xu G, Takahashi E, Folkerth RD, Haynes RL, Volpe JJ, Grant PE, Kinney HC. 2014. Radial coherence of diffusion tractography in the cerebral white matter of the human fetus: neuroanatomic insights. *Cerebral Cortex* **24**:579–592. DOI: https://doi.org/10.1093/cercor/bhs330, PMID: 23131806

Yakovlev PI, Locke S, Koskoff DY, Patton RA. 1960. Limbic nuclei of thalamus and connections of limbic cortex. *Archives of Neurology* **3**:620–641. DOI: https://doi.org/10.1001/archneur.1960.00450060008002, PMID: 13787071

Zanin E, Ranjeva J-P, Confort-Gouny S, Guye M, Denis D, Cozzone PJ, Girard N. 2011. White matter maturation of normal human fetal brain. An in vivo diffusion tensor tractography study. *Brain and Behavior* **1**:95–108. DOI: https://doi.org/10.1002/brb3.17, PMID: 22399089

Chapter 9.

Local minima in tissue microstructure precedes sulcal formation in the human fetal brain.

9.1 Abstract

The structural scaffolding of the human brain is assembled during the fetal period through a series of rapid, dynamic, and intersecting processes. The third trimester of gestation is characterised by the emergence of complex cortical folding patterns, the development of white matter connections and dissolution of transient compartments such as the subplate. Multiple hypotheses have been proposed to explain how these processes interact to drive the formation of cortical convolutions, however there are no data-driven analyses during the fetal period to address them empirically.

To explore this gap in understanding, we analyse the relationship between the in utero formation of cortical folds and underlying tissue microstructure, using high angular resolution multi-shell diffusion-weighted imaging (HARDI) as part of the Developing Human Connectome Project (dHCP). We find cytoarchitectural differences between gyral and sulcal regions, previously observed in adults and non-human primates, are already present at the onset of gyrification in utero. Our analysis reveals local minima in tissue microstructure prior to the formation of sulcal pits, suggesting that microstructural changes precede the onset of primary cortical fold development. This result provides fundamental mechanistic insight into the co-maturation of cortical macro and microstructure in early human life and has implications for understanding the developmental biology of cortical folding abnormalities.

9.2 Introduction

The gyrification of the human brain refers to the formation of grooves (sulci) and ridges (gyri) on surface of the brain through the folding of the cortex. From an evolutionary perspective, it allows the expansion of cortical surface area within the confined space of the skull (Fernandez et al., 2016), optimizing the efficiency of brain circuitry by bringing interconnected cortical areas closer together, increasing the speed of information transmission. Perturbing the course of neurodevelopment can alter the morphology of the cerebral cortex and result in lifelong deleterious effects on brain function, that may manifest as intellectual disability, autism and treatment-resistant epilepsy (Nordahl et al., 2007, Barkovich 2012, Subramanian et al., 2020). These clinical observations motivate the need to better understand the mechanistic framework behind the development of complex folding patterns.

At the end of the second trimester, after the bulk of neuronal migration has finished (~27 gestational weeks), the human brain is still a relatively smooth structure. Cortical folding then rapidly proceeds across the third trimester of gestation, with all major sulcal landmarks of the adult brain evident by the time of normal birth (Chi et al., 1977; Cachia et al., 2016; Yun et al., 2020). The deepest areas of the sulci, the sulcal pits, are the first to develop and are the most invariant across time, remaining spatially consistent even as other convolutions form (Im et al., 2010, Lohmann et al., 2008). Although the timeline for the development of surface features has been thoroughly described, the underlying in utero biology that drives cortical folding and determines individual variations in surface morphology is not well understood.

There are many hypotheses and empirical studies about the biological mechanisms that drive cortical gyrification (Van Essen 1997, 2020, Lefèvre et al., 2010, Xu et al., 2010, Tallinen et al., 2014, 2016). The probable role of other key developmental processes in cortical gyrification has been alluded to by previous work, such as the dissipation of the subplate (Rana et al., 2019), ingrowth of thalamocortical

axons (Van Essen 2020), neuronal proliferation (Kriegstein et al., 2006), and differential expansion of cortical layers (Richmann et al., 1975). However very few studies have been conducted in the human fetal brain during the time window when gyrification begins. It is hypothesised that the highly conserved nature of primary cortical sulci between individuals, compared to the secondary and tertiary sulci, would suggest that they are under closer genetic control than later developing sulci (Im and Grant 2019). By extension, the mechanisms governing the formation of cortical convolutions may differ pre- and post-natally, becoming more influenced by environmental cues at later stages of development.

Diffusion MRI can be used to quantify structural maturation of the brain and can provide detailed information about intracellular and extracellular water diffusion over the second to third trimester. Modelling the diffusion signal allows a refined interpretation of the dynamic changes seen in image contrast in terms of the underlying cellular biology. This has been demonstrated in rodents (Sizonenko et al., 2007, Aggarwal et al., 2015), primates (Wang et al 2017), human fetuses (Huang et al., 2014), and preterm infants (McKinstry et al., 2002, Ball et al., 2013, Batalle et al., 2019). However, the relationship between the maturation of tissue microstructure and the development of cortical sulci has not been characterized.

Using T2-weighted and HARDI data acquired as part of the dHCP, we quantify the relationship between the emerging macroscopic features on the surface of the brain and the microstructural properties of the underlying tissue layers, including the cortical plate and subplate (or developing white matter). We studied 112 imaging datasets from fetuses aged between 24 and 36 gestational weeks (GW), to quantitatively describe the relationship between tissue architecture, gyral and sulcal formation across gestational age (GA). We describe the folding of the cortex using sulcal depth and mean curvature. We then model the diffusion MR signal using a combination of the diffusion tensor imaging (DTI) and multi-shell multi-tissue constrained spherical deconvolution (MSMT-CSD) to characterize how the microstructure of the underlying subplate and cortical plate layers change with gestational age. Correlating these metrics at the individual subject level within sulcal areas reveals a brain-wide inverse relationship between tissue microstructure and sulcal depth that crucially, is independent of age-related

maturation. We then analyse the predictive power of microstructure to anticipate the emergence of cortical folds using age-mismatched analysis across the cross-sectional cohort. We identified local minima in tissue fraction during the second trimester, prior to the formation of cortical folds, in regions which subsequently mature into sulcal pits. This provides novel mechanistic insight into the emergence of cortical folding and has implications for understanding how folding abnormalities arise in utero.

9.3 Results

9.3.1 General trends in surface metrics across gestational age

The vertex-wise correlation between surface metrics (sulcal depth, surface area and curvature) and GA of the subject, demonstrated expected patterns of areal expansion and gyrification across the cortex (Yun et al., 2020). Sulcal depth, area and curvature maps demonstrated the appearance of major primary sulci over this timeframe, with high magnitude Pearson r values across the cortex (Figure 1a). Manually defined labels of the 19 major primary sulci were propagated from the surface template to each subject, and the mean sulcal depth within the sulcus was charted against GA. Changes in sulcal depth at each primary sulcal landmark were best fitted by sigmoidal curves over this developmental window (Supplementary Figure 2).

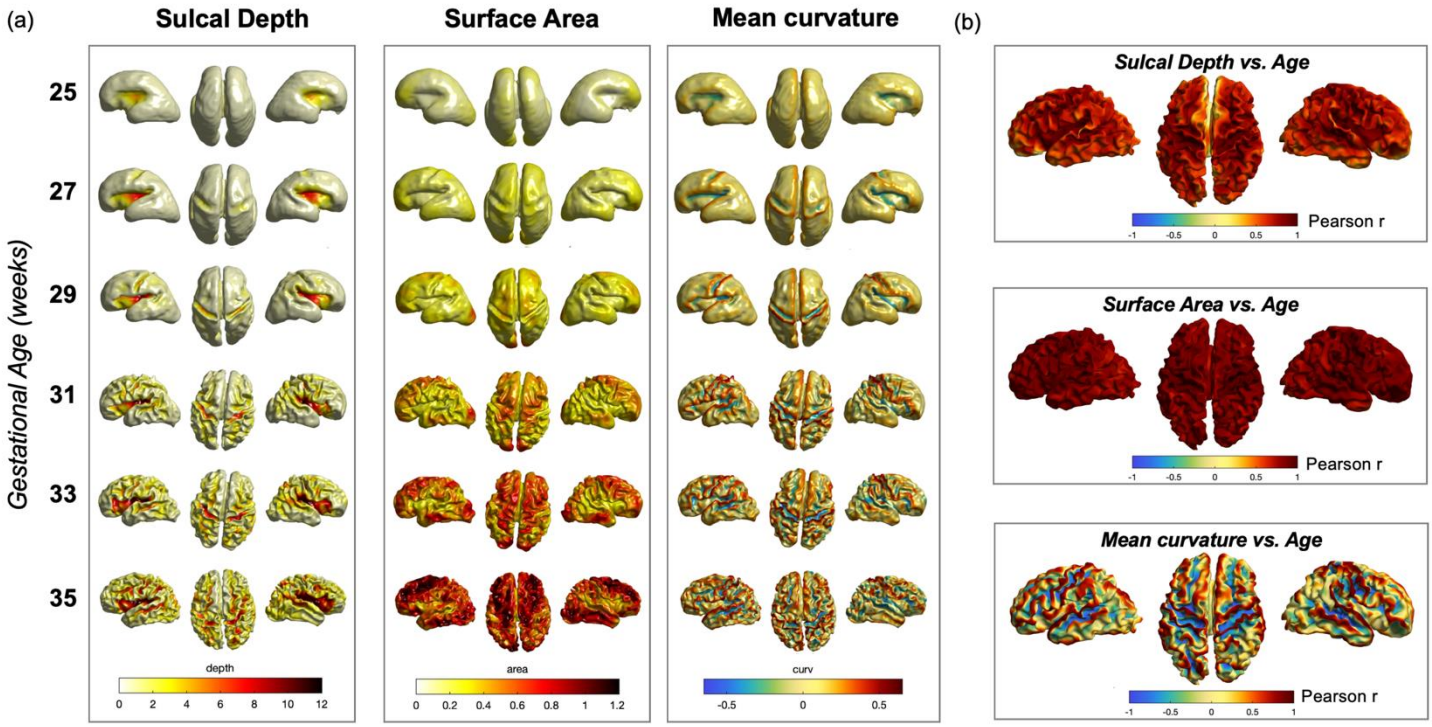

Figure 1. *Age related changes in surface features (a) Mean surface metrics (depth, area, curvature) in each gestational week (b) Pearson r correlation coefficient between surface metrics and gestational age.*

9.3.2 Age-dependent trends in diffusion metrics

To quantify variations in microstructure across the surface, DTI and MSMT-CSD models were both fitted to the individual subject HARDI data. Both approaches have been used to describe fetal brain maturation in previous literature (Wilson et al., 2021, Wilson et al., 2023, Jaimes et al., 2020 Chen et al., 2022). We aligned the surfaces, T2 and DWI volumes for each subject, and used the surface normal, a straight line of 1mm in length which is perpendicular to the tangent, to project inside and outside the white matter boundary. In this way we were able to obtain diffusion metrics of the subplate and cortical plate at each vertex. Projecting these values to the white matter surface highlighted regionally variant patterns of diffusion metrics across the brain that change with GA (Figure 2).

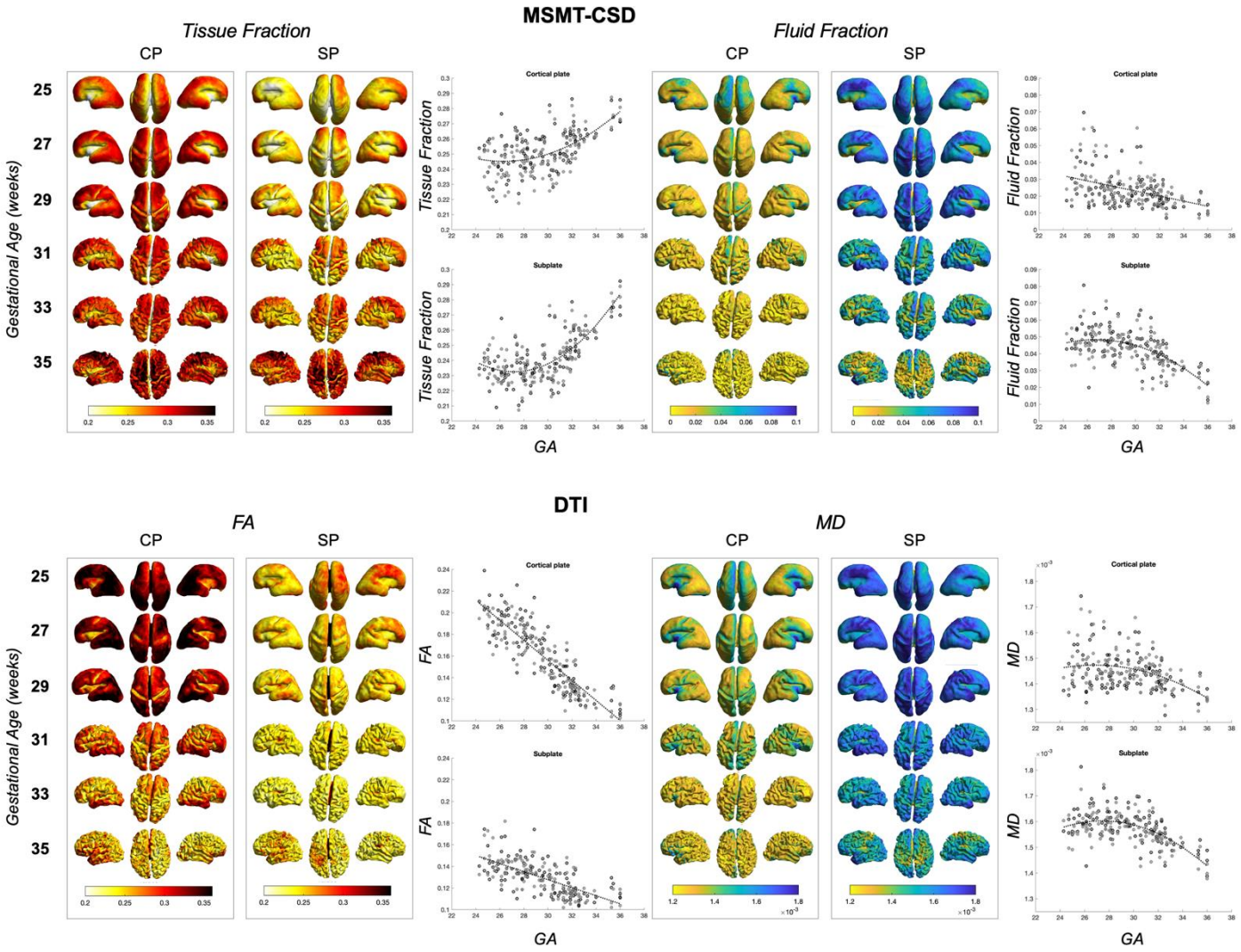

Figure 2. *Biweekly mean cortical plate (CP) and subplate (SP) microstructure projected to the white matter surface for MSMT-CSD derived metrics (tissue and fluid fraction) and DTI metrics (fractional anisotropy (FA), and mean diffusivity (MD)). Right hand side plots show mean diffusion metrics (grey = left, black = right) across the whole brain in the cortical plate and subplate of each subject, charted against the GA of the subject. Certain metrics were best fit with a linear trend, others using a 2nd order polynomial curve.*

To summarise the general trend across the second to third trimester, the mean value for each diffusion metric was calculated across all vertices within the CP and SP and plotted against GA (Figure 2). This analysis highlighted specific maturational trends for each diffusion metric across the surface between 24 and 36 GW, with both the mean fluid fraction and mean MD showing decreasing with age in the

cortical plate and subplate (Figure 2). In contrast, FA and tissue fraction showed opposite trends, with FA decreasing linearly towards term, and tissue fraction increasing (Figure 2).

9.3.3 Tissue fraction decreases as a function of sulcal depth, independent of age.

To test the hypothesis that microstructural change accompanies the formation of cortical folds independent of the effect of age-related change, we analysed the coupling between cortical folding and diffusion metrics within local areas in individual subjects. We calculated the correlation between tissue fraction and sulcal depth in each vertex neighbourhood (i.e patch of cortex). The size of all the neighbourhoods was fixed to 5 degrees of separation from the central point (Figure 3a).

In the majority of sulcal areas, within-subject cortical plate and subplate tissue fraction were negatively associated with sulcal depth in the neighbourhood coupling analysis (Figure 3), implying that sulcal pits have the lowest tissue fraction. At the level of individual subjects, this relationship was not only present at the onset of gyrification in the early emerging sulcus such as central sulcus (27 GW), but also through to the later stages of the third trimester as cortical folds became more mature (Figure 3). When exploring this relationship across the cohort, subjects were grouped every two weeks to calculate the mean Pearson's correlation coefficient at each vertex. After statistical testing, this association was robust to FDR correction ($q = 0.05$, $p < 0.02$) and for every biweekly GA group, in brain regions where sulci were appearing (Figure 5e,f). At 25 GW, significant neighbourhood associations were only seen in the sylvian fissure with progression then seen at 27 GW in the central sulcus, and by 35 GW in most primary sulci (Figure 3).

We then performed a linear regression to quantify the rate of change in this association across age, projecting the beta coefficient onto the white matter surface (3e). This beta reflects the change in the strength of the correlation between sulcal depth and tissue fraction for each gestational week. Only beta

coefficients where model fit was significant after correction for multiple comparisons using FDR (q = 0.05, p < 0.02) are displayed (Figure 3e). We observed that the magnitude of beta did not vary between brain regions, suggesting that the association between sulcal depth and tissue fraction strengthens uniformly and proportionally with age across the cerebral cortex.

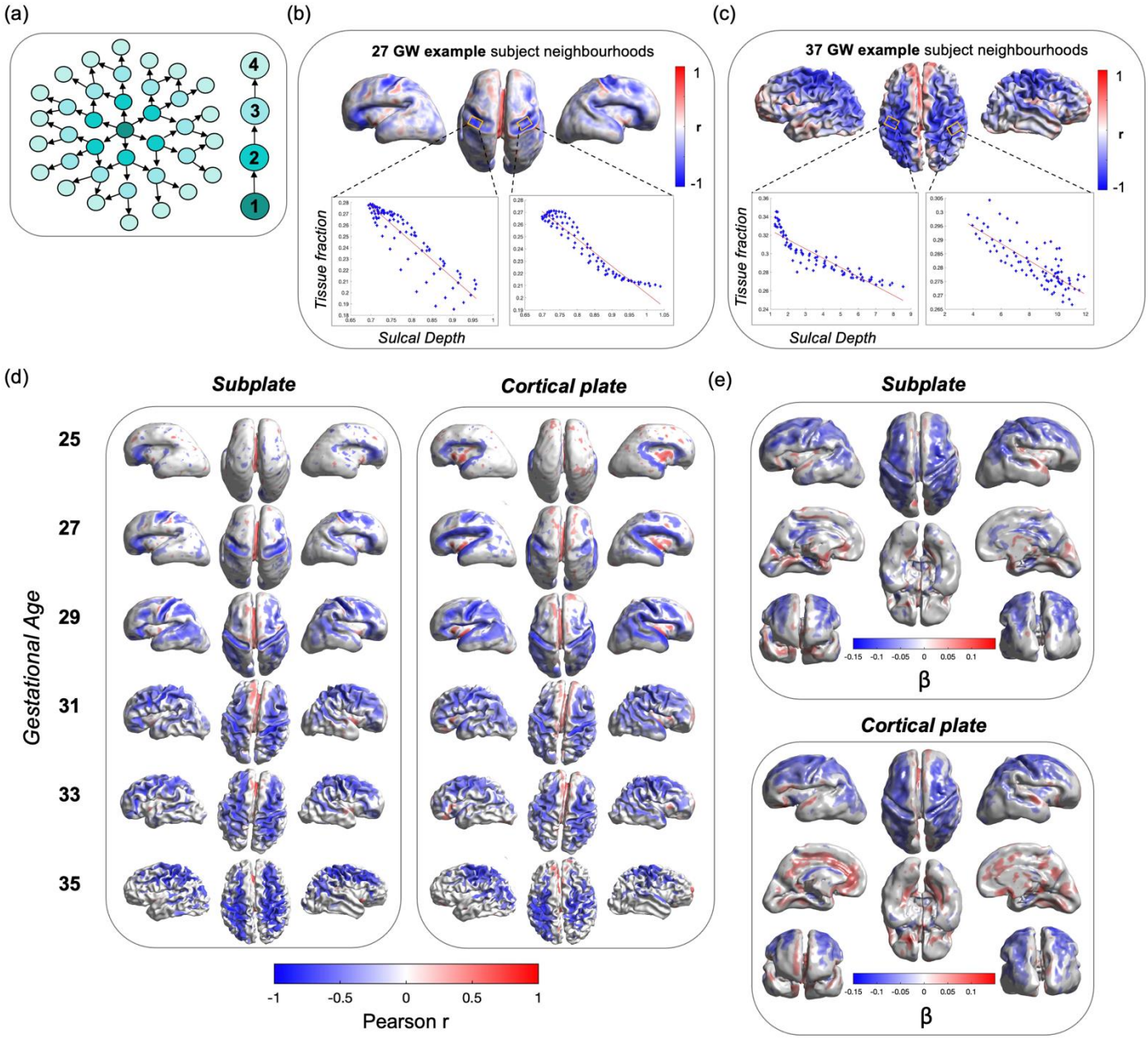

Figure 3. *Within-subject tissue fraction vs. sulcal depth neighbourhood analysis (a) Schematic to demonstrate the neighbourhood concept, and the degrees of separation between the central vertex and surrounding neighbours (1-4 shown). (b) Example of coupling in different aged subjects. Plots show example of how 'r' value is derived, in the central sulcus area at 27 GW and (c) 37 GW. (d) Mean r for subjects grouped into two-weekly bins, representing tissue fraction vs. sulcal depth in cortical plate and subplate. Only significant r values shown after FDR correction. (e) Linear regression (beta) at each vertex for the Pearson r value across gestational age, for subplate and cortical plate. Only values shown that are significant after FDR correction.*

9.3.4 Microstructural changes in sulcal regions precedes the formation of the sulcus

To investigate whether changes in microstructure precede the emergence of cortical convolutions, we quantified the coupling between tissue fraction in the younger half of the cohort (25 GW – 30 GW) and mature sulcal depth values (35 GW average). This age-mismatched analysis (Figure 4) highlighted microstructural variations across a sulcal area prior to presence of a fold. We identified numerous brain regions across the surface where tissue fraction in younger subjects correlated with future sulcal depth values. Significant trends were identified in different major sulcal landmarks, including the inferior frontal sulcus, superior temporal sulcus and post-central sulcus (indicated with arrows). To explore this relationship in more detail, the analysis was repeated just for specific sulcal regions of interest (ROIs) in each gestational week (Figure 4b). In the central sulcus at 25 GW there was marked variability between subjects and thus no consistent trend was seen between tissue fraction and future depth. However, by 26 GW a negative relationship (blue) was evident at more vertices which is then consistently seen from 27 GW onwards across the central sulcus. In the other sulcal ROIs, all gestational weeks, from 25 to 30, showed similar correlation patterns between subjects and across the sulcus, that were consistent with age (Supplementary info).

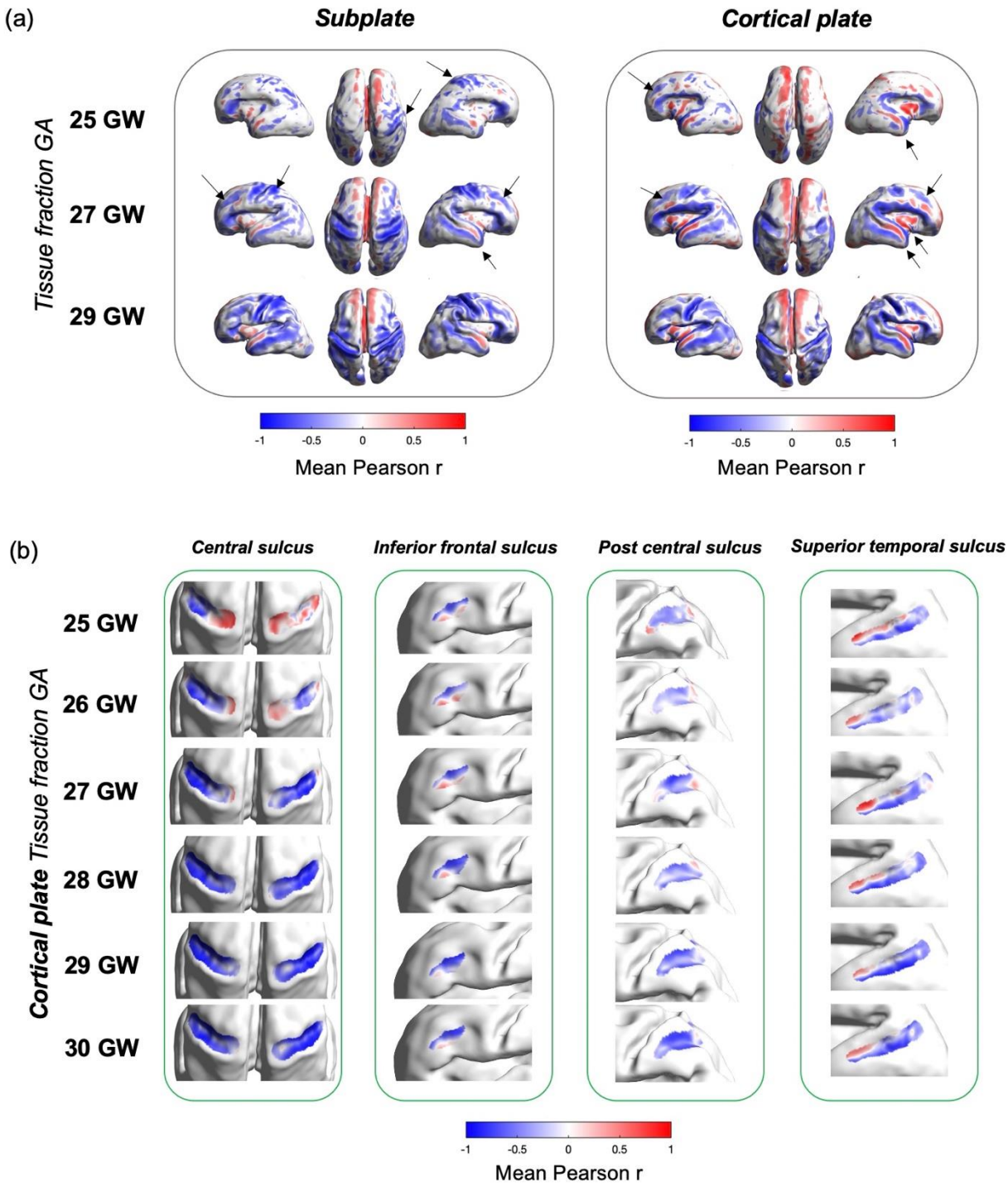

Figure 4. *Age-mismatched analysis highlights brain regions where changes in microstructure precede the formation of sulcal folds. (a) Whole-brain mean Pearson r correlation coefficient values for the correlation between mature 35 GW average sulcal depth values and native individual subject tissue fraction. Arrows indicate areas of change between top and bottom panel, including the inferior frontal*

sulcus, superior temporal sulcus, post-central sulcus and insula. (b) Close-up, repeating analysis of specific primary sulci using cortical plate tissue fraction values and mature 35 GW sulcal depth.

9.4 Discussion

In this study, we investigate how the microstructure of the fetal brain transitions to initiate the cortical folding process, in the human brain in vivo. Specialised acquisition and image reconstruction techniques were designed to overcome the unique challenges associated with the in utero environment, such as motion and distortion artefacts. The bespoke pipelines significantly enhanced data quality and enabled us to reconstruct T2w-derived surfaces and multi-shell DWI data for a large cohort of healthy fetuses spanning the second to third trimester. With this unique dataset, it was possible to explore the relationship between the underlying cytoarchitecture of the cortex and the macrostructural appearance of sulci and gyri. We found regionally heterogenous patterns of cortical microstructural and macrostructural development with GA, and a robust brain-wide inverse relationship between tissue microstructure and sulcal depth. We then establish that this 'local minima' in tissue microstructure precedes the emergence of cortical folds later in gestation, providing insight on the mechanistic biology underlying human gyrification.

9.4.1 DTI and MSMT-CSD-derived metrics are sensitive to different developmental cortical processes.

The microstructure of the cortex matures over the same timeframe that primary and secondary cortical folds emerge (Huang 2009, McKinstry et al., 2002, Ball et al., 2013, Batalle et al., 2019), however the relationship between them has not been investigated during this developmental window *in vivo.* There are a multitude of biological processes occurring simultaneously in the cortical plate and subplate in the third trimester which create a complex microstructural environment. Transitions in the cellular architecture and morphological maturation can be quantified with diffusion-derived metrics. While DTI provides a benchmark to compare results to previous studies, the MSMT-CSD overcomes the crossing

fiber limitations of DTI methods, offering more reliable decomposition of the diffusion MRI signal into tissue and fluid components. This offers improved characterisation of the biological complexity of developing brain tissue, which was not previously possible with in utero imaging (Alexander et al., 2002, Tournier 2010).

We found distinct trends between the DTI and MSMT-CSD metrics that allow a refined interpretation about the underlying biology of cortical microstructural maturation. Although tissue fraction and FA are considered complementary metrics to describe microstructural maturity, and coherently aligned tissue-like signal, we found opposite trends in the whole-brain average of these metrics in the cortex (Figure 2). FA decreases linearly in both the subplate and the cortical plate, with a higher rate of change in the cortical plate. Previous work has shown that maturing axonal and dendritic morphology affects the diffusion signal in the immature cerebral cortex, bridging the gap between MR imaging and the underlying developmental biology in post-mortem tissue (Wang et al., 2017, Dean et al., 2013, Sizonenko et al., 2007). In the developing cortex, the biological correlate of decreasing FA is a loss of radial glial morphology, dendritic arborization and axonal branching (Wang et al., 2017), while decreasing MD is the result of increasing cellular and organelle density (Dean et al., 2013, Sizonenko et al., 2007). For the first time in the human fetal brain in utero, we show decreasing FA in the cortex over this timeframe, implying the in utero MR signal changes are sensitive to the loss of radial alignment in the cortical plate, the disassembly of radial scaffolding in the subplate (as neuronal migration is largely complete at the end of the second trimester) and the restriction of water movement equally in all directions as dendritic arborization occurs (Rakic 2003). Decreasing cortical FA has also been observed in preterm infants over a comparable timeframe in early development (McKinstry et al., 2002, Dudink et al., 2010, Vinall et al., 2013, Ball et al., 2013, Batalle et al., 2019), and in post-mortem tissue from other gyrencephalic mammals such as ferrets and macaques (Kroenke et al., 2007, 2009; Yu et al., 2016, Wang et al., 2017).

On the other hand, when we model the diffusion signal with MSMT-CSD, we observe tissue fraction increases with GA over the third trimester, that likely reflect maturing neuronal morphology and

reductions in extracellular water, as dendritic trees develop and thalamocortical fibers synapse in the cortical plate and subplate (Kostovic and Judas 2010). Tissue fraction increases linearly in the cortical plate, whereas in the subplate a rapid increase is not seen until after 30 GW (Figure 3). This difference in maturational trend between compartments highlights the sensitivity of MSMT-CSD to the differentiation of radial glial cells into astrocytes, which takes place at approximately 30 GW in subplate regions (Kostovic et al., 2014). With this result, we demonstrate how the richly informative diffusion signal can be modelled with complementary approaches to understand the neurobiology of the human cortex as it matures in vivo.

9.4.2 Tissue fraction is higher in gyral than sulcal areas, recapitulating adult neuroanatomy in utero

We then explored the hypothesis that the microstructural maturation in the subplate and cortical plate plays a mechanistic role in cortical folding. To disentangle the effect of gestational age, we quantified the co-maturation of microstructure and macrostructure within local patches of cortex in individual fetuses. We calculated the correlation between sulcal depth and tissue fraction (in the cortical plate and subplate) for each vertex neighbourhood and found a clear, significant, brain-wide relationship in all subjects, showing sulcal depth is inversely correlated with tissue fraction (Figure 3).

We describe this brain-wide feature as ‘local minima in tissue fraction’, which represents the deepest parts of sulci, from their initial formation to maturity at the end of the third trimester. Linear regression of the correlation values revealed significant negative beta values across the surface, suggesting this relationship between tissue microstructure and sulcal depth strengthens as the folds mature. With this result, we recapitulate the structural differences between gyral crowns and sulcal pits observed in the mature brain (Figure 5). In gyral crowns there is lower neuronal cell density, higher myelinated fiber density, greater vertical alignment of pyramidal neurons, and longer more elaborate dendritic trees than in sulcal pits (Hiletag and Barbas 2005, Llinares-Benadero and Borrell, 2019). Primate studies have

shown that there are up to 50% fewer white matter neurons in sulcal pits than gyral crown areas (Mortazavi et al 2017). Another study by Nie et al., quantified the fraction of axonal fibers connected to gyri vs sulci within local cortical surface patches, in human, chimpanzee, and macaque brains, finding increased axonal fiber density near the gyral crowns across species (Nie et al., 2012). Furthermore, these differences are likely to have mechanistic importance, as the cortex is thicker in gyral crowns than sulcal pits (Von-economo 1925, Fischl and Dale 2000) and the degree of cortical folding is inversely correlated with local cortical thickness, irrespective of subject age (Hogstrom et al. 2013). A functional correlate to support the differences in structural connectivity was also identified in a brain-wide analysis, which noted the strongest functional connectivity exists between gyri, the weakest connectivity between sulci, and an intermediate level between gyri and sulci (Deng et al., 2014). Overall, the higher white matter fiber density, dendritic branching, and alignment of cellular structures in gyral crowns in comparison to the sulcal pits is consistent with higher tissue fractions at the top of a sulcus, decreasing towards the pits. Our analysis reveals that there are quantifiable differences in cytoarchitectural organisation of sulcal and gyral areas at the onset of gyrification in human neurodevelopment during the second to third trimester, and based on previous literature, they appear to persist into adulthood.

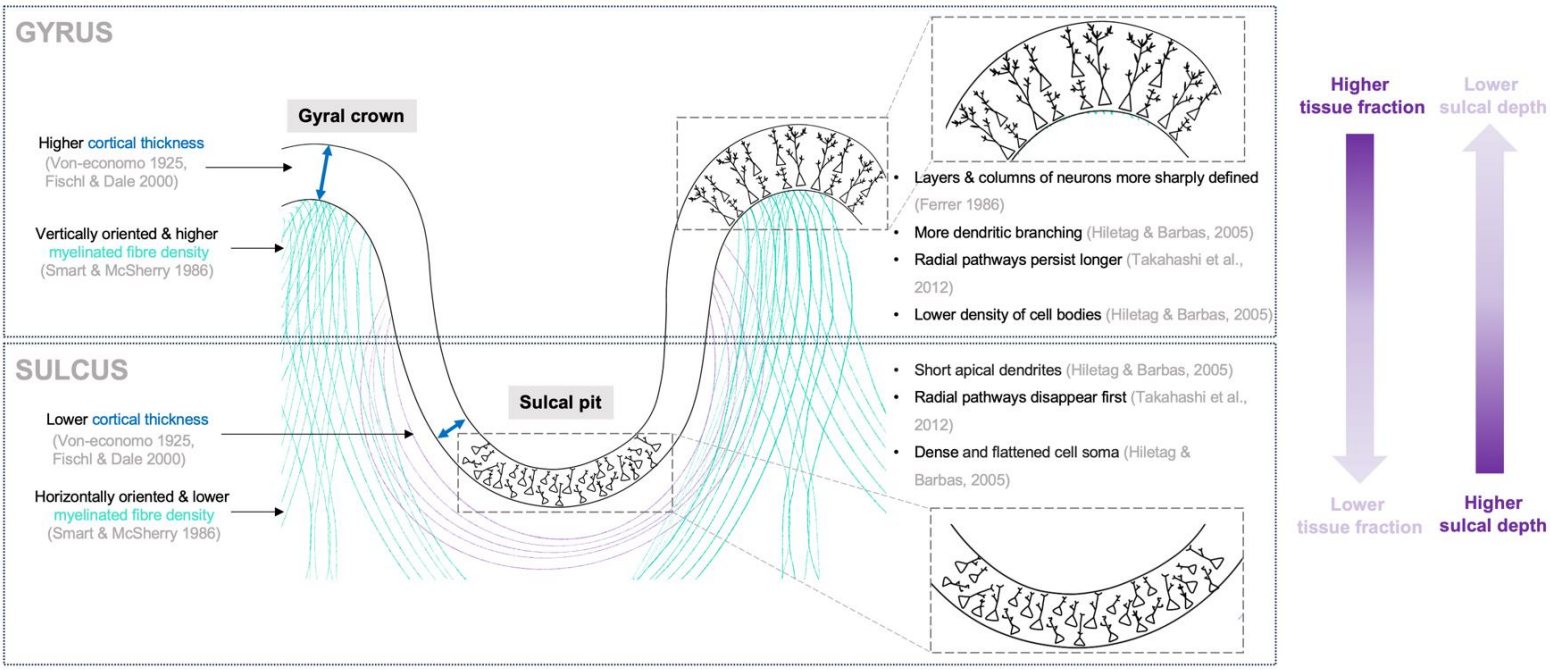

Figure 5. *Schematic summary of literature to date, illustrating the anatomical differences between gyral and sulcal areas. This includes macrostructural features such as cortical thickness, and microstructural differences in fibre density, cellular organisation and neuronal morphology that may explain the trends in tissue fraction as a function of sulcal depth (far right).*

9.4.3 Local minima in tissue fraction precedes the formation of cortical folds

To investigate if the differences in microstructure between gyral and sulcal areas offer mechanistic insight about the processes involved in gyrification, we carried out an age-mismatched analysis, examining the hypothesis that local minima in tissue fraction precede the formation of cortical folds. We identified numerous brain regions across the surface where tissue fraction in the second trimester correlated with sulcal depth values in the third trimester. This cross-sectional analysis highlights the predictive power of dynamic changes in the MR signal to anticipate the formation of cortical folds. It also suggests that the biological processes known to affect the diffusion signal in the cortical plate and subplate, precede and facilitate the formation of cortical folds.

The developmental processes affecting the diffusion signal in utero were investigated by Takahashi et al., 2012, using a small number of *ex vivo* human fetal specimens. This study identified a difference in the timing of the regression of radial pathways between gyral crests and sulcal depths, and a greater density of fiber bundles in developing gyral areas compared to sulcal areas (Takahashi 2012). At the crests of gyri, radial pathways persisted longer than those to the depths of the sulci and horizontal fiber pathways tended to emerge before gyri and sulci (Takahashi 2012). The higher tissue microstructure we observe in gyral crowns is analogous to the observations by Takahashi et al., suggesting our analysis

approach was able to replicate the ex vivo post-mortem results and capture these developmental processes across a large human sample in vivo.

Many studies point towards a complex role of fiber connectivity in determining cortical folding patterns (Van Essen 2020). Experiments disrupting the development of cortical afferent fibers have shown a profound effect on the pattern of cortical folding (Goldman and Galkin, 1978; Goldman-Rakic, 1980; Rakic, 1988). Our results support the hypotheses that cortical folding is driven by differences in structural connectivity, as the decreasing tissue microstructure in sulcal regions precedes the onset of cortical folding in specific locations across the cortex. In the context of previous work, this is likely to reflect the differential maturation and wiring of fiber bundles underlying gyral and sulcal areas, observed by Takahashi et al., 2012. Thus, our analysis reveals structural differences across the cortex between gyri and sulci at the onset of their development, which has crucial mechanistic importance for understanding cortical folding abnormalities. We find evidence in the diffusion MR signal over the second to third trimester, that in utero brain microstructure in the cortical plate and subplate changes dynamically to initiate the formation of cortical convolutions.

9.5 Conclusion

With this unique dataset acquired as part of the dHCP, we demonstrate the utility of the fetal MR signal as an investigate tool to understand the mechanisms of cortical folding in vivo. With advanced in utero imaging techniques (Christiaens et al., 2019, 2021), we modelled HARDI signal and T2 tissue surface reconstructions to investigate the microstructural changes that accompany the development of primary sulci in the fetal brain. In this whole-brain characterisation in vivo, we quantify the direct role of transient compartments in the formation of cortical convolutions. We show that cytoarchitectural differences between gyral and sulcal regions, previously observed in adults and non-human primates, are already present at the onset of gyrification in utero. Moreover, we find local minima in tissue fraction across the cortex, that precedes the formation of primary cortical folds. In this analysis, we uncover a

direct, crucial link between micro and macrostructure that offers mechanistic insight about how gyrification begins in the fetal brain, and by extension how folding abnormalities might arise in utero.

9.6 Methods

9.6.1 Acquisition and pre-processing

112 in utero fetal T2 and diffusion MRI datasets were acquired on a Philips Achieva 3T system with a 32-channel cardiac coil (Price 2019 ISMRM). T2 acquisition involved multiple single-shot turbo spin echo sequences with TE = 250ms, TR = 2265ms (Price et al., 2019). DWI was acquired with a combined spin echo and field echo (SAFE) sequence at 2 mm isotropic resolution and diffusion encoding (15 volumes at b=0s/mm², 46 volumes at b=400s/mm², and 80 volumes at b=1000s/mm²) (Christiaens et al., 2019). T2 datasets were reconstructed to 0.5 mm isotropic using an automated bespoke pipeline, including dynamic distortion correction and slice-to-volume motion correction (Cordero-Grande et al., 2019, Christiaens et al., 2021).

9.6.2 Image registration and segmentation

Alignment between diffusion and T2w volumes for each subject used FLIRT boundary-based registration in FSL (Jenkinson et al., 2001, Jenkinson et al., 2012). For registration of individual subject T2s to a common space, a spatiotemporal atlas of the fetal brain was used, which has been made publicly available (https://gin.g-node.org/kcl_cdb/fetal_brain_mri_atlas). The atlas was constructed using the Medical Image Registration ToolKit (MIRTK) atlas generation pipeline (Schuh et al., 2018) (https://biomedia.doc.ic.ac.uk/software/mirtk/). Cortex, white matter and CSF probability maps were generated using the Developing brain Region Annotation With Expectation-Maximization (Draw-EM) module of MIRTK. Then, an automated deep learning pipeline was used to segment T2w brain images into different tissue types, including deep grey matter, white matter, CSF and cortex (Makropoulos 2014). The deep learning network was trained on manually refined labels propagated from the fetal

dHCP atlas (Schuh et al., 2018, Makropoulos et al., 2018). For each subject, a combination of the T2w volume and the cortex probability map was used for multi-channel ANTs non-linear symmetric diffeomorphic image registration, creating warps between native T2 space and age-matched weeks of the atlas. The multi-channel approach improved accuracy at cortical boundaries.

9.6.3 Surface reconstruction, registration, and vertex correspondence

The cortical plate segmentation was used to reconstruct a surface on the white matter boundary. The inner volume of the segmented cortical plate was smoothed using 1.5 mm full width at half-maximum (FWHM) kernel. On the smoothed volume, the hemispheric (left and right) triangular surface meshes were extracted with the "isosurface" function in MATLAB 2018b (MathWorks Inc., Natick, MA). Resulting surfaces meshes were registered to a 28 GW template surface (Serag et al., 2012), using a 2D sphere-to-sphere warping method (Yun et al., 2020, Robbins et al., 2004), such that there was vertex correspondence between all aligned surfaces.

9.6.4 Surface metric calculation

Three metrics describing surface features were chosen for this study, mean curvature, surface area and sulcal depth. The mean curvature and surface area were computed according to the angular deviation from a patch around each vertex on the surface model and the Voronoi region around each vertex on the cortical surface (Meyer et al., 2003). Sulcal depth was calculated using the adaptive distance transform (ADT) method (Yun et al. 2013).

9.6.5 Diffusion modelling: DTI and MSMT-CSD derived maps of diffusion metrics.

Two different approaches to modelling the DWI signal were used, the traditional diffusion tensor method (DTI) (Basser et al., 1994) and multi-shell multi-tissue constrained spherical deconvolution (MSMT-CSD) (Jeurissen et al., 2014). The diffusion tensor was estimated by extracting the b=0 and b=1000 volumes for each subject, using the iteratively reweighted linear least squares estimator in MRtrix3 (Tournier et al., 2019). Subsequently FA/MD maps were calculated from the tensor (Basser et al., 1994).

For MSMT-CSD derived metrics, in each subject, white matter response functions were extracted from areas of relatively mature white matter (corticospinal tract and corpus callosum) using the 'tournier' algorithm (Tournier et al., 2019; Tournier et al., 2013). CSF responses were extracted using masks of the ventricles using the 'dhollander' algorithm in MRtrix3 (Jeurissen et al., 2014; Tournier et al., 2019; Tournier et al., 2013). To obtain group-average response functions, the white matter response functions of the oldest 20 subjects were averaged (approximating relatively mature white matter), and the CSF group-average response function was calculated from the whole cohort. Using these two average response functions, the dMRI signal of all subjects was subsequently decomposed into a tissue and fluid component, using the tournier algorithm applied via the MRtrix3 software package (Tournier et al., 2019), and resulting components were intensity normalised for each subject (Raffelt et al., 2011). The tissue and fluid component maps were normalised to 1, for ease of interpretation, then labelled and tissue and fluid 'fraction'.

9.6.6 Projecting from the surface boundary into diffusion maps

The inverse transform was applied to the surfaces to register them back to native T2 space, and surface coordinates were converted to cartesian space (x,y,z). This preserved the vertex correspondence between all subjects and the 28 GW surface template, such that the surface normal could be used to extrapolate from the white matter boundary into the T2-aligned diffusion maps at equivalent points

across the surface. The surface normal was multiplied by 2, to project 2 mm perpendicular to the white matter surface boundary, sampling the values in different diffusion maps. The maps used were:

1. Fractional Anisotropy (FA) (DTI)
2. Mean Diffusivity (FA) (DTI)
3. Tissue Fraction (MSMT-CSD)
4. Fluid Fraction (MSMT-CSD)

To obtain estimates of microstructure in the cortical plate, we projected twice the surface normal outside the white matter boundary. To estimate microstructure of the subplate, we projected twice the surface normal inside the white matter boundary.

9.6.7 Coupling analysis within-subject

To understand the local relationships within cortical areas of individual subjects, correlation analysis was performed within vertex neighbourhoods, to calculate the 'coupling' between microstructure and macrostructure (adapted from Vandekar et al., 2016). Custom-built MATLAB analysis pipelines were written, to find neighbours around a central vertex up to 5 degrees of separation. Then the Pearson correlation coefficient (r) and corresponding p value was calculated to describe the relationship between diffusion and surface metrics in each neighbourhood. The subjects were grouped into bi-weekly bins, and a single sample t-test was used on the Pearson r values at each vertex, within each age group, to identify significant vertices. To correct for multiple comparisons across all vertices, we controlled for the false discovery rate (FDR) (Benjamini and Hochberg 1995), to identify significant features while incurring a relatively low proportion of false positives. The mean r value is displayed at the vertices which survived FDR correction in each age bin (23, 25, 27…35 GW).

9.6.8 Age-mismatched coupling analysis

To investigate whether the microstructure in the youngest subjects preceded the formation of cortical folds, we repeated the above coupling neighbourhood analysis, but correlated the mature sulcal depth values (population average at each vertex 35 GW to 37 GW) against the native tissue fraction values in the youngest subjects. The same statistics were used as above to correct for multiple comparisons across all surface vertices.

Chapter 10.

Fetal brain anatomical development converges on neonatal functional resting state networks.

10.1 Abstract

During the second half of human gestation, the structural networks of the human brain are rapidly established. Evidence suggests that the earliest hubs in the functional connectome also start to emerge across the same period. However, establishing how brain structure and function intersect and modulate each other in very early development is challenging. This chapter describes the analysis of dHCP fetal anatomical MRI data, using Independent Component Analysis (ICA), to provide a data-driven decomposition of the T2w volumes into spatial components that represent independent modes of variation in brain structure across all participants. In this case, the aim was to investigate whether structural growth over the fetal period has spatial similarity to neonatal functional networks. We hypothesised that coherent spatial patterns of anatomical development over the fetal period would spatially overlap with mature neonatal functional networks.

10.2 Introduction

The human connectome is organised to optimise the structural integration and functional specification of brain systems (Passingham et al., 2002; Sporns et al., 2005). Optimal "wiring" of this connectome during human brain development is crucial for healthy mental functioning later in life. Previous work suggests that the foundations for the brains' structural and functional connectivity networks are laid in utero, through a complex series of molecular and cellular processes. However, the intersection of these processes is challenging to study ex vivo, as they occur in a spatiotemporally heterogeneous and precisely regulated pattern across the brain. To address this high dimensionality problem, we use a data-driven analysis technique to analyse T2 log jacobian maps, independent component analysis. With this method we explore the image contrast in a model-free approach, to explore how the substrates of the fetal brain structure assemble and converge on neonatal functional networks.

There are many hypotheses concerning what develops first, and the earliest interactions between structural and functional connectivity. At the cellular level, spontaneous activity has been recorded in subplate neurons as early as the mid-fetal period (between 15 and 23 gestational weeks) (Moore et al., 2014, Khazipov and Luhman 2006). These neurons serve as input and output targets for fibers projecting to and from the developing cortex, forming active endogenous cortical circuitry (Kostovic and Rakic 1990). Although connectivity between brain regions becomes significantly more efficient after postnatal myelination, there is widespread, coordinated functional activity in the developing cortex that precedes the presence of myelin. There is also evidence to suggest that myelination induction is dependent on neuronal maturation and electrical activity (Barres and Raff 1993; Demerens, et al. 1996; Gyllensten and Malmfors 1963; Kinney, et al. 1988). Furthermore, in certain circuits, such as the auditory system, the extent of myelination is uncorrelated with functional maturation (Dubois, et al. 2013).

There are numerous methodological challenges associated with the acquisition and analysis of fetal functional imaging data. Since it is challenging to administer specific stimuli to the developing fetus, resting state EEG and fMRI have been used, which do not require active participation from the subject. Resting state recording methods are based on the premise that regions of the brain which are functionally connected continue to communicate while the subject is resting. The covariance in spontaneous brain activity across spatially discrete brain regions can therefore be used to delineate functional activity networks. The first published example of resting state networks in the fetal brain was 10 years ago (Schöpf et al., 2012), and there have since been several studies examining the emergence of network architecture in the second and third trimester (Karolis et al., 2023, Thomason et al., 2013, 2015; Turk et al., 2019; van den Heuvel et al., 2018).

Preliminary studies using fetal resting-state fMRI have identified highly interconnected regions, or 'hubs', in visual and motor areas of the human fetal brain (Thomason et al., 2014 van den Heuvel et al., 2018), which is consistent with observations in infant studies (Fenn-Moltu et al., 2022, De Asis-Cruz et al., 2015; Fransson et al., 2011). Studies in preterm infants over the second to third trimester have shown the maturation of hubs (Van den Heuvel et al., 2018, Doria et al., 2010, Ball et al., 2014), increasing long-range and interhemispheric connectivity (van den Heuvel, et al. 2014), and distinct age-related patterns of development exist across different networks (Doria et al. 2010; Smyser, et al. 2010). By term age, certain networks such as the primary sensory and motor regions, have bilateral network architecture comparable to mature adult resting state networks (Doria et al., 2010; Fransson et al., 2009; van den Heuvel et al., 2014).

Previous work aiming to establish the relationship between structure and function in neonatal development has analysed functional activity and the correlates of myelination. One study estimated white matter myelination using DTI metrics, and recorded functional responses with EEG (Dubois, et al. 2008). This study examined the developing neonatal visual system to demonstrate how fiber myelination leads to a dramatic increase in the conduction speed of the nerve impulses (Baumann and Pham-Dinh 2001). Other studies have linked structure to function at the level of different cognitive systems and found positive associations between working memory performance and microstructural maturation of white matter pathways (Chung, et al. 2018). Similarly, expressive, and receptive language abilities are correlated with myelin water fraction in frontal and temporal white matter regions in toddlers (O'Muircheartaigh, et al. 2014). While simple linear relationships have been found between certain features of structural and functional maturation, the interaction at the systems level to inform network development is likely to be more complex.

Structural brain development is often analysed using measures that describe volumetric growth, by segmenting T2-weighted volumes into different tissue types, using prior anatomical knowledge and imaging contrast as priors. This approach has been used to quantify the growth of fetal brain structures across large representative populations, establishing the maturational trajectories of different tissue types across the second to third trimester (Grossman et al., 2006, Clouchoux et al., 2012, Ren et al., 2022, Scott et al., 2011, Jarvis et al., 2016, Machado-Rivas 2022, Kyriakopoulou et al., 2017). However, with this approach, it is difficult to infer the co-maturation and modes of variation between brain areas as they develop.

Overall, the literature to date has identified several different brain regions that play a crucial role in early human brain development and are involved in the assembly of functional network

architecture. Similarly, the development of brain structures and cortical expansion has been described in previous chapters (Wilson et al., 2021, 2023, Jaimes et al., 2021, Song et al., 2017). However, establishing the relationship between developing structure and function remains a challenge. There are very few studies describing how brain structure and function modulate each other in very early development, and none address the relationship between morphometry, volumetric growth, and functional activity.

The aim of this work was to use a data-driven approach, independent component analysis (ICA) (Comon 1994), to identify brain regions with coherent structural expansion and spatially independent maturational trajectories. ICA is an unsupervised learning method that separates independent signals out from a linear mixture. This approach to data processing can be used to find the modes of variation in neuroimaging data across a group of subjects. ICA was run on the Jacobians of the dHCP fetal anatomical MRI data, with the aim to separate out networks of brain regions that have coordinated expansion and growth over the second to third trimester. We then investigate whether these 'structural networks' are spatially similar to neonatal functional networks (Eyre et al., 2021) using the Jaccard Index. We hypothesised that coherent spatial patterns of anatomical development over the fetal period will map onto the most mature functional networks observed in neonates.

10.4 Results

ICA applied to the fetal T2 Jacobian maps was successful in separating the mixed signal into spatially independent components. All components were either bilateral and symmetrical or had a complementary separate component in the opposite hemisphere. After running a GLM to extract component weightings, these were correlated against the gestational age of the subject. All 20 ICA anatomical components had strong age-related trends, linear and exponential, in subject weightings (Figure 1). The largest variation in component weighting between subjects of the same age was observed in the ventricle components (IC 6 and 14). Many of the component weighting trends increased up to 30 weeks, then plateaued and more variability was introduced between subjects, (IC 0, 4, 7, 9, 17), many of these were in the CSF/outer cortical tissue.

I identified five distinct groups based on tissue type and maturational trend across subjects, including deep grey matter areas, white matter, CSF, ventricles, and primary cortical areas (Figure 1). For independent components of the same tissue type, I observe the same trends in component weighting with age, suggesting that primary cortical areas for example share similar developmental trajectories but their maturation is not dependent on each other. To compare the fetal structural networks to the dHCP neonatal functional networks (Eyre et al., 2021), we calculated the spatial similarity between them, and the top 15 overlapping network combinations are shown (Figure 4) Four components shared high spatial similarity with neonatal fMRI resting state networks (Jaccard indices higher than 0.25) (Figure 3). These included the medial visual, posterior parietal, medial motor, and motor association functional networks. Most of the T2 components did not overlap with fMRI resting state networks and shared less than 10% of similar voxels (Figure 4).

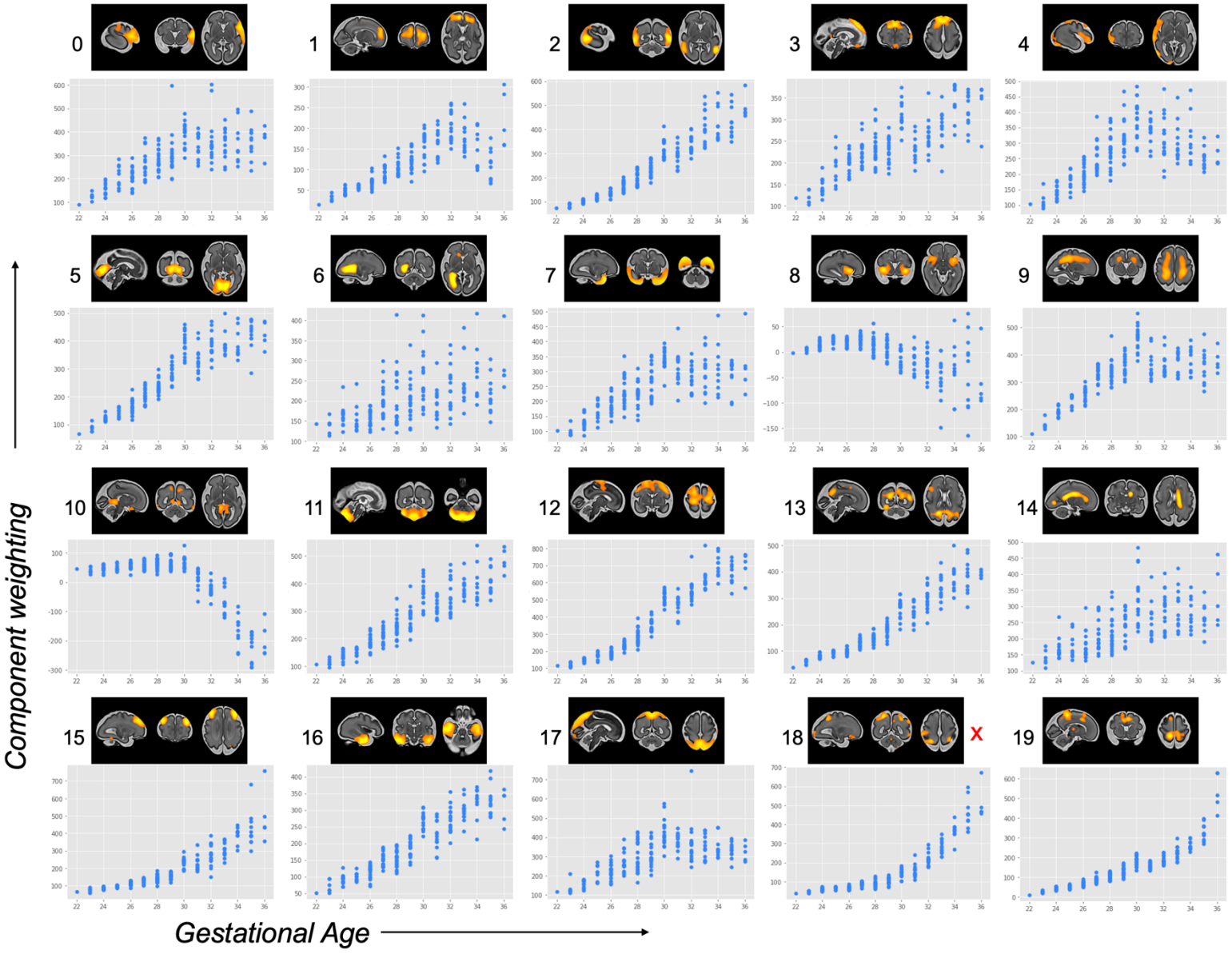

Figure 1. *All 20 ICA anatomical components had strong age-related trends, either linear or exponential, in subject weightings. The weighting of each component in each subject (y axis) is plotted against the gestational age of the subject (x axis). Red cross indicates components that were identified as noise.*

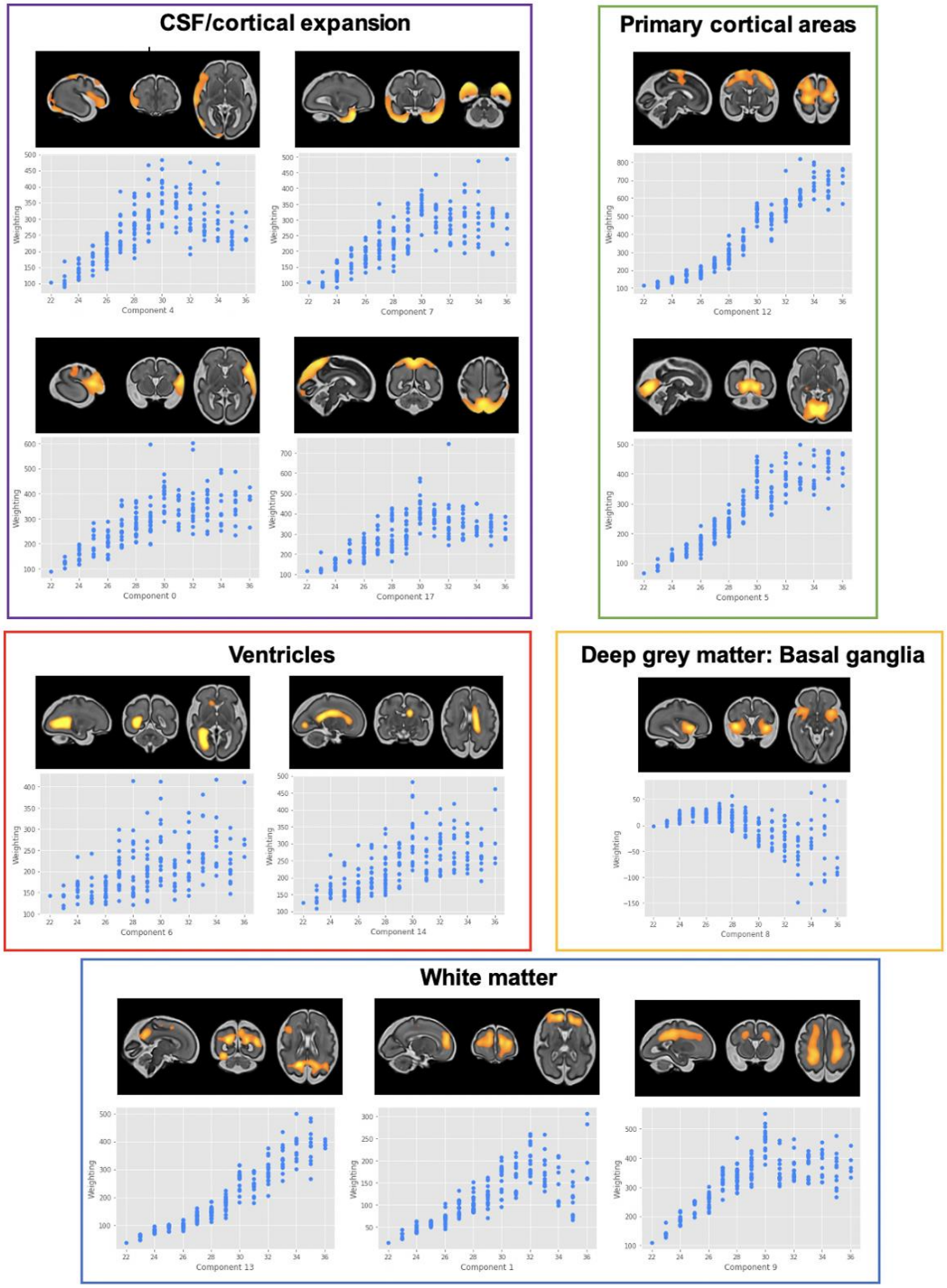

Figure 2. *Independent components could be clustered according to similar tissue types, which showed similarity in the relationship between component weighting and gestational age.*

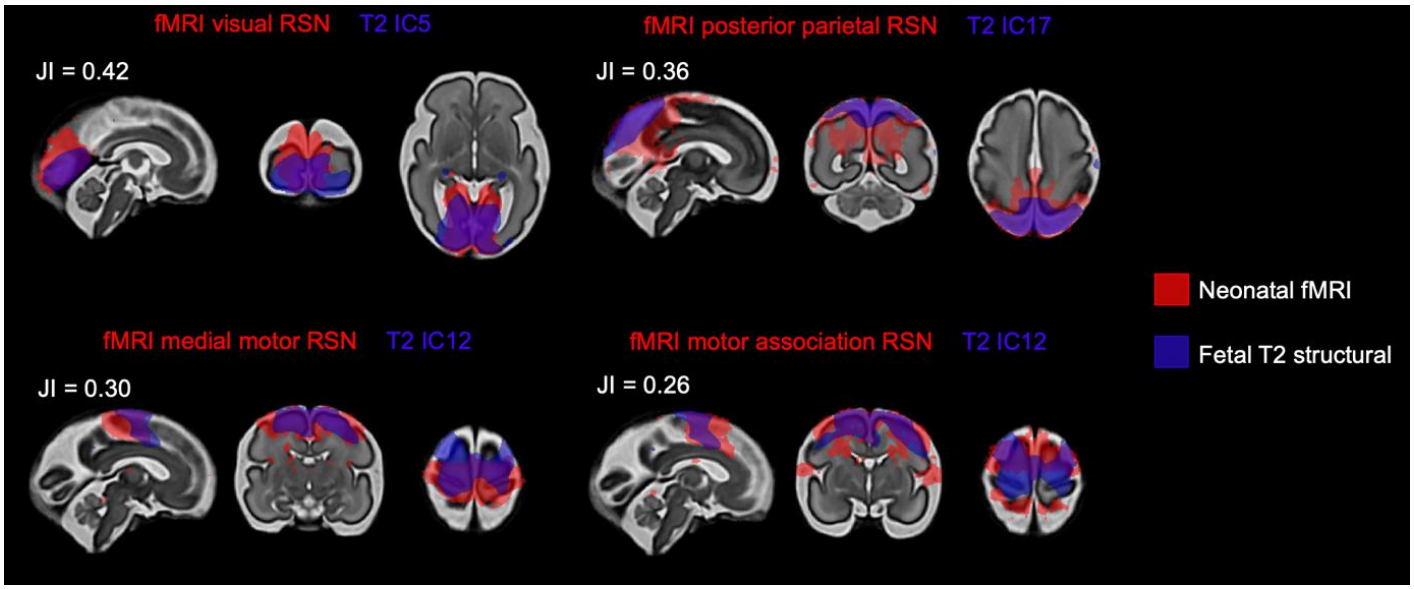

Figure 3. *The 4 pairs of regions with the largest Jaccard Index (JI), indicating the largest spatial similarity, were the visual, medial motor and motor association regions and the posterior parietal network.*

Fetal T2 networks	Neonatal fMRI resting state networks	Jaccard Index
IC_0005	Visual	0.41998
IC_0017	Posterior parietal	0.360525
IC_0012	Medial motor	0.299256
IC_0012	Motor association	0.261523
IC_0017	Visual Association	0.17578
IC_0000	Auditory	0.157734
IC_0004	Auditory	0.150481
IC_0012	Lateral motor	0.142554
IC_0003	Prefrontal	0.129214
IC_0012	Frontoparietal	0.126407
IC_0002	Temporoparietal	0.123491
IC_0004	Temporoparietal	0.119671
IC_0000	Somatosensory	0.116873
IC_0013	Posterior parietal	0.115302

Figure 4. *Spatial similarity between fetal T2 and neonatal fMRI resting state networks according to Jaccard Index.*

10.5 Discussion

The results suggest that during the second and third trimester, there is coordinated maturation of brain anatomy in specific regions which parallel the development of functional network architecture. The linear and exponential trends we observe between component weightings and gestational age imply that structural foundations are being built throughout the second and third trimester, between 22 and 36 weeks.

Each spatial component represents a mode of variation of brain structure across all participants, we observed very similar component weights between subjects of the same gestational age, particularly in the second trimester, suggesting gestational age effects drive most of the variation between subjects. Components that were CSF-dominated in younger subjects (which become the outer cortex in older subjects), plateaued at in component weighting at approximately 30 weeks (IC 0, 4, 7, 9, 17). This coincides with the fast-growth phase of gyrification across the brain (Yun et al., 2020) and is likely reflective of the increasing macrostructural maturity (cortical folding) in these areas. The primary cortical area components (IC 5, 12) showed linearly increased weights, while the white matter components in the cingulum and periventricular cross-roads showed inflection points at ~30 and 32 GW, which may reflect the change in T2w contrast at the onset of pre-myelination which occurs around this timepoint (Kinney et al., 1998).

ICA also extracted components which were a combination of cortical and subcortical grey matter, with known connectivity between them, such as the LGN and the primary visual area, suggesting that there is coordinated, uniform expansion of brain tissue in the subcortical and cortical areas. Many imaging studies and post-mortem analysis have quantified the differences

in MR contrast that reflect tissue maturation, and their biological underpinnings, but have largely been exploring DWI data (Wilson et al., 2021, 2023, Jaimes et al., 2020, Khan 2019, Zanin et al., 2011 Takahashi et al., 2012). The results presented here highlight that there is developmental contrast in the T2 volumes, that may be informative and complementary to diffusion data analysis.

When I calculated the spatial similarity between the T2-derived components and the neonatal resting state networks, the largest spatial overlap between anatomical and functional network development was seen in the visual and motor regions. This result is consistent with studies of functional activity which have identified these areas as critical functional hubs in perinatal development (Doria, et al. 2010; Fransson, et al. 2009; van den Heuvel, et al. 2014). Previous literature has also described the evolution of network architecture in preterm infants, during the same timeframe in development. Analysis of functional activity in preterm infants observed a rich club of interconnected cortical hubs already present by 30 GW, sharing similarities with adult network connectivity (Ball et al., 2014). This was supported by separate studies describing properties of centrality in the network organization in primary (visual cortex, precentral gyrus) and association brain regions (inferior temporal gyrus, medial temporal lobe) before birth and in neonates (Turk 2019, Fenn-Moltu et al., 2022). The combination of the findings presented in this chapter, together with previous work in fetal and preterm cohorts makes a strong case for the early maturation of sensorimotor networks, both in terms of their structure and function.

Selecting imaging markers a priori can bias observations, whereas ICA allows for non-subjective analysis of the imaging data and other co-variates. When applied in the spatial domain to anatomical data, ICA can detect and separate spatial features that are strongly

associated with demographic and behavioral variables (Douad et al., 2014, Llera et al., 2019). Previous studies have used this method for a variety of applications, including the identification of biomarkers to understand the encephalopathy of prematurity (Ball et al., 2017) and neurodegeneration (Douad et al., 2014). Ball et al., used a combination of ICA and canonical-correlation analysis (CCA) to reveal patterns of structural development that were associated with specific clinical risk factors, which in turn correlated with cognitive and motor outcomes at 2 years (Ball et al., 2017). Another study used ICA to parcellate developing white matter into regions with consistent growth trajectories and found associations with cognitive ability in a subset of components (O'Muircheartaigh et al., 2014). These results suggest that it could be informative to perform similar analysis in the fetal cohort, exploring if in utero brain structure is associated with cognitive outcomes later in life.

The different dimensions and resolution of structural and functional imaging data make multi-modal analysis challenging, particularly in the fetal brain where both imaging modalities are also accompanied by their own unique set of challenges and are highly sensitive to motion and distortion. In theory, introducing other imaging contrasts, such as diffusion maps would be beneficial to this analysis. With DWI metrics it would be possible to explore microstructural changes underlying the independent growth trajectories of these brain regions, that accompanies cortical expansion. This would be possible using linked independent component analysis (FLICA) implemented in FSL (Groves et al., 2011; Smith et al., 2004). FLICA is an extension of ICA that facilitates multi-modal data integration, where multiple ICA factorizations are simultaneously performed, characterising biophysically plausible modes of variability across all subjects' images. FLICA aims to overcome the difficulties associated with analysing multiple modalities in separate pathways. However, in practice, FLICA was challenging to implement with fetal data because it relies on accurate registration between

imaging modalities and standard space. Image registration was more accurate with T2-weighted volumes than the diffusion volumes, which are more prone to distortion and lower SNR. There are also differences in the acquired resolution between modalities (DWI = 2 mm^3, T2 = 0.8 mm^3) that drive the registration error at the cortical boundary, due to greater partial voluming in the lower resolution DWI. In the fetal data, certain diffusion contrasts have less noise and greater contrast between tissues than others eg. MD, and therefore dominate the FLICA decomposition.

This analysis paves the way for future investigations of the structural imaging contrast. The networks extracted herein also provide a meaningful way to parcellate the anatomical data, for future work to extend this analysis and create structural connectomes. Another avenue to pursue in future work would be to repeat this unbiased analysis of T2 signal in a fetal clinical cohort, such as in fetuses with congenital heart disease, where there is a known alteration in structural brain development that is associated with functional, cognitive consequences later in life. With the data acquired, we only explored the variation between components due to gestational age, but the extraction of meaningful anatomical regions implies this approach could be extended to explore how other co-variates, such as socioeconomic status, or maternal health introduce modes of variation into the developmental contrast and affect structural brain growth.

This exploratory analysis of the T2 contrast examined if independent features were detectable and could support our understanding about structural brain development in utero. Although this analysis cannot reveal any causative links between structural and functional development, it demonstrates with two independent cohorts and imaging modalities, that there is a coherent change in the fetal T2 image contrast supporting previous functional imaging work in neonates.

The data-driven approach extracted meaningful anatomical networks, such as the thalamic LGN and primary visual cortices, without any manual intervention or priors beyond specifying the number of components. The success of this method is a testament to the quality of the fetal imaging reconstructions, suggesting meaningful developmental contrast exists between tissue types.

10.6 Methods

10.6.1 Cohort, acquisition, and pre-processing

For this analysis, we used a subset (n = 190) of the Developing Human Connectome Project (dHCP) fetal cohort (http://www.developingconnectome.org/), scanned at the Newborn Imaging Centre at Evelina London Children's Hospital, London, UK, ethical approval (14/LO/1169, IRAS 138070). All pregnant participants gave written informed consent prior to scanning. T2-weighted MRI datasets (range: 22 to 36 weeks gestational age) were acquired with the dHCP acquisition protocol (see earlier Methods section) on a Philips Achieva 3T system with a 32-channel cardiac coil, using multiple single-shot turbo spin echo sequences with TE = 250ms, TR = 2265ms (Price et al., 2019). Datasets were reconstructed to 0.5 mm^3 resolution using an automated bespoke pipeline, including dynamic distortion correction and slice-to-volume motion correction (Cordero-Grande et al., 2019).

All MRI data was reviewed by an expert perinatal neuroradiologist and any subjects with brain abnormalities were excluded. All remaining subjects were visually checked and scored (0-4) based on the field of view, residual motion, distortion, and artefacts (for more detail see 4.5 Quality Control).

10.6.2 Image registration

To run ICA, all subject volumes must be aligned to a common space. ANTs non-linear symmetric diffeomorphic image registration (Avants et al., 2008) was used to register subjects T2 to the 30w template of the dHCP atlas (via age-matched weekly template intermediates). The dHCP spatio-temporal fetal brain atlas (https://gin.g-node.org/kcl_cdb/fetal_brain_mri_atlas) was constructed using a modified version of the MIRTK atlas generation pipeline (Schuh et al., 2018). Both the subject T2 and the MIRTK-generated cortex probability maps were used as inputs to the non-linear registration, which improved accuracy at cortical boundaries. After image registration to the dHCP fetal atlas, a further quality control step was introduced to visually assess the alignment of each subject.

10.6.3 Jacobian determinant ICA analysis

Non-linear deformation fields were created to transform the native subject T2 to the age-matched template of the dHCP fetal atlas (https://doi.gin.g-node.org/10.12751/g-node.ysgsy1/) using ANTs (Avants et al., 2008). Warps were then compiled between native T2 and 30 GW template space (Avants et al., 2008), and the log Jacobian determinant calculated. In the resultant log Jacobian maps, higher log-Jacobian values represent brain regions that contracted during image registration (i.e., larger brain volumes), while smaller values represent volume reductions (Avants and Gee, 2004). A single 4D file was created by concatenating the log Jacobian volumes for all subjects. This was used as the input for subsequent analysis in Python (Van Rossum and Drake, 1995; Varoquaux et al., 2010).

The canonical ICA algorithm (Varoquaux et al., 2010), implemented in python using the nilearn package (Abraham et al., 2014), was applied to the 4D Jacobian volume. ICA is a technique that extracts salient patterns embedded in the data, by separating out the multivariate

signal into a maximally independent set of components. The ICA algorithm transforms the input data into components that represent an 'unmixing' of the signal, such that the independent components have distributions that are non-Gaussian. In this way, it can reduce the dimensionality of the data (from many thousands of individual voxels) into a set of interpretable variants. The optimal number of components for this case was chosen to balance robustness and interpretability (Eyre et al., 2021). I observed that increasing the ICA dimensionality above 20 lead to a division of cortical regions and splitting bilateral components into left/right lateralised areas.

Components were inspected and only one artefact component was identified and excluded from further analysis. The criteria for excluding components were (a) majority of the signal occurring in edge voxels indicating misregistration (b) sparse, randomly distributed signal with low total area.

To extract component weightings for each individual subject, FSL's general linear model was applied to the component maps, co-varying for gestational age (Winkler et al., 2014; Anderson and Robinson 2001). For each component, the weighting for each subject was plotted against gestational age to visualise any trends across the second to third trimester.

10.6.4 Neonatal functional resting state networks

The estimation of neonatal fMRI resting state networks is described in detail by previous work (Eyre et al., 2021). Briefly, probabilistic group ICA was performed using FSL melodic on temporally concatenated data across term-born infants scanned at 43.5–44.5 weeks PMA (n = 24). The result was eleven spontaneous BOLD activity patterns (RSNs), categorised by their

neuroanatomy into primary and association networks. Five RSNs included primary motor or sensory cortical areas and were categorized as primary networks: medial motor, lateral motor, somatosensory, auditory, and visual. The remaining six were categorized as association networks: motor association, temporoparietal, posterior parietal, frontoparietal, prefrontal and visual association.

10.6.5 Calculating spatial similarity with the Jaccard Index

To transform the neonatal resting state networks into 30w fetal template space, a non-linear warp was calculated between neonatal 40w template and fetal 30w template, using ANTS SyN (Avants et al., 2008). The Jaccard index (J) (Jaccard, 1912) was used to compare the spatial similarity between fetal structural components (A) with the neonatal RSNs (B):

$$J(A,B) = \frac{|A \cap B|}{|A \cup B|}$$

This index quantifies the similarity between the two sets of data, with a range from 0 to 1, where 0 is no overlap and 1 is spatially identical. The closer to 1, the more similar the two components.

V. Conclusions

11. The main findings

There is a very limited amount of literature in the field of fetal MRI and therefore the focus of this thesis was to pilot neuroimaging methods for exploratory analysis, aiming to understand the MRI signal and what it represents in the context of the fetal brain. Diffusion MRI has high sensitivity but low specificity to a variety of biological processes, and therefore the precise biological underpinnings of signal change are ambiguous. The first two results chapters of this thesis describe the use of complementary diffusion modelling techniques to quantify and describe white matter development over the second to third trimester. Acquiring multi-shell HARDI allowed the fitting of microstructure models that capture more of the information within the diffusion signal than DTI, enabling the extraction of more informative parameters from the data. While DTI provides a benchmark for comparisons to be made with previous literature, when this was combined with MSMT-CSD-derived metrics, a more refined interpretation of the dynamic contrast changes was possible.

In the first results chapter, I use tractography to delineate exemplary developing white matter bundles, and quantified microstructural change with DTI (to provide a reference to previous work) and MSMT-CSD metrics. This analysis demonstrates distinct developmental trajectories for major association, projection, and commissural fibers, with nonlinear changes in tract microstructure. 2^{nd} order polynomial trends were fitted to describe the overall changes in microstructure, which align with post-mortem studies and provide insight into early

neurodevelopmental processes. Changes in FA and MD were observed, reflecting maturational changes in water content, tissue organization, and axonal coherence. The results in this chapter highlight the unique maturational trends of different white-matter tracts and the heterogeneity of white-matter development during the late second to third trimesters of gestation, serving as a resource for future research and clinical comparisons.

The second results chapter details an extension of this analysis of white matter development, to dissect the changes in diffusion signal at the level of transient fetal tissue compartments. By segmenting the tracts, it was possible to characterise tissue properties continuously along the developing fiber bundles, with higher spatial and temporal specificity. This facilitated better interpretation of the dynamic changes in MR contrast in each compartment, relating them to the well-established developmental biology occurring during the early, mid, and late prenatal periods. This method worked especially well in the thalamic-motor and sensory tracts which showed comparable microstructural trajectories. During the early period, there was a higher tissue fraction in the middle of the tract, where migrating neurons form a radial scaffold. In the mid prenatal period, as this scaffold dissipates, there is a decrease in tissue fraction in the middle of the tract and an increase towards the termination of the tracts, aligning with the maturation of neurons in the cortical plate. During the late prenatal period, the start and end of the axis exhibit the highest tissue fraction values, indicating the onset of the pre-myelination phase of white matter development. This chapter illustrates how the dMRI signal can be utilized to model in vivo spatiotemporal trajectories, capturing underlying neurobiological properties, and aligning with trends observed in post-mortem histology (Kostović, 2020).

The third chapter of this thesis examined the hypothesis that there are microstructural changes in the cortical plate and subplate that predict the emergence of sulci. The analysis combined

microstructural and macrostructural metrics across gestation and within subject to test this hypothesis. The challenge to address this research question was to disentangle broader maturational changes from a specific change in microstructure that is directly linked to cortical folding. To approach this, neighbourhood analysis was used at the level of individual subjects, correlating diffusion metrics extracted from specific fetal compartments with the local change in sulcal depth. A clear inverse relationship was observed in all subjects, independent of gestational age, that showed tissue fraction decreases as a function of sulcal depth in all neighbourhoods, with a partially or fully formed sulcus. This correlation was robust and significant after multiple-comparison correction across a large proportion of surface vertices in sulcal areas, implying that there are local minima in tissue microstructure across the surface that denote the presence of sulcal pits.

A plausible biological reason for this trend is the variation in fiber density and connectivity between gyral and sulcal regions, which has been repeatedly observed by a variety of different studies using diverse research methods (Nie et al., 2012, Deng et al., 2014, Takahashi 2012, Mortazavi et al 2017). Previous work has noted up to a 50% reduction in white matter neurons in sulcal pits compared to gyral crown areas (Mortazavi et al 2017). Studies drawing comparisons across including human, chimpanzee, and macaque brains, found higher axonal fiber density near the gyral crowns (Nie et al., 2012). Imaging analysis of HARDI data in humans also identified differences in fiber density between gyral and sulcal areas, indicating that gyri are connected by denser tractography streamline fibers than sulci (Takahashi et al., 2012). Additionally, to support the structural findings, stronger functional connectivity has been shown between gyri, weaker connectivity between sulci, and moderate connectivity between gyri and sulci (Deng et al., 2014). Overall, the analysis presented in this thesis builds

on previous knowledge of neuroanatomy and suggests that microstructural changes can serve as predictors for the onset of primary cortical fold development.

The final chapter details a data-driven decomposition of the anatomical data, using independent component analysis (ICA) to separate mixed spatial features within developmental T2 contrast. The first goal of this investigation was to explore coordinated maturation of brain anatomy during the second and third trimester. The second goal of this analysis was a brief inquiry to link structural components to the development of functional network architecture. Unlike previous chapters that were guided by *a priori* theories and selection of anatomical regions of interest, ICA offers an model-free approach to analysing the data. I successfully extracted meaningful anatomical networks, which highlighted a developmental synchrony between all the primary cortical areas, as demonstrated by their similar component weighting trajectories across age. Other components identified included deep grey matter, periventricular cross-roads, and outer CSF, reflecting general cortical expansion over the fetal period. The trends in component weightings across gestational age were similar for each tissue type, highlighting the developmental contrast and morphological maturation in T2w volumes, which could complement diffusion data analysis in future work.

When compared with neonatal functional networks, the highest spatial similarity between anatomical and functional network development was observed in the visual and motor regions. These areas have been identified as critical functional hubs in perinatal development (Doria, et al. 2010; Fransson, et al. 2009; van den Heuvel, et al. 2014). Supporting the notion that the earliest maturing networks have coordinated development of both structure and function. This exploratory analysis investigated using T2 contrast to detect independent features and enhance our understanding of structural brain development in utero. Although this brief analysis could

not establish causal links between structural and functional development, the results demonstrate a meaningful way to parcellate the brain for future analysis, showing coherent changes in fetal T2 image contrast in areas of the brain that also show the greatest functional maturity in utero.

12. Future directions for fetal imaging

An essential hypothesis that has not yet been studied is the difference between in utero and ex utero development. This is vital for clinical understanding of why infants born preterm have an increased risk of adverse neurodevelopmental outcomes. Furthermore, they have a greater risk of developing autism, schizophrenia, and psychosis later in life. The 'Fetal Origins of Disease' hypothesis stipulates that neurodevelopment in utero is a critical determinant of neurological health later in life. The comparison between fetal and preterm development is essential to test this theory, quantifying differences in in utero and ex utero development will improve clinical understanding about the encephalopathy of prematurity. However, this is a non-trivial hypothesis to test, due to the need to harmonize between fetal and preterm MR scans. In addition to differences in diffusion acquisition parameters (such as the strength and number of b shells), there is also a greater susceptibility to motion and other artefacts in utero. A thoughtful and creative approach to data analysis is required to overcome these confounding factors. Adapting the methods outlined in this thesis could provide important insight about windows of vulnerability for preterm infants, compartmental differences in microstructural development and the link between microstructure and cortical folding.

Other imaging modalities may also provide complementary insight about fetal brain development and build on the results outlined in this thesis. T1w contrasts were also part of the dHCP fetal acquisition protocol but were not analysed due to time constraints. Previous literature has used intensity normalized and calibrated T1w and T2w contrasts to create a T1/T2 ratio map. The T1/T2 contrast is used as a quantitative measure of tissue integrity, suggested as a measure of myelin content (Glasser and Van Essen 2010, Ganzetti et al., 2014). Since the T1/T2 ratio accentuates contrast between myelinated and less myelinated structures, it may provide useful qualitative mapping of pre-myelination and its spread across the brain in the late fetal period. Mapping the spatial spread of myelination would complement this work and further understanding about white matter development in the third trimester.

The recent development of cerebral organoids from human cells has the potential to bridge the gap between in vivo MRI and cellular mechanisms (Lancaster and Knoblich 2014, Lancaster et al., 2013). Organoids are three-dimensional structures derived from human pluripotent stem cells that can be used to recapitulate key features of human brain development in a simplified and controlled environment. They have become a valuable tool for studying brain development and disease. Spontaneous electrical activity has been recorded within organoid cultures and early evidence of neural circuits (Zourray et al., 2022). By combining organoid cultures with advanced imaging techniques, such as calcium imaging or functional magnetic resonance imaging (fMRI), it is possible to investigate patterns of neuronal activity and the earliest phases of structural and functional development. However, a major challenge in this field currently is the non-overlapping timescales between in vivo and ex vivo work, such that cell cultures, human tissue work and organoids can be used to model processes in the first trimester, then in vivo imaging only becomes possible in the second to third trimester. Formulating approaches to acquire imaging earlier and tissue work later in development would facilitate links between

volumetric whole-brain imaging and cellular analysis techniques. Bridging the gap of scales, from whole brain voxels to the cellular level removes the ambiguity in the biological interpretations that are littered throughout this thesis, and more broadly is a coveted goal for neuroscience researchers.

In a similar vein, ultra-high field imaging of human fetal tissue also provides mechanistic insight that would complement MR analysis with greater granularity at the cellular level. Imaging *ex vivo* at ultra-high field strength offers improved spatial resolution and tissue contrast.. Ultra-high field MR in conjunction with histology on the same specimens provides a direct link between dynamic MR signals and their biophysical correlates. It would enhance confidence in the biological interpretations described in this thesis if they were accompanied by histological stains to validate the hypotheses.

13. Concluding remarks

The goal throughout this work was to deepen understanding about fetal MRI as a research tool to investigate the developing brain, and to establish a normative reference for the contrast changes underpinning the maturation of cerebral tissues across the gestational timeline. Quantifying the spatiotemporal maturation of MR contrast for different tissue types, provides a benchmark to identify deviations from the norm in clinical cases and establishes guideposts for its use in general clinical practice. The work in this thesis involves a combination of data driven techniques, such as independent component analysis and methods guided by prior understanding of developmental neuroanatomy, such as diffusion tractography. When these various methodological approaches were tailored specifically to the fetal population, it was

possible to address all the research hypotheses set out in the start of this thesis, demonstrating the promise of high-quality fetal MR data for a variety of multi-modal research applications.

The use of MRI as a quantitative method relies on the assumption that a given tissue is represented by similar voxel intensities throughout the data. If the images are corrupted, due to distortion, motion or other artefacts, the quantitative parameters computed from corrupted data will likely be erroneous. Correcting or reducing the effects of these artefacts is thus a crucial issue for the use of MRI in quantitative analysis (Belaroussi et al., 2006). Adequate image processing, motion and distortion correction algorithms that are specifically tailored to the fetal context, are a requirement for accurate quantification of signal in utero. Thus, the absence of fetal specific image processing pipelines has been a major confound in previous fetal studies, limiting the reliability and interpretation of developmental contrast.

It was a priority of the dHCP to generate research-quality fetal MR data, by dedicating resources to the development of bespoke pre-processing pipelines, significantly enhancing the quality of fetal data for research use. This quality across modalities made it possible to conduct joint analysis of different imaging contrasts and further understanding about the complementary information between them, despite the differences in artefact susceptibility, noise, and resolution. After addressing the challenges of spatial normalisation across modalities and using stringent quality control, the fetal imaging contrasts were richly informative, reliably reflecting biological changes with a consistency between subjects of the same age. Consequently, the work in this thesis supports the use of as much multi-modal information as possible to characterise in utero neurodevelopment at the individual and group level. On the other hand, this work also highlights constraints and limitations of the data that must be considered when linking MR results to the underlying biology. Overall, the work in this thesis

will hopefully encourage the medical imaging community to take advantage of fetal MRI, and the open access dHCP dataset, for clinical and general research applications.

VI. Appendix I

Supplementary Information for Results Chapter 7:

Development of white matter pathways over the second to third trimester in the human fetal brain,

Wilson et al., 2021 PNAS

PNAS
www.pnas.org

Supplementary Information for
Regional Development of Human White Matter pathways in utero over the 2nd and 3rd Trimester

Siân Wilson, Maximilian Pietsch, Lucilio Cordero-Grande, Anthony N Price, Jana Hutter, Jiaxin Xiao, Laura McCabe, Mary A Rutherford, Emer J Hughes, Serena J Counsell, Jacques-Donald Tournier, Tomoki Arichi, Joseph V Hajnal, A David Edwards, Daan Christiaens, Jonathan O'Muircheartaigh

Corresponding author: Tomoki Arichi
Email: tomoki.arichi@kcl.ac.uk

This PDF file includes:

Supplementary Information

The dHCP data collection and analysis was approved by the UK NHS research ethics committee (REC code: 14/LO/1169). Informed written consent was obtained from each subject prior to participation.

1. Acquisition, pre-processing and quality control. Gestational age was determined by sonography at 12 post-ovulatory weeks as part of their routine clinical care. Fetal MRI data were acquired with a Philips Achieva 3T system with a 32-channel cardiac coil in maternal supine position. dMRI data were collected with a combined spin echo and field echo (SAFE) sequence [1,2] at 2 mm isotropic resolution, using a multi-shell diffusion encoding that consists of 15 volumes at b= 0 s/mm^2, 46 volumes at b= 400 s/mm^2, and 80 volumes at b= 1000 s/mm^2 lasting 14 minutes [3,4]. The protocol also included the collection of structural T2w, T1w, and fMRI data, for a total imaging time of approximately 45 minutes.

Raw data were processed using a bespoke processing and quality assessment pipeline [5] that includes Generalized Singular Value Shrinkage (GSVS) MP-PCA image denoising and Rician bias correction in the acquired magnitude, complex data dynamic distortion correction of susceptibility-induced B0 field changes using the SAFE method [1,6,7] and slice-to-volume motion

correction based on a multi-shell spherical harmonics and radial decomposition (SHARD) representation[5].

Quality control was based on summary metrics designed to detect the amount of motion (based on the gradient of the motion parameters over time) and the percentage of slice dropouts in the data [5]. This was followed up with expert visual assessment, which considered any residual or uncorrected artefacts due to motion, noise and distortion. Of the 151 subjects that were pre-processed, 113 were classified as high quality reconstructions based on the above criteria and were included in this study.

2. Modelling diffusion weighted imaging data. For each subject, the motion and distortion-corrected *b=0* and *b=1000* volumes were extracted and used to estimate the diffusion tensor, using the iteratively reweighted linear least squares estimator in *MRtrix3* [8] and FA/MD maps were calculated [9].

For spatial alignment, orientation density functions (ODFs) were estimated in *MRtrix3* using constrained spherical deconvolution [10,11]. Individual subject ODFs were compiled into weekly templates through a series of coarse pose normalisation and nonlinear diffeomorphic image registration steps [12–14]. The resulting ODF templates were then iteratively nonlinearly aligned to a joint population template using median aggregation [13,14]. The resulting transformations were composed to obtain pairs of inverse consistent diffeomorphic subject-to-template and template-to-subject warps.

For analysis, WM and CSF response functions were estimated for each subject in subject-native space using co-registered age-matched T2-based tissue segmentations [15] as inclusion areas. WM response functions were extracted from the CST and CC using the *tournier* algorithm and CSF responses using the *dhollander* algorithm in *MRtrix3* [8,16]. The WM response functions of the oldest 20 subjects were averaged to obtain a group-average response function of relatively mature WM, a group-average CSF response function was calculated from the whole cohort of subjects. All subjects' dMRI signal was subsequently deconvolved into tissue ODF and scalar fluid components using multi-shell multi-tissue constrained spherical deconvolution [11] and the two corresponding group-average response functions. For each subject, the resulting components were intensity normalised [13] and, to be able to compare FA values with tissue anisotropy, the power spectrum in the tissue component was calculated from the square root of the power in the l=2 band of the spherical harmonics on the normalised ODF. Finally, all normalised quantities were transformed to their respective template-space using the subject-to-template warps.

3. Tractography. The ODF templates were used as a guideline for selecting regions of interest (ROIs) to perform tractography. Targeted probabilistic streamline tractography as implemented in *MRtrix3*, was performed in 5 different weekly templates (at intervals of ~3 weeks) on the normalised age-averaged tissue ODFs to delineate the CST, ILF, OR and CC (Figure 2). This approach was used in order to maintain a standardised region of interest for calculating microstructural metrics. Tractography was performed independently in the left and right hemispheres of each template, due to the recorded hemispheric asymmetry of the fetal brain [17]. Tracts were defined based on multiple spatially independent ROIs, originating in seed regions, with at least one further specific inclusion zone and with exclusion zones to limit tracts to a single hemisphere if appropriate (specific details of how each tract was delineated are described below). Template-to-subject warps were constructed using the FNIRT package in FSL [18] and used to transform tracts from the age-matched template to individual subject space. Tracts were sifted for spurious streamlines using tcksift [8,19].

3.1 Cortico-spinal tract (CST). For tracking both the left and right CST, the cerebral peduncle of the lower brain stem was used as a seed region, with waypoints in the left and right posterior limb of the internal capsule (PLIC). Both masks were drawn using axial brain slices and were 3 slices thick. The left and right primary motor cortices, were used as respective tract endpoint regions.

The central sulcus was used as a reference point to identify this region in the 3D-volumetric reconstruction of the brain. An angulation threshold of 15° was used.

3.2 Inferior lateral fasciculus (ILF). Seed-region masks were placed in coronal slices in the left and right anterior temporal lobes, with a waypoint mask placed along part of the lateral and inferior wall of the lateral ventricle. To avoid inclusion of fibres crossing the midline, an exclusion zone was placed through the corpus callosum with a sagittal mask along the midline. Angular threshold of 20° was used.

3.3 Optic radiation (OR). The left and right optic radiations were tracked separately, using the left and right lateral geniculate nucleus as a seed region. A waypoint was drawn in coronal slices, in the posterior occipital lobe, estimating the location of the primary visual cortex. The exclusion zone consisted of a multi-slice sagittal mask along the midline and a multi-slice axial mask immediately superior to the corpus callosum. Angular threshold of 20° was used.

3.4 Corpus callosum (CC). The genu and the splenium of the corpus callosum were tracked independently, due to an *ex utero* autopsy study reporting different sequences of myelination in the subregions of the corpus callosum [20]. Exclusion zones were placed in axial slices above and below the corpus callosum and in mid-coronal slices. Due to the curvature of the tracts, angulation thresholds were set higher at 45°.

4. Analysis of microstructural change metrics. Diffusion tensor model: Tracts were overlaid onto the FA and MD maps and then the mean FA and MD values were calculated within the overlaid streamlines. Multi-shell multi-tissue constrained spherical deconvolution: Tracts were overlaid onto the normalised fluid ODF, and onto the square root of the power in the l=2 band of the tissue ODF, representing tissue anisotropy and the mean value within the streamlines was calculated.

5. Statistical modelling. Akaike information criterion (AIC) was used to evaluate the most suitable model across different degrees of polynomial fit (1-4), to describe the relationship between gestational age and FA/MD [21]. This was determined according to the lowest AIC value and highest rounded Akaike weight (w_i). Where a linear trend was identified, Spearman's rank correlation coefficients (ρ) were calculated to illustrate the strength and direction of the association between the mean FA/MD of each tract and gestational age of the subject.

SI References

1. Hutter, J. *et al.* Quiet echo planar imaging for functional and diffusion MRI. *Magn. Reson. Med.* **79**, 1447–1459 (2018).
2. Ferrazzi, G. *et al.* An efficient sequence for fetal brain imaging at 3T with enhanced T1 contrast and motion robustness. *Magn. Reson. Med.* **80**, 137–146 (2018).
3. Tournier, J. *et al.* A data-driven approach to optimising the encoding for multi-shell diffusion MRI with application to neonatal imaging. *NMR Biomed.* **33**, (2020).
4. Hutter, J. *et al.* Slice-level diffusion encoding for motion and distortion correction. *Med. Image Anal.* **48**, 214–229 (2018).
5. Christiaens, D. *et al.* Scattered slice SHARD reconstruction for motion correction in multi-shell diffusion MRI. *Neuroimage* **225**, 117437 (2021).
6. Cordero-Grande, L., Christiaens, D., Hutter, J., Price, A. N. & Hajnal, J. V. Complex diffusion-weighted image estimation via matrix recovery under general noise models. *Neuroimage* **200**, 391–404 (2019).
7. Ghiglia, D. C. & Romero, L. A. Robust two-dimensional weighted and unweighted phase unwrapping that uses fast transforms and iterative methods. *J. Opt. Soc. Am. A* **11**, 107 (1994).
8. Tournier, J. D. *et al.* MRtrix3: A fast, flexible and open software framework for medical image processing and visualisation. *NeuroImage* vol. 202 (2019).
9. Basser, P. J., Mattiello, J. & Lebihan, D. Estimation of the Effective Self-Diffusion Tensor from the NMR Spin Echo. *J. Magn. Reson. Ser. B* **103**, 247–254 (1994).

10. Tournier, J. D., Calamante, F. & Connelly, A. Robust determination of the fibre orientation distribution in diffusion MRI: Non-negativity constrained super-resolved spherical deconvolution. *Neuroimage* **35**, 1459–1472 (2007).
11. Jeurissen, B., Tournier, J. D., Dhollander, T., Connelly, A. & Sijbers, J. Multi-tissue constrained spherical deconvolution for improved analysis of multi-shell diffusion MRI data. *Neuroimage* **103**, 411–426 (2014).
12. Jenkinson, M., Bannister, P., Brady, M. & Smith, S. Improved optimization for the robust and accurate linear registration and motion correction of brain images. *Neuroimage* **17**, 825–841 (2002).
13. Raffelt, D. *et al.* Symmetric diffeomorphic registration of fibre orientation distributions. *Neuroimage* **56**, 1171–1180 (2011).
14. Pietsch, M. *et al.* A framework for multi-component analysis of diffusion MRI data over the neonatal period. *Neuroimage* **186**, 321–337 (2019).
15. Serag, A. *et al. A. SERAG ET AL.: A 4D PROBABILISTIC ATLAS OF THE DEVELOPING BRAIN A Multi-channel 4D Probabilistic Atlas of the Developing Brain: Application to Fetuses and Neonates*. *Annals of the BMVA* vol. 2012 www.brain-development.org. (2012).
16. Tournier, J. D., Calamante, F. & Connelly, A. Determination of the appropriate b value and number of gradient directions for high-angular-resolution diffusion-weighted imaging. *NMR Biomed.* **26**, 1775–1786 (2013).
17. Bracco, L., Tiezzi, A., Ginanneschi, A., Campanella, C. & Amaducci, L. Lateralization of choline acetyltransferase (ChAT) activity in fetus and adult human brain. *Neurosci. Lett.* **50**, 301–305 (1984).
18. Jenkinson, M., Beckmann, C. F., Behrens, T. E. J., Woolrich, M. W. & Smith, S. M. Review FSL. *Neuroimage* **62**, 782–790 (2012).
19. Tournier, J.-D., Calamante, F. & Connelly, A. MRtrix: Diffusion tractography in crossing fiber regions. *Int. J. Imaging Syst. Technol.* **22**, 53–66 (2012).
20. Kinney, H. C., Brody, B. A., Kloman, A. S. & Gilles, F. H. Sequence of central nervous system myelination in human infancy: II. Patterns of myelination in autopsied infants. *J. Neuropathol. Exp. Neurol.* **47**, 217–234 (1988).
21. Akaike, H. Information theory and an extension of the maximum likelihood principle. Proceedings of the 2nd international symposium on information theory. *Second Int. Symp. Inf. Theory* (1973).

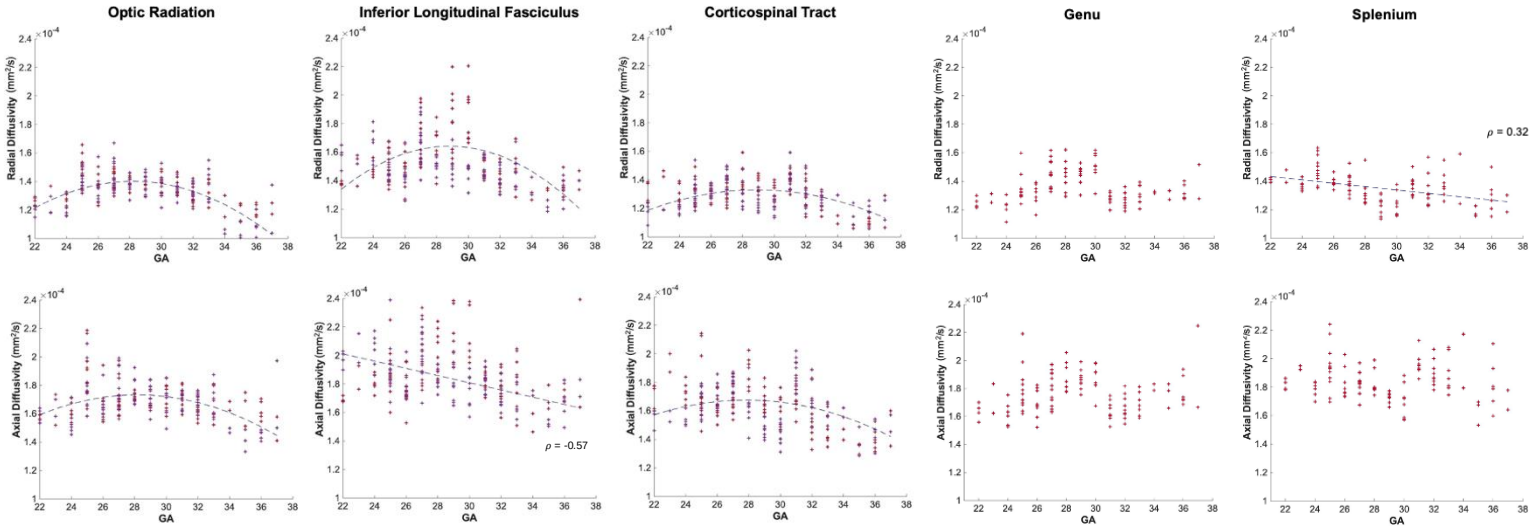

Figure S1. Axial (AD) and radial diffusivities (RD) for each tract over gestational age. Mean AD and RD values underlying the left (red) and right (purple) CST, ILF, OR, Genu and Splenium for

each fetal subject, plotted according to the gestational age (GA) of the subject in weeks. A second degree polynomial curve is fitted for the AD in the CST and OR, the RD in the CST, ILF, and OR (navy dashed line) ($p < 0.05$). The AD in the ILF and the RD in the splenium have linear relationships with gestational age, described by a Spearman's rank correlation coefficient (ρ), ($p < 0.05$). No significant relationship found between AD and GA in the splenium and genu.

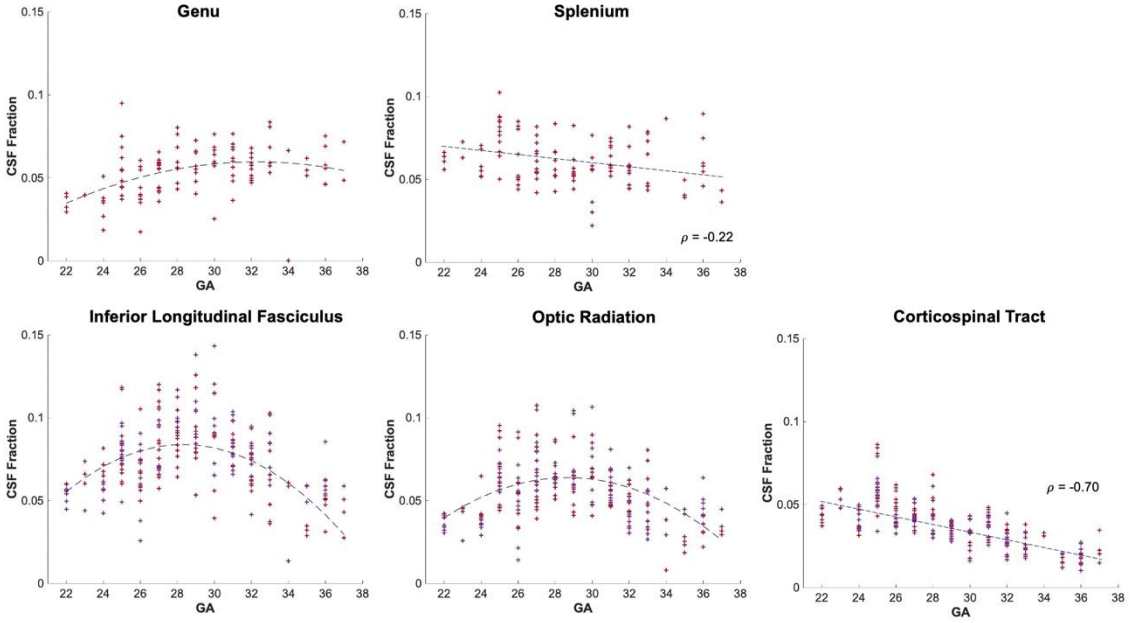

Figure S2. Fluid fraction changes with gestational age. Linear relationships between CSF fraction and GA in the splenium and CST, quantified using Spearman's rank correlations (ρ). In the Genu, ILF, and OR, 2nd degree polynomial trends were fit (according to AIC).

VII. Appendix II

Supplementary Information for Results Chapter 8:

Spatiotemporal tissue maturation of thalamocortical pathways over the second to third trimester in the human fetal brain

Wilson et al., 2023 eLife

Appendix 1

Extended details about the methodological decision-making process

Sociodemographic information

One of the aims of the dHCP was to ensure that the cohort analysed were representative of the diverse sociodemographic spread within the London population. We compared our cohort with information derived from the Mayor of London database (https://data.london.gov.uk/dataset/indices-of-deprivation) to check if the distributions were similar (***Appendix 1—figure 1***). We find that socioeconomic status, according to the index of multiple deprivation, and the ethnicity is comparable between our cohort and London. This suggests that our sample is representative, and our results should be generalisable across the London population. To ensure that we were not observing the effect of a preterm pregnancy, we also provide information on the GA at birth of the fetal cohort and the baby birth weight.

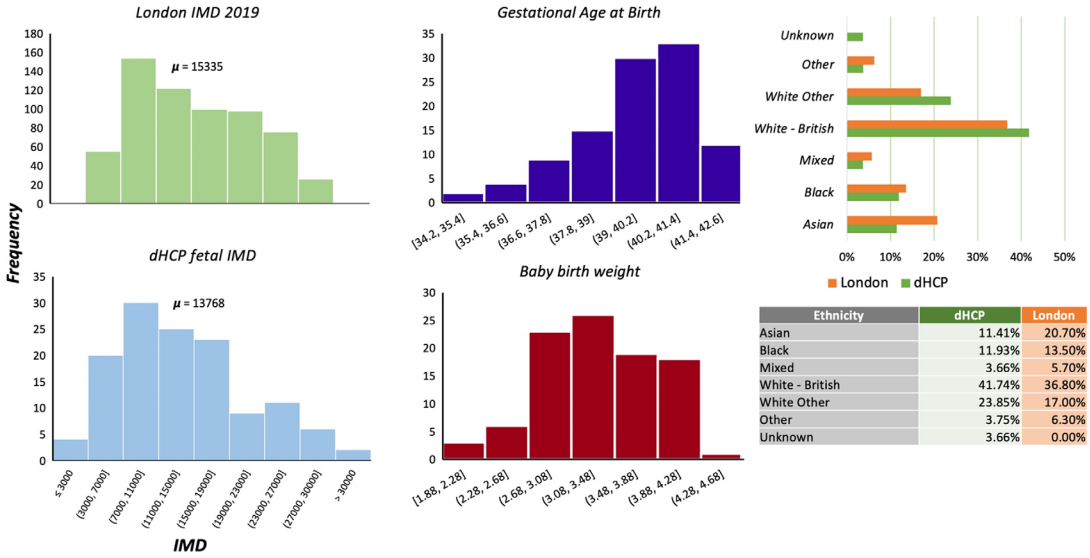

Ethnicity	dHCP	London
Asian	11.41%	20.70%
Black	11.93%	13.50%
Mixed	3.66%	5.70%
White - British	41.74%	36.80%
White Other	23.85%	17.00%
Other	3.75%	6.30%
Unknown	3.66%	0.00%

Appendix 1—figure 1. Sociodemographic and neonatal follow-up information. Including index of multiple deprivation (IMD), London. Gestational age at birth, birth weight, and ethnicity.

Quality control

QC was implemented using summary metrics based on the gradient of the motion parameters over time and the percentage of slice dropouts in the data (***Christiaens et al., 2021***). This was followed up with expert visual assessment, which considered any residual or uncorrected artefacts. Image sharpness, residual distortion, and motion artefacts were visually assessed and scored between 0 and 3, based on the mean b=0, b=400, and b=1000 images. The scoring system was as follows: 0=failure, brain outside field of view, 1=banding and large distortion, 2=blurring but no major artefacts, 3=relatively high quality.

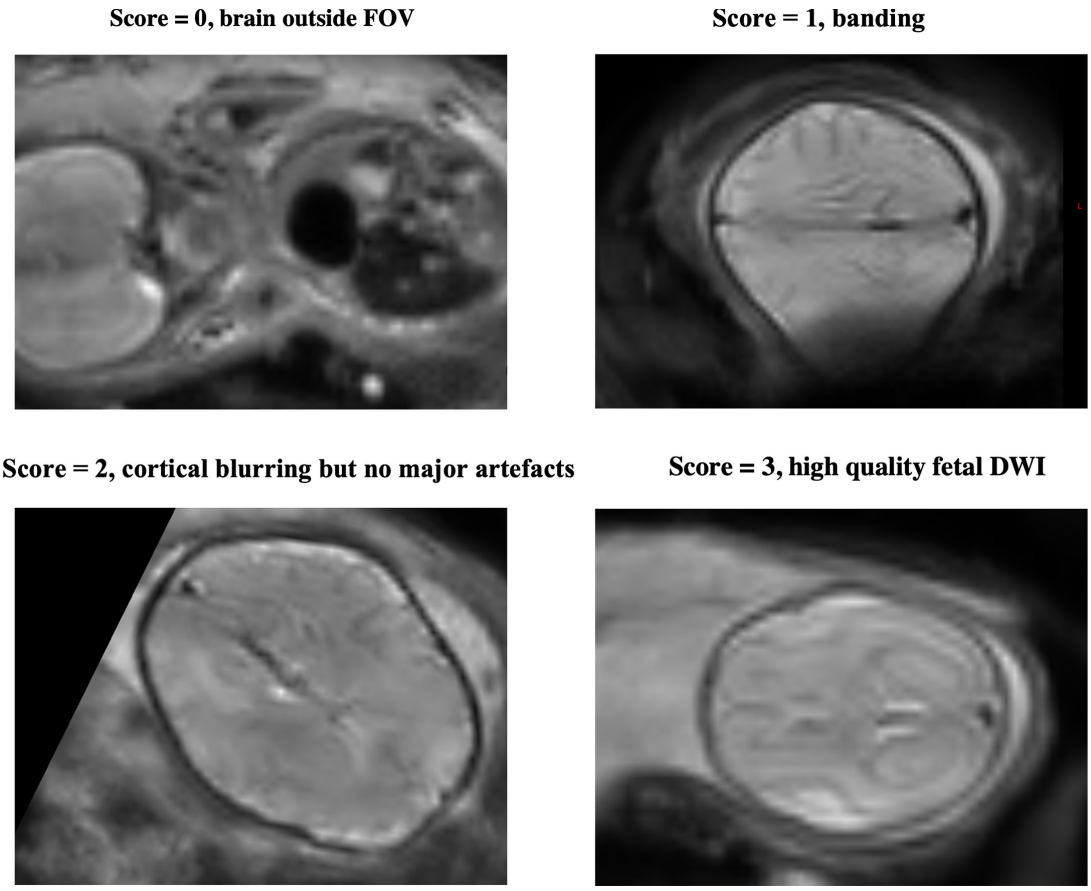

Appendix 1—figure 2. Examples of QC scoring scale for subjects, between 0 and 3, with 0 (=failure, e.g. subject moved out of the field of view) to 3 (=high quality).

As an additional check to see if the extent of motion affected our results, we correlated the indices derived from the SHARD pipeline with GA. There are three output parameters per subject, which are signal-to-noise ratio (SNR), rotation, and translation. SNR = mean b=0 signal/mean noise level, measured in the reconstruction mask using MP-PCA denoising. Rotation = mean change in rotation of the subject pose between slices (degrees). Translation = mean change in translation of the subject pose between slices (mm).

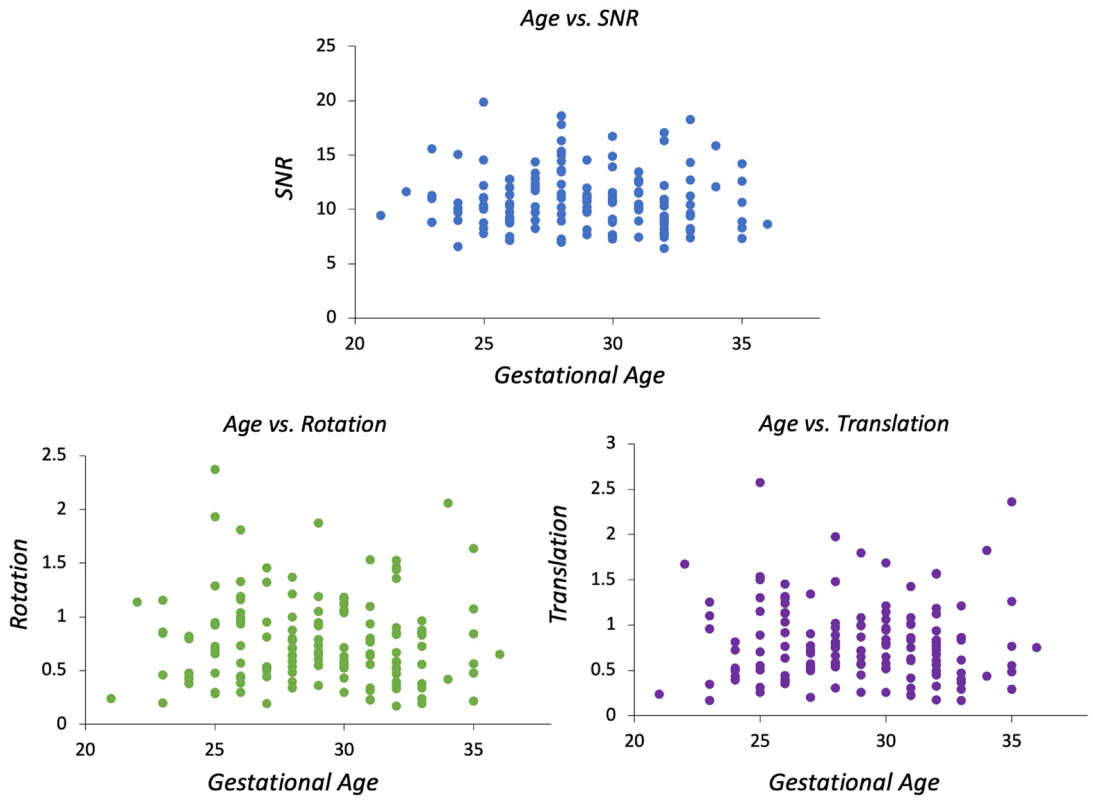

Appendix 1—figure 3. Correlations between spherical harmonics and radial decomposition (SHARD)-derived indices describing subject motion and gestational age (signal-to-noise ratio [SNR], rotation and translation).

Diffusion data modelling

Previous publications provide detail on the optimisation process used to define the b-shell values used (***Tournier et al., 2019*** and ***Christiaens et al., 2019b***; ***Christiaens et al., 2019a***). This work demonstrates that there is a marked loss of signal at higher b-shells (>1000 s/mm^3) in the neonatal brain compared to adults, due to the tissue being inherently much less restricted. There is also increased noise at higher b-shells. Both issues are amplified in the fetal brain, there are long relaxation times in the water-rich, relatively unrestricted fetal brain tissues and the amount of noise is higher.

To demonstrate the suitability of MSMT-CSD for this dataset, an important consideration is that the MSMT-CSD approach doesn't mandate a specific set of b-values which are required for the modelling process, only that there are multiple shells in addition to b=0. The technique depends on the signals related to different tissue types having sufficiently distinct behaviours across the b-values sampled, and so depends inherently on the characteristics of the tissue. To demonstrate the distinct properties of the different compartments in the fetal brain, we have now included a figure in the Appendix (***Appendix 1—figure 4***) showing the signal amplitude per tissue type as a function of b-value, and the ODFs after MSMT-CSD has been applied.

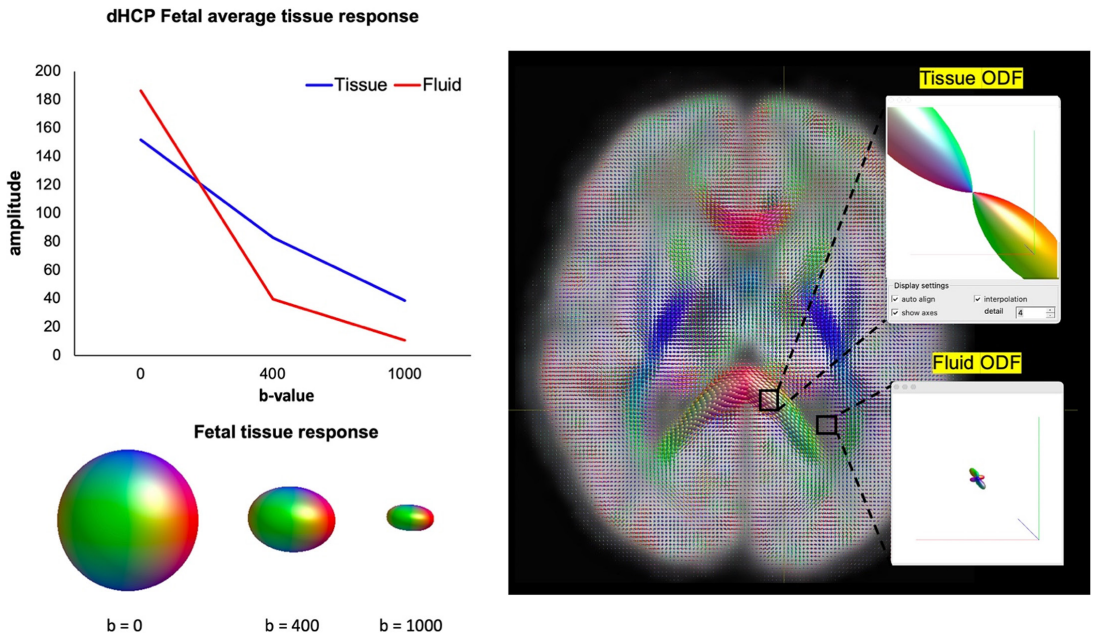

Appendix 1—figure 4. Signal amplitude decay in tissue vs. fluid response functions at different b-shells (left). Polar plots of the distinct orientation density functions (ODFs) between the corpus callosum (white matter, tissue compartment) and ventricle (cortical spinal fluid [CSF], fluid compartment) after multi-shell multi-tissue constrained spherical deconvolution (MSMT-CSD) is applied to the data (right).

Along-tract changes for specific gestational weeks

Prior to grouping the data as seen in ***Figure 5***. The analysis was conducted for individual subjects, then averaged for each gestational week. We present these trajectories (***Appendix 1—figures 5 and 6***) to demonstrate how there are gradual changes in the diffusion signal, on a weekly basis, that justify our decision (for easier interpretation) to group the data into early, mid, and late prenatal groups.

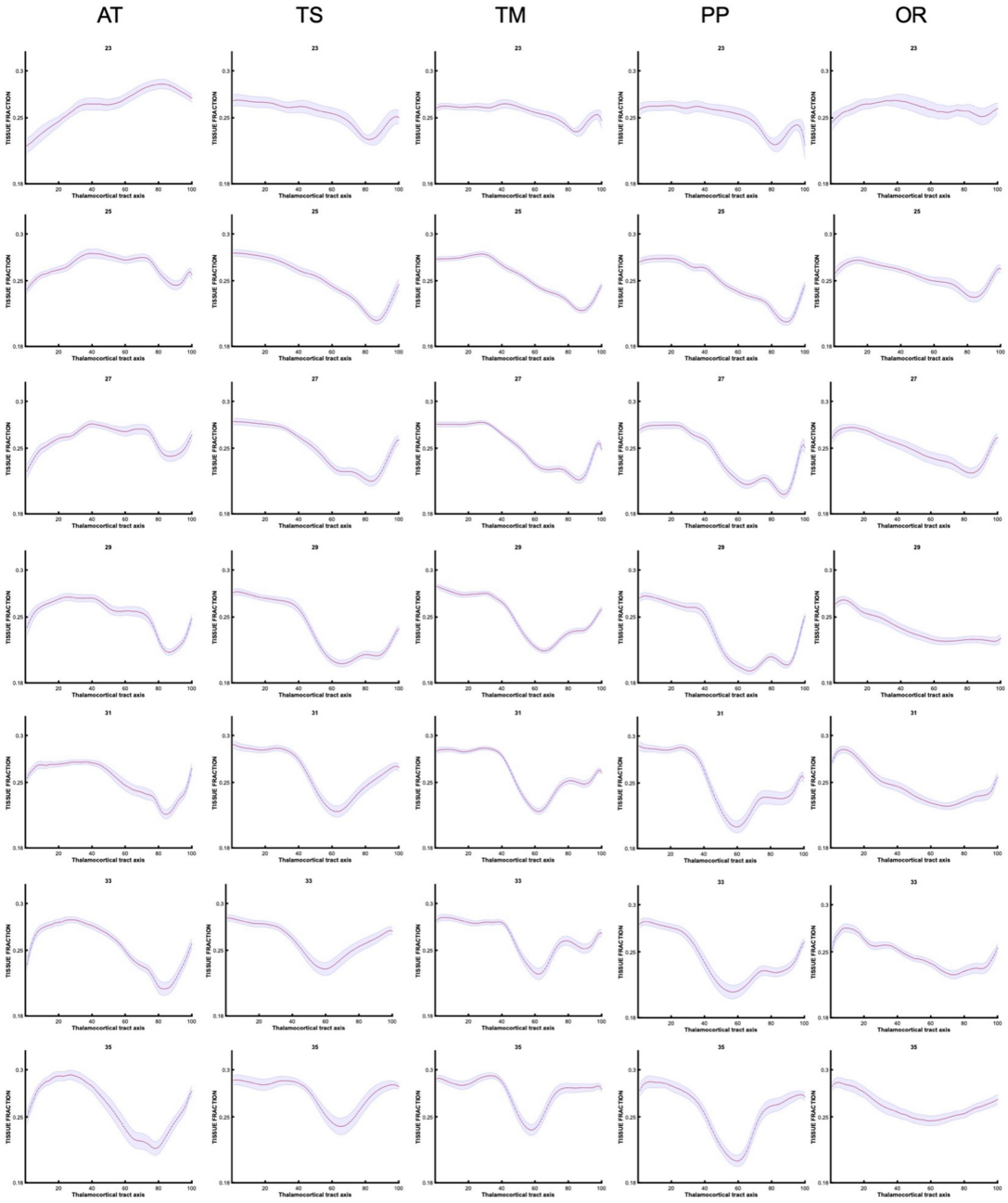

Appendix 1—figure 5. Tissue fraction trajectories along thalamocortical tract axis in each gestational week, prior to grouping into early, mid, and late prenatal (every other week shown).

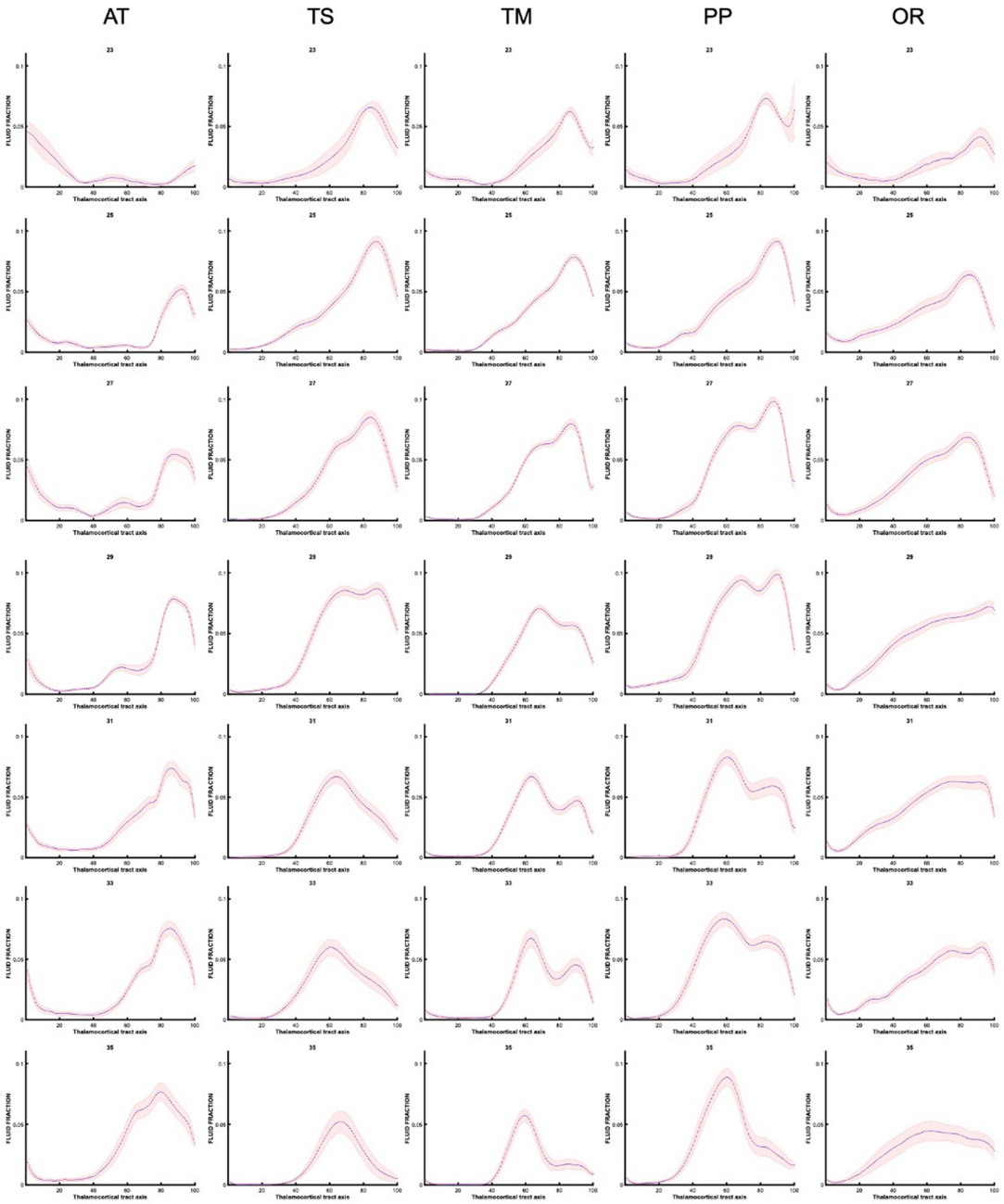

Appendix 1—figure 6. Fluid fraction trajectories along thalamocortical tract axis in each gestational week, prior to grouping into early, mid, and late prenatal (every other week shown).

VIII. Appendix III

Supplementary Information for Results Chapter 9:

Local minima in tissue microstructure precedes sulcal formation in the human fetal brain

Cohort

Participants were recruited and scanned according to dHCP protocol, which was approved by the UK Health Research Authority (Research Ethics Committee reference number: 14/LO/1169). Written parental consent was obtained in every case for imaging and open data release of the anonymised data. All data was acquired in St Thomas Hospital, London, United Kingdom. GA was determined by sonography at 12 post-ovulatory weeks as part of routine clinical care. Consenting mothers were scanned between 24 and 38 GW with a Philips Achieva 3T system, with a 32-channel cardiac coil in maternal supine position.

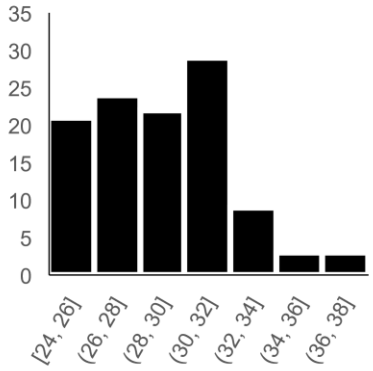

Supplementary Figure 1. Gestational Age (GA) distribution of fetal cohort (n = 112 subjects, 68 male and 44 female)

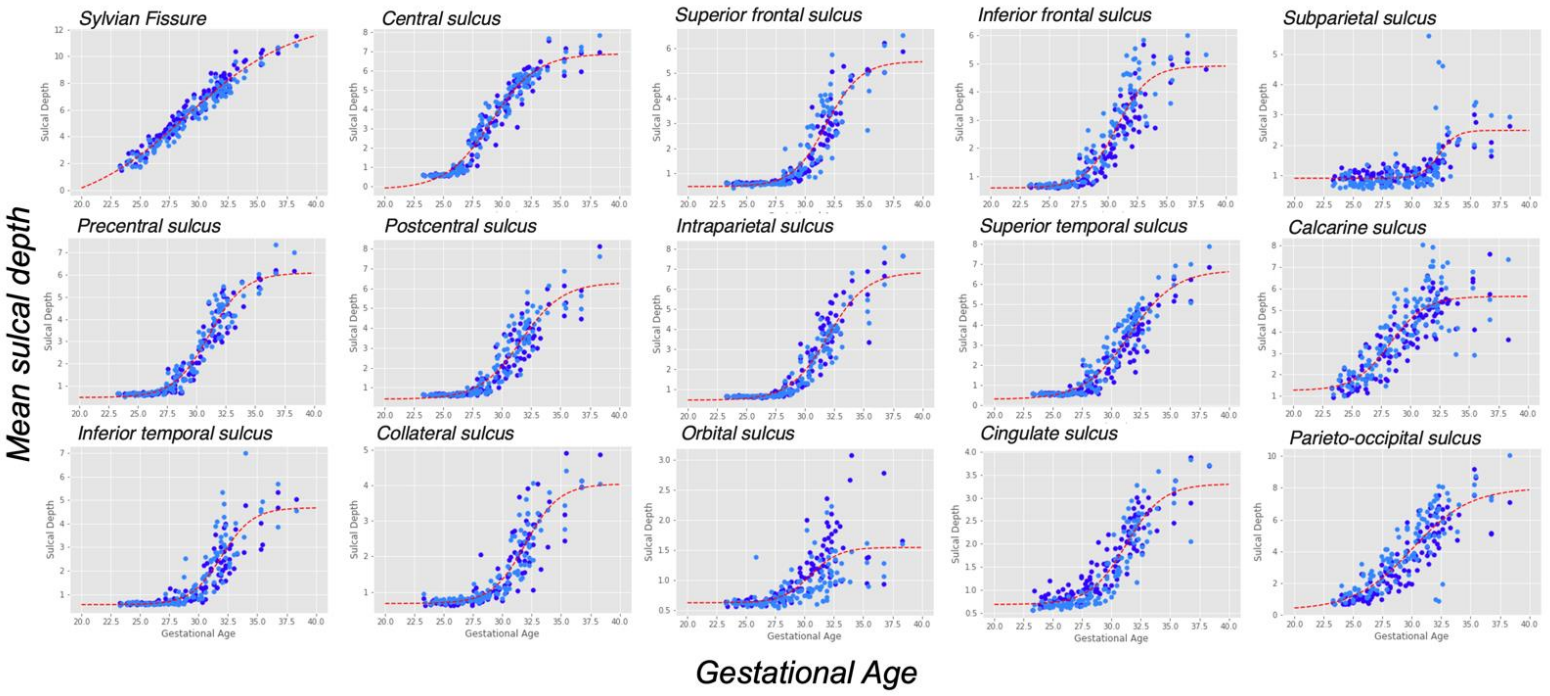

Supplementary Figure 2. Mean sulcal depth in each subject in 15 major primary sulci, for the left (light blue) and right (dark blue) hemispheres. All growth curves were best fit with a sigmoid to describe the growth and formation of the sulci.

IX. Bibliography

Abbott, L. C., & Nigussie, F. (2020). Adult neurogenesis in the mammalian dentate gyrus. *Anatomia, Histologia, Embryologia*, *49*(1), 3–16. https://doi.org/10.1111/ahe.12496

Abraham, A., Pedregosa, F., Eickenberg, M., Gervais, P., Mueller, A., Kossaifi, J., Gramfort, A., Thirion, B., & Varoquaux, G. (2014). Machine learning for neuroimaging with scikit-learn. *Frontiers in Neuroinformatics*, *8*. https://doi.org/10.3389/fninf.2014.00014

Aggarwal, M., Gobius, I., Richards, L. J., & Mori, S. (2015). Diffusion MR Microscopy of Cortical Development in the Mouse Embryo. *Cerebral Cortex*, *25*(7), 1970–1980. https://doi.org/10.1093/cercor/bhu006

Alcauter, S., Lin, W., Smith, J. K., Short, S. J., Goldman, B. D., Reznick, J. S., Gilmore, J. H., & Gao, W. (2014). Development of Thalamocortical Connectivity during Infancy and Its Cognitive Correlations. *Journal of Neuroscience*, *34*(27), 9067–9075. https://doi.org/10.1523/JNEUROSCI.0796-14.2014

Alexander, A. L., Hasan, K. M., Lazar, M., Tsuruda, J. S., & Parker, D. L. (2001). Analysis of partial volume effects in diffusion-tensor MRI. *Magnetic Resonance in Medicine*, *45*(5), 770–780. https://doi.org/10.1002/mrm.1105

Alexander, D. C., Barker, G. J., & Arridge, S. R. (2002a). Detection and modeling of non-Gaussian apparent diffusion coefficient profiles in human brain data. *Magnetic Resonance in Medicine*, *48*(2), 331–340. https://doi.org/10.1002/mrm.10209

Alexander, D. C., Barker, G. J., & Arridge, S. R. (2002b). Detection and modeling of non-Gaussian apparent diffusion coefficient profiles in human brain data. *Magnetic Resonance in Medicine*, *48*(2), 331–340. https://doi.org/10.1002/mrm.10209

Allendoerfer, K. L., & Shatz, C. J. (1994). The Subplate, A Transient Neocortical Structure: Its Role in the Development of Connections between Thalamus and Cortex. *Annual Review of Neuroscience*, *17*(1), 185–218. https://doi.org/10.1146/annurev.ne.17.030194.001153

Alvarez-Buylla, A., García-Verdugo, J. M., & Tramontin, A. D. (2001). A unified hypothesis on the lineage of neural stem cells. *Nature Reviews Neuroscience*, *2*(4), 287–293. https://doi.org/10.1038/35067582

Alvarez-Buylla, A., & Nottebohm, F. (1988). Migration of young neurons in adult avian brain. *Nature*, *335*(6188), 353–354. https://doi.org/10.1038/335353a0

Alzu'bi, A., Homman-Ludiye, J., Bourne, J. A., & Clowry, G. J. (2019). Corrigendum: Thalamocortical Afferents Innervate the Cortical Subplate much Earlier in Development in Primate than in Rodent. *Cerebral Cortex*, *29*(12), 5316–5316. https://doi.org/10.1093/cercor/bhz056

Anderson, M. J., & Robinson, J. (2001). Permutation Tests for Linear Models. *Australian & New Zealand Journal of Statistics*, *43*(1), 75–88. https://doi.org/10.1111/1467-842X.00156

Andescavage, N. N., du Plessis, A., McCarter, R., Serag, A., Evangelou, I., Vezina, G., Robertson, R., & Limperopoulos, C. (2016). Complex Trajectories of Brain Development in the Healthy Human Fetus. *Cerebral Cortex*, cercor;bhw306v1. https://doi.org/10.1093/cercor/bhw306

André, M., Lamblin, M.-D., d'Allest, A. M., Curzi-Dascalova, L., Moussalli-Salefranque, F., Nguyen The Tich, S., Vecchierini-Blineau, M.-F., Wallois, F., Walls-Esquivel, E., & Plouin, P. (2010). Electroencephalography in premature and full-term infants. Developmental features and glossary. *Neurophysiologie Clinique/Clinical Neurophysiology*, *40*(2), 59–124. https://doi.org/10.1016/j.neucli.2010.02.002

Angevine, J. B., & Sidman, R. L. (1961). Autoradiographic Study of Cell Migration during Histogenesis of Cerebral Cortex in the Mouse. *Nature*, *192*(4804), 766–768. https://doi.org/10.1038/192766b0

Anticevic, A., Cole, M. W., Repovs, G., Murray, J. D., Brumbaugh, M. S., Winkler, A. M., Savic, A., Krystal, J. H., Pearlson, G. D., & Glahn, D. C. (2014). Characterizing Thalamo-Cortical Disturbances in Schizophrenia and Bipolar Illness. *Cerebral Cortex*, *24*(12), 3116–3130. https://doi.org/10.1093/cercor/bht165

Avants, B., Epstein, C., Grossman, M., & Gee, J. (2008). Symmetric diffeomorphic image registration with cross-correlation: Evaluating automated labeling of elderly and neurodegenerative brain. *Medical Image Analysis*, *12*(1), 26–41. https://doi.org/10.1016/j.media.2007.06.004

Back, S. A., Luo, N. L., Borenstein, N. S., Levine, J. M., Volpe, J. J., & Kinney, H. C. (2001). Late Oligodendrocyte Progenitors Coincide with the Developmental Window of Vulnerability for Human Perinatal White Matter Injury. *The Journal of Neuroscience*, *21*(4), 1302–1312. https://doi.org/10.1523/JNEUROSCI.21-04-01302.2001

Back, S. A., Luo, N. L., Borenstein, N. S., Volpe, J. J., & Kinney, H. C. (2002). Arrested oligodendrocyte lineage progression during human cerebral white matter development: Dissociation between the timing of progenitor differentiation and myelinogenesis. *Journal of Neuropathology and Experimental Neurology*, *61*(2), 197–211. https://doi.org/10.1093/jnen/61.2.197

Back, S. A., & Volpe, J. J. (1997). Cellular and molecular pathogenesis of periventricular white matter injury. *Mental Retardation and Developmental Disabilities Research Reviews*, *3*(1), 96–107. https://doi.org/10.1002/(SICI)1098-2779(1997)3:1<96::AID-MRDD12>3.0.CO;2-M

Ball, G., Aljabar, P., Nongena, P., Kennea, N., Gonzalez-Cinca, N., Falconer, S., Chew, A. T. M., Harper, N., Wurie, J., Rutherford, M. A., Counsell, S. J., & Edwards, A. D. (2017). Multimodal image analysis of clinical influences on preterm brain development: Clinical Factors and Preterm Brain Development. *Annals of Neurology*, *82*(2), 233–246. https://doi.org/10.1002/ana.24995

Ball, G., Aljabar, P., Zebari, S., Tusor, N., Arichi, T., Merchant, N., Robinson, E. C., Ogundipe, E., Rueckert, D., Edwards, A. D., & Counsell, S. J. (2014). Rich-club organization of the newborn human brain. *Proceedings of the National Academy of Sciences*, *111*(20), 7456–7461. https://doi.org/10.1073/pnas.1324118111

Ball, G., Boardman, J. P., Aljabar, P., Pandit, A., Arichi, T., Merchant, N., Rueckert, D., Edwards, A. D., & Counsell, S. J. (2013). The influence of preterm birth on the developing thalamocortical connectome. *Cortex*, *49*(6), 1711–1721. https://doi.org/10.1016/j.cortex.2012.07.006

Ball, G., Boardman, J. P., Rueckert, D., Aljabar, P., Arichi, T., Merchant, N., Gousias, I. S., Edwards, A. D., & Counsell, S. J. (2012). The Effect of Preterm Birth on Thalamic and Cortical Development. *Cerebral Cortex*, *22*(5), 1016–1024. https://doi.org/10.1093/cercor/bhr176

Ball, G., Pazderova, L., Chew, A., Tusor, N., Merchant, N., Arichi, T., Allsop, J. M., Cowan, F. M., Edwards, A. D., & Counsell, S. J. (2015). Thalamocortical Connectivity Predicts Cognition in Children Born Preterm. *Cerebral Cortex (New York, N.Y.: 1991)*, *25*(11), 4310–4318. https://doi.org/10.1093/cercor/bhu331

Ball, G., Srinivasan, L., Aljabar, P., Counsell, S. J., Durighel, G., Hajnal, J. V., Rutherford, M. A., & Edwards, A. D. (2013). Development of cortical microstructure in the preterm human brain. *Proceedings of the National Academy of Sciences*, *110*(23), 9541–9546. https://doi.org/10.1073/pnas.1301652110

Bammer, R. (2003). Basic principles of diffusion-weighted imaging. *European Journal of Radiology*, *45*(3), 169–184. https://doi.org/10.1016/S0720-048X(02)00303-0

Barker, D. J. P. (1995). Fetal origins of coronary heart disease. *BMJ*, *311*(6998), 171–174. https://doi.org/10.1136/bmj.311.6998.171

Barkovich, A. J. (2000). Concepts of myelin and myelination in neuroradiology. *AJNR. American Journal of Neuroradiology*, *21*(6), 1099–1109.

Barkovich, A. J., Guerrini, R., Kuzniecky, R. I., Jackson, G. D., & Dobyns, W. B. (2012). A developmental and genetic classification for malformations of cortical development: Update 2012. *Brain*, *135*(5), 1348–1369. https://doi.org/10.1093/brain/aws019

Barkovich, A. J., Kjos, B. O., Jackson, D. E., & Norman, D. (1988). Normal maturation of the neonatal and infant brain: MR imaging at 1.5 T. *Radiology*, *166*(1), 173–180. https://doi.org/10.1148/radiology.166.1.3336675

Basser, P. J., Mattiello, J., & Lebihan, D. (1994). Estimation of the Effective Self-Diffusion Tensor from the NMR Spin Echo. *Journal of Magnetic Resonance, Series B*, *103*(3), 247–254. https://doi.org/10.1006/jmrb.1994.1037

Basser, P. J., Mattiello, J., & LeBihan, D. (1994). MR diffusion tensor spectroscopy and imaging. *Biophysical Journal*, *66*(1), 259–267. https://doi.org/10.1016/S0006-3495(94)80775-1

Basser, P. J., Pajevic, S., Pierpaoli, C., Duda, J., & Aldroubi, A. (2000). In vivo fiber tractography using DT-MRI data. *Magnetic Resonance in Medicine*, *44*(4), 625–632. https://doi.org/10.1002/1522-2594(200010)44:4<625::AID-MRM17>3.0.CO;2-O

Batalle, D., Hughes, E. J., Zhang, H., Tournier, J.-D., Tusor, N., Aljabar, P., Wali, L., Alexander, D. C., Hajnal, J. V., Nosarti, C., Edwards, A. D., & Counsell, S. J. (2017). Early development of structural networks and the impact of prematurity on brain connectivity. *NeuroImage*, *149*, 379–392. https://doi.org/10.1016/j.neuroimage.2017.01.065

Batalle, D., O'Muircheartaigh, J., Makropoulos, A., Kelly, C. J., Dimitrova, R., Hughes, E. J., Hajnal, J. V., Zhang, H., Alexander, D. C., Edwards, A. D., & Counsell, S. J. (2019). Different patterns of cortical maturation before and after 38 weeks gestational age demonstrated by diffusion MRI in vivo. *NeuroImage*, *185*, 764–775. https://doi.org/10.1016/j.neuroimage.2018.05.046

Bayer, S. A., & Altman, J. (1991). *Neocortical development*. Raven Press.

Bayly, P. V., Okamoto, R. J., Xu, G., Shi, Y., & Taber, L. A. (2013). A cortical folding model incorporating stress-dependent growth explains gyral wavelengths and stress patterns in the developing brain. *Physical Biology*, *10*(1), 016005. https://doi.org/10.1088/1478-3975/10/1/016005

Behrens, T. E. J., Johansen-Berg, H., Woolrich, M. W., Smith, S. M., Wheeler-Kingshott, C. A. M., Boulby, P. A., Barker, G. J., Sillery, E. L., Sheehan, K., Ciccarelli, O., Thompson, A. J., Brady, J. M., & Matthews, P. M. (2003). Non-invasive mapping of connections between human thalamus and cortex using diffusion imaging. *Nature Neuroscience*, *6*(7), 750–757. https://doi.org/10.1038/nn1075

Belmonte-Mateos, C., & Pujades, C. (2022). From Cell States to Cell Fates: How Cell Proliferation and Neuronal Differentiation Are Coordinated During Embryonic Development. *Frontiers in Neuroscience*, *15*, 781160. https://doi.org/10.3389/fnins.2021.781160

Benders, M. J., Palmu, K., Menache, C., Borradori-Tolsa, C., Lazeyras, F., Sizonenko, S., Dubois, J., Vanhatalo, S., & Hüppi, P. S. (2015). Early Brain Activity Relates to Subsequent Brain Growth in Premature Infants. *Cerebral Cortex*, *25*(9), 3014–3024. https://doi.org/10.1093/cercor/bhu097

Benjamini, Y., & Hochberg, Y. (1995). Controlling the False Discovery Rate: A Practical and Powerful Approach to Multiple Testing. *Journal of the Royal Statistical Society: Series B (Methodological)*, *57*(1), 289–300. https://doi.org/10.1111/j.2517-6161.1995.tb02031.x

Berman, J. I., Lanza, M. R., Blaskey, L., Edgar, J. C., & Roberts, T. P. L. (2013). High angular resolution diffusion imaging probabilistic tractography of the auditory radiation. *AJNR. American Journal of Neuroradiology*, *34*(8), 1573–1578. https://doi.org/10.3174/ajnr.A3471

Bloch, F., Hansen, W. W., & Packard, M. (1946). Nuclear Induction. *Physical Review*, *69*(3–4), 127–127. https://doi.org/10.1103/PhysRev.69.127

Bond, R. F., Vildibill, H. D., Krech, L. H., & Hershey, J. C. (1991). Influence of histaminergic receptors on denervated canine gracilis muscle vascular tone during endotoxemia. *The American Journal of Physiology*, *261*(3 Pt 2), H882-891. https://doi.org/10.1152/ajpheart.1991.261.3.H882

Brady, S. T., Witt, A. S., Kirkpatrick, L. L., de Waegh, S. M., Readhead, C., Tu, P.-H., & Lee, V. M.-Y. (1999). Formation of Compact Myelin Is Required for Maturation of the Axonal Cytoskeleton. *The Journal of Neuroscience*, *19*(17), 7278–7288. https://doi.org/10.1523/JNEUROSCI.19-17-07278.1999

Brodmann, K. (1909). *Vergleichende Lokalisationslehre der Grosshirnrinde in ihren Prinzipien dargestellt auf Grund des Zellenbaues*. Barth.

Brody, B. A., Kinney, H. C., Kloman, A. S., & Gilles, F. H. (1987). Sequence of Central Nervous System Myelination in Human Infancy. I. An Autopsy Study of Myelination: *Journal of Neuropathology and Experimental Neurology*, *46*(3), 283–301. https://doi.org/10.1097/00005072-198705000-00005

Budday, S., Raybaud, C., & Kuhl, E. (2014). A mechanical model predicts morphological abnormalities in the developing human brain. *Scientific Reports*, *4*(1), 5644. https://doi.org/10.1038/srep05644

Bui, T., Daire, J.-L., Chalard, F., Zaccaria, I., Alberti, C., Elmaleh, M., Garel, C., Luton, D., Blanc, N., & Sebag, G. (2006). Microstructural development of human brain assessed in utero by diffusion tensor imaging. *Pediatric Radiology*, *36*(11), 1133–1140. https://doi.org/10.1007/s00247-006-0266-3

Bystron, I., Blakemore, C., & Rakic, P. (2008). Development of the human cerebral cortex: Boulder Committee revisited. *Nature Reviews Neuroscience*, *9*(2), 110–122. https://doi.org/10.1038/nrn2252

Bystron, I., Rakic, P., Molnár, Z., & Blakemore, C. (2006). The first neurons of the human cerebral cortex. *Nature Neuroscience*, *9*(7), 880–886. https://doi.org/10.1038/nn1726

Cachia, A., Roell, M., Mangin, J.-F., Sun, Z. Y., Jobert, A., Braga, L., Houde, O., Dehaene, S., & Borst, G. (2018). How interindividual differences in brain anatomy shape reading accuracy. *Brain Structure and Function*, *223*(2), 701–712. https://doi.org/10.1007/s00429-017-1516-x

Calamante, F. (2019). The Seven Deadly Sins of Measuring Brain Structural Connectivity Using Diffusion MRI Streamlines Fibre-Tracking. *Diagnostics (Basel, Switzerland)*, *9*(3), 115. https://doi.org/10.3390/diagnostics9030115

Calamante, F., Tournier, J.-D., Jackson, G. D., & Connelly, A. (2010). Track-density imaging (TDI): Super-resolution white matter imaging using whole-brain track-density mapping. *NeuroImage*, *53*(4), 1233–1243. https://doi.org/10.1016/j.neuroimage.2010.07.024

Cajal, S. R. (1909). "Histologie du système nerveux central de lhomme et des vertébrés." Paris, Maloine Editeurs.

Casarosa, S., Bozzi, Y., & Conti, L. (2014). Neural stem cells: Ready for therapeutic applications? *Molecular and Cellular Therapies*, *2*(1), 31. https://doi.org/10.1186/2052-8426-2-31

Chen, R., Sun, C., Liu, T., Liao, Y., Wang, J., Sun, Y., Zhang, Y., Wang, G., & Wu, D. (2022). Deciphering the developmental order and microstructural patterns of early white matter pathways in a diffusion MRI based fetal brain atlas. *NeuroImage*, *264*, 119700. https://doi.org/10.1016/j.neuroimage.2022.119700

Chenn, A., & Walsh, C. A. (2002). Regulation of Cerebral Cortical Size by Control of Cell Cycle Exit in Neural Precursors. *Science*, *297*(5580), 365–369. https://doi.org/10.1126/science.1074192

Chi, J. G., Dooling, E. C., & Gilles, F. H. (1977). Gyral development of the human brain. *Annals of Neurology*, *1*(1), 86–93. https://doi.org/10.1002/ana.410010109

Christiaens, D. (n.d.). *Fetal diffusion MRI acquisition and analysis in the developing Human Connectome Project*.

Christiaens, D., Cordero-Grande, L., Pietsch, M., Hutter, J., Price, A. N., Hughes, E. J., Vecchiato, K., Deprez, M., Edwards, A. D., Hajnal, J. V., & Tournier, J.-D. (2021). Scattered slice SHARD reconstruction for motion correction in multi-shell diffusion MRI. *NeuroImage*, *225*, 117437. https://doi.org/10.1016/j.neuroimage.2020.117437

Christiaens, D., Cordero-Grande, L., Price, A. N., Hutter, J., Hughes, E., Counsell, S. J., Tournier, J.-D., & Hajnal, J. V. (2019). Fetal diffusion MRI acquisition and analysis in the developing Human Connectome Project. *Proceedings of the Annual Meeting of the International Society of Magnetic Resonance in Medicine (ISMRM)*.

Christiaens, D., Slator, P. J., Cordero-Grande, L., Price, A. N., Deprez, M., Alexander, D. C., Rutherford, M., Hajnal, J. V., & Hutter, J. (2019). In Utero Diffusion MRI: Challenges, Advances, and Applications. *Topics in Magnetic Resonance Imaging*, *28*(5), 255–264. https://doi.org/10.1097/RMR.0000000000000211

Clascá, F., Rubio-Garrido, P., & Jabaudon, D. (2012). Unveiling the diversity of thalamocortical neuron subtypes: Thalamocortical neuron diversity. *European Journal of Neuroscience*, *35*(10), 1524–1532. https://doi.org/10.1111/j.1460-9568.2012.08033.x

Clouchoux, C., Guizard, N., Evans, A. C., Du Plessis, A. J., & Limperopoulos, C. (2012). Normative fetal brain growth by quantitative in vivo magnetic resonance imaging. *American Journal of Obstetrics and Gynecology*, *206*(2), 173.e1-173.e8. https://doi.org/10.1016/j.ajog.2011.10.002

Comon, P. (1994). Independent component analysis, A new concept? *Signal Processing*, *36*(3), 287–314. https://doi.org/10.1016/0165-1684(94)90029-9

Corbin, J. G., Nery, S., & Fishell, G. (2001). Telencephalic cells take a tangent: Non-radial migration in the mammalian forebrain. *Nature Neuroscience*, *4*(S11), 1177–1182. https://doi.org/10.1038/nn749

Cordero-Grande, L., Christiaens, D., Hutter, J., Price, A. N., & Hajnal, J. V. (2019). Complex diffusion-weighted image estimation via matrix recovery under general noise models. *NeuroImage*, *200*, 391–404. https://doi.org/10.1016/j.neuroimage.2019.06.039

Cordero-Grande1, L., et al., (2019). Automating Motion Compensa- tion in 3T Fetal Brain Imaging: Localize, Align and Reconstruct, in: ISMRM 2019, p. 1000.

Counsell, S. J., Allsop, J. M., Harrison, M. C., Larkman, D. J., Kennea, N. L., Kapellou, O., Cowan, F. M., Hajnal, J. V., Edwards, A. D., & Rutherford, M. A. (2003). Diffusion-Weighted Imaging of the Brain in Preterm Infants With Focal and Diffuse White Matter Abnormality. *Pediatrics*, *112*(1), 1–7. https://doi.org/10.1542/peds.112.1.1

Counsell, S. J., Maalouf, E. F., Fletcher, A. M., Duggan, P., Battin, M., Lewis, H. J., Herlihy, A. H., Edwards, A. D., Bydder, G. M., & Rutherford, M. A. (2002). MR imaging assessment of myelination in the very preterm brain. *AJNR. American Journal of Neuroradiology*, *23*(5), 872–881.

Dawson, M. (2003). NG2-expressing glial progenitor cells: An abundant and widespread population of cycling cells in the adult rat CNS. *Molecular and Cellular Neuroscience*, *24*(2), 476–488. https://doi.org/10.1016/S1044-7431(03)00210-0

De Asis-Cruz, J., Bouyssi-Kobar, M., Evangelou, I., Vezina, G., & Limperopoulos, C. (2015). Functional properties of resting state networks in healthy full-term newborns. *Scientific Reports*, *5*(1), 17755. https://doi.org/10.1038/srep17755

De Vareilles, H., Rivière, D., Mangin, J., & Dubois, J. (2023). Development of cortical folds in the human brain: An attempt to review biological hypotheses, early neuroimaging investigations

and functional correlates. *Developmental Cognitive Neuroscience*, *61*, 101249. https://doi.org/10.1016/j.dcn.2023.101249

Dean, J. M., McClendon, E., Hansen, K., Azimi-Zonooz, A., Chen, K., Riddle, A., Gong, X., Sharifnia, E., Hagen, M., Ahmad, T., Leigland, L. A., Hohimer, A. R., Kroenke, C. D., & Back, S. A. (2013). Prenatal Cerebral Ischemia Disrupts MRI-Defined Cortical Microstructure Through Disturbances in Neuronal Arborization. *Science Translational Medicine*, *5*(168). https://doi.org/10.1126/scitranslmed.3004669

deIpolyi, A. R., Mukherjee, P., Gill, K., Henry, R. G., Partridge, S. C., Veeraraghavan, S., Jin, H., Lu, Y., Miller, S. P., Ferriero, D. M., Vigneron, D. B., & Barkovich, A. J. (2005). Comparing microstructural and macrostructural development of the cerebral cortex in premature newborns: Diffusion tensor imaging versus cortical gyration. *NeuroImage*, *27*(3), 579–586. https://doi.org/10.1016/j.neuroimage.2005.04.027

Deng, F., Jiang, X., Zhu, D., Zhang, T., Li, K., Guo, L., & Liu, T. (2014). A functional model of cortical gyri and sulci. *Brain Structure and Function*, *219*(4), 1473–1491. https://doi.org/10.1007/s00429-013-0581-z

Deprez, M., Price, A., Christiaens, D., Lockwood Estrin, G., Cordero-Grande, L., Hutter, J., Daducci, A., Tournier, J.-D., Rutherford, M., Counsell, S. J., Cuadra, M. B., & Hajnal, J. V. (2020). Higher Order Spherical Harmonics Reconstruction of Fetal Diffusion MRI With Intensity Correction. *IEEE Transactions on Medical Imaging*, *39*(4), 1104–1113. https://doi.org/10.1109/TMI.2019.2943565

Dimitrova, R., Pietsch, M., Christiaens, D., Ciarrusta, J., Wolfers, T., Batalle, D., Hughes, E., Hutter, J., Cordero-Grande, L., Price, A. N., Chew, A., Falconer, S., Vecchiato, K., Steinweg, J. K., Carney, O., Rutherford, M. A., Tournier, J.-D., Counsell, S. J., Marquand, A. F., … O'Muircheartaigh, J. (2020). Heterogeneity in Brain Microstructural Development Following Preterm Birth. *Cerebral Cortex*, *30*(9), 4800–4810. https://doi.org/10.1093/cercor/bhaa069

Doetsch, F., Caillé, I., Lim, D. A., García-Verdugo, J. M., & Alvarez-Buylla, A. (1999). Subventricular Zone Astrocytes Are Neural Stem Cells in the Adult Mammalian Brain. *Cell*, *97*(6), 703–716. https://doi.org/10.1016/S0092-8674(00)80783-7

Doria, V., Beckmann, C. F., Arichi, T., Merchant, N., Groppo, M., Turkheimer, F. E., Counsell, S. J., Murgasova, M., Aljabar, P., Nunes, R. G., Larkman, D. J., Rees, G., & Edwards, A. D. (2010). Emergence of resting state networks in the preterm human brain. *Proceedings of the National Academy of Sciences*, *107*(46), 20015–20020. https://doi.org/10.1073/pnas.1007921107

Douaud, G., Groves, A. R., Tamnes, C. K., Westlye, L. T., Duff, E. P., Engvig, A., Walhovd, K. B., James, A., Gass, A., Monsch, A. U., Matthews, P. M., Fjell, A. M., Smith, S. M., & Johansen-Berg, H. (2014). A common brain network links development, aging, and vulnerability to disease. *Proceedings of the National Academy of Sciences*, *111*(49), 17648–17653. https://doi.org/10.1073/pnas.1410378111

Drobyshevsky, A. (2005). Developmental Changes in Diffusion Anisotropy Coincide with Immature Oligodendrocyte Progression and Maturation of Compound Action Potential. *Journal of Neuroscience*, *25*(25), 5988–5997. https://doi.org/10.1523/JNEUROSCI.4983-04.2005

Duboc, V., Dufourcq, P., Blader, P., & Roussigné, M. (2015). Asymmetry of the Brain: Development and Implications. *Annual Review of Genetics*, *49*(1), 647–672. https://doi.org/10.1146/annurev-genet-112414-055322

Dubois, J., Benders, M., Cachia, A., Lazeyras, F., Ha-Vinh Leuchter, R., Sizonenko, S. V., Borradori-Tolsa, C., Mangin, J. F., & Huppi, P. S. (2008). Mapping the Early Cortical Folding Process in the Preterm Newborn Brain. *Cerebral Cortex*, *18*(6), 1444–1454. https://doi.org/10.1093/cercor/bhm180

Dubois, J., & Dehaene-Lambertz, G. (2015). Fetal and Postnatal Development of the Cortex: MRI and Genetics. In *Brain Mapping* (pp. 11–19). Elsevier. https://doi.org/10.1016/B978-0-12-397025-1.00194-9

Dudink, J., Buijs, J., Govaert, P., Van Zwol, A. L., Conneman, N., Van Goudoever, J. B., & Lequin, M. (2010). Diffusion tensor imaging of the cortical plate and subplate in very-low-birth-weight infants. *Pediatric Radiology*, *40*(8), 1397–1404. https://doi.org/10.1007/s00247-010-1638-2

Dudink, J., Lequin, M., Van Pul, C., Buijs, J., Conneman, N., Van Goudoever, J., & Govaert, P. (2007). Fractional anisotropy in white matter tracts of very-low-birth-weight infants. *Pediatric Radiology*, *37*(12), 1216–1223. https://doi.org/10.1007/s00247-007-0626-7

Duncan, G. J., Simkins, T. J., & Emery, B. (2021). Neuron-Oligodendrocyte Interactions in the Structure and Integrity of Axons. *Frontiers in Cell and Developmental Biology*, *9*, 653101. https://doi.org/10.3389/fcell.2021.653101

Edgar, J. M., & Garbern, J. (2004). The myelinated axon is dependent on the myelinating cell for support and maintenance: Molecules involved. *Journal of Neuroscience Research*, *76*(5), 593–598. https://doi.org/10.1002/jnr.20063

Edwards, A. D., Rueckert, D., Smith, S. M., Abo Seada, S., Alansary, A., Almalbis, J., Allsop, J., Andersson, J., Arichi, T., Arulkumaran, S., Bastiani, M., Batalle, D., Baxter, L., Bozek, J., Braithwaite, E., Brandon, J., Carney, O., Chew, A., Christiaens, D., … Hajnal, J. V. (2022). The Developing Human Connectome Project Neonatal Data Release. *Frontiers in Neuroscience*, *16*, 886772. https://doi.org/10.3389/fnins.2022.886772

Emos, M. C., Khan Suheb, M. Z., & Agarwal, S. (2022). Neuroanatomy, Internal Capsule. In *StatPearls*. StatPearls Publishing. http://www.ncbi.nlm.nih.gov/books/NBK542181/

Essen, D. C. V. (1997). A tension-based theory of morphogenesis and compact wiring in the central nervous system. *Nature*, *385*(6614), 313–318. https://doi.org/10.1038/385313a0

Eyre, M., Fitzgibbon, S. P., Ciarrusta, J., Cordero-Grande, L., Price, A. N., Poppe, T., Schuh, A., Hughes, E., O'Keeffe, C., Brandon, J., Cromb, D., Vecchiato, K., Andersson, J., Duff, E. P., Counsell, S. J., Smith, S. M., Rueckert, D., Hajnal, J. V., Arichi, T., … Edwards, A. D. (2021). The Developing Human Connectome Project: Typical and disrupted perinatal functional connectivity. *Brain*, *144*(7), 2199–2213. https://doi.org/10.1093/brain/awab118

Fabrizi, L., Slater, R., Worley, A., Meek, J., Boyd, S., Olhede, S., & Fitzgerald, M. (2011). A Shift in Sensory Processing that Enables the Developing Human Brain to Discriminate Touch from Pain. *Current Biology*, *21*(18), 1552–1558. https://doi.org/10.1016/j.cub.2011.08.010

Fenn-Moltu, S., Fitzgibbon, S. P., Ciarrusta, J., Eyre, M., Cordero-Grande, L., Chew, A., Falconer, S., Gale-Grant, O., Harper, N., Dimitrova, R., Vecchiato, K., Fenchel, D., Javed, A., Earl, M., Price, A. N., Hughes, E., Duff, E. P., O'Muircheartaigh, J., Nosarti, C., … Batalle, D. (2022). Development of neonatal brain functional centrality and alterations associated with preterm birth. *Cerebral Cortex*, bhac444. https://doi.org/10.1093/cercor/bhac444

Fernández, V., Llinares-Benadero, C., & Borrell, V. (2016). Cerebral cortex expansion and folding: What have we learned? *The EMBO Journal*, *35*(10), 1021–1044. https://doi.org/10.15252/embj.201593701

Ferrazzi, G., Price, A. N., Teixeira, R. P. A. G., Cordero-Grande, L., Hutter, J., Gomes, A., Padormo, F., Hughes, E., Schneider, T., Rutherford, M., Kuklisova Murgasova, M., & Hajnal, J. V. (2018). An efficient sequence for fetal brain imaging at 3T with enhanced T_1 contrast and motion robustness: Fetal T_1. *Magnetic Resonance in Medicine*, *80*(1), 137–146. https://doi.org/10.1002/mrm.27012

Fields, R. D. (2008). White matter in learning, cognition and psychiatric disorders. *Trends in Neurosciences*, *31*(7), 361–370. https://doi.org/10.1016/j.tins.2008.04.001

Fischl, B., & Dale, A. M. (2000). Measuring the thickness of the human cerebral cortex from magnetic resonance images. *Proceedings of the National Academy of Sciences*, *97*(20), 11050–11055. https://doi.org/10.1073/pnas.200033797

Flechsig, P. E. (1920). *Anatomie des menschlichen Gehirns und Rückenmarks auf myelogenetischer Grundlage* (Vol. 1). G. Thieme.

Fortin, J.-P., Parker, D., Tunç, B., Watanabe, T., Elliott, M. A., Ruparel, K., Roalf, D. R., Satterthwaite, T. D., Gur, R. C., Gur, R. E., Schultz, R. T., Verma, R., & Shinohara, R. T. (2017). Harmonization of multi-site diffusion tensor imaging data. *NeuroImage*, *161*, 149–170. https://doi.org/10.1016/j.neuroimage.2017.08.047

Fransson, P., Åden, U., Blennow, M., & Lagercrantz, H. (2011). The Functional Architecture of the Infant Brain as Revealed by Resting-State fMRI. *Cerebral Cortex*, *21*(1), 145–154. https://doi.org/10.1093/cercor/bhq071

Friede, R. L. (1972). Control of myelin formation by axon caliber. (With a model of the control mechanism). *The Journal of Comparative Neurology*, *144*(2), 233–252. https://doi.org/10.1002/cne.901440207

Gadisseux, J. F., Evrard, P., Misson, J. P., & Caviness, V. S. (1989). Dynamic structure of the radial glial fiber system of the developing murine cerebral wall. An immunocytochemical analysis. *Developmental Brain Research*, *50*(1), 55–67. https://doi.org/10.1016/0165-3806(89)90126-0

Garel, C., Chantrel, E., Brisse, H., Elmaleh, M., Luton, D., Oury, J.-F., Sebag, G., & Hassan, M. (2001). *Fetal Cerebral Cortex: Normal Gestational Landmarks Identified Using Prenatal MR Imaging*. 6.

Ghashghaei, H. T., Lai, C., & Anton, E. S. (2007). Neuronal migration in the adult brain: Are we there yet? *Nature Reviews Neuroscience*, *8*(2), 141–151. https://doi.org/10.1038/nrn2074

Ghiglia, D. C., & Romero, L. A. (1994). Robust two-dimensional weighted and unweighted phase unwrapping that uses fast transforms and iterative methods. *Journal of the Optical Society of America A*, *11*(1), 107. https://doi.org/10.1364/JOSAA.11.000107

Gholipour, A., Estroff, J. A., Barnewolt, C. E., Robertson, R. L., Grant, P. E., Gagoski, B., Warfield, S. K., Afacan, O., Connolly, S. A., Neil, J. J., Wolfberg, A., & Mulkern, R. V. (2014). Fetal MRI: A technical update with educational aspirations: Fetal Mri: A Technical Update With Educational Aspirations. *Concepts in Magnetic Resonance Part A*, *43*(6), 237–266. https://doi.org/10.1002/cmr.a.21321

Gholipour, A., Rollins, C. K., Velasco-Annis, C., Ouaalam, A., Akhondi-Asl, A., Afacan, O., Ortinau, C. M., Clancy, S., Limperopoulos, C., Yang, E., Estroff, J. A., & Warfield, S. K. (2017). A normative spatiotemporal MRI atlas of the fetal brain for automatic segmentation and analysis of early brain growth. *Scientific Reports*, *7*(1), 476. https://doi.org/10.1038/s41598-017-00525-w

Ghosh, A., Antonini, A., McConnell, S. K., & Shatz, C. J. (1990). Requirement for subplate neurons in the formation of thalamocortical connections. *Nature*, *347*(6289), 179–181. https://doi.org/10.1038/347179a0

Glenn, O. A. (2009). Normal Development of the Fetal Brain by MRI. *Seminars in Perinatology*, *33*(4), 208–219. https://doi.org/10.1053/j.semperi.2009.04.009

Goldman, P. S., & Galkin, T. W. (1978). Prenatal removal of frontal association cortex in the fetal rhesus monkey: Anatomical and functional consequences in postnatal life. *Brain Research*, *152*(3), 451–485. https://doi.org/10.1016/0006-8993(78)91103-4

Goldman, S. A., & Nottebohm, F. (1983). Neuronal Production, Migration, and Differentiation in a Vocal Control Nucleus of the Adult Female Canary Brain. *Proceedings of the National Academy of Sciences of the United States of America*, *80*(8), 2390–2394. JSTOR.

Goldman-Rakic, P. S. (1980). Morphological consequences of prenatal injury to the primate brain. *Progress in Brain Research*, *53*, 1–19.

Golgi, C. (1885). *Sulla fina anatomia degli organi centrali del sistema nervoso*. S. Calderini. https://books.google.co.uk/books?id=AIVAAAAAYAAJ

Götz, M., Hartfuss, E., & Malatesta, P. (2002). Radial glial cells as neuronal precursors: A new perspective on the correlation of morphology and lineage restriction in the developing cerebral cortex of mice. *Brain Research Bulletin*, *57*(6), 777–788. https://doi.org/10.1016/S0361-9230(01)00777-8

Govaert, P., Triulzi, F., & Dudink, J. (2020). The developing brain by trimester. In *Handbook of Clinical Neurology* (Vol. 171, pp. 245–289). Elsevier. https://doi.org/10.1016/B978-0-444-64239-4.00014-X

Grant, E., Hoerder-Suabedissen, A., & Molnár, Z. (2012). Development of the Corticothalamic Projections. *Frontiers in Neuroscience*, *6*. https://doi.org/10.3389/fnins.2012.00053

Gray, G. E., Leber, S. M., & Sanes, J. R. (1990). Migratory patterns of clonally related cells in the developing central nervous system. *Experientia*, *46*(9), 929–940. https://doi.org/10.1007/BF01939386

Greve, D. N., & Fischl, B. (2009). Accurate and robust brain image alignment using boundary-based registration. *NeuroImage*, *48*(1), 63–72. https://doi.org/10.1016/j.neuroimage.2009.06.060

Grossman, R., Hoffman, C., Mardor, Y., & Biegon, A. (2006). Quantitative MRI measurements of human fetal brain development in utero. *NeuroImage*, *33*(2), 463–470. https://doi.org/10.1016/j.neuroimage.2006.07.005

Grover, V. P. B., Tognarelli, J. M., Crossey, M. M. E., Cox, I. J., Taylor-Robinson, S. D., & McPhail, M. J. W. (2015). Magnetic Resonance Imaging: Principles and Techniques: Lessons

for Clinicians. *Journal of Clinical and Experimental Hepatology*, *5*(3), 246–255. https://doi.org/10.1016/j.jceh.2015.08.001

Hadders-Algra, M., Boxum, A. G., Hielkema, T., & Hamer, E. G. (2017). Effect of early intervention in infants at very high risk of cerebral palsy: A systematic review. *Developmental Medicine & Child Neurology*, *59*(3), 246–258. https://doi.org/10.1111/dmcn.13331

Hartline, D. K., & Colman, D. R. (2007). Rapid Conduction and the Evolution of Giant Axons and Myelinated Fibers. *Current Biology*, *17*(1), R29–R35. https://doi.org/10.1016/j.cub.2006.11.042

Hatten, M. E. (1999). Central Nervous System Neuronal Migration. *Annual Review of Neuroscience*, *22*(1), 511–539. https://doi.org/10.1146/annurev.neuro.22.1.511

Hatten, M., Liem, R., & Mason, C. (1986). Weaver mouse cerebellar granule neurons fail to migrate on wild-type astroglial processes in vitro. *The Journal of Neuroscience*, *6*(9), 2676–2683. https://doi.org/10.1523/JNEUROSCI.06-09-02676.1986

Haubensak, W., Attardo, A., Denk, W., & Huttner, W. B. (2004). Neurons arise in the basal neuroepithelium of the early mammalian telencephalon: A major site of neurogenesis. *Proceedings of the National Academy of Sciences*, *101*(9), 3196–3201. https://doi.org/10.1073/pnas.0308600100

Hawkes, R. C., Holland, G. N., Moore, W. S., & Worthington, B. S. (1980). Nuclear Magnetic Resonance (NMR) Tomography of the Brain: A Preliminary Clinical Assessment with Demonstration of Pathology. *Journal of Computer Assisted Tomography*, *4*(5), 577–586. https://doi.org/10.1097/00004728-198010000-00001

Haynes, R. L., Borenstein, N. S., Desilva, T. M., Folkerth, R. D., Liu, L. G., Volpe, J. J., & Kinney, H. C. (2005). Axonal development in the cerebral white matter of the human fetus

and infant. *The Journal of Comparative Neurology*, *484*(2), 156–167. https://doi.org/10.1002/cne.20453

He, W., Ingraham, C., Rising, L., Goderie, S., & Temple, S. (2001). Multipotent Stem Cells from the Mouse Basal Forebrain Contribute GABAergic Neurons and Oligodendrocytes to the Cerebral Cortex during Embryogenesis. *The Journal of Neuroscience*, *21*(22), 8854–8862. https://doi.org/10.1523/JNEUROSCI.21-22-08854.2001

Hilgetag, C. C., & Barbas, H. (2005). Developmental mechanics of the primate cerebral cortex. *Anatomy and Embryology*, *210*(5–6), 411–417. https://doi.org/10.1007/s00429-005-0041-5

Hoerder-Suabedissen, A., & Molnár, Z. (2013). Molecular Diversity of Early-Born Subplate Neurons. *Cerebral Cortex*, *23*(6), 1473–1483. https://doi.org/10.1093/cercor/bhs137

Hoerder-Suabedissen, A., & Molnár, Z. (2015). Development, evolution and pathology of neocortical subplate neurons. *Nature Reviews Neuroscience*, *16*(3), 133–146. https://doi.org/10.1038/nrn3915

Hogstrom, L. J., Westlye, L. T., Walhovd, K. B., & Fjell, A. M. (2013). The Structure of the Cerebral Cortex Across Adult Life: Age-Related Patterns of Surface Area, Thickness, and Gyrification. *Cerebral Cortex*, *23*(11), 2521–2530. https://doi.org/10.1093/cercor/bhs231

Holland, B. A., Haas, D. K., Norman, D., Brant-Zawadzki, M., & Newton, T. H. (1986). MRI of normal brain maturation. *AJNR. American Journal of Neuroradiology*, *7*(2), 201–208.

Huang, H., & Vasung, L. (2014). Gaining insight of fetal brain development with diffusion MRI and histology. *International Journal of Developmental Neuroscience*, *32*(1), 11–22. https://doi.org/10.1016/j.ijdevneu.2013.06.005

Hubbard, A. M., Harty, M. P., & States, L. J. (1999). A new tool for prenatal diagnosis: Ultrafast fetal MRI. *Seminars in Perinatology*, *23*(6), 437–447. https://doi.org/10.1016/S0146-0005(99)80023-8

Hüppi, P. S., Murphy, B., Maier, S. E., Zientara, G. P., Inder, T. E., Barnes, P. D., Kikinis, R., Jolesz, F. A., & Volpe, J. J. (2001). Microstructural Brain Development After Perinatal Cerebral White Matter Injury Assessed by Diffusion Tensor Magnetic Resonance Imaging. *Pediatrics*, *107*(3), 455–460. https://doi.org/10.1542/peds.107.3.455

Huttenlocher, P. R. (1979). Synaptic density in human frontal cortex—Developmental changes and effects of aging. *Brain Research*, *163*(2), 195–205. https://doi.org/10.1016/0006-8993(79)90349-4

Huttenlocher, P. R., & Dabholkar, A. S. (1997). Regional differences in synaptogenesis in human cerebral cortex. *The Journal of Comparative Neurology*, *387*(2), 167–178. https://doi.org/10.1002/(SICI)1096-9861(19971020)387:2<167::AID-CNE1>3.0.CO;2-Z

Hutter, J., Christiaens, D. J., Schneider, T., Cordero-Grande, L., Slator, P. J., Deprez, M., Price, A. N., Tournier, J.-D., Rutherford, M., & Hajnal, J. V. (2018). Slice-level diffusion encoding for motion and distortion correction. *Medical Image Analysis*, *48*, 214–229. https://doi.org/10.1016/j.media.2018.06.008

Hutter, J., Slator, P. J., Christiaens, D., Teixeira, R. P. A. G., Roberts, T., Jackson, L., Price, A. N., Malik, S., & Hajnal, J. V. (2018). Integrated and efficient diffusion-relaxometry using ZEBRA. *Scientific Reports*, *8*(1), 15138. https://doi.org/10.1038/s41598-018-33463-2

Hutter, J., Tournier, J. D., Price, A. N., Cordero-Grande, L., Hughes, E. J., Malik, S., Steinweg, J., Bastiani, M., Sotiropoulos, S. N., Jbabdi, S., Andersson, J., Edwards, A. D., & Hajnal, J. V. (2018). Time-efficient and flexible design of optimized multishell HARDI diffusion: Time-Efficient Flexible dMRI. *Magnetic Resonance in Medicine*, *79*(3), 1276–1292. https://doi.org/10.1002/mrm.26765

Ikeda, T., Murata, Y., Quilligan, E. J., Choi, B. H., Parer, J. T., Doi, S., & Park, S.-D. (1998). Physiologic and histologic changes in near-term fetal lambs exposed to asphyxia by partial

umbilical cord occlusion. *American Journal of Obstetrics and Gynecology*, *178*(1), 24–32. https://doi.org/10.1016/S0002-9378(98)70621-0

Im, K., & Grant, P. E. (2019). Sulcal pits and patterns in developing human brains. *NeuroImage*, *185*, 881–890. https://doi.org/10.1016/j.neuroimage.2018.03.057

Im, K., Jo, H. J., Mangin, J.-F., Evans, A. C., Kim, S. I., & Lee, J.-M. (2010). Spatial Distribution of Deep Sulcal Landmarks and Hemispherical Asymmetry on the Cortical Surface. *Cerebral Cortex*, *20*(3), 602–611. https://doi.org/10.1093/cercor/bhp127

Im, K., Pienaar, R., Lee, J.-M., Seong, J.-K., Choi, Y. Y., Lee, K. H., & Grant, P. E. (2011). Quantitative comparison and analysis of sulcal patterns using sulcal graph matching: A twin study. *NeuroImage*, *57*(3), 1077–1086. https://doi.org/10.1016/j.neuroimage.2011.04.062

Jaccard, P. (1912). THE DISTRIBUTION OF THE FLORA IN THE ALPINE ZONE.1. *New Phytologist*, *11*(2), 37–50. https://doi.org/10.1111/j.1469-8137.1912.tb05611.x

Jaimes, C., Machado-Rivas, F., Afacan, O., Khan, S., Marami, B., Ortinau, C. M., Rollins, C. K., Velasco-Annis, C., Warfield, S. K., & Gholipour, A. (2020a). In vivo characterization of emerging white matter microstructure in the fetal brain in the third trimester. *Human Brain Mapping*, *41*(12), 3177–3185. https://doi.org/10.1002/hbm.25006

Jaimes, C., Machado-Rivas, F., Afacan, O., Khan, S., Marami, B., Ortinau, C. M., Rollins, C. K., Velasco-Annis, C., Warfield, S. K., & Gholipour, A. (2020b). In vivo characterization of emerging white matter microstructure in the fetal brain in the third trimester. *Human Brain Mapping*, *41*(12), 3177–3185. https://doi.org/10.1002/hbm.25006

Jakab, A., Pogledic, I., Schwartz, E., Gruber, G., Mitter, C., Brugger, P. C., Langs, G., Schöpf, V., Kasprian, G., & Prayer, D. (2015). Fetal Cerebral Magnetic Resonance Imaging Beyond Morphology. *Seminars in Ultrasound, CT and MRI*, *36*(6), 465–475. https://doi.org/10.1053/j.sult.2015.06.003

Jakab, A., Tuura, R., Kellenberger, C., & Scheer, I. (2017). In utero diffusion tensor imaging of the fetal brain: A reproducibility study. *NeuroImage: Clinical*, *15*, 601–612. https://doi.org/10.1016/j.nicl.2017.06.013

Jakovcevski, I., Filipovic, R., Mo, Z., Rakic, S., & Zecevic, N. (2009). Oligodendrocyte development and the onset of myelination in the human fetal brain. *Frontiers in Neuroanatomy*, *3*, 5. https://doi.org/10.3389/neuro.05.005.2009

Jarvis, D., Akram, R., Mandefield, L., Paddock, M., Armitage, P., & Griffiths, P. D. (2016). Quantification of total fetal brain volume using 3D MR imaging data acquired in utero: Quantification of fetal brain volume. *Prenatal Diagnosis*, *36*(13), 1225–1232. https://doi.org/10.1002/pd.4961

Jenkinson, M., Bannister, P., Brady, M., & Smith, S. (2002). Improved Optimization for the Robust and Accurate Linear Registration and Motion Correction of Brain Images. *NeuroImage*, *17*(2), 825–841. https://doi.org/10.1006/nimg.2002.1132

Jenkinson, M., Beckmann, C. F., Behrens, T. E. J., Woolrich, M. W., & Smith, S. M. (2012). FSL. *NeuroImage*, *62*(2), 782–790. https://doi.org/10.1016/j.neuroimage.2011.09.015

Jenkinson, M., & Smith, S. (2001). A global optimisation method for robust affine registration of brain images. *Medical Image Analysis*, *5*(2), 143–156. https://doi.org/10.1016/S1361-8415(01)00036-6

Jeurissen, B., Leemans, A., Tournier, J.-D., Jones, D. K., & Sijbers, J. (2013). Investigating the prevalence of complex fiber configurations in white matter tissue with diffusion magnetic resonance imaging: Prevalence of Multifiber Voxels in WM. *Human Brain Mapping*, *34*(11), 2747–2766. https://doi.org/10.1002/hbm.22099

Jeurissen, B., Tournier, J.-D., Dhollander, T., Connelly, A., & Sijbers, J. (2014). Multi-tissue constrained spherical deconvolution for improved analysis of multi-shell diffusion MRI data. *NeuroImage*, *103*, 411–426. https://doi.org/10.1016/j.neuroimage.2014.07.061

Johansen-Berg, H., Behrens, T. E. J., Sillery, E., Ciccarelli, O., Thompson, A. J., Smith, S. M., & Matthews, P. M. (2005). Functional–Anatomical Validation and Individual Variation of Diffusion Tractography-based Segmentation of the Human Thalamus. *Cerebral Cortex*, *15*(1), 31–39. https://doi.org/10.1093/cercor/bhh105

Jones, D. K. (2008). Tractography Gone Wild: Probabilistic Fibre Tracking Using the Wild Bootstrap With Diffusion Tensor MRI. *IEEE Transactions on Medical Imaging*, *27*(9), 1268–1274. https://doi.org/10.1109/TMI.2008.922191

Jones, E. G. (2007). *The thalamus* (2nd ed). Cambridge University Press.

Judaš, M., Sedmak, G., & Kostović, I. (2013). The significance of the subplate for evolution and developmental plasticity of the human brain. *Frontiers in Human Neuroscience*, *7*. https://doi.org/10.3389/fnhum.2013.00423

Kanold, P. O. (2019). The first cortical circuits: Subplate neurons lead the way and shape cortical organization. *Neuroforum*, *25*(1), 15–23. https://doi.org/10.1515/nf-2018-0010

Kanold, P. O., & Luhmann, H. J. (2010). The Subplate and Early Cortical Circuits. *Annual Review of Neuroscience*, *33*(1), 23–48. https://doi.org/10.1146/annurev-neuro-060909-153244

Kasprian, G., Brugger, P. C., Weber, M., Krssák, M., Krampl, E., Herold, C., & Prayer, D. (2008). In utero tractography of fetal white matter development. *NeuroImage*, *43*(2), 213–224. https://doi.org/10.1016/j.neuroimage.2008.07.026

Kasprian, G., Langs, G., Brugger, P. C., Bittner, M., Weber, M., Arantes, M., & Prayer, D. (2011). The Prenatal Origin of Hemispheric Asymmetry: An In Utero Neuroimaging Study. *Cerebral Cortex*, *21*(5), 1076–1083. https://doi.org/10.1093/cercor/bhq179

Kelly, R. E., & Hoptman, M. J. (2022). Replicability in Brain Imaging. *Brain Sciences*, *12*(3), 397. https://doi.org/10.3390/brainsci12030397

Kershman, J. (1938). THE MEDULLOBLAST AND THE MEDULLOBLASTOMA: A STUDY OF HUMAN EMBRYOS. *Archives of Neurology & Psychiatry*, *40*(5), 937. https://doi.org/10.1001/archneurpsyc.1938.02270110091007

Kessaris, N., Fogarty, M., Iannarelli, P., Grist, M., Wegner, M., & Richardson, W. D. (2006). Competing waves of oligodendrocytes in the forebrain and postnatal elimination of an embryonic lineage. *Nature Neuroscience*, *9*(2), 173–179. https://doi.org/10.1038/nn1620

Keunen, K., van der Burgh, H. K., de Reus, M. A., Moeskops, P., Schmidt, R., Stolwijk, L. J., de Lange, S. C., Išgum, I., de Vries, L. S., Benders, M. J., & van den Heuvel, M. P. (2018). Early human brain development: Insights into macroscale connectome wiring. *Pediatric Research*, *84*(6), 829–836. https://doi.org/10.1038/s41390-018-0138-1

Khan, S., Vasung, L., Marami, B., Rollins, C. K., Afacan, O., Ortinau, C. M., Yang, E., Warfield, S. K., & Gholipour, A. (2019). Fetal brain growth portrayed by a spatiotemporal diffusion tensor MRI atlas computed from in utero images. *NeuroImage*, *185*, 593–608. https://doi.org/10.1016/j.neuroimage.2018.08.030

Khazipov, R., & Luhmann, H. J. (2006). Early patterns of electrical activity in the developing cerebral cortex of humans and rodents. *Trends in Neurosciences*, *29*(7), 414–418. https://doi.org/10.1016/j.tins.2006.05.007

Kim, J. S., Singh, V., Lee, J. K., Lerch, J., Ad-Dab'bagh, Y., MacDonald, D., Lee, J. M., Kim, S. I., & Evans, A. C. (2005). Automated 3-D extraction and evaluation of the inner and outer cortical surfaces using a Laplacian map and partial volume effect classification. *NeuroImage*, *27*(1), 210–221. https://doi.org/10.1016/j.neuroimage.2005.03.036

Kim, K., Habas, P. A., Rousseau, F., Glenn, O. A., Barkovich, A. J., & Studholme, C. (2010). Intersection Based Motion Correction of Multislice MRI for 3-D *in Utero* Fetal Brain Image Formation. *IEEE Transactions on Medical Imaging*, *29*(1), 146–158. https://doi.org/10.1109/TMI.2009.2030679

Kinney, H. C., Ann brody, B., Kloman, A. S., & Gilles, F. H. (1988). Sequence of Central Nervous System Myelination in Human Infancy. II. Patterns of Myelination in Autopsied Infants: *Journal of Neuropathology and Experimental Neurology*, *47*(3), 217–234. https://doi.org/10.1097/00005072-198805000-00003

Kinney, H. C., Karthigasan, J., Borenshteyn, N. I., Flax, J. D., & Kirschner, D. A. (1994). Myelination in the developing human brain: Biochemical correlates. *Neurochemical Research*, *19*(8), 983–996. https://doi.org/10.1007/BF00968708

Klingner, C. M., Langbein, K., Dietzek, M., Smesny, S., Witte, O. W., Sauer, H., & Nenadic, I. (2014). Thalamocortical connectivity during resting state in schizophrenia. *European Archives of Psychiatry and Clinical Neuroscience*, *264*(2), 111–119. https://doi.org/10.1007/s00406-013-0417-0

Knaap, M. S. van der, Valk, J., & Valk, J. (1995). *Magnetic resonance of myelin, myelination, and myelin disorders* (2nd ed). Springer.

Kostovic, I. (2002). Laminar Organization of the Human Fetal Cerebrum Revealed by Histochemical Markers and Magnetic Resonance Imaging. *Cerebral Cortex*, *12*(5), 536–544. https://doi.org/10.1093/cercor/12.5.536

Kostović, I. (2020). The enigmatic fetal subplate compartment forms an early tangential cortical nexus and provides the framework for construction of cortical connectivity. *Progress in Neurobiology*, *194*, 101883. https://doi.org/10.1016/j.pneurobio.2020.101883

Kostovic, I., & Goldman-Rakic, P. S. (1983). Transient cholinesterase staining in the mediodorsal nucleus of the thalamus and its connections in the developing human and monkey brain. *The Journal of Comparative Neurology*, *219*(4), 431–447. https://doi.org/10.1002/cne.902190405

Kostović, I., Išasegi, I. Ž., & Krsnik, Ž. (2019). Sublaminar organization of the human subplate: Developmental changes in the distribution of neurons, glia, growing axons and extracellular matrix. *Journal of Anatomy*, *235*(3), 481–506. https://doi.org/10.1111/joa.12920

Kostović, I., & Jovanov-Milosević, N. (2006). The development of cerebral connections during the first 20-45 weeks' gestation. *Seminars in Fetal & Neonatal Medicine*, *11*(6), 415–422. https://doi.org/10.1016/j.siny.2006.07.001

Kostović, I., Jovanov-Milošević, N., Radoš, M., Sedmak, G., Benjak, V., Kostović-Srzentić, M., Vasung, L., Čuljat, M., Radoš, M., Hüppi, P., & Judaš, M. (2014). Perinatal and early postnatal reorganization of the subplate and related cellular compartments in the human cerebral wall as revealed by histological and MRI approaches. *Brain Structure and Function*, *219*(1), 231–253. https://doi.org/10.1007/s00429-012-0496-0

Kostovic, I., & Judas, M. (2006). Prolonged coexistence of transient and permanent circuitry elements in the developing cerebral cortex of fetuses and preterm infants. *Developmental Medicine and Child Neurology*, *48*(5), 388–393. https://doi.org/10.1017/S0012162206000831

Kostovic, I., & Judas, M. (2007). Transient patterns of cortical lamination during prenatal life: Do they have implications for treatment? *Neuroscience & Biobehavioral Reviews*, *31*(8), 1157–1168. https://doi.org/10.1016/j.neubiorev.2007.04.018

Kostović, I., & Judaš, M. (2010). The development of the subplate and thalamocortical connections in the human foetal brain: Human foetal cortical circuitry. *Acta Paediatrica*, *99*(8), 1119–1127. https://doi.org/10.1111/j.1651-2227.2010.01811.x

Kostović, I., & Judaš, M. (2015). Embryonic and Fetal Development of the Human Cerebral Cortex. In *Brain Mapping* (pp. 167–175). Elsevier. https://doi.org/10.1016/B978-0-12-397025-1.00193-7

Kostović, I., & Molliver, ME. (1974). New interpretation of laminar development of cerebral-cortex-synaptogenesis in different layers of neopallium in human fetus. *Anatomical Record*, *178*(2), 395–395.

Kostovic, I., & Rakic, P. (1980). Cytology and time of origin of interstitial neurons in the white matter in infant and adult human and monkey telencephalon. *Journal of Neurocytology*, *9*(2), 219–242. https://doi.org/10.1007/BF01205159

Kostovic, I., & Rakic, P. (1984). Development of prestriate visual projections in the monkey and human fetal cerebrum revealed by transient cholinesterase staining. *The Journal of Neuroscience: The Official Journal of the Society for Neuroscience*, *4*(1), 25–42. https://doi.org/10.1523/JNEUROSCI.04-01-00025.1984

Kostovic, I., & Rakic, P. (1990). Developmental history of the transient subplate zone in the visual and somatosensory cortex of the macaque monkey and human brain. *The Journal of Comparative Neurology*, *297*(3), 441–470. https://doi.org/10.1002/cne.902970309

Kostović, I., Sedmak, G., Vukšić, M., & Judaš, M. (2015). The Relevance of Human Fetal Subplate Zone for Developmental Neuropathology of Neuronal Migration Disorders and Cortical Dysplasia. *CNS Neuroscience & Therapeutics*, *21*(2), 74–82. https://doi.org/10.1111/cns.12333

Kostovic, I., & Vasung, L. (2009). Insights From In Vitro Fetal Magnetic Resonance Imaging of Cerebral Development. *Seminars in Perinatology*, *33*(4), 220–233. https://doi.org/10.1053/j.semperi.2009.04.003

Kroenke, C. D., Taber, E. N., Leigland, L. A., Knutsen, A. K., & Bayly, P. V. (2009). Regional Patterns of Cerebral Cortical Differentiation Determined by Diffusion Tensor MRI. *Cerebral Cortex*, *19*(12), 2916–2929. https://doi.org/10.1093/cercor/bhp061

Kroenke, C. D., Van Essen, D. C., Inder, T. E., Rees, S., Bretthorst, G. L., & Neil, J. J. (2007). Microstructural Changes of the Baboon Cerebral Cortex during Gestational Development Reflected in Magnetic Resonance Imaging Diffusion Anisotropy. *The Journal of Neuroscience*, *27*(46), 12506–12515. https://doi.org/10.1523/JNEUROSCI.3063-07.2007

Krsnik, Ž., Majić, V., Vasung, L., Huang, H., & Kostović, I. (2017). Growth of Thalamocortical Fibers to the Somatosensory Cortex in the Human Fetal Brain. *Frontiers in Neuroscience*, *11*, 233. https://doi.org/10.3389/fnins.2017.00233

Kuklisova-Murgasova, M., Quaghebeur, G., Rutherford, M. A., Hajnal, J. V., & Schnabel, J. A. (2012). Reconstruction of fetal brain MRI with intensity matching and complete outlier removal. *Medical Image Analysis*, *16*(8), 1550–1564. https://doi.org/10.1016/j.media.2012.07.004

Kurugol, S., Marami, B., Afacan, O., Warfield, S. K., & Gholipour, A. (2017). Motion-Robust Spatially Constrained Parameter Estimation in Renal Diffusion-Weighted MRI by 3D Motion Tracking and Correction of Sequential Slices. In M. J. Cardoso, T. Arbel, F. Gao, B. Kainz, T. van Walsum, K. Shi, K. K. Bhatia, R. Peter, T. Vercauteren, M. Reyes, A. Dalca, R. Wiest, W. Niessen, & B. J. Emmer (Eds.), *Molecular Imaging, Reconstruction and Analysis of Moving Body Organs, and Stroke Imaging and Treatment* (Vol. 10555, pp. 75–85). Springer International Publishing. https://doi.org/10.1007/978-3-319-67564-0_8

Kyriakopoulou, V. (2012). *Brain development in fetal ventriculomegaly*. https://doi.org/10.25560/11086

Kyriakopoulou, V., Vatansever, D., Davidson, A., Patkee, P., Elkommos, S., Chew, A., Martinez-Biarge, M., Hagberg, B., Damodaram, M., Allsop, J., Fox, M., Hajnal, J. V., & Rutherford, M. A. (2017). Normative biometry of the fetal brain using magnetic resonance imaging. *Brain Structure and Function*, *222*(5), 2295–2307. https://doi.org/10.1007/s00429-016-1342-6

Kyriakopoulou, V., Vatansever, D., Elkommos, S., Dawson, S., McGuinness, A., Allsop, J., Molnar, Z., Hajnal, J., & Rutherford, M. (2014). Cortical Overgrowth in Fetuses With Isolated Ventriculomegaly. *Cerebral Cortex*, *24*(8), 2141–2150. https://doi.org/10.1093/cercor/bht062

Labusch, M., Mancini, L., Morizet, D., & Bally-Cuif, L. (2020). Conserved and Divergent Features of Adult Neurogenesis in Zebrafish. *Frontiers in Cell and Developmental Biology*, *8*, 525. https://doi.org/10.3389/fcell.2020.00525

Lang, K. R., & Gingerich, O. (Eds.). (1979). *A Source Book in Astronomy and Astrophysics, 1900–1975:* Harvard University Press. https://doi.org/10.4159/harvard.9780674366688

Lange, C., Rost, F., Machate, A., Reinhardt, S., Lesche, M., Weber, A., Kuscha, V., Dahl, A., Rulands, S., & Brand, M. (2020). Single cell sequencing of radial glia progeny reveals diversity of newborn neurons in the adult zebrafish brain. *Development*, 1855951. https://doi.org/10.1242/dev.185595

Le Gros Clark, W. E. (1936). The Topography and Homologies of the Hypothalamic Nuclei in Man. *Journal of Anatomy*, *70*(Pt 2), 203-214.3.

Lefèvre, J., & Mangin, J.-F. (2010). A Reaction-Diffusion Model of Human Brain Development. *PLoS Computational Biology*, *6*(4), e1000749. https://doi.org/10.1371/journal.pcbi.1000749

Levine, D., Barnes, P. D., Madsen, J. R., Li, W., & Edelman, R. R. (1997). Fetal central nervous system anomalies: MR imaging augments sonographic diagnosis. *Radiology*, *204*(3), 635–642. https://doi.org/10.1148/radiology.204.3.9280237

Levine, D., Barnes, P. D., Sher, S., Semelka, R. C., Li, W., McArdle, C. R., Worawattanakul, S., & Edelman, R. R. (1998). Fetal fast MR imaging: Reproducibility, technical quality, and conspicuity of anatomy. *Radiology*, *206*(2), 549–554. https://doi.org/10.1148/radiology.206.2.9457211

Lin, S., & Bergles, D. E. (2004). Synaptic signaling between GABAergic interneurons and oligodendrocyte precursor cells in the hippocampus. *Nature Neuroscience*, *7*(1), 24–32. https://doi.org/10.1038/nn1162

Liu, T., Gao, F., Zheng, W., You, Y., Zhao, Z., Lv, Y., Chen, W., Zhang, H., Ji, C., & Wu, D. (2021). Diffusion MRI of the infant brain reveals unique asymmetry patterns during the first-

half-year of development. *NeuroImage*, *242*, 118465. https://doi.org/10.1016/j.neuroimage.2021.118465

Llera, A., Wolfers, T., Mulders, P., & Beckmann, C. F. (2019). Inter-individual differences in human brain structure and morphology link to variation in demographics and behavior. *ELife*, *8*, e44443. https://doi.org/10.7554/eLife.44443

Llinares-Benadero, C., & Borrell, V. (2019). Deconstructing cortical folding: Genetic, cellular and mechanical determinants. *Nature Reviews Neuroscience*, *20*(3), 161–176. https://doi.org/10.1038/s41583-018-0112-2

Luhmann, H. J., & Khazipov, R. (2018). Neuronal Activity Patterns in the Developing Barrel Cortex. *Neuroscience*, *368*, 256–267. https://doi.org/10.1016/j.neuroscience.2017.05.025

Luskin, M., & Shatz, C. (1985). Studies of the earliest generated cells of the cat's visual cortex: Cogeneration of subplate and marginal zones. *The Journal of Neuroscience*, *5*(4), 1062–1075. https://doi.org/10.1523/JNEUROSCI.05-04-01062.1985

Machado-Rivas, F., Afacan, O., Khan, S., Marami, B., Velasco-Annis, C., Lidov, H., Warfield, S. K., Gholipour, A., & Jaimes, C. (2021). Spatiotemporal changes in diffusivity and anisotropy in fetal brain tractography. *Human Brain Mapping*, *42*(17), 5771–5784. https://doi.org/10.1002/hbm.25653

Machado-Rivas, F., Gandhi, J., Choi, J. J., Velasco-Annis, C., Afacan, O., Warfield, S. K., Gholipour, A., & Jaimes, C. (2022). Normal Growth, Sexual Dimorphism, and Lateral Asymmetries at Fetal Brain MRI. *Radiology*, *303*(1), 162–170. https://doi.org/10.1148/radiol.211222

MacKay, A. L., & Laule, C. (2016). Magnetic Resonance of Myelin Water: An in vivo Marker for Myelin. *Brain Plasticity*, *2*(1), 71–91. https://doi.org/10.3233/BPL-160033

Mahmoudzadeh, M., Dehaene-Lambertz, G., Fournier, M., Kongolo, G., Goudjil, S., Dubois, J., Grebe, R., & Wallois, F. (2013). Syllabic discrimination in premature human infants prior to

complete formation of cortical layers. *Proceedings of the National Academy of Sciences*, *110*(12), 4846–4851. https://doi.org/10.1073/pnas.1212220110

Makropoulos, A., Gousias, I. S., Ledig, C., Aljabar, P., Serag, A., Hajnal, J. V., Edwards, A. D., Counsell, S. J., & Rueckert, D. (2014). Automatic Whole Brain MRI Segmentation of the Developing Neonatal Brain. *IEEE Transactions on Medical Imaging*, *33*(9), 1818–1831. https://doi.org/10.1109/TMI.2014.2322280

Makropoulos, A., Robinson, E. C., Schuh, A., Wright, R., Fitzgibbon, S., Bozek, J., Counsell, S. J., Steinweg, J., Vecchiato, K., Passerat-Palmbach, J., Lenz, G., Mortari, F., Tenev, T., Duff, E. P., Bastiani, M., Cordero-Grande, L., Hughes, E., Tusor, N., Tournier, J.-D., … Rueckert, D. (2018). The developing human connectome project: A minimal processing pipeline for neonatal cortical surface reconstruction. *NeuroImage*, *173*, 88–112. https://doi.org/10.1016/j.neuroimage.2018.01.054

Malatesta, P., & Götz, M. (2013). Radial glia – from boring cables to stem cell stars. *Development*, *140*(3), 483–486. https://doi.org/10.1242/dev.085852

Malatesta, P., Hartfuss, E., & Götz, M. (2000). Isolation of radial glial cells by fluorescent-activated cell sorting reveals a neuronal lineage. *Development*, *127*(24), 5253–5263. https://doi.org/10.1242/dev.127.24.5253

Marenco, S., Stein, J. L., Savostyanova, A. A., Sambataro, F., Tan, H.-Y., Goldman, A. L., Verchinski, B. A., Barnett, A. S., Dickinson, D., Apud, J. A., Callicott, J. H., Meyer-Lindenberg, A., & Weinberger, D. R. (2012). Investigation of Anatomical Thalamo-Cortical Connectivity and fMRI Activation in Schizophrenia. *Neuropsychopharmacology*, *37*(2), 499–507. https://doi.org/10.1038/npp.2011.215

Marín, O., & Rubenstein, J. L. R. (2001). A long, remarkable journey: Tangential migration in the telencephalon. *Nature Reviews Neuroscience*, *2*(11), 780–790. https://doi.org/10.1038/35097509

Marín, O., & Rubenstein, J. L. R. (2003). Cell Migration in the Forebrain. *Annual Review of Neuroscience*, *26*(1), 441–483. https://doi.org/10.1146/annurev.neuro.26.041002.131058

Marin, O., Valiente, M., Ge, X., & Tsai, L.-H. (2010). Guiding Neuronal Cell Migrations. *Cold Spring Harbor Perspectives in Biology*, *2*(2), a001834–a001834. https://doi.org/10.1101/cshperspect.a001834

Marshall, C. A. G., & Goldman, J. E. (2002). Subpallial *Dlx2* -Expressing Cells Give Rise to Astrocytes and Oligodendrocytes in the Cerebral Cortex and White Matter. *The Journal of Neuroscience*, *22*(22), 9821–9830. https://doi.org/10.1523/JNEUROSCI.22-22-09821.2002

Mathur, A., & Inder, T. (2009). Magnetic resonance imaging—Insights into brain injury and outcomes in premature infants. *Journal of Communication Disorders*, *42*(4), 248–255. https://doi.org/10.1016/j.jcomdis.2009.03.007

McKinstry, R. C. (2002). Radial Organization of Developing Preterm Human Cerebral Cortex Revealed by Non-invasive Water Diffusion Anisotropy MRI. *Cerebral Cortex*, *12*(12), 1237–1243. https://doi.org/10.1093/cercor/12.12.1237

Meyer, G., Schaaps, J. P., Moreau, L., & Goffinet, A. M. (2000). Embryonic and Early Fetal Development of the Human Neocortex. *The Journal of Neuroscience*, *20*(5), 1858–1868. https://doi.org/10.1523/JNEUROSCI.20-05-01858.2000

Meyer, M., Desbrun, M., Schröder, P., & Barr, A. H. (2003). Discrete Differential-Geometry Operators for Triangulated 2-Manifolds. In H.-C. Hege & K. Polthier (Eds.), *Visualization and Mathematics III* (pp. 35–57). Springer Berlin Heidelberg. https://doi.org/10.1007/978-3-662-05105-4_2

Miller, F. D., & Gauthier, A. S. (2007). Timing Is Everything: Making Neurons versus Glia in the Developing Cortex. *Neuron*, *54*(3), 357–369. https://doi.org/10.1016/j.neuron.2007.04.019

Miller, J. A., Ding, S.-L., Sunkin, S. M., Smith, K. A., Ng, L., Szafer, A., Ebbert, A., Riley, Z. L., Royall, J. J., Aiona, K., Arnold, J. M., Bennet, C., Bertagnolli, D., Brouner, K., Butler, S.,

Caldejon, S., Carey, A., Cuhaciyan, C., Dalley, R. A., … Lein, E. S. (2014). Transcriptional landscape of the prenatal human brain. *Nature*, *508*(7495), 199–206. https://doi.org/10.1038/nature13185

Miller, M. W., & Nowakowski, R. S. (1988). Use of bromodeoxyuridine-immunohistochemistry to examine the proliferation, migration and time of origin of cells in the central nervous system. *Brain Research*, *457*(1), 44–52. https://doi.org/10.1016/0006-8993(88)90055-8

Mitter, C., Prayer, D., Brugger, P. C., Weber, M., & Kasprian, G. (2015). In Vivo Tractography of Fetal Association Fibers. *PLOS ONE*, *10*(3), e0119536. https://doi.org/10.1371/journal.pone.0119536

Miyazaki, Y., Song, J. W., & Takahashi, E. (2016). Asymmetry of Radial and Symmetry of Tangential Neuronal Migration Pathways in Developing Human Fetal Brains. *Frontiers in Neuroanatomy*, *10*. https://doi.org/10.3389/fnana.2016.00002

Mojsilović, J., & Zečević, N. (1991). Early development of the human thalamus: Golgi and Nissl study. *Early Human Development*, *27*(1–2), 119–144. https://doi.org/10.1016/0378-3782(91)90033-Y

Molliver, M. E., Kostovic´, I., & Van Der Loos, H. (1973). The development of synapses in cerebral cortex of the human fetus. *Brain Research*, *50*(2), 403–407. https://doi.org/10.1016/0006-8993(73)90741-5

Molnár, Z., Adams, R., & Blakemore, C. (1998). Mechanisms Underlying the Early Establishment of Thalamocortical Connections in the Rat. *The Journal of Neuroscience*, *18*(15), 5723–5745. https://doi.org/10.1523/JNEUROSCI.18-15-05723.1998

Molnár, Z., & Blakemore, C. (1995). How do thalamic axons find their way to the cortex? *Trends in Neurosciences*, *18*(9), 389–397. https://doi.org/10.1016/0166-2236(95)93935-q

Molnár, Z., Clowry, G. J., Šestan, N., Alzu'bi, A., Bakken, T., Hevner, R. F., Hüppi, P. S., Kostović, I., Rakic, P., Anton, E. S., Edwards, D., Garcez, P., Hoerder-Suabedissen, A., &

Kriegstein, A. (2019). New insights into the development of the human cerebral cortex. *Journal of Anatomy*, *235*(3), 432–451. https://doi.org/10.1111/joa.13055

Molnár, Z., Garel, S., López-Bendito, G., Maness, P., & Price, D. J. (2012). Mechanisms controlling the guidance of thalamocortical axons through the embryonic forebrain: Mechanisms controlling the guidance of thalamocortical axons. *European Journal of Neuroscience*, *35*(10), 1573–1585. https://doi.org/10.1111/j.1460-9568.2012.08119.x

Molnár, Z., & Hoerder-Suabedissen, A. (2016). Regional scattering of primate subplate. *Proceedings of the National Academy of Sciences*, *113*(35), 9676–9678. https://doi.org/10.1073/pnas.1611194113

Moore, A. R., Zhou, W.-L., Sirois, C. L., Belinsky, G. S., Zecevic, N., & Antic, S. D. (2014). Connexin hemichannels contribute to spontaneous electrical activity in the human fetal cortex. *Proceedings of the National Academy of Sciences*, *111*(37). https://doi.org/10.1073/pnas.1405253111

Morel, A., Magnin, M., & Jeanmonod, D. (1997). Multiarchitectonic and stereotactic atlas of the human thalamus. *The Journal of Comparative Neurology*, *387*(4), 588–630. https://doi.org/10.1002/(SICI)1096-9861(19971103)387:4<588::AID-CNE8>3.0.CO;2-Z

Morrow, T., Song, M.-R., & Ghosh, A. (2001). Sequential specification of neurons and glia by developmentally regulated extracellular factors. *Development*, *128*(18), 3585–3594. https://doi.org/10.1242/dev.128.18.3585

Mortazavi, F., Romano, S. E., Rosene, D. L., & Rockland, K. S. (2017). A Survey of White Matter Neurons at the Gyral Crowns and Sulcal Depths in the Rhesus Monkey. *Frontiers in Neuroanatomy*, *11*, 69. https://doi.org/10.3389/fnana.2017.00069

Moseley, M. E., Cohen, Y., Mintorovitch, J., Chileuitt, L., Shimizu, H., Kucharczyk, J., Wendland, M. F., & Weinstein, P. R. (1990). Early detection of regional cerebral ischemia in

cats: Comparison of diffusion- and T2-weighted MRI and spectroscopy. *Magnetic Resonance in Medicine*, *14*(2), 330–346. https://doi.org/10.1002/mrm.1910140218

Mrzljak, L., Uylings, H. B. M., Kostovic, I., & van Eden, C. G. (1992). Prenatal development of neurons in the human prefrontal cortex. II. A quantitative Golgi study. *The Journal of Comparative Neurology*, *316*(4), 485–496. https://doi.org/10.1002/cne.903160408

Nair, A., Treiber, J. M., Shukla, D. K., Shih, P., & Müller, R.-A. (2013). Impaired thalamocortical connectivity in autism spectrum disorder: A study of functional and anatomical connectivity. *Brain*, *136*(6), 1942–1955. https://doi.org/10.1093/brain/awt079

Najdenovska, E., Alemán-Gómez, Y., Battistella, G., Descoteaux, M., Hagmann, P., Jacquemont, S., Maeder, P., Thiran, J.-P., Fornari, E., & Bach Cuadra, M. (2018). In-vivo probabilistic atlas of human thalamic nuclei based on diffusion- weighted magnetic resonance imaging. *Scientific Data*, *5*(1), 180270. https://doi.org/10.1038/sdata.2018.270

Nakagawa, Y. (2019). Development of the thalamus: From early patterning to regulation of cortical functions. *WIREs Developmental Biology*, *8*(5). https://doi.org/10.1002/wdev.345

Nie, J., Guo, L., Li, G., Faraco, C., Stephen Miller, L., & Liu, T. (2010). A computational model of cerebral cortex folding. *Journal of Theoretical Biology*, *264*(2), 467–478. https://doi.org/10.1016/j.jtbi.2010.02.002

Nie, J., Guo, L., Li, K., Wang, Y., Chen, G., Li, L., Chen, H., Deng, F., Jiang, X., Zhang, T., Huang, L., Faraco, C., Zhang, D., Guo, C., Yap, P.-T., Hu, X., Li, G., Lv, J., Yuan, Y., … Liu, T. (2012). Axonal Fiber Terminations Concentrate on Gyri. *Cerebral Cortex*, *22*(12), 2831–2839. https://doi.org/10.1093/cercor/bhr361

Niemann, K., Mennicken, V. R., Jeanmonod, D., & Morel, A. (2000). The Morel Stereotactic Atlas of the Human Thalamus: Atlas-to-MR Registration of Internally Consistent Canonical Model. *NeuroImage*, *12*(6), 601–616. https://doi.org/10.1006/nimg.2000.0650

Noctor, S. C., Cunningham, C. L., & Kriegstein, A. R. (2020). Radial migration in the developing cerebral cortex. In *Cellular Migration and Formation of Axons and Dendrites* (pp. 323–344). Elsevier. https://doi.org/10.1016/B978-0-12-814407-7.00015-8

Noctor, S. C., Flint, A. C., Weissman, T. A., Dammerman, R. S., & Kriegstein, A. R. (2001). Neurons derived from radial glial cells establish radial units in neocortex. *Nature*, *409*(6821), 714–720. https://doi.org/10.1038/35055553

Noctor, S. C., Martínez-Cerdeño, V., Ivic, L., & Kriegstein, A. R. (2004). Cortical neurons arise in symmetric and asymmetric division zones and migrate through specific phases. *Nature Neuroscience*, *7*(2), 136–144. https://doi.org/10.1038/nn1172

Nordahl, C. W., Dierker, D., Mostafavi, I., Schumann, C. M., Rivera, S. M., Amaral, D. G., & Van Essen, D. C. (2007). Cortical Folding Abnormalities in Autism Revealed by Surface-Based Morphometry. *The Journal of Neuroscience*, *27*(43), 11725–11735. https://doi.org/10.1523/JNEUROSCI.0777-07.2007

Nosarti, C., Nam, K. W., Walshe, M., Murray, R. M., Cuddy, M., Rifkin, L., & Allin, M. P. G. (2014). Preterm birth and structural brain alterations in early adulthood. *NeuroImage: Clinical*, *6*, 180–191. https://doi.org/10.1016/j.nicl.2014.08.005

O'Muircheartaigh, J., Dean, D. C., Ginestet, C. E., Walker, L., Waskiewicz, N., Lehman, K., Dirks, H., Piryatinsky, I., & Deoni, S. C. L. (2014). White matter development and early cognition in babies and toddlers. *Human Brain Mapping*, *35*(9), 4475–4487. https://doi.org/10.1002/hbm.22488

Ortinau, C. M., Rollins, C. K., Gholipour, A., Yun, H. J., Marshall, M., Gagoski, B., Afacan, O., Friedman, K., Tworetzky, W., Warfield, S. K., Newburger, J. W., Inder, T. E., Grant, P. E., & Im, K. (2019). Early-Emerging Sulcal Patterns Are Atypical in Fetuses with Congenital Heart Disease. *Cerebral Cortex*, *29*(8), 3605–3616. https://doi.org/10.1093/cercor/bhy235

Parker, G. J. M. (2010). Probabilistic Fiber Tracking. In D. K. Jones, PhD (Ed.), *Diffusion MRI* (pp. 396–408). Oxford University Press. https://doi.org/10.1093/med/9780195369779.003.0023

Passingham, R. E., Stephan, K. E., & Kötter, R. (2002). The anatomical basis of functional localization in the cortex. *Nature Reviews Neuroscience*, *3*(8), 606–616. https://doi.org/10.1038/nrn893

Pietsch, M. (n.d.). *ADVANCED DIFFUSION MRI ANALYSIS METHODS FOR NEONATAL IMAGING*. 301.

Pietsch, M., Christiaens, D., Hutter, J., Cordero-Grande, L., Price, A. N., Hughes, E., Edwards, A. D., Hajnal, J. V., Counsell, S. J., & Tournier, J.-D. (2019). A framework for multi-component analysis of diffusion MRI data over the neonatal period. *NeuroImage*, *186*, 321–337. https://doi.org/10.1016/j.neuroimage.2018.10.060

Poliak, S., & Peles, E. (2003). The local differentiation of myelinated axons at nodes of Ranvier. *Nature Reviews Neuroscience*, *4*(12), 968–980. https://doi.org/10.1038/nrn1253

Pollen, A. A., Nowakowski, T. J., Chen, J., Retallack, H., Sandoval-Espinosa, C., Nicholas, C. R., Shuga, J., Liu, S. J., Oldham, M. C., Diaz, A., Lim, D. A., Leyrat, A. A., West, J. A., & Kriegstein, A. R. (2015). Molecular Identity of Human Outer Radial Glia during Cortical Development. *Cell*, *163*(1), 55–67. https://doi.org/10.1016/j.cell.2015.09.004

Poole-Wilson, P. A., & Langer, G. A. (1975). Effect of pH on ionic exchange and function in rat and rabbit myocardium. *The American Journal of Physiology*, *229*(3), 570–581. https://doi.org/10.1152/ajplegacy.1975.229.3.570

Price, A., Cordero-Grande, L., Hughes, E., Rutherford, M., Edwards, A. D., & Hajnal, J. V. (2019.). *The Developing Human Connectome Project (dHCP): Fetal Acquisition Protocol*. ISMRM.

Price, D. J., Kennedy, H., Dehay, C., Zhou, L., Mercier, M., Jossin, Y., Goffinet, A. M., Tissir, F., Blakey, D., & Molnár, Z. (2006). The development of cortical connections. *European Journal of Neuroscience*, *23*(4), 910–920. https://doi.org/10.1111/j.1460-9568.2006.04620.x

Purcell, E. M., Torrey, H. C., & Pound, R. V. (1946). Resonance Absorption by Nuclear Magnetic Moments in a Solid. *Physical Review*, *69*(1–2), 37–38. https://doi.org/10.1103/PhysRev.69.37

Raffelt, D., Tournier, J.-D., Fripp, J., Crozier, S., Connelly, A., & Salvado, O. (2011). Symmetric diffeomorphic registration of fibre orientation distributions. *NeuroImage*, *56*(3), 1171–1180. https://doi.org/10.1016/j.neuroimage.2011.02.014

Rajagopalan, V., Scott, J., Habas, P. A., Kim, K., Corbett-Detig, J., Rousseau, F., Barkovich, A. J., Glenn, O. A., & Studholme, C. (2011). Local Tissue Growth Patterns Underlying Normal Fetal Human Brain Gyrification Quantified In Utero. *Journal of Neuroscience*, *31*(8), 2878–2887. https://doi.org/10.1523/JNEUROSCI.5458-10.2011

Rakic, P. (1975). Timing of Major Ontogenetic Events in the Visual Cortex of the Rhesus Monkey. In *Brain Mechanisms in Mental Retardation* (pp. 3–40). Elsevier. https://doi.org/10.1016/B978-0-12-139050-1.50008-2

Rakic, P. (1977). Prenatal development of the visual system in rhesus monkey. *Philosophical Transactions of the Royal Society of London. B, Biological Sciences*, *278*(961), 245–260. https://doi.org/10.1098/rstb.1977.0040

Rakic, P. (1978). Neuronal migration and contact guidance in the primate telencephalon. *Postgraduate Medical Journal*, *54 Suppl 1*, 25–40.

Rakic, P. (1988). Specification of Cerebral Cortical Areas. *Science*, *241*(4862), 170–176. https://doi.org/10.1126/science.3291116

Rakic, P. (1990). Principles of neural cell migration. *Experientia*, *46*(9), 882–891. https://doi.org/10.1007/BF01939380

Rakic, P. (1995). A small step for the cell, a giant leap for mankind: A hypothesis of neocortical expansion during evolution. *Trends in Neurosciences*, *18*(9), 383–388. https://doi.org/10.1016/0166-2236(95)93934-P

Rakic, P. (2003). Elusive radial glial cells: Historical and evolutionary perspective. *Glia*, *43*(1), 19–32. https://doi.org/10.1002/glia.10244

Rakic, P. (2005). Less is more: Progenitor death and cortical size. *Nature Neuroscience*, *8*(8), 981–982. https://doi.org/10.1038/nn0805-981

Rakic, P. (2009). Evolution of the neocortex: A perspective from developmental biology. *Nature Reviews Neuroscience*, *10*(10), 724–735. https://doi.org/10.1038/nrn2719

Rakic, P., & Yakovlev, P. I. (1968). Development of the corpus callosum and cavum septi in man. *The Journal of Comparative Neurology*, *132*(1), 45–72. https://doi.org/10.1002/cne.901320103

Raybaud, C., Ahmad, T., Rastegar, N., Shroff, M., & Al Nassar, M. (2013). The premature brain: Developmental and lesional anatomy. *Neuroradiology*, *55*(S2), 23–40. https://doi.org/10.1007/s00234-013-1231-0

Rees, S., Stringer, M., Just, Y., Hooper, S. B., & Harding, R. (1997). The vulnerability of the fetal sheep brain to hypoxemia at mid-gestation. *Developmental Brain Research*, *103*(2), 103–118. https://doi.org/10.1016/S0165-3806(97)81787-7

Reid, C. B., Tavazoie, S. F., & Walsh, C. A. (1997). Clonal dispersion and evidence for asymmetric cell division in ferret cortex. *Development*, *124*(12), 2441–2450. https://doi.org/10.1242/dev.124.12.2441

Reillo, I., De Juan Romero, C., García-Cabezas, M. Á., & Borrell, V. (2011). A Role for Intermediate Radial Glia in the Tangential Expansion of the Mammalian Cerebral Cortex. *Cerebral Cortex*, *21*(7), 1674–1694. https://doi.org/10.1093/cercor/bhq238

Ren, J.-Y., Zhu, M., Wang, G., Gui, Y., Jiang, F., & Dong, S.-Z. (2022). Quantification of Intracranial Structures Volume in Fetuses Using 3-D Volumetric MRI: Normal Values at 19 to 37 Weeks' Gestation. *Frontiers in Neuroscience*, *16*, 886083. https://doi.org/10.3389/fnins.2022.886083

Richman, D. P., Stewart, R. M., Hutchinson, J., & Caviness, V. S. (1975). Mechanical Model of Brain Convolutional Development: Pathologic and experimental data suggest a model based on differential growth within the cerebral cortex. *Science*, *189*(4196), 18–21. https://doi.org/10.1126/science.1135626

Robbins, S. (2004). Tuning and comparing spatial normalization methods. *Medical Image Analysis*, *8*(3), 311–323. https://doi.org/10.1016/j.media.2004.06.009

Rollins, C. K., Ortinau, C. M., Stopp, C., Friedman, K. G., Tworetzky, W., Gagoski, B., Velasco-Annis, C., Afacan, O., Vasung, L., Beaute, J. I., Rofeberg, V., Estroff, J. A., Grant, P. E., Soul, J. S., Yang, E., Wypij, D., Gholipour, A., Warfield, S. K., & Newburger, J. W. (2021). Regional Brain Growth Trajectories in Fetuses with Congenital Heart Disease. *Annals of Neurology*, *89*(1), 143–157. https://doi.org/10.1002/ana.25940

Romanes, G. J. (1965). Cunningham's textbook of anatomy. *Academic Medicine*, *40*(1), xix.

Ronan, L., & Fletcher, P. C. (2015). From genes to folds: A review of cortical gyrification theory. *Brain Structure and Function*, *220*(5), 2475–2483. https://doi.org/10.1007/s00429-014-0961-z

Rossum, G. van, & Drake, F. L. (2010). *The Python language reference* (Release 3.0.1 [Repr.]). Python Software Foundation.

Rowitch, D. H., & Kriegstein, A. R. (2010). Developmental genetics of vertebrate glial–cell specification. *Nature*, *468*(7321), 214–222. https://doi.org/10.1038/nature09611

Rutherford, M. A. (2009). Magnetic resonance imaging of the fetal brain. *Current Opinion in Obstetrics & Gynecology*, *21*(2), 180–186. https://doi.org/10.1097/GCO.0b013e32832947ab

Samuelsen, G. B. (2003). The Changing Number of Cells in the Human Fetal Forebrain and its Subdivisions: A Stereological Analysis. *Cerebral Cortex*, *13*(2), 115–122. https://doi.org/10.1093/cercor/13.2.115

Saraceno, B., Laviola, F., Sternai, E., Terzian, E., & Tognoni, G. (1994). Consequences of mental distress recognition in general practice in Italy: A follow-up study. Italian Cooperative Group on Mental Distress in General Practice. *Social Science & Medicine (1982)*, *39*(6), 789–796. https://doi.org/10.1016/0277-9536(94)90040-x

Schilling, K., Gao, Y., Janve, V., Stepniewska, I., Landman, B. A., & Anderson, A. W. (2018). Confirmation of a gyral bias in diffusion MRI fiber tractography. *Human Brain Mapping*, *39*(3), 1449–1466. https://doi.org/10.1002/hbm.23936

Schneider, J. F., Confort-Gouny, S., Le Fur, Y., Viout, P., Bennathan, M., Chapon, F., Fogliarini, C., Cozzone, P., & Girard, N. (2007). Diffusion-weighted imaging in normal fetal brain maturation. *European Radiology*, *17*(9), 2422–2429. https://doi.org/10.1007/s00330-007-0634-x

Schuh, A., Makropoulos, A., Robinson, E. C., Cordero-Grande, L., Hughes, E., Hutter, J., Price, A. N., Murgasova, M., Teixeira, R. P. A. G., Tusor, N., Steinweg, J. K., Victor, S., Rutherford, M. A., Hajnal, J. V., Edwards, A. D., & Rueckert, D. (2018). *Unbiased construction of a temporally consistent morphological atlas of neonatal brain development* [Preprint]. Neuroscience. https://doi.org/10.1101/251512

Schummers, J., Sharma, J., & Sur, M. (2005). Bottom-up and top-down dynamics in visual cortex. In *Progress in Brain Research* (Vol. 149, pp. 65–81). Elsevier. https://doi.org/10.1016/S0079-6123(05)49006-8

Schwabbauer, M. L. (1975). Use of the latent image technique to develop and evaluate problem-solving skills. *The American Journal of Medical Technology*, *41*(12), 457–462.

Scott, J. A., Habas, P. A., Kim, K., Rajagopalan, V., Hamzelou, K. S., Corbett-Detig, J. M., Barkovich, A. J., Glenn, O. A., & Studholme, C. (2011). Growth trajectories of the human fetal brain tissues estimated from 3D reconstructed in utero MRI. *International Journal of Developmental Neuroscience: The Official Journal of the International Society for Developmental Neuroscience*, *29*(5), 529–536. https://doi.org/10.1016/j.ijdevneu.2011.04.001

Serag, A., Aljabar, P., Ball, G., Counsell, S. J., Boardman, J. P., Rutherford, M. A., Edwards, A. D., Hajnal, J. V., & Rueckert, D. (2012). Construction of a consistent high-definition spatio-temporal atlas of the developing brain using adaptive kernel regression. *NeuroImage*, *59*(3), 2255–2265. https://doi.org/10.1016/j.neuroimage.2011.09.062

Sharma, J., Angelucci, A., & Sur, M. (2000). Induction of visual orientation modules in auditory cortex. *Nature*, *404*(6780), 841–847. https://doi.org/10.1038/35009043

Shi, Y., Lai, R., Kern, K., Sicotte, N., Dinov, I., & Toga, A. W. (2008). Harmonic Surface Mapping with Laplace-Beltrami Eigenmaps. In D. Metaxas, L. Axel, G. Fichtinger, & G. Székely (Eds.), *Medical Image Computing and Computer-Assisted Intervention – MICCAI 2008* (Vol. 5242, pp. 147–154). Springer Berlin Heidelberg. https://doi.org/10.1007/978-3-540-85990-1_18

Sidman, R. L., & Rakic, P. (1973). Neuronal migration, with special reference to developing human brain: A review. *Brain Research*, *62*(1), 1–35. https://doi.org/10.1016/0006-8993(73)90617-3

Sizonenko, S. V., Camm, E. J., Garbow, J. R., Maier, S. E., Inder, T. E., Williams, C. E., Neil, J. J., & Huppi, P. S. (2007). Developmental Changes and Injury Induced Disruption of the Radial Organization of the Cortex in the Immature Rat Brain Revealed by In Vivo Diffusion Tensor MRI. *Cerebral Cortex*, *17*(11), 2609–2617. https://doi.org/10.1093/cercor/bhl168

Smart, I. H., & McSherry, G. M. (1986). Gyrus formation in the cerebral cortex of the ferret. II. Description of the internal histological changes. *Journal of Anatomy*, *147*, 27–43.

Smith, F., Adam, A.H, & Phillips, W.D.P. (1983). NMR IMAGING IN PREGNANCY. *The Lancet*, *321*(8314–8315), 61–62. https://doi.org/10.1016/S0140-6736(83)91588-X

Smith, F. W., MacLennan, F., Abramovich, D. R., MacGilivray, I., & Hutchison, J. M. S. (1984). NMR imaging in human pregnancy: A preliminary study. *Magnetic Resonance Imaging*, *2*(1), 57–64. https://doi.org/10.1016/0730-725X(84)90126-7

Smith, R. E., Tournier, J.-D., Calamante, F., & Connelly, A. (2012). Anatomically-constrained tractography: Improved diffusion MRI streamlines tractography through effective use of anatomical information. *NeuroImage*, *62*(3), 1924–1938. https://doi.org/10.1016/j.neuroimage.2012.06.005

Smith, R. E., Tournier, J.-D., Calamante, F., & Connelly, A. (2013). SIFT: Spherical-deconvolution informed filtering of tractograms. *NeuroImage*, *67*, 298–312. https://doi.org/10.1016/j.neuroimage.2012.11.049

Sporns, O., Tononi, G., & Kötter, R. (2005). The human connectome: A structural description of the human brain. *PLoS Computational Biology*, *1*(4), e42. https://doi.org/10.1371/journal.pcbi.0010042

Stejskal, E. O., & Tanner, J. E. (1965a). Spin Diffusion Measurements: Spin Echoes in the Presence of a Time-Dependent Field Gradient. *The Journal of Chemical Physics*, *42*(1), 288–292. https://doi.org/10.1063/1.1695690

Stejskal, E. O., & Tanner, J. E. (1965b). Spin Diffusion Measurements: Spin Echoes in the Presence of a Time-Dependent Field Gradient. *The Journal of Chemical Physics*, *42*(1), 288–292. https://doi.org/10.1063/1.1695690

Stiles, J., & Jernigan, T. L. (2010). The Basics of Brain Development. *Neuropsychology Review*, *20*(4), 327–348. https://doi.org/10.1007/s11065-010-9148-4

Subramanian, L., Calcagnotto, M. E., & Paredes, M. F. (2020). Cortical Malformations: Lessons in Human Brain Development. *Frontiers in Cellular Neuroscience*, *13*, 576. https://doi.org/10.3389/fncel.2019.00576

Sur, M., & Rubenstein, J. L. R. (2005). Patterning and plasticity of the cerebral cortex. *Science (New York, N.Y.)*, *310*(5749), 805–810. https://doi.org/10.1126/science.1112070

Susuki, K., & Rasband, M. N. (2008). Molecular mechanisms of node of Ranvier formation. *Current Opinion in Cell Biology*, *20*(6), 616–623. https://doi.org/10.1016/j.ceb.2008.09.007

Takahashi, E., Folkerth, R. D., Galaburda, A. M., & Grant, P. E. (2012). Emerging Cerebral Connectivity in the Human Fetal Brain: An MR Tractography Study. *Cerebral Cortex*, *22*(2), 455–464. https://doi.org/10.1093/cercor/bhr126

Tallinen, T., Chung, J. Y., Biggins, J. S., & Mahadevan, L. (2014). Gyrification from constrained cortical expansion. *Proceedings of the National Academy of Sciences*, *111*(35), 12667–12672. https://doi.org/10.1073/pnas.1406015111

Tallinen, T., Chung, J. Y., Rousseau, F., Girard, N., Lefèvre, J., & Mahadevan, L. (2016). On the growth and form of cortical convolutions. *Nature Physics*, *12*(6), 588–593. https://doi.org/10.1038/nphys3632

Thomason, M. E., Scheinost, D., Manning, J. H., Grove, L. E., Hect, J., Marshall, N., Hernandez-Andrade, E., Berman, S., Pappas, A., Yeo, L., Hassan, S. S., Constable, R. T., Ment, L. R., & Romero, R. (2017). Weak functional connectivity in the human fetal brain prior to preterm birth. *Scientific Reports*, *7*(1), 39286. https://doi.org/10.1038/srep39286

Toga, A. W. (Ed.). (2015). *Brain mapping: An encyclopedic reference*. Elsevier/AP, Academic Press is an imprint of Elsevier.

Toga, A. W., & Thompson, P. M. (2003). Mapping brain asymmetry. *Nature Reviews Neuroscience*, *4*(1), 37–48. https://doi.org/10.1038/nrn1009

Tolner, E. A., Sheikh, A., Yukin, A. Y., Kaila, K., & Kanold, P. O. (2012). Subplate Neurons Promote Spindle Bursts and Thalamocortical Patterning in the Neonatal Rat Somatosensory Cortex. *The Journal of Neuroscience*, *32*(2), 692–702. https://doi.org/10.1523/JNEUROSCI.1538-11.2012

Toro, R., & Burnod, Y. (2005). A Morphogenetic Model for the Development of Cortical Convolutions. *Cerebral Cortex*, *15*(12), 1900–1913. https://doi.org/10.1093/cercor/bhi068

Toulmin, H., Beckmann, C. F., O'Muircheartaigh, J., Ball, G., Nongena, P., Makropoulos, A., Ederies, A., Counsell, S. J., Kennea, N., Arichi, T., Tusor, N., Rutherford, M. A., Azzopardi, D., Gonzalez-Cinca, N., Hajnal, J. V., & Edwards, A. D. (2015). Specialization and integration of functional thalamocortical connectivity in the human infant. *Proceedings of the National Academy of Sciences*, *112*(20), 6485–6490. https://doi.org/10.1073/pnas.1422638112

Toulmin, H., O'Muircheartaigh, J., Counsell, S. J., Falconer, S., Chew, A., Beckmann, C. F., & Edwards, A. D. (2021). Functional thalamocortical connectivity at term equivalent age and outcome at 2 years in infants born preterm. *Cortex*, *135*, 17–29. https://doi.org/10.1016/j.cortex.2020.09.022

Tournier, J., Christiaens, D., Hutter, J., Price, A. N., Cordero-Grande, L., Hughes, E., Bastiani, M., Sotiropoulos, S. N., Smith, S. M., Rueckert, D., Counsell, S. J., Edwards, A. D., & Hajnal, J. V. (2020). A data-driven approach to optimising the encoding for multi-shell diffusion MRI with application to neonatal imaging. *NMR in Biomedicine*, *33*(9). https://doi.org/10.1002/nbm.4348

Tournier, J.-D. (2010). The Biophysics of Crossing Fibers. In D. K. Jones, PhD (Ed.), *Diffusion MRI* (pp. 465–482). Oxford University Press. https://doi.org/10.1093/med/9780195369779.003.0028

Tournier, J.-D., Calamante, F., & Connelly, A. (2007). Robust determination of the fibre orientation distribution in diffusion MRI: Non-negativity constrained super-resolved spherical deconvolution. *NeuroImage*, *35*(4), 1459–1472. https://doi.org/10.1016/j.neuroimage.2007.02.016

Tournier, J.-D., Calamante, F., & Connelly, A. (2013). Determination of the appropriate *b* value and number of gradient directions for high-angular-resolution diffusion-weighted imaging: APPROPRIATE *b* VALUE AND NUMBER OF GRADIENT DIRECTIONS FOR HARDI. *NMR in Biomedicine*, *26*(12), 1775–1786. https://doi.org/10.1002/nbm.3017

Tournier, J.-D., Calamante, F., Gadian, D. G., & Connelly, A. (2004). Direct estimation of the fiber orientation density function from diffusion-weighted MRI data using spherical deconvolution. *NeuroImage*, *23*(3), 1176–1185. https://doi.org/10.1016/j.neuroimage.2004.07.037

Tournier, J.-D., Smith, R., Raffelt, D., Tabbara, R., Dhollander, T., Pietsch, M., Christiaens, D., Jeurissen, B., Yeh, C.-H., & Connelly, A. (2019). MRtrix3: A fast, flexible and open software framework for medical image processing and visualisation. *NeuroImage*, *202*, 116137. https://doi.org/10.1016/j.neuroimage.2019.116137

Tsuchiya, K., Mizutani, Y., & Hachiya, J. (1996). Surface anatomy MR scanning of the brain using HASTE sequences. *American Journal of Roentgenology*, *167*(6), 1585–1587. https://doi.org/10.2214/ajr.167.6.8956602

Turk, E., van den Heuvel, M. I., Benders, M. J., de Heus, R., Franx, A., Manning, J. H., Hect, J. L., Hernandez-Andrade, E., Hassan, S. S., Romero, R., Kahn, R. S., Thomason, M. E., & van den Heuvel, M. P. (2019). Functional Connectome of the Fetal Brain. *The Journal of Neuroscience*, *39*(49), 9716–9724. https://doi.org/10.1523/JNEUROSCI.2891-18.2019

Tustison, N. J., Avants, B. B., Cook, P. A., Yuanjie Zheng, Egan, A., Yushkevich, P. A., & Gee, J. C. (2010). N4ITK: Improved N3 Bias Correction. *IEEE Transactions on Medical Imaging*, *29*(6), 1310–1320. https://doi.org/10.1109/TMI.2010.2046908

Uehara, H., Yoshioka, H., Kawase, S., Nagai, H., Ohmae, T., Hasegawa, K., & Sawada, T. (1999). A new model of white matter injury in neonatal rats with bilateral carotid artery occlusion. *Brain Research*, *837*(1–2), 213–220. https://doi.org/10.1016/S0006-8993(99)01675-3

van den Heuvel, M. I., Turk, E., Manning, J. H., Hect, J., Hernandez-Andrade, E., Hassan, S. S., Romero, R., van den Heuvel, M. P., & Thomason, M. E. (2018). Hubs in the human fetal brain network. *Developmental Cognitive Neuroscience*, *30*, 108–115. https://doi.org/10.1016/j.dcn.2018.02.001

Van Essen, D. C. (1997). A tension-based theory of morphogenesis and compact wiring in the central nervous system. *Nature*, *385*(6614), 313–318. https://doi.org/10.1038/385313a0

Van Essen, D. C. (2020). A 2020 view of tension-based cortical morphogenesis. *Proceedings of the National Academy of Sciences*, *117*(52), 32868–32879. https://doi.org/10.1073/pnas.2016830117

Vandekar, S. N., Shinohara, R. T., Raznahan, A., Hopson, R. D., Roalf, D. R., Ruparel, K., Gur, R. C., Gur, R. E., & Satterthwaite, T. D. (2016). Subject-level measurement of local cortical coupling. *NeuroImage*, *133*, 88–97. https://doi.org/10.1016/j.neuroimage.2016.03.002

Varoquaux, G., Sadaghiani, S., Pinel, P., Kleinschmidt, A., Poline, J. B., & Thirion, B. (2010). A group model for stable multi-subject ICA on fMRI datasets. *NeuroImage*, *51*(1), 288–299. https://doi.org/10.1016/j.neuroimage.2010.02.010

Varoquaux, G., Sadaghiani, S., Poline, J. B., & Thirion, B. (2009). *CanICA: Model-based extraction of reproducible group-level ICA patterns from fMRI time series*. https://doi.org/10.48550/ARXIV.0911.4650

Vasung, L., Rollins, C. K., Velasco-Annis, C., Yun, H. J., Zhang, J., Warfield, S. K., Feldman, H. A., Gholipour, A., & Grant, P. E. (2020). Spatiotemporal Differences in the Regional Cortical Plate and Subplate Volume Growth during Fetal Development. *Cerebral Cortex*, *30*(8), 4438–4453. https://doi.org/10.1093/cercor/bhaa033

Veraart, J., Novikov, D. S., Christiaens, D., Ades-aron, B., Sijbers, J., & Fieremans, E. (2016). Denoising of diffusion MRI using random matrix theory. *NeuroImage*, *142*, 394–406. https://doi.org/10.1016/j.neuroimage.2016.08.016

Vinall, J., Grunau, R. E., Brant, R., Chau, V., Poskitt, K. J., Synnes, A. R., & Miller, S. P. (2013). Slower Postnatal Growth Is Associated with Delayed Cerebral Cortical Maturation in Preterm Newborns. *Science Translational Medicine*, *5*(168). https://doi.org/10.1126/scitranslmed.3004666

Volpe, J. J. (2001). Neurobiology of Periventricular Leukomalacia in the Premature Infant. *Pediatric Research*, *50*(5), 553–562. https://doi.org/10.1203/00006450-200111000-00003

Volpe, J. J. (2009). The Encephalopathy of Prematurity—Brain Injury and Impaired Brain Development Inextricably Intertwined. *Seminars in Pediatric Neurology*, *16*(4), 167–178. https://doi.org/10.1016/j.spen.2009.09.005

Volpe, J. J. (Ed.). (2018). *Volpe's neurology of the newborn* (Sixth edition). Elsevier.

von Economo, C. F., & Koskinas, G. N. (1925). *Die cytoarchitektonik der hirnrinde des erwachsenen menschen*. J. Springer.

Walsh, C., & Cepko, C. L. (1988). Clonally Related Cortical Cells Show Several Migration Patterns. *Science*, *241*(4871), 1342–1345. https://doi.org/10.1126/science.3137660

Walsh, Ch., & Cepko, C. L. (1990). Cell lineage and cell migration in the developing cerebral cortex. *Experientia*, *46*(9), 940–947. https://doi.org/10.1007/BF01939387

Wang, X., Chun, S.-J., Treloar, H., Vartanian, T., Greer, C. A., & Strittmatter, S. M. (2002). Localization of Nogo-A and Nogo-66 Receptor Proteins at Sites of Axon–Myelin and

Synaptic Contact. *The Journal of Neuroscience*, *22*(13), 5505–5515. https://doi.org/10.1523/JNEUROSCI.22-13-05505.2002

Wang, X., Studholme, C., Grigsby, P. L., Frias, A. E., Cuzon Carlson, V. C., & Kroenke, C. D. (2017). Folding, But Not Surface Area Expansion, Is Associated with Cellular Morphological Maturation in the Fetal Cerebral Cortex. *The Journal of Neuroscience*, *37*(8), 1971–1983. https://doi.org/10.1523/JNEUROSCI.3157-16.2017

Ware, M. L. (1999). Coexistence of Widespread Clones and Large Radial Clones in Early Embryonic Ferret Cortex. *Cerebral Cortex*, *9*(6), 636–645. https://doi.org/10.1093/cercor/9.6.636

Weidenheim, K. M., Kress, Y., Epshteyn, I., Rashbaum, W. K., & Lyman, W. D. (1992). Early Myelination in the Human Fetal Lumbosacral Spinal Cord: Characterization by Light and Electron Microscopy. *Journal of Neuropathology and Experimental Neurology*, *51*(2), 142–149. https://doi.org/10.1097/00005072-199203000-00004

Widjaja, E., Geibprasert, S., Mahmoodabadi, S. Z., Blaser, S., Brown, N. E., & Shannon, P. (2010). Alteration of Human Fetal Subplate Layer and Intermediate Zone During Normal Development on MR and Diffusion Tensor Imaging. *American Journal of Neuroradiology*, *31*(6), 1091–1099. https://doi.org/10.3174/ajnr.A1985

Wiegell, M. R., Larsson, H. B. W., & Wedeen, V. J. (2000). Fiber Crossing in Human Brain Depicted with Diffusion Tensor MR Imaging. *Radiology*, *217*(3), 897–903. https://doi.org/10.1148/radiology.217.3.r00nv43897

Wilkinson, M., Kane, T., Wang, R., & Takahashi, E. (2017). Migration Pathways of Thalamic Neurons and Development of Thalamocortical Connections in Humans Revealed by Diffusion MR Tractography. *Cerebral Cortex*, *27*(12), 5683–5695. https://doi.org/10.1093/cercor/bhw339

Wilson, S., Pietsch, M., Cordero-Grande, L., Christiaens, D., Uus, A., Karolis, V. R., Kyriakopoulou, V., Colford, K., Price, A. N., Hutter, J., Rutherford, M. A., Hughes, E. J., Counsell, S. J., Tournier, J.-D., Hajnal, J. V., Edwards, A. D., O'Muicheartaigh, J., & Arichi, T. (2023). Spatiotemporal tissue maturation of thalamocortical pathways in the human fetal brain. *ELife*, *12*, e83727. https://doi.org/10.7554/eLife.83727

Wilson, S., Pietsch, M., Cordero-Grande, L., Price, A. N., Hutter, J., Xiao, J., McCabe, L., Rutherford, M. A., Hughes, E. J., Counsell, S. J., Tournier, J.-D., Arichi, T., Hajnal, J. V., Edwards, A. D., Christiaens, D., & O'Muircheartaigh, J. (2021). Development of human white matter pathways in utero over the second and third trimester. *Proceedings of the National Academy of Sciences*, *118*(20), e2023598118. https://doi.org/10.1073/pnas.2023598118

Wimberger, D. M., Roberts, T. P., Barkovich, A. J., Prayer, L. M., Moseley, M. E., & Kucharczyk, J. (1995). Identification of "Premyelination" by Diffusion-Weighted MRI: *Journal of Computer Assisted Tomography*, *19*(1), 28–33. https://doi.org/10.1097/00004728-199501000-00005

Winkler, A. M., Ridgway, G. R., Webster, M. A., Smith, S. M., & Nichols, T. E. (2014). Permutation inference for the general linear model. *NeuroImage*, *92*, 381–397. https://doi.org/10.1016/j.neuroimage.2014.01.060

Xu, G., Knutsen, A. K., Dikranian, K., Kroenke, C. D., Bayly, P. V., & Taber, L. A. (2010). Axons Pull on the Brain, But Tension Does Not Drive Cortical Folding. *Journal of Biomechanical Engineering*, *132*(7), 071013. https://doi.org/10.1115/1.4001683

Xu, G., Takahashi, E., Folkerth, R. D., Haynes, R. L., Volpe, J. J., Grant, P. E., & Kinney, H. C. (2014). Radial coherence of diffusion tractography in the cerebral white matter of the human fetus: Neuroanatomic insights. *Cerebral Cortex (New York, N.Y.: 1991)*, *24*(3), 579–592. https://doi.org/10.1093/cercor/bhs330

Yakovlev, P. I., Locke, S., Koskoff, D. Y., & Patton, R. A. (1960). Limbic Nuclei of Thalamus and Connections of Limbic Cortex. *Archives of Neurology*, *3*(6), 620–641. https://doi.org/10.1001/archneur.1960.00450060008002

Yamashita, Y., Namimoto, T., Abe, Y., Takahashi, M., Iwamasa, J., Miyazaki, K., & Okamura, H. (1997). MR imaging of the fetus by a HASTE sequence. *American Journal of Roentgenology*, *168*(2), 513–519. https://doi.org/10.2214/ajr.168.2.9016238

Yu, Q., Ouyang, A., Chalak, L., Jeon, T., Chia, J., Mishra, V., Sivarajan, M., Jackson, G., Rollins, N., Liu, S., & Huang, H. (2016). Structural Development of Human Fetal and Preterm Brain Cortical Plate Based on Population-Averaged Templates. *Cerebral Cortex*, *26*(11), 4381–4391. https://doi.org/10.1093/cercor/bhv201

Yue, X., Mehmet, H., Penrice, J., Cooper, C., Cady, E., Wyatt, J. S., Reynolds, E. O., Edwards, A. D., & Squier, M. V. (1997). Apoptosis and necrosis in the newborn piglet brain following transient cerebral hypoxia-ischaemia. *Neuropathology and Applied Neurobiology*, *23*(1), 16–25.

Yun, H. J., Im, K., Jin-Ju Yang, Yoon, U., & Lee, J.-M. (2013). Automated Sulcal Depth Measurement on Cortical Surface Reflecting Geometrical Properties of Sulci. *PLoS ONE*, *8*(2), e55977. https://doi.org/10.1371/journal.pone.0055977

Yun, H. J., Vasung, L., Tarui, T., Rollins, C. K., Ortinau, C. M., Grant, P. E., & Im, K. (2020). Temporal Patterns of Emergence and Spatial Distribution of Sulcal Pits During Fetal Life. *Cerebral Cortex*, *30*(7), 4257–4268. https://doi.org/10.1093/cercor/bhaa053

Zambusi, A., & Ninkovic, J. (2020). Regeneration of the central nervous system-principles from brain regeneration in adult zebrafish. *World Journal of Stem Cells*, *12*(1), 8–24. https://doi.org/10.4252/wjsc.v12.i1.8

Zanin, E., Ranjeva, J., Confort-Gouny, S., Guye, M., Denis, D., Cozzone, P. J., & Girard, N. (2011). White matter maturation of normal human fetal brain. An in vivo diffusion tensor tractography study. *Brain and Behavior*, *1*(2), 95–108. https://doi.org/10.1002/brb3.17